Trinity River Restoration Program

Technical Report: TR-TRRP-2020-1

WY2016-2017 Trinity River Gravel Augmentation Monitoring Report

Prepared by:

David Gaeuman
The Yurok Tribe
Fisheries Department
Klamath, California

January 2020

Contents

Abstract 1
Introduction 2
Geographic Context 3
Flow Management 4
Gravel Augmentations 5
  The Diversion Pool 6
  Lowden Ranch 7
  The 2016 and 2017 Flow Releases 9
Methods 12
  Topographic Surveys 12
  Topographic Change Analysis 14
  Sediment Monitoring 17
  Uncertainty 17
  PIT-tagged Tracer Stones 21
Results of Reach-Scale Monitoring 23
  Gravel Budgets in the Lewiston Bridges Reach 23
    The 2016 Flow Release 24
    The 2017 Flow Release 25
  Gravel Budgets in the Lowden/THG Reach 29
    The 2016 Flow Release 29
    The 2017 Flow Release 32
  Gravel Activity in the Lewiston Bridges Reach 36
  Gravel Activity in the Lowden/THG Reach 37
  PIT-tagged Tracers 38
    Tracer Recovery Efficiency 38
Integration of Gravel Budget and Tracer Results 45
Results of Pool Depth Monitoring 51
  Background 51
  Quantifying Changes in Pool Morphology 51
  Pool Selection 52
  Depth Changes by Time Interval 56
Conclusions 61
Recommendations 63
References 64

Appendix A: Assessment of Elevation Bias in 2017 Sonar Data
Appendix B: Bedload Sampling Uncertainty
Appendix C: Morphodynamic Modeling
Appendix D: Pool Polygon Location Maps
Appendix E: Pool Depth Statistics
Appendix F: Cumulative Pool Depth-frequency Curves
Appendix G: Pool Depth Change Statistics

Abstract

Gravel augmentation is a method for restoring gravel-bed stream reaches in which coarse bed material that would otherwise be delivered from upstream is captured in impoundments behind dams. The Trinity River, located in far northern California, is regulated by two dams that divert a portion of its flow to the Sacramento River as part of California's Central Valley Project. This report describes gravel augmentations implemented in the Trinity River by the Trinity River Restoration Program in water years 2016 and 2017, and presents the results of 2016 and 2017 monitoring activities designed to assess how those augmentations affected gravel transport and bed morphology in the reaches downstream from the augmentation points. Augmentations in those years were performed at the Diversion Pool augmentation site and at two locations at Lowden Ranch during spring high flow releases from Lewiston Dam. Monitoring conducted in the reaches downstream from those sites consisted of repeated topographic surveys, bedload transport sampling, and relocation of bedload tracer particles. The topographic data support development of morphology-based gravel budgets, whereas the bedload measurements provide boundary conditions that support estimation of gravel fluxes throughout the study reaches. Tracer locations delineate gravel transport distances and transport pathways, and provide insight into the dynamics of mass exchanges between the augmentation material and the native substrate. At 12,000 ft^3/s, the peak discharge attained by the 2017 flow release was 26% greater than the peak of 9,500 ft^3/s reach during the 2016 release. Sediment budget results for 2016 show that a large share of the gravel introduced into the river that year was deposited close to the augmentation points. The 2017 budgets indicate that gravel fluxes were between 50 and 170% greater in 2017 than in 2016, and that the areas immediately downstream from the augmentations experienced net erosion. Deposition of the 2016 and 2017 augmentation material occurred farther downstream, and significant gravel fluxes exited the downstream boundaries of both study reaches. The increase in gravel mobility during the 2017 flow release relative to the 2016 release appears to have been due in large part to the larger magnitude of the 2017 release peak. The tracer data, however, suggest that vertical and lateral sorting processes may have prevented the augmentation gravel from fully participating in the downstream transport. This report also presents data quantifying depth changes over a six-year period in 105 pool locations distributed between Lewiston Dam and the North Fork Trinity River. Those data reveal that the depths of most pools remained essentially constant between 2011 and 2017.

Introduction

Gravel augmentation is a method for restoring gravel-bed stream reaches in which coarse bed material that would otherwise be delivered from upstream is captured in impoundments behind dams. Elimination of bed material inputs downstream from dams can lead to channel incision, coarsening of the streambed, decreased bed mobility, and a loss of topographic and habitat diversity (Williams and Wolman, 1984; Lisle et al. 1993; Church, 1995; Viparelli et al. 2011). In such instances, gravel augmentation has the potential to decrease bed surface particle sizes and increase bed mobility, thereby stimulating increased rates of geomorphic activity. Processes such as bed scour and fill, bank erosion, and channel migration create and maintain the pools, bars, and riffles that drive variations in flow depth, velocity, and direction that constitute the diversity in meso- and micro-scale habitats needed to support the range of species and life stages present in the aquatic ecosystem (Petts and Maddock 1996; Kondolf and Wilcock 1996; Stanford et al. 1996; Richter et al. 1997; Milhous 1998; Ock et al. 2015).

Despite its potential for ecological benefit, however, there is also a risk for coarse sediment augmentations to produce unfavorable outcomes. There is considerable evidence that large increases in sediment supplies can cause topographic relief and physical habitat diversity to decrease (Lisle 1982; Madej 1999; Bartley and Rutherfurd 2005; Madej and Ozaki 2006; Yarnell et al. 2006; Madej and Ozaki 2009; Zunka et al. 2015). Adding very large quantities of gravel to a stream can also interfere with recreation and navigation, and may threaten property and infrastructure through bank erosion or increased flood stages due to bed aggradation. Regardless of whether these various outcomes are considered to be positive or negative, it is incumbent on resource managers to be aware of them and attempt to anticipate them. The current state of the science, however, is inadequate to predict precisely where and when these various potential outcomes will be realized (Lisle et al. 1997; Sklar et al. 2009; Humphries et al. 2012; Pace et al. 2016; Gaeuman et al. 2017). Direct monitoring of changes in stream topography, substrate condition, and habitat quality is therefore necessary to assess the consequences of past gravel augmentations and improve restoration practices through an adaptive management process.

This report describes gravel augmentations implemented in the Trinity River of northern California in 2016 and 2017, and presents the results of monitoring designed to assess how those augmentations affected gravel transport and bed morphology in the reaches downstream from the augmentation points. These management and monitoring activities are implemented by the Trinity River Restoration Program (TRRP) in accordance with the Trinity River Mainstem Fishery Record of Decision (ROD) issued by the U.S. Department of the Interior (USDOI 2000). The ROD authorizes the TRRP to supplement the gravel supply downstream from a pair of dams that have eliminated the natural gravel supply downstream from the dams and regulated streamflows in downstream reaches since 1960. TRRP gravel augmentations and physical monitoring results for 2012-2015 are described by Gaeuman et al. (2017) as well as by Gaeuman and Stewart (2019), and results from 2003-2011 can be found in Gaeuman (2011) and Gaeuman (2014). Krause (2012) provides background information on gravel management in the Trinity River prior to establishment of the TRRP in 2002. This report, however, does not attempt to link the physical effects of gravel augmentation directly to ecological function, as those complex issues are addressed

elsewhere. Gaeuman and Boyce (2018) and Gaeuman et al. (2019) describe some initial investigations into how morphological changes associated with gravel augmentations have affected salmon rearing habitat quality in one reach of the Trinity River, whereas the nexus between stream morphology and salmon habitat is to be considered more generally in an upcoming TRRP habitat synthesis report.

Geographic Context

The Trinity River drains the south side of the Scott Mountains and Trinity Alps in northern California and joins into the Klamath River about 43 miles upstream from where the Klamath discharges into the Pacific Ocean. The river is regulated by two dams: Trinity Dam impounds a large storage reservoir about 112 miles from its mountain headwaters, whereas Lewiston Dam located about 8 miles farther downstream regulates trans-basin water diversions to the California's Central Valley, as well as flows to downstream reaches of the Trinity (Figure 1). The river downstream from the dams is gravel-bedded with typical channel widths between about 100 and 150 ft and, under current dam operating guidelines, a mean annual flood of about 6500 to 8500 ft^3/s, depending on distance from the dam.

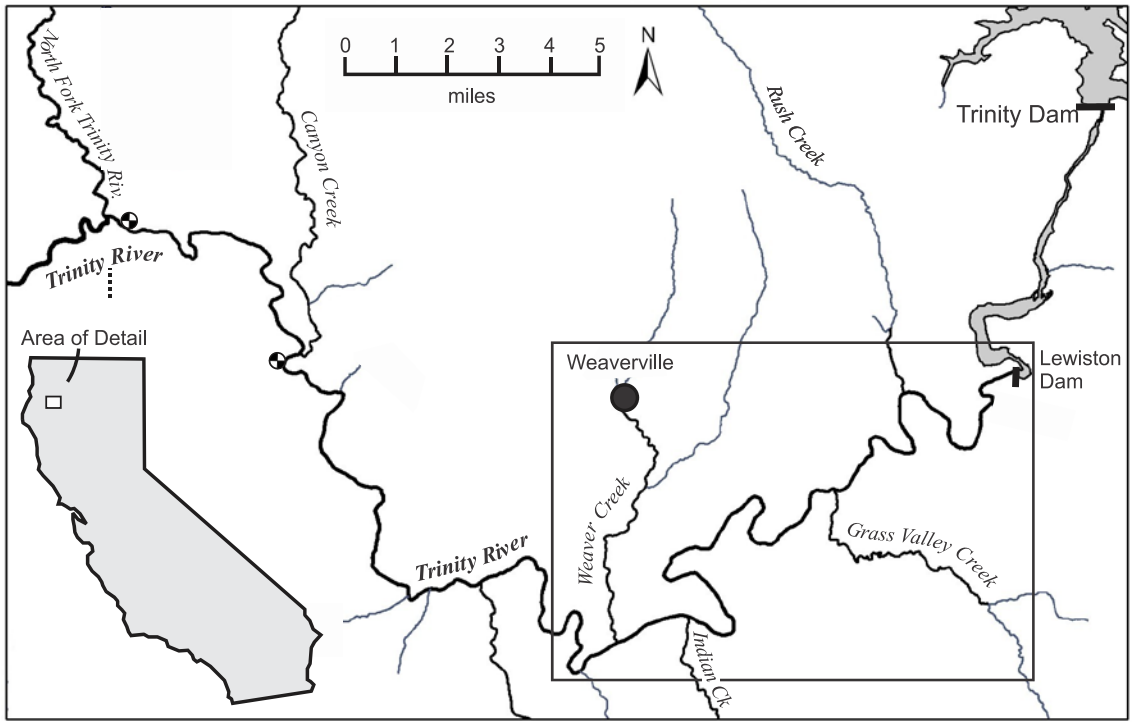

Figure 1: Map of the Trinity River between Lewiston Dam and the North Fork Trinity River. Boxed portion of the river is shown in greater detail in Figure 2.

The TRRP manages gravel supplies in a segment of the Trinity River that extends from Lewiston Dam to Indian Creek, located 16.4 river miles downstream. According to scientific studies and administrative documents that established the Program (USFWS and HVT 1999;

USDOI 2000), the cumulative sediment deliveries from Indian Creek and upstream tributaries are sufficiently large that gravel augmentation is unnecessary downstream from that point. All TRRP gravel augmentations intended to increase the supply of mobile gravel and all monitoring focussed on the fate of that material has therefore been performed upstream from Indian Creek. However, a persistent belief exists among some public stakeholders that TRRP gravel additions have contributed to the widespread filling of deep pools used as holding habitat by adult salmonids throughout a stretch of river extending 40 miles downstream to the confluence of the Trinity River and the North Fork Trinity River. Consequently, this report also presents new data collected 2016 and 2017 and updates an earlier analysis by Gaeuman and Krause (2013) that addressed changes in pool depths and volumes between 2009 and 2012.

Flow Management

Streamflow in the Trinity River downstream from Lewiston Dam is managed in accordance with guidelines contained in the ROD (USDOI 2000), which defines five annual hydrographs, each of which corresponds to a water year type – critically dry, dry, normal, wet, and extremely wet – defined according to the total water yield from the Trinity River catchment upstream from the dams (Table 1). Each water year type is associated with a probability of occurance in any given water year, and each of the five hydrographs specifies a total water volume available for release from Lewiston Dam for that water year and a recommended peak magnitude for the annual spring high-flow release.

Table 1: Water year and release hydrograph types defined for Trinity River management. Catchment yield thresholds and release volumes are given in thousand acre-ft (Kaf).

WY Type	Critically Dry	Dry	Normal	Wet	Extremely Wet
Catchment Yield (Kaf)	--	650	1025	1350	2000
Probability	0.12	0.28	0.20	0.28	0.12
Release Volume (Kaf)	369	453	647	701	815
Nominal Release Peak (ft^3/s)	1500	4500	6000	8500	11000

In recent years, peak flow releases from Lewiston Dam have often deviated somewhat from the ROD-recommended values as managers attempt to craft hydrographs designed to accomplish specific geomorphic or biological objectives. For example, 2011 was classified as a wet year, but TRRP chose to maximize geomorphic change by planning to release a peak of 11,000 ft^3/s, the largest flow authorized by the ROD. Likewise, a peak of 8,500 ft^3/s was targeted in 2015 even though that year was classified as a dry year. The total annual release volumes, however, cannot exceed the volumes authorized by the ROD. Any increase in the flow peak must be balanced by a decrease in the magnitude or duration of some other hydrograph component.

Discharge in the Trinity River is gaged at six locations between Lewiston Dam and the North Fork Trinity River, four of which are relevant to this report (Figure 2). The U.S. Geological Survey (USGS) operates three of those gages. From upstream to downstream, the relevant

USGS gages are Trinity River at Lewiston (USGS 11525500), Trinity River below Limekiln Gulch (USGS 11525655), and Trinity River at Douglas City (USGS 11525854). The fourth relevant gage, Trinity River above Grass Valley Creek (TRGVC), is operated by a contractor during annual spring high-flow releases from Lewiston Dam (Figure 2). Only the Lewiston gage and TRGVC are directly tied to gravel dynamics at the gravel augmentation locations discussed herein.

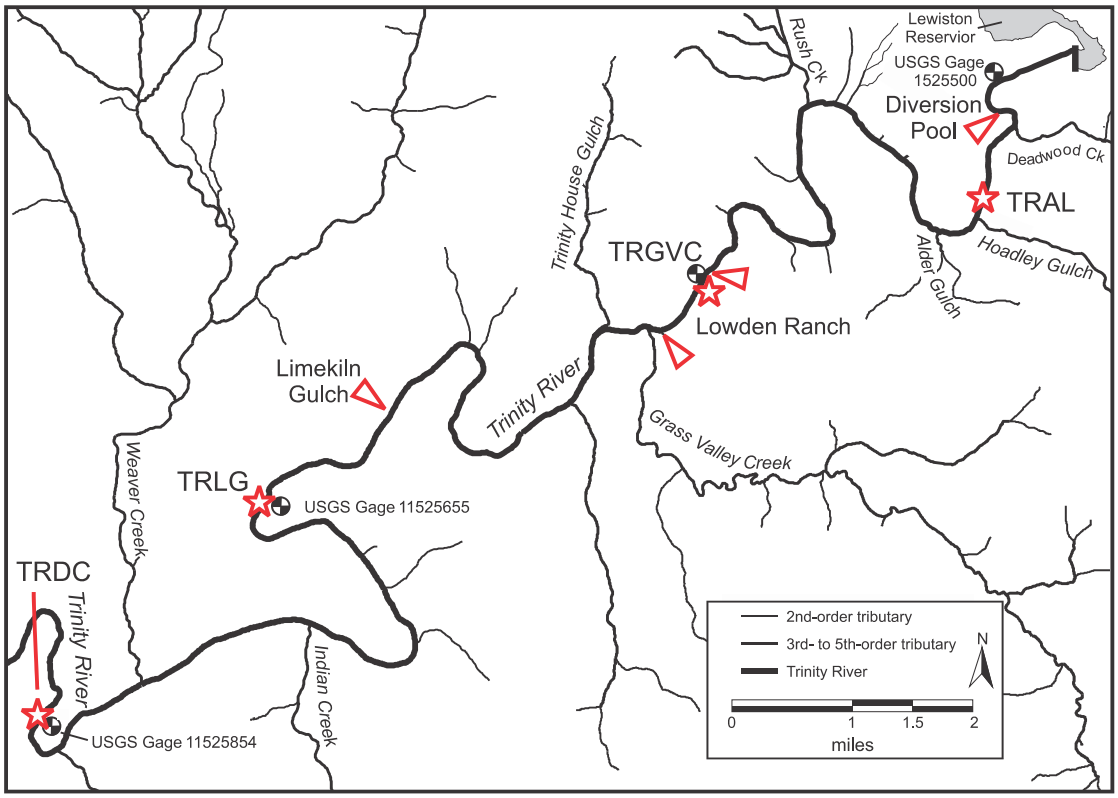

Figure 2: Map of the Trinity River between Lewiston Dam and the Trinity River stream gage at Douglas City. Red triangles point to gravel augmentation locations referred to in the text; red stars labelled TRAL, TRGVC, TRLG, and TRDC indicate sediment monitoring locations discussed in the methods section.

Gravel Augmentations

Since its inception, TRRP has used two basic methods to implement gravel augmentations: gravel "injections" in which gravel is pushed or dumped directly into the main flow on the rising limb of high-flow releases from Lewiston Dam, and bar construction associated with mechanical channel rehabilitation projects implemented during low-flow periods. Prior to 2011, 80% of all TRRP additions of mobile gravel were associated with the placement of designed bars at rehabilitation project sites. By the end of 2010, however, most of the sites slated for mechanical restoration upstream from Indian Creek had been completed, so gravel injections have taken a progressively larger role in ensuring that the upper river receives an adequate supply of gravel. In 2015 through 2017, 98% of augmentations totaling 9,030 yd^3 of

mobile gravel were injected into the flow on the rising limbs of spring floods released from Lewiston Dam at one of three locations – the Diversion Pool gravel injection point and at two points within the Lowden Ranch reach of the river (Table 2; Figure 2). The remaining 2% of the gravel introduced during that period was placed during summer low flow in conjunction with the 2015 Limekiln Gulch mechanical rehabilitation project. The Limekiln placement, which consisted of just 200 yd^3 of gravel used to create a channel crossing for heavy equipment, is considered too small to produce a detectable change in downstream channel morphology and is discussed no further in this report.

Table 2: Additions of mobile gravel in the Trinity River in 2015 through 2017.

Year	Location	Type	Volume yd^3
2015	Lowden Ranch, upstream	Injection	680
2015	Diversion Pool	Injection	1000
2015	Limekiln Gulch Rehab Project	Low-flow placement	200
2016	Lowden Ranch, upstream	Injection	1600
2016	Diversion Pool	Injection	2000
2017	Lowden Ranch, upstream	Injection	1400
2017	Lowden Ranch, downstream	Injection	600
2017	Diversion Pool	Injection	1550

The Diversion Pool

The Diversion Pool gravel injection point, located 0.9 miles from Lewiston Dam, has been the most frequently used site for gravel augmentations since TRRP augmentations began in 2003. Gravel injections were performed at the site every year from 2008 through 2017 except the drought year of 2014 when no flood flows were released from Lewiston Dam. Overall, 54% (12,015 of 22,290 yd^3) of all gravel TRRP has introduced into the channel on the rising limb of high-flow releases has been injected at the Diversion Pool. The Diversion Pool site is located immediately downstream from a concrete weir that spans nearly the entire valley floor and constricts flow into a narrow rapid characterized by large standing waves and strong turbulence capable of immediately entraining the injected material. A level surface above flood stage on river right is suitable for stockpiling coarse sediment and operating heavy equipment that can inject gravel directly into the main flow during flood events (Figure 3). Discharge at the Diversion Pool is measured by the USGS gage at Lewiston, located about half a mile upstream (Figure 2).

Figure 3: Aerial photograph of the Diversion Pool gravel injection location. The red triangle indicates the gravel injection point and the white arrow indicates flow direction.

Lowden Ranch

The first gravel injection in the Lowden Ranch area was performed during the 2010 spring flow release, prior to construction of the Lowden Ranch channel rehabilitation project in the fall of 2010. That injection was performed at the downstream end of the project area, about 7.5 miles downstream from Lewiston Dam and immediately upstream from the mouth of Grass Valley Creek (Figure 2; Figure 4). Rehabilitation work upstream from that injection featured terrace lowering and minor channel widening that was explicitly intended to encourage bar deposition in response to planned gravel injections farther upstream (Gaeuman 2014a). The first gravel injection performed for that purpose was implemented during the 2011 spring flow release, when 2050 yd^3 of gravel were pushed into the flow at the upstream end of the site (Figure 4). No further gravel injections were performed at Lowden Ranch until 2015, when 680 yd^3 of gravel were injected at the upstream injection point. About 1600 yd^3 of gravel were injected at the upstream location in 2016, whereas both injection points were utilized to inject a total of 2000 yd^3 in 2017.

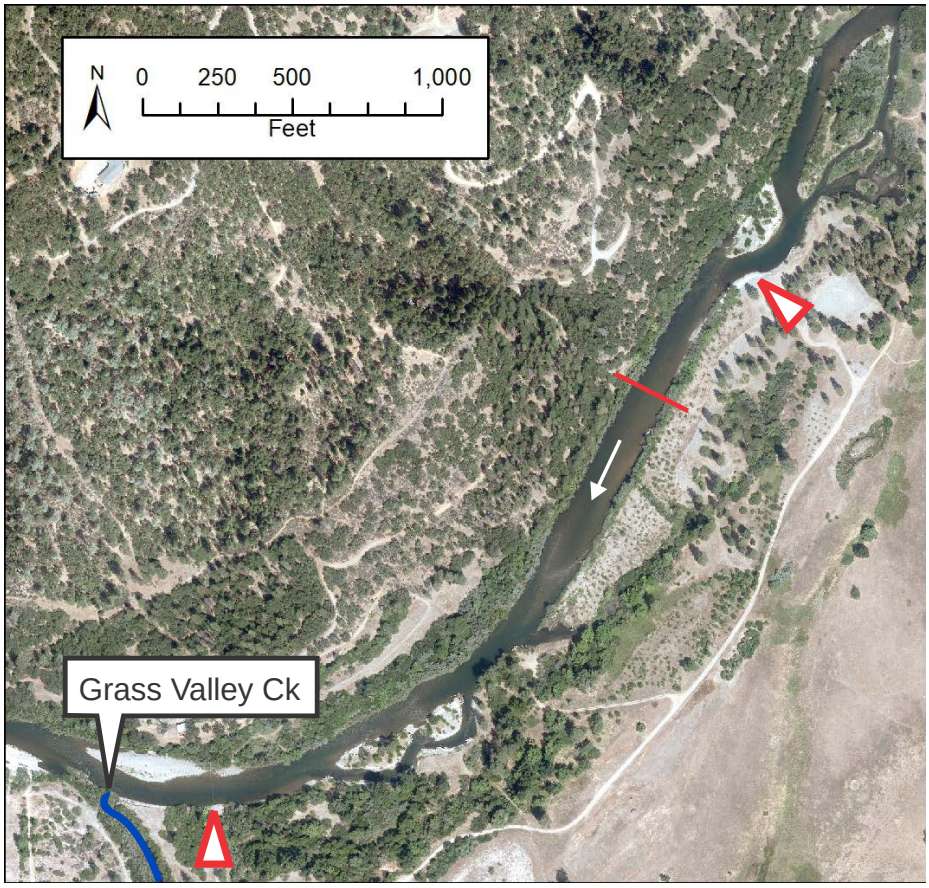

Figure 4: Aerial photograph of the Lowden Ranch gravel injection locations. The red triangles indicate the upstream and downstream gravel injection points, the red line indicates the TRGVC gage and sediment transport sampling transect, and the white arrow indicates flow direction.

Discharge at the Lowden Ranch injection points is measured at the TRGVC gage. In addition to quantifying flows within Lowden Ranch itself, that gage provides a good approximation of gravel-transporting flows downstream from Grass Valley Creek. Although that tributary can contribute peak flows in excess of 1000 ft^3/s during brief winter storm events, those flood events occur almost exclusively during the months of December through March when releases from Lewiston Dam are small. By April and May, when annual floods are released from the dam, typical flows in Grass Valley Creek are in the neighborhood of 50 ft^3/s. Given that flows of 4500 ft^3/s or more are needed to generate significant gravel transport in the Lowden Reach (Gaeuman et al. 2017), inflow from Grass Valley Creek represents a negligible contribution to flows capable of transporting gravel. Indeed, a comparison of the records from TRGVC and the Limekiln Gulch gage, located about 5.5 miles downstream from the Grass Valley Creek confluence, verifies that differences in the durations of competent flows at the two gages are small. Discharges equalling or exceeding 4500 ft^3/s occur 2% of the time in the 10-year TRGVC record of average daily flows and 2.2% of the time in the record from Limekiln Gulch for the same period (Figure 5). Moreover, the maximum daily flow at Limekiln Gulch during that period exceeded the maximum daily

peak at TRGVC by just 6.5%, which is well within the error margin for “good” discharge measurements defined by the USGS (Rantz et al. 1982).

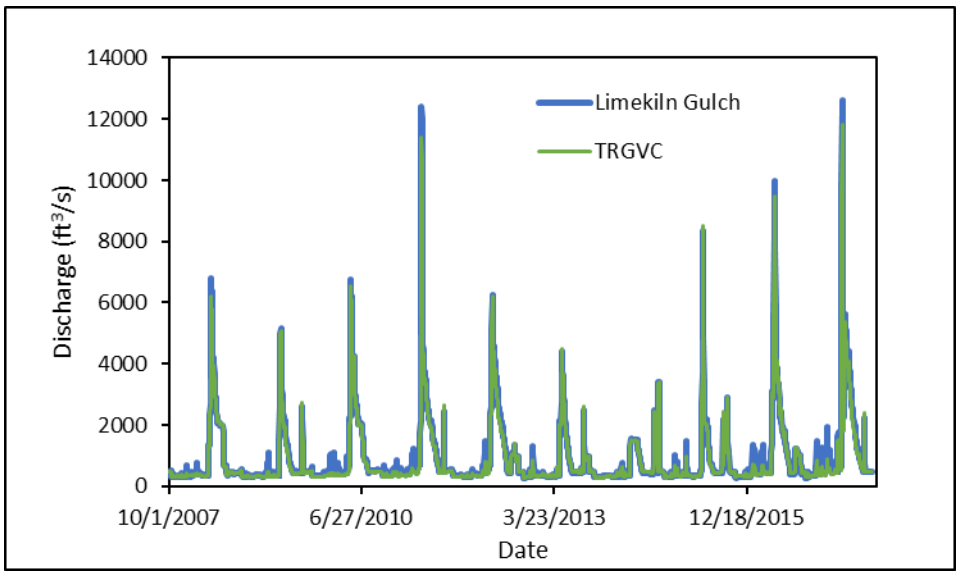

Figure 5: Daily mean discharge over the 10-year period of overlapping records at the USGS Trinity River stream gage below Limekiln Gulch and the TRGVC gage.

The 2016 and 2017 Flow Releases

In the wet water year of 2016, TRRP chose to release a spring flood from Lewiston Dam consisting of two peaks, each of which briefly peaked near 9,500 ft^3/s (Figure 6). Sediment transport monitoring in prior years had shown that bedload transport rates often reach a maximum in the first hours of the annual flood peak, then decrease by as much as 50% by the second or third day of a steady flow peak. The double-peaked hydrograph implemented in 2016 was designed to test the hypothesis that the rise to a second discharge peak might produce a second peak in bedload transport. The 2016 gravel injections took advantage of this experimental hydrograph by splitting the total gravel injection volumes of 2,000 yd^3 at the Diversion Pool and 1,600 yd^3 at Lowden Ranch into four equal batches, where each batch consisted of either 500 yd^3 or 400 yd^3 at the respective sites. At each site, the first batch of gravel was injected early on the rising limb of the first peak, and the second batch was injected about 24 hours later as the peak discharge was attained (Figure 6). The third and fourth batches were deployed in a similar fashion on the second flood peak. In all cases, the gravel was simply dumped into the flow with front-end loaders. This injection schedule was selected to explore potential differences in the mobility of gravel injected on the rising limb of a flood versus the peak of the flood, as well as differences in mobility of gravel injected on the first versus the second peak. This investigation into the effect of injection timing was facilitated by the inclusion of tracer particles in the injection material, as described in a later section of this report.

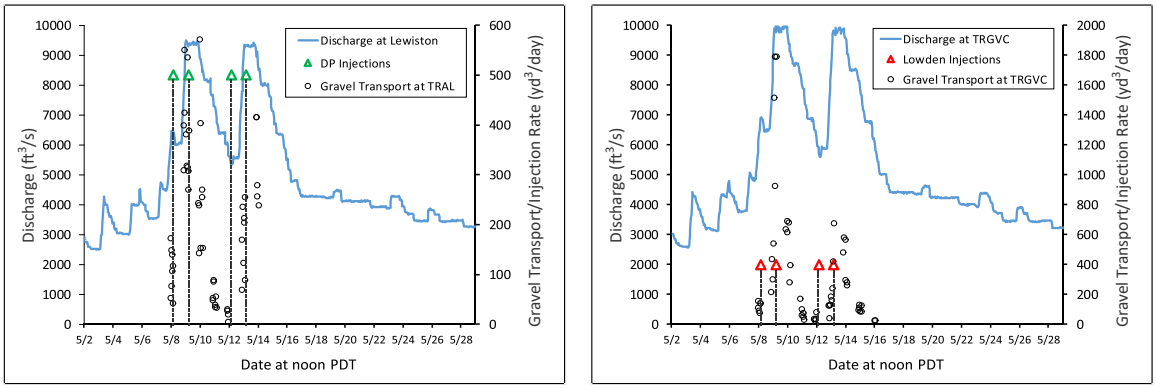

Figure 6: Flow release hydrographs, gravel injection rates, and sampled gravel transport rates during the 2016 spring flow release at the Diversion Pool (left) and Lowden Ranch (right). Transport rates converted to gravel stockpile volume units as described in the text.

Water year 2017 was classified as extremely wet, so TRRP planned to release the maximum spring flood authorized by the ROD of 11,000 ft^3/s. Difficulties in precisely operating the gates at Lewiston Dam, however, caused the actual peak to exceed that target by several hundred ft^3/s over most of its duration, and even to reach an instantaneous peak of 12,000 ft^3/s (Figure 7). After maintaining a relatively steady peak flow for 3 days, flows were rapidly lowered to a level well below the threshold for gravel entrainment. That relatively small discharge was maintained for more than a week before flow was again increased to a moderate flood level slightly larger than the threshold for significant coarse bedload transport. After about five days at that moderate flood level, flows began a gradual decrease that would take three months to reach the summer baseflow of 450 ft^3/s. Although the second peak in the 2017 was competent to generate some gravel transport, it was not designed with a geomorphic objective in mind. Rather, that portion of the 2017 hydrograph was intended to promote riparian development in floodplain areas by maintaining high ground water levels and preventing soil moisture from receding faster than the rate at which the roots of cottonwood and other tree seedlings can grow downward.

At the Diversion Pool, the 2017 release was accompanied by a single gravel injection totaling 1,500 yd^3 on the rising limb of the flood when discharge was increasing from about 6,000 to 7,000 ft^3/s (Figure 7). At Lowden Ranch, however, observations regarding how previous gravel augmentation had altered channel morphology in that reach led to the development of a new injection strategy for that location. It had become apparent that a large proportion of the gravel injected at the upstream end of the Lowden Reach had been deposited in a relatively high gravel ridge extending downstream along the left channel margin. Previous work, including initial results from tracking the 2016 tracer particles, suggested that this outcome was the result of pushing the gravel into the flow near the left bank at relatively high discharge levels when flows can push gravel to high elevations and heavy equipment cannot enter the channel itself. Consequently, in 2017, the decision was made to inject the gravel at the very beginning of the release period when discharge was approximately 1,500 ft^3/s and machinery could enter the water. At the upstream injection point, the injection was accomplished with a front-end loader that would bring loads of gravel from a nearby

stockpile and place it in shallow water near the edge of the channel where it could be reached by an excavator positioned farther into the channel. After picking up gravel delivered by the loader, the excavator would pivot 180 degrees and reach as far out as possible to drop the gravel near the channel thalweg. Although the discharge during this operation was insufficient to generate gravel transport from the streambed itself, it was sufficient to spread the material dumped by the excavator downstream far enough to prevent the pile of injected material from growing above the water surface. About 1,400 yd^3 of gravel was injected at the upstream locations in this manner. About two-thirds of the material was injected on April 18 and the remainder was injected on the following day (Figure 7). Following the injection, releases from Lewiston Dam were gradually reduced to less than 400 ft^2/s by April 21. Flows began to gradually rise again late on April 22, and a steep rise to the flood peak commenced in earnest on April 24.

Another 600 yd^3 of gravel was injected on April 19 at the downstream Lowden injection point, bringing the total for the Lowden reach to 2,000 yd^3. For that injection, end-dump haul trucks were backed up to the edge of the channel and dumped. A loader would then push the pile left by the truck as far out into the river as possible. The loader eventually built a high spit-like point of gravel into the river. Gravel pushed to the tip of the spit was spread a few tens of meters distance downstream during the injection operation, but the bulk of the material remained where it was placed until the rise to the flood peak.

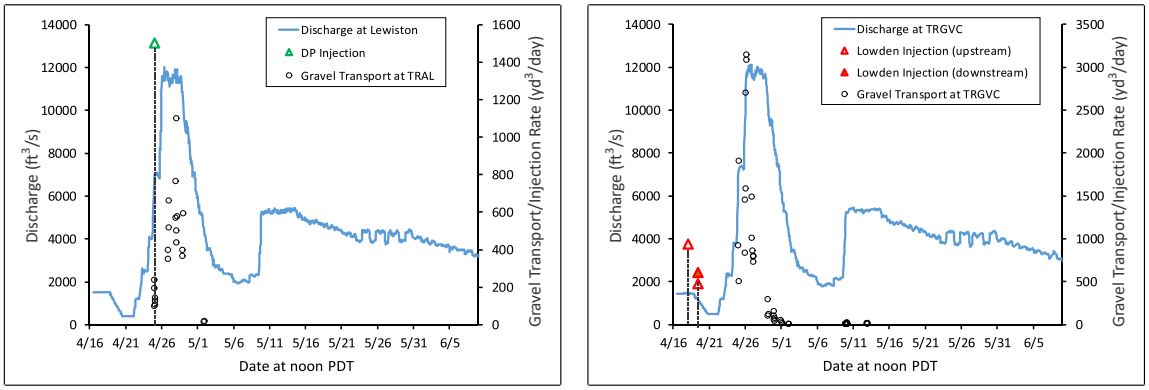

Figure 7: Flow release hydrographs, gravel injection rates, and sampled gravel transport rates during the 2017 spring flow release at the Diversion Pool (left) and Lowden Ranch (right). Transport rates converted to gravel stockpile volume units as described in the text.

The material used for the Lowden Ranch gravel injections came from a stockpile processed at the site during the 2010 Lowden Ranch rehabilitation project, when gravel processing specification called for oversize rock to be removed with a 5-inch screen. This resulted in a particle size distribution similar to that of the bed surface at Lowden Ranch, particularly for size fractions larger than the median (Figure 8). Pebble counts with stockpiled gravel yield median and 90th percentile particle sizes for the injection material of 64 and 120 mm, respectively, whereas pebble counts performed at Lowden Ranch in 2015 indicate that the same percentiles for the bed surface are 55 and 118 mm. The particles size distribution of the

gravel injected at the Diversion Pool differed slightly from year to year, depending on the source of the material. A portion of the material injected in 2016 consisted of leftover material processed at a time when oversize rock was still removed with a 5-inch screen, whereas more recent processing specifications call for a 4-inch screen. The material injected at the Diversion Pool in 2016 was therefore similar in size to the material injected at Lowden Ranch. The gravel injected at the Diversion Pool in 2017, however, was processed later with a 4-inch screen. Consequently, that injection was somewhat finer than the bed surface at Lowden Ranch, especially through the coarsest quartile of its distribution. In all cases, however, size distribution of the bed surface material at Lowden Ranch has a finer tail than the injection gravel. Similar comparisons involving substrate at the Diversion Pool are unavailable because that reach consists of deep pools and a steep rapid where in-channel substrate sampling is impractical.

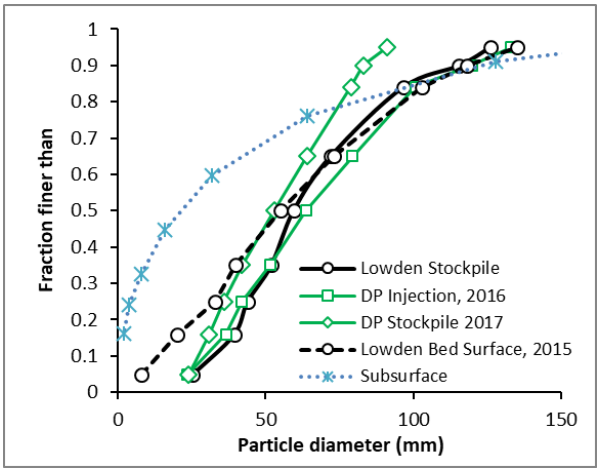

Figure 8: Particle size distributions of injection gravel compared with the bed surface particle size in the in the reach between the Lowden Ranch injection points. Subsurface data as reported by Viparelli et al. (2011).

Methods

Topographic Surveys

The initial conditions dataset used for the analyses presented herein consist of two digital terrain models representing 2015 topography. One of the terrain models begins about 950 ft upstream from the upstream Lowden Ranch gravel injection point and extends about 1,700 ft downstream from that point. The other terrain model spans a reach extending about 2,600 ft downstream from the Diversion Pool gravel injection point. At Lowden Ranch, 2015 topography is based primarily on high-resolution sonar obtained on the falling limb of the 2015 flow release with a Norbit iWBMSc multibeam system mounted on a jet boat. This sonar system features 256 sonar beams sampling at up to 40 Hz, making it possible to obtain several million sonar soundings in a matter of hours. Data were logged using Hypack surveying software to ensure complete areal coverage in real time, and post-processed in Caris HIPS & SIPS to create a grid surface with 1-ft resolution (GMA 2017a). Virtually the entire channel in the vicinity of Lowden Ranch can be accessed with the multibeam, but

small amounts of conventional ground survey data were collected with real time kinematic (RTK) GPS along the channel margins where the presence of vegetation or water depths less than about 1.5 ft prohibited sonar collection.

In contrast to the Lowden Reach, much of the reach downstream from the Diversion Pool consists of a steep rapid containing large boulders and abundant whitewater upstream from the New Lewiston Bridge (Figure 3). Furthermore, the reach downstream from the New Lewiston Bridge contains a large heavily vegetated island and several small channels. Use of the multibeam sonar system is limited due to the presence of boulders, shallow water, strong currents, and aerated water, whereas dense canopy interferes with the use of GPS. The 2015 terrain model in that area is therefore based on a combination of single-beam sonar and conventional ground surveys collected over a period spanning August 2015 through March 2016. Sonar surveys near the Diversion Pool were performed using a Ross Laboratories 875-8 portable hydrographic sonar sweep system. This system accommodates an array of seven sonar transducers spaced 3.28 ft apart. Positioning information is provided by integrated RTK GPS with multiple antennae and a Honeywell HMR 3000 attitude sensor. The channel through much of the reach downstream from the Diversion Pool, however, is too swift and rocky to safely deploy the sonar array, and bubbles in the water column interfere with sonar transmission in many of the deeper areas. Thus, only about 20% of the reach was accessible to the sonar system. The remaining 80% of the reach was surveyed using RTK-GPS or a laser total station, and the combined data were processed to produce an elevation grid with a 3-ft horizontal resolution and a root-mean-square vertical error of 0.19 ft (GMA 2016).

In 2016, TRRP produced a terrain model covering the river and entire valley bottom from Lewiston Dam to the North Fork Trinity River. The vast majority of the bathymetric data that defines the river channel in this terrain model was collected with the same Norbit iWBMSc multibeam sonar system used to map Lowden Ranch in 2015. As before, conventional surveys were used to fill in along the channel margins throughout the survey domain, and the reach immediately downstream from the Diversion Pool was again surveyed using a combination of the sweep sonar system employed in 2015 and conventional methods. In addition, airborne LiDAR covering the terrestrial valley bottom area was acquired using a Leica ALS80 dually mounted with a Phase One IQ180 in a Cessna Caravan aircraft (GMA 2017b). The LiDAR collection produced an average elevation point density over the project area of about one point per ft^2, and the data were processed to generate a bare earth triangulated surface model and exported to a grid surface with 3-ft resolution. Data from these various survey sources were ultimately stitched together to create a single terrain model covering the entire TRRP project area.

Topographic surveys in 2017 spanned 9 miles of the main channel from the Diversion Pool to a point about 2.5 miles downstream from the Lowden Ranch downstream injection point. Main channel bathymetry was again collected with the Norbit iWBMSc multibeam sonar system, except for in the first 0.7 miles downstream from the Diversion Pool where the sweep sonar system and conventional survey methods were employed. The survey in that area also included a floodplain area on the inside of a bend immediately downstream from the Diversion Pool, which was surveyed with a combination of conventional techniques and structure-from-motion (SfM) photogrammetry. Aerial imagery used to develop the SfM point

cloud was collected with a DJI Matrice 600 Pro drone, and image processing was performed with Agisoft Photoscan Pro software (GMA 2018). Elsewhere, the 2017 terrain model incorporates terrestrial data only in the Lowden Ranch area, where conventional surveys were used to supplement portions of the channel margin missed by the multibeam.

For each of the terrains discussed above, the topographic data from the different sources were merged to create contiguous triangular irregular network (TIN) surfaces. Those surfaces were then resampled to create multiple reach-scale elevation grids with 2-ft resolution and a common coordinate origin. Down-sampling from the higher original resolution of the multibeam and LiDAR data helped to reduce file sizes and processing time, whereas gridding to a common origin ensures that elevation points in grids for different years fall in precisely the same locations.

Topographic Change Analysis

The primary objective of gravel augmentation is to improve aquatic habitat by increasing topographic complexity, so the outcome of gravel augmentations is primarily monitored with topographic surveys that document morphologic change and quantify channel complexity. Rates of change can be quantified in terms of volumes of coarse bed material eroded or deposited within a stream reach over time. Volumetric changes in bed material storage are determined by developing morphology-based sediment budgets in which a terrain model representing topography at one point in time is subtracted from a terrain model representing topography at a later time, such that negative changes indicate erosion and positive changes indicate deposition (Ashmore and Church 1998). The bed of the Trinity River in the study area is primarily composed of clast-supported gravel and cobbles (Viparelli et al. 2011), so changes in the bed material volumes determined by topographic differencing is insensitive to the presence of sand because the fine bed material fractions occupy the pore spaces between the larger grains (Gaeuman 2014a). Changes in bed material volumes are therefore taken to be equivalent to changes in the volume of the gravel and cobble fractions.

Gravel budgets are herein developed for stream reaches containing the Diversion Pool and Lowden Ranch gravel injection points. The first of these budget reaches, referred to as the Lewiston bridges reach, extends from the Diversion Pool to the bifurcation of the Cemetery Side Channel 1.4 miles downstream (Figure 9). Two bridges over the Trinity River exist within this reach: the New Lewiston Bridge near the upstream end of the reach and the Old Lewiston Bridge near the downstream end. The Lewiston Bridges gravel budget is terminated at that point because the topographic survey data do not extend into the side channel and surrounding low floodplain areas where undetected deposition may have occurred. A preliminary main channel gravel budget, however, was carried downstream as far at the confluence with Rush Creek (Figure 2) for quality control purposes, as described in Appendix A. The second budget reach begins about 1,500 ft upstream from the upstream Lowden Ranch gravel augmentation point, and extends 1.4 miles downstream through the Lowden Ranch site and another recent rehabilitation project site called Trinity House Gulch. This reach, which is herein denoted as the Lowden/THG budget reach, terminates at the downstream end of a bend in the river containing relatively deep pools known as the SP-Ponderosa Pools (Figure 10).

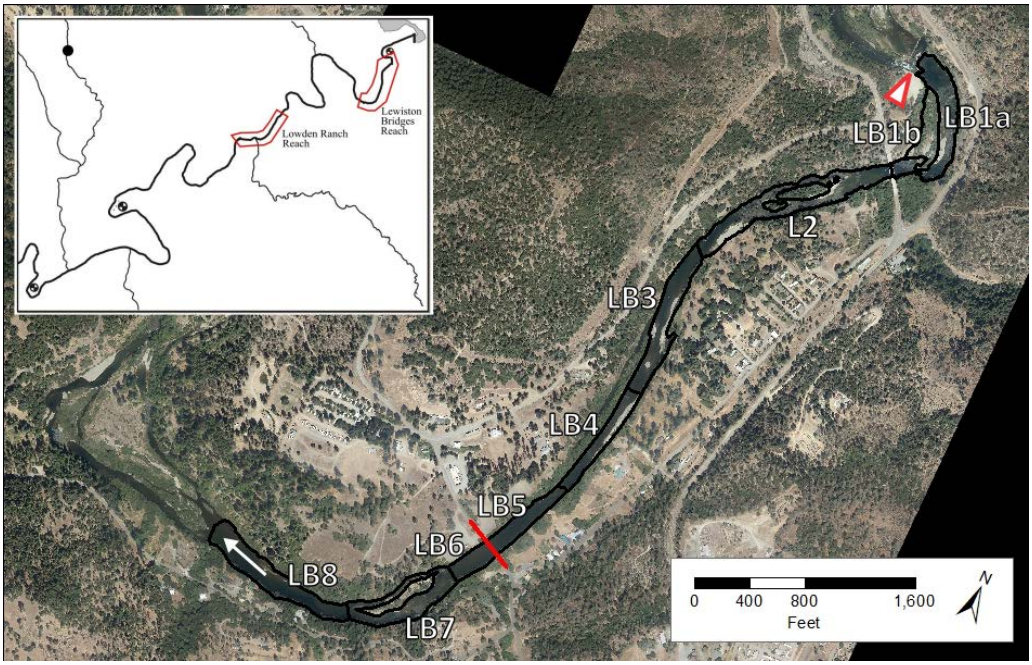

Figure 9: Aerial photo of the Lewiston Bridges gravel budget reach. Labeled gravel budget analysis zones outlined in black. The red triangle indicates the gravel injection point, the red line indicates the TRAL bedload sampling transect, and the white arrow indicates flow direction and points at the Cemetery Side Channel bifurcation.

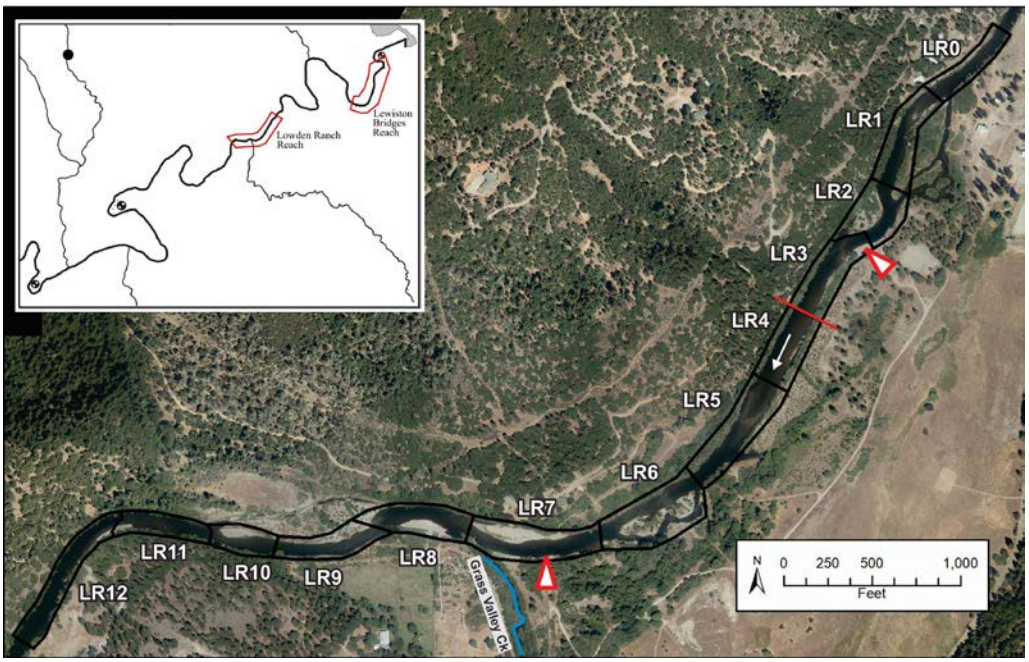

Figure 10: Aerial photo of the Lowden/THG gravel budget reach. Labeled gravel budget analysis zones are outlined in black. Red triangles indicate gravel injection points, the red line indicates the TRGVC gage and bedload sampling transect, and the white arrow indicates flow direction.

Both budget reaches are sub-divided into multiple longitudinal analysis zones in which the local change in gravel storage (ΔV_b) is computed as the difference between the volumes of gravel erosion (E_G) and gravel deposition (D_G) within the zone. Gravel fluxes at the boundaries between zones can then be estimated if the flux at one zonal boundary is known. For zone boundaries downstream from a known boundary flux:

$$F_i = F_{i-1} + \Delta V_b \qquad (1a)$$

where F_i is the gravel flux across the downstream boundary of analysis zone i, and the subscript i increments in the downstream direction. In the case of zone boundaries upstream from a known flux:

$$F_i = F_{i+1} - \Delta V_b \qquad (1b)$$

Rates of geomorphic change can also be quantified in terms of the volumes of bed material eroded and deposited between successive surveys. In their study of geomorphic change on the Chilliwack River, Ham and Church (2000) introduced "channel activity" as the sum of erosion and deposition within a stream reach. Gaeuman et al. (2003) adapted that concept to define a metric of gravel activity:

$$G_i = (D_{Gi} + E_{Gi})/L_i \qquad (2)$$

where L_i is the longitudinal distance through analysis zone i. This measure of geomorphic process rates has the advantage of being robust with respect to relative bias between a pair of topographic surveys. A bias that exaggerates the volume of bed material eroded within an area will necessarily also diminish the volume of bed material deposited in the area by an equal amount, provided the magnitude of the bias is smaller than the magnitude of the actual difference between the average surface elevations. In that case, G_i for a given area is entirely insensitive to survey bias. A disadvantage of this metric, however, is that it represents a minimum gravel activity during a flow event rather than the total activity. Only the final terrain contributes to the erosion and deposition volumes that comprise G_i. Transient topographic features, such as a bar that forms during a flood and subsequently erodes away before the end of the flood, register zero activity. The proportion of the total activity associated with an event captured in G_i depends on the types of topographic changes that occur, as well as their actual magnitudes.

The lateral extents of the analysis zones were determined by a variety of factors, some of which are logistical in nature. In most places, the edges of the analysis areas correspond to the boundary where the gravel streambed transitions to overbank areas composed of finer materials with riparian cover. In areas where that transition is more gradual, it is necessary to replace sonar data collection with ground-based surveying methods or LiDAR data collection. As different surveying methods are associated with different types of potential errors, the uncertainty analyses described in a later section require that some analysis zone boundaries correspond to interfaces between areas where different survey methods were used.

Sediment Monitoring

TRRP monitors sediment transport rates during the annual high-flow releases from Lewiston Dam at four locations along the Trinity River. Bedload transport rates at the monitoring locations are determined with physical samples obtained with a TR-2 bedload sampler. These measurements are used to define quantitative relationships linking water flow and sediment discharge, which are then used to estimate total gravel loads transported past the monitoring locations during the annual flow releases (details on the sampling and analysis methods can be found in annual sediment monitoring reports issued by the contractor, e.g. GMA 2018).

One of the monitoring stations [Trinity River above Grass Valley Creek (TRGVC)] is located 500 ft downstream from the upstream gravel injection point in the Lowden/THG reach (Figure 2; Figure 4). Another [Trinity River at Lewiston (TRAL)] is located at the Old Lewiston Bridge 1 mile downstream from the Diversion Pool injection point (Figure 2; Figure 9). Due to their proximity to gravel injection points, gravel loads estimated from bedload sampling at these locations serve as boundary conditions that make it possible to convert ΔV_b determined from topographic changes to actual gravel flux rates through the budget reaches. These two monitoring stations plus the Trinity River below Limekiln Gulch (TRLG) station farther downstream (Figure 2) also support assessments of how transport rates are changing over time in response to continued upstream augmentations. The fourth monitoring location, Trinity River at Douglas City (TRDC), is located downstream from Indian Creek and is primarily used to set target transport rates in the more upstream reaches where gravel supplies are believed to be limited (Gaeuman 2014b).

In addition to physical sediment samples, gravel transport rates at TRAL have also been monitored using passive acoustic methods since 2016. Sediment generated noise (SGN) is recorded with a pair of hydrophones installed on either side of the river near the sediment monitoring transect (Marineau et al. 2016). Each hydrophone records 1-minute audio samples as 44.1 kHz, 16-bit stereo (2-channel) .wav files at 20-minute intervals over the flow release. The acoustic data collected in 2016 and 2017 were processed and converted to bedload transport rates by researchers at the US Geological Survey's California Water Science Center. Of the four gravel budgets discussed herein, only the 2017 budget for the Lewiston Bridges reach relies on a gravel flux estimated from SGN. Gravel budgets for both years in the Lowden/THG reach rely on fluxes estimated from bedload samples, whereas the 2016 Lewiston Bridges budget includes no flux estimates.

Uncertainty

Three types of error potentially contribute to the uncertainty in bed elevations and sediment volume changes derived from topographic survey data. These are 1) random errors in the elevation data, 2) systematic bias in the elevation data, and 3) uncertainty in the bulk densities of the substrate and augmented gravel. Random errors are considered first.

Gaeuman (2014a) presents an extensive uncertainty analysis suggesting that the total uncertainty in individual elevations due to all sources of random error in the 2015 survey

data is less than 0.3 ft, and errors associated with individual measurements in the later surveys are likely similar or smaller. These survey errors are assumed to be independent and randomly distributed. The expected error over n random, mutually independent elevation measurements is equal to the standard error of the estimate, which is defined by the expected error divided by $n^{0.5}$ (Hamilton 1990), which tends to zero in the limit of $n \rightarrow .\infty$. Uncertainty due to random errors therefore have negligible net effect on the mean bed elevations or volumetric changes estimated over large portions of the study area where the topography is characterized by large numbers of survey points (Grams et al. 2013; Gaeuman 2014a). In the present case, the dataset with the fewest measurement within the analysis area (the 2015 survey) contains on the order of 10^6 individual survey points. This value of n coupled with individual random errors of 0.3 ft corresponds to a standard error of about 0.0003 ft. Values of n for all other years are much larger and so yield smaller standard errors. Random errors therefore usually have a negligible effect on the bed material storage changes and depth statistics computed for this study.

The potential for systematic errors that result in survey bias, however, is extremely important in that the resulting error increases linearly with the spatial extent of the survey. Denoted herein by ε_b, bias is expressed by a non-zero expected error that persists regardless of the magnitude of n. Possible sources of survey bias include various errors associated with equipment dimensions or set-up, such as imperfect measurement of GPS antenna offsets, as well as issues with instrument calibration or parameterization. Because ε_b applies uniformly to the entire survey, it is propagated to total uncertainty in the estimated difference in sediment volumes between two surveys:

$$\delta V_b = A\varepsilon_b \tag{3}$$

where δV_b is the total volumetric uncertainty over an area A (Gaeuman et al. 2017). Bias accumulates in proportion to the area being considered, so even a relatively small value of ε_b can eventually produce large uncertainties when accumulated over a large study area. For example, ε_b = +0.1 ft between a survey conducted at time 1 and another survey conducted at time 2 would produce a volumetric error of +3 yd^3 if the study area covered 90 yd^2. But that same bias would produce a volumetric error of +161 yd^3 if the survey were extended over an acre. Whether uncertainties of these magnitudes are acceptable will depend on the magnitude of the actual changes the surveys are intended to detect. It is therefore a critical factor in any assessment of geomorphic change. Gaeuman (2014a) reported that the potential survey-to-survey bias associated with the sweep sonar system deployed in the reach downstream from the Diversion Pool was empirically estimated at 0.04 ft, whereas tests with the multibeam system used farther downstream suggested a potential bias of less than 0.033 ft (Gaeuman et al. 2017). Analysis of the 2017 multibeam data, however, revealed a systematic bias of between 0.07 and 0.1 ft between the 2016 and 2017 surveys (Appendix A). The source of the relative bias in the 2017 data could not be identified, but one possibility is that, although the same model of multibeam sonar was deployed in 2015 through 2017, the equipment was rented and the actual sonar units supplied by the vendor may have differed. The bias detected in the 2017 data was corrected by adding 0.1 ft to the 2017 elevations, and assigning ε_b a value of 0.05 ft computing the uncertainty margins for volumetric changes involving multibeam and sweep sonar measurements. The estimate for ε_b of 0.05 ft was retained for

elevation changes detected with sonar during the 2016 flow release, but no bias correction was applied.

Volumetric changes computed for the floodplain area on the inside of the bend downstream from the Diversion Pool are subject to uncertainties similar to those estimated for the sonar data. The presence of dune-like lobes of fresh gravel on that surface show that it is subject to gravel deposition and erosion even though it also supports patches of dense vegetation. In 2015, the area was surveyed using conventional ground-based methods, whereas in 2016 it was surveyed with airborne LiDAR. Ground surveys were used again in 2017, but those data were supplemented with SfM data collected where open ground can be seen from above the vegetation canopy. These methods differ substantially in the measurement density that can be achieved, as well as in their capacities to penetrate vegetation. SfM techniques can achieve very high point densities, but cannot penetrate vegetation. Conventional surveys can penetrate vegetation, but point densities may be too low to accurately represent the terrain. LiDAR can penetrate vegetation to a point, but the potential for false returns increases with the density of the vegetation. The likely magnitude of bias that could arise from these differences was evaluated by comparing the 2016 LiDAR data with a previous LiDAR flight conducted in 2012. The 2012 LiDAR surface was subtracted from the 2016 LiDAR surface in vegetated terrestrial areas near the Diversion Pool where no real change is believed to have occurred. The surface of difference nonetheless showed a mean difference of −0.085 ft with a standard deviation of 0.53 ft. Inspection of the differenced surface revealed that areas with large negative errors coincide with locations where brush or other thick vegetation is visible on the digital imagery collected during the LiDAR flights. Together, these results show that the 2016 LiDAR penetrated vegetation much more effectively than did the 2012 LiDAR. Because the bare-earth model derived from the 2016 LiDAR lacks topographic features that appear to correspond to vegetation visible on the imagery, it is assumed that its mean difference from the 2012 LiDAR represents its maximum likely bias relative to the ground surveys. Elevation changes in terrestrial areas near the Diversion Pool were therefore assigned an uncertainty of 0.085 ft for both flow releases.

Errors in gravel budgets derived from topographic differencing can also arise from differences between the bulk densities of the gravel substrate versus stockpiled gravel used for gravel injections and in the conversion factor used to convert gravel loads determined from physical sediment sampling to substrate volume equivalents. Gaeuman (2014a) measured the bulk density of stockpiled gravel at 1.45 tons per yd^3 and used published data to estimate the typical density of the gravel component of gravel-bed river substrate of to be 1.61 tons per yd^3. These values are used below to convert stockpiled material and sampled gravel bedload to volumetric units that are comparable to the results of topographic differencing. All such conversions are assigned uncertainty margins of ± 10%. As these types of errors are independent of survey errors, they can be combined as the root sum of squared errors (Ham and Church 2000; Lane et al. 2003; Gaeuman et al. 2003).

The potential for error in the bedload flux computed from physical samples at TRGVC and TRAL represents another source of uncertainty in the gravel budgets developed for the Lewiston Bridges and Lowden/THG reaches. Sediment sampling and load computations are subject to numerous types of errors, including failure to properly account for temporal

variations in transport rates when interpolating between samples with rating curves that relate transport rates to water discharge, as well as to logistical difficulties that limit the accuracy of the physical samples themselves. Gaeuman (2014a) estimated the uncertainty associated with interpolation methods by comparing loads computed with rating curves developed from 2011 data using different interpolation methods, and suggested that the 28% difference in the estimates could be considered the uncertainty margin related to that potential source of error. Where two independent rating curve estimates are involved, however, a 28% uncertainty in their difference is equivalent to the root sum of squared uncertainties of 20% in each estimate. The availability of total bedload fluxes computed from passive acoustics at TRAL offers a means for evaluating this result. The total flux estimated from calibrated SGN for the 2016 flow release is 2445 tons, whereas the flux estimated from rating curves based on discharge is 2140 tons. For the 2017 flow release, the calibrated SGN yields a coarse bedload (> 8 mm) flux of 3646 tons and the corresponding estimate from discharge-based rating curves is 4330 tons. Because SGN provides a continuous record of sediment transport intensity and is more closely correlated with measured transport rates than is discharge (Marineau et al. 2016), the SGN-derived loads are almost certainly more accurate than the loads computed from the discharge-based rating curves. Assuming the SGN-derived loads are the superior estimates, their respective 12% and 19% differences from the rating curve values can be taken as typical margins of error for individual rating curve estimates. The larger error in the 2017 rating curve estimates is likely due to the fact that just 21 bedload samples were collected at TRAL in 2017, compared to 64 bedload samples collected in 2016. This reduction in sampling effort reflects TRRP's decision to rely on the acoustic monitoring to quantify bedload transport at TRAL in 2017 and use the physical samples primarily for calibration purposes. These considerations suggest the adoption of an uncertainty margin related to rating curve interpolation of no more than 20%.

Gaeuman (2014a) also assessed the uncertainty due to sampling error with an analysis of multiple pairs of consecutive coarse bedload samples collected during the 2011 flow release at near constant discharge. Those paired samples differed by an average factor of 2.17, suggesting an average error due to sampling variability of near 40% if it is assumed that the actual transport rate lies between the paired sample rates. That rather crude error assessment, which neglected any consideration of the number of bedload samples collected in each sampling campaign, is replaced herein with a new analysis of the error inherent in sampled bedload transport rates based on tests of sample variability performed during the 2016 and 2017 spring flow releases. That analysis, which is presented in Appendix B, yields a much smaller uncertainty margin associated with sampling error of 11%. As sampling errors and data interpolation errors are independent, it would be technically acceptable to combine them as the root sum of squared errors to yield a total uncertainty margin of 23%. However, because the uncertainty estimate derived in Appendix B is so much smaller than the prior estimate, it is perhaps prudent to be more conservative. The total uncertainty in bedload flux estimates used herein is therefore assumed equal to the sum of the component uncertainties, that is, 31%.

PIT-tagged Tracer Stones

Previous monitoring (Gaeuman 2011; Gaeuman 2014a; Gaeuman 2014b, Gaeuman et al. 2017) has shown that gravel injected or otherwise added to the Trinity River travels relatively short distances in a typical flow release, and so may take many years to arrive at downstream sites where gravel supplies are currently low. In 2016, TRRP undertook a multi-year study designed to demonstrate the travel characteristics of augmented gravel by seeding the 2016 gravel injections at Lowden Ranch with tracer stones containing passive integrated transponder (PIT) tags. PIT tags, which are frequently applied in river science to track the movements of fish, transmit a unique ID when stimulated with a magnetic field generated by an alternating current passing through an antenna consisting of one or more close loops of wire in a non-conductive housing. The electrical current flowing through the antenna produces a magnetic field that induces a current in any near-by PIT tags, causing them to transmit a radio frequency signal that is received by the antenna. Because they have no internal power source, they can be used to track individual stones over many years. Their use for tracking gravel particles in streams has become increasingly common in recent years (Bradley and Tucker 2012; Liébault et al. 2012; Gaeuman 2013; Phillips et al. 2013; Phillips and Jerolmack 2014; Olinde and Johnson 2015; Arnaud et al. 2015; Bradley 2017).

A total of 2,000 PIT-tagged tracers was prepared by embedding in stones collected from gravel injection stockpiles along the Trinity River. Stones of two sizes were selected: smaller stones with a shortest diameter (c-axis) measuring between 28 and 37 mm and a maximum diameter (a-axis) of no more than 80 mm, and larger stones with c-axes between 37 and 42 mm and a maximum diameter of no more than 100 mm. Holes parallel to the c-axes and 6 mm in diameter were drilled in the stones with a hole-core diamond bit. PIT tags measuring 32 or 23 mm in length were inserted into the holes in the larger and smaller stones, respectively, and the holes were then sealed with epoxy glue.

To assess how the timing of gravel injections affected subsequent transport, 250 PIT-tagged tracers were fed evenly into the injection gravel with each of the four batches of gravel injected at Lowden Ranch and the Diversion Pool in 2016 (Figure 6). The tracers had been sorted into bags according to their unique identification numbers prior to the release, making it relatively easy to record the timing of when individual tracers were introduced into the river. In all, 1,000 tracers were introduced at each site.

The tracers were subsequently relocated in late fall of 2016 after releases from Lewiston Dam reached low winter baseflow levels and again in the fall of 2017 using a radio-frequency backpack reader manufactured by Oregon RFID. The reader was connected via a twinax cable to one of two different antennae, depending on search conditions. A pole antenna purchased from Oregon RFID was used when searching in vegetated areas or other areas where obsticals limit mobility. The field-generating loop on that antenna is about 1.6 ft in diameter and, according to product specifications, can detect 32-mm tags at ranges exceeding 3 ft. The detection range for 23-mm tags is expected to be about 25% shorter, in proportion to their size. A larger custom-made antenna with a loop 3.3 ft wide and 6.6 ft long was constructed and used in 2017 for searching in more open areas, such as in the wetted channel and on open gravel bars. Its design, featuring a structural frame composed of wood and water-proof glue, allows it to be deployed in various ways depending on local conditions.

Long articulating handles make the antenna relatively easy for two people to carry in open terrestrial setting or to push below the water surface when deployed from a boat in deep water. In shallow water, a typical deployment is to remove one handle and float the wooden loop on the water surface. Tests showed that, when connected to this larger antenna, the backpack reader could detect 32-mm tags at distances of up to 5 ft.

Both the search strategy and geo-location of PIT tag detections rely on GPS. Hand-held GPS units were used to record trackline positions at 1 s intervals that helped the search crews maintain orderly search patterns in the field. An internal clock in the backpack reader was synchronized with GPS time at the beginning of each search day so that the time stamps on individual PIT-tag detections logged in the reader could be subsequently matched to the GPS positions. The detection range coupled with the antenna size, the imprecision if the hand-held GPS units used, and other logistical difficulties means that the tag positions are not determined precisely. In most case, the coordinates assigned to the tags located with the large antenna are believed to be accurate to within about 16 ft and about half that for tags located with the smaller pole antenna. Given that the phenomenon being investigated potentially spans longitudinal extents on the order of 10^3 ft, that level of uncertainty in the tag positions is of little consequence.

Results of Reach-Scale Monitoring

Gravel Budgets in the Lewiston Bridges Reach

Terrain models covering the Lewiston Bridges reach were developed for 2016 and 2017 using a combination of multibeam sonar, a multi-transducer sonar sweep system, airborne LiDAR, and conventional grounds surveys. These terrain models support analyses to estimate gravel storage changes and gravel fluxes during the 2017 spring flow release between the Diversion Pool gravel injection site and the bifurcation point for the Cemetery side channel 1.4 miles downstream (Figure 9). In 2015, however, topographic surveys covered only the first half mile downstream from the Diversion Pool, so gravel dynamics during the 2016 flow release can be assessed only in zones LB1a, LB1b, and LB2 (Figure 11). As this limited spatial domain does not encompass the TRAL sediment monitoring transect, the 2016 budget lacks gravel flux estimates at the analysis zone boundaries. The topographic data collected before and after the 2017 flow release, however, span the entire reach. The gravel budget for that year therefore includes estimated gravel fluxes at all zone boundaries.

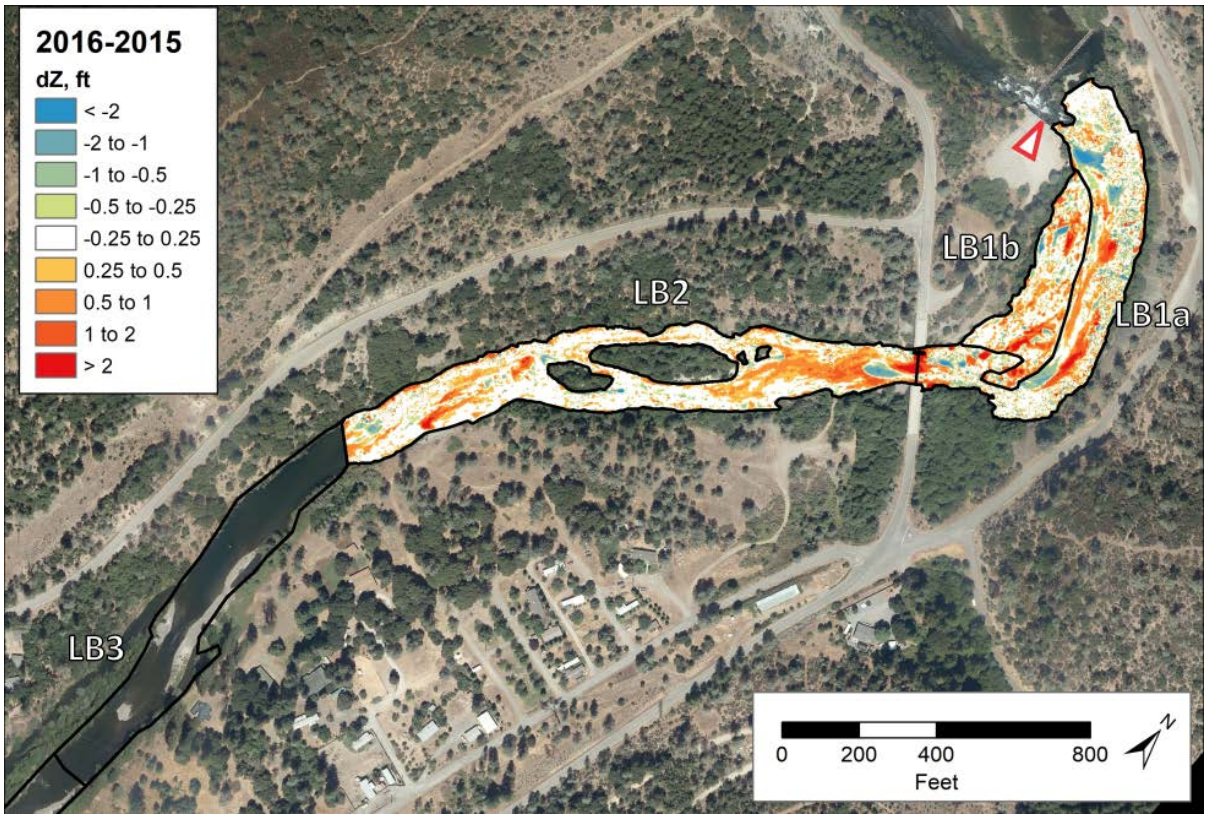

Figure 11: Bed elevation changes during the 2016 spring flow release at the upstream end of the Lewiston Bridges reach. *dZ* = change in bed elevation. The red triangle indicates the Diversion Pool gravel injection point.

The 2016 Flow Release

Topographic differencing revealed widespread deposition during the 2016 spring flow release, whereas just a few scattered patches of erosion were detected (Figure 11). Deposition was particularly common in LB1b, in the central portion of LB1a, and in the upstream third of LB2 between the New Lewiston Bridge and a large mid-channel island. This distribution of deposition suggests that most of the gravel injected at the Diversion Pool in 2016 and perhaps in prior years deposited within about 1,500 ft of the injection point. There is, however, another region of concentrated deposition farther downstream halfway between the islands and boundary with zone LB3. A patch of deep red near the left bank in that area corresponds to the downstream face of a large lobe of gravel that prograded about 30 ft downstream during the 2016 release. Patches of erosion are most prominent near the upstream end of LB1a immediately downstream from the injection point.

The 2016 gravel budget for the region of topographic differencing confirms the dominance of deposition, with an estimated increase in gravel storage in those three analysis zones of 2509 yd^3 (Table 3). This storage increase is about 39% larger than the volume of gravel augmented at the Diversion Pool in 2016 when converted to substrate bulk density), suggesting that as much as 708 yd^3 of gravel moved into the study reach from upstream. This volume of input seems unlikely, given the proximity of the study area to Lewiston Dam and a general lack of upstream gravel sources. The uncertainty margins for the volume change estimate, however, are larger than the implied influx from upstream and indicate that the actual storage change could be anywhere between 0.88 and 1.9 times the 2016 augmentation volume. Indeed, subtracting an assumed relative bias of 0.04 ft between the 2015 and 2016 terrain models from the vertical changes in all analysis zones listed in Table 3 yields an approximate balance between the 2016 augmentation volume and the total storage increase. As that magnitude of potential bias is well within the uncertainty bounds assigned to the topographic changes in those budget analysis zones, it is tentatively concluded that gravel deliveries to the upstream boundary of LB1a in 2016 were near zero.

Table 3: 2016 gravel budget for the upstream end of the Lewiston Bridges reach. dZ = mean change in bed elevation, ΔV_b = change in gravel storage volume, G_a (yd^3) = augmentation volume, δV_b = uncertainty in gravel volume, δV_T = total uncertainty in storage change volume. All volumes given in substrate equivalent bulk density. Flux inside the box was estimated from field measurements.

Zone	dZ (ft)	ΔV_b (yd^3)	G_a (yd^3)	δV_b (yd^3)	δV_T (yd^3)
Gravel augmentation input			1801	± 180	
LB1a	0.051	291		± 285	
LB1b	0.254	662		± 222	
LB2	0.199	1556		± 391	
Total		2509			± 915

Gravel fluxes at the boundaries of budget analysis zones cannot be computed for the 2016 release in the Lewiston Bridges reach because the bedload sampling transect needed to define a boundary condition lies outside of the 2016 budget area.

The 2017 Flow Release

The effects of the 2017 flow release immediately downstream from the Diversion Pool gravel augmentation differed markedly from those observed in 2016 in that erosion dominated in analysis zone LB1a (Figure 12). In particular, a patch of scour in excess of 2 ft covers more than 4,300 ft^2 near the right bank at the upstream end of that analysis zone. Change in much of the zone was less than 0.25 ft, and deposition is limited to a scattering of small patches. The dominance of erosion apparent in the figure is reflected in the 2017 gravel budget for the Lewiston Bridges reach (Table 4), which shows the value of $\Delta V_b = -861\ yd^3$ computed for zone LB1a to be the largest negative value for any zone in the reach. The pattern of 2017 change in zone LB1b also differs from 2016 in that 2017 deposition is concentrated in the downstream half of the zone, whereas in 2016 patches of deposition were distributed throughout LB1b. Overall, the magnitude of deposition in LB1b in 2017 is considerably smaller than it was in 2016 – a comparison between Table 3 and Table 4 shows the value of ΔV_b computed for zone LB1b in 2017 to be just 40% of the value computed for 2016. The results indicate that the 2017 flow release was considerably more effective at transporting the injected gravel away from the injection point than was the previous release.

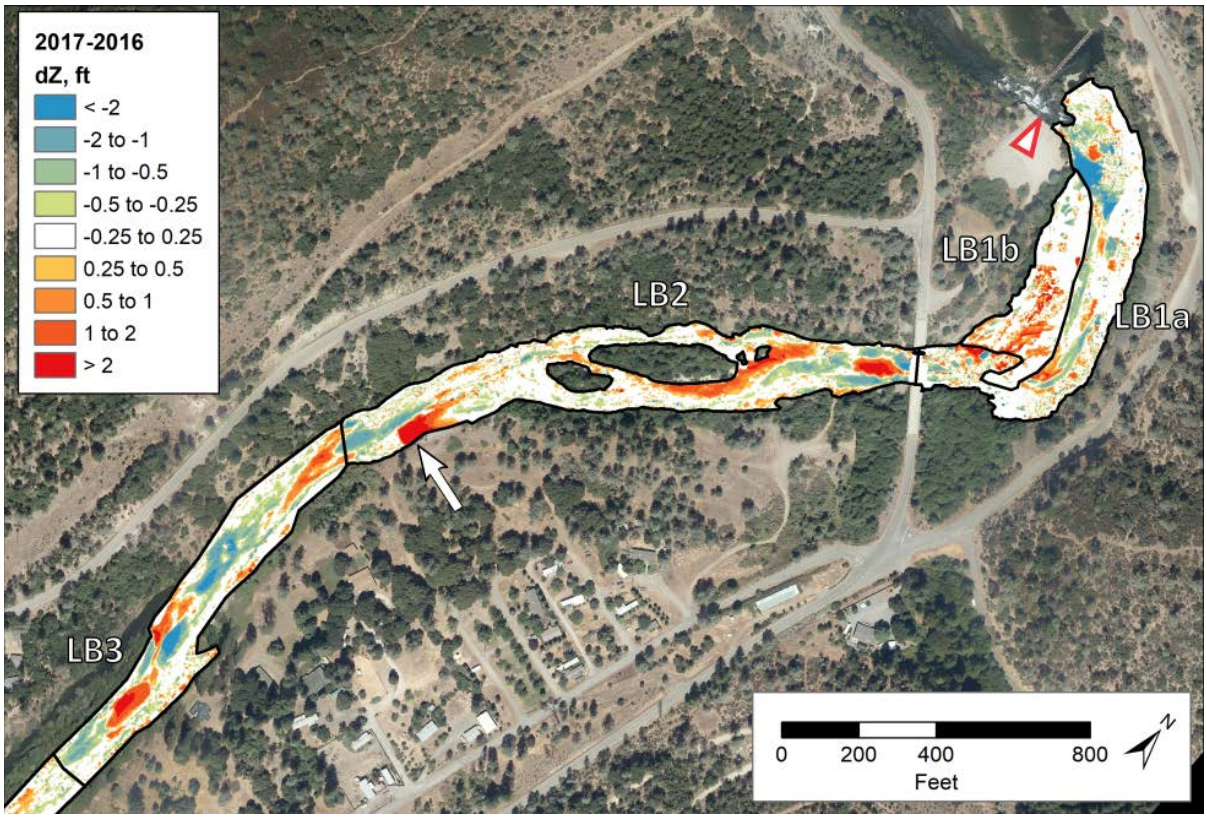

Figure 12: Bed elevation changes during the 2017 spring flow release in the upstream half of the Lewiston Bridges reach. *dZ* = change in bed elevation. The white arrow indicates the position of the prograding gravel lobe described in the text. The red triangle indicates the Diversion Pool gravel injection point.

The 2017 bed level changes observed in zone LB2 are broadly similar to those seen in 2016 in that relatively large areas of deposition exists along the upstream edge of the large island in zone LB2. However, the 2017 results for LB2 also include large regions of erosion in that area, as well as at the downstream boundary of the zone. Consequently, ΔV_b computed for zone LB2 in 2017 is just 45% of the 2016 value. Another difference between the 2016 and 2017 is in the magnitude of deposition along the left bank near the downstream end of LB2. The summary of 2016 changes above noted the presence of a large gravel lobe in that area that had prograded a short distance downstream during the 2016 release. In 2017, the rate at which the gravel lobe advanced quadrupled such that its leading edge moved about 140 ft downstream and doubled in width (Figure 12; Figure 13). Thus, not only were erosion volumes in LB2 larger in 2017 than in 2016, but a larger proportion of the 2017 deposition in LB2 was close to the zone's downstream boundary.

Figure 13: Leading edge of the prograding gravel lobe on the left bank near the downstream end of LB2. 2017 photo.

The increased effectiveness of the 2017 flow release for transporting augmented gravel downstream compared to the 2016 release is strikingly evident when the storage changes in zones LB1a, LB1b, and LB2 are considered together. The total 2017 storage increase across those three zones is just 119 yd^3, whereas the total for 2016 is 21 times larger at 2509 yd^3. Moreover, the combined 2017 gravel storage increase in those zones is less than one-twelfth of the substrate equivalent volume of 1351 yd^3 injected at the Diversion pool that year. Given that the stated purpose of TRRP gravel augmentations is to promote bed mobility and the fluvial processes that drive morphologic change, the considerably greater mobility of the augmentation material injected at the Diversion Pool in 2017 suggests that the 2017 material meets Program objectives better than the coarser material injected in 2016. This appears to

validate recommendations made in 2015 to change the maximum screen size called for in the Program's gravel processing specifications from 5 inches to 4 inches.

The distribution of erosion and deposition in zone LB3 is suggestive of bedform migration through the area (Figure 12). The patch of deposition at the upstream boundary of that zone is in the form of a linguoid bar, whereas the patch of erosion at the downstream end of zone LB2 likely represents the bar's location prior to the flow release. Another set of matching patches of erosion and deposition are located in the downstream half of LB3, where an approximately oval-shaped red patch indicating deposition lies slightly downstream from a patch of blue of a similar shape and size. Overall, erosion dominates over deposition in this zone, as quantified by a net decrease in storage by 678 yd^3. This imbalance in erosion and deposition partially masks the imprint of bedform migration through the area.

Table 4: 2017 gravel budget for a portion of the Lewiston Bridges reach downstream from the Diversion Pool. Variables are: dZ = mean change in bed elevation, ΔV_b = change in gravel storage volume, G_a (yd^3) = augmentation volume, δV_b = uncertainty in gravel volume, F_i = gravel flux at downstream boundary of zone i, δF = cumulative uncertainty in gravel flux. All volumes given in substrate-equivalent bulk density. Flux inside the box was estimated from field measurements.

Zone	dZ (ft)	ΔV_b (yd^3)	G_a (yd^3)	δV_b (yd^3)	F_i (yd^3)	δF (yd^3)
Flux from upstream					548	± 1428
Gravel augmentation input			1351	± 135		
LB1a	−0.158	−861		± 273	2760	± 1166
LB1b	0.202	266		± 221	2235	± 967
LB2	0.093	714		± 382	1521	± 654
LB3	−0.143	−678		± 237	2199	± 510
LB4	−0.163	−405		± 124	2604	± 466
LB5	−0.153	−339		± 466	2265	± 453
LB6	−0.352	−559		± 79	2824	± 504
LB7	0.134	492		± 184	2332	± 598
LB8	0.034	206		± 302	2125	± 821

The next three zones farther downstream appear to have functioned primarily as transport pipelines during the 2017 release. Deposition is almost entirely absent from both LB4 and LB5, and they contain only two coherent patches of erosion – one at the downstream end of LB4 and one near the center of LB5 (Figure 14). Deposition is also entirely lacking in zone LB6, although it does contain a sizable area of scour deeper than 1 ft. Although static bed elevations alone do not imply efficient bedload throughput, a static bed combined with a measured boundary flux does. In this case, the gravel flux at the downstream boundary of LB5 was monitored during the flow release through a combination of bedload transport sampling and passive acoustic techniques. The flux estimated by these methods is highlighted with a boxed cell in Table 4. That flux is an internal boundary condition that is then propagated upstream and downstream to all other zone boundaries in the reach. As can be seen in the table, the uncertainty associated with the propagated fluxes increases with distance from the known boundary condition. As LB5 contains the known boundary and LB4 is just one zone away, it can be stated with high confidence that the gravel transport fluxes

through this part of the study reach in 2017 were in the neighborhood of 2,200-2,600 yd^3 with uncertainty margins of ±500 yd^3 or less. Propagation of the known boundary flux analysis zone LB1a results in an estimated gravel delivery from upstream of the Diversion Pool of 548 ± 1428 yd^3. Due to the large magnitude of the uncertainty at that location, no definitive conclusion can be drawn regarding whether the 0.9 miles of river upstream delivered significant quantities of gravel to the Lewiston Bridges reach. Given that the general lack of gravel sources between LB1a and Lewiston Dam, a large positive error in the estimated flux to LB1 seems unlikely. It is therefore assumed that the actual gravel flux to the Lewiston Bridges reach in 2017 was similar to or perhaps much less than the figure of 548 yd^3 given in Table 4. The tentative conclusion stated earlier that gravel deliveries to LB1a were negligible in 2016, when the peak of the release hydrograph was 20% lower than the 2017 peak, seems appropriate.

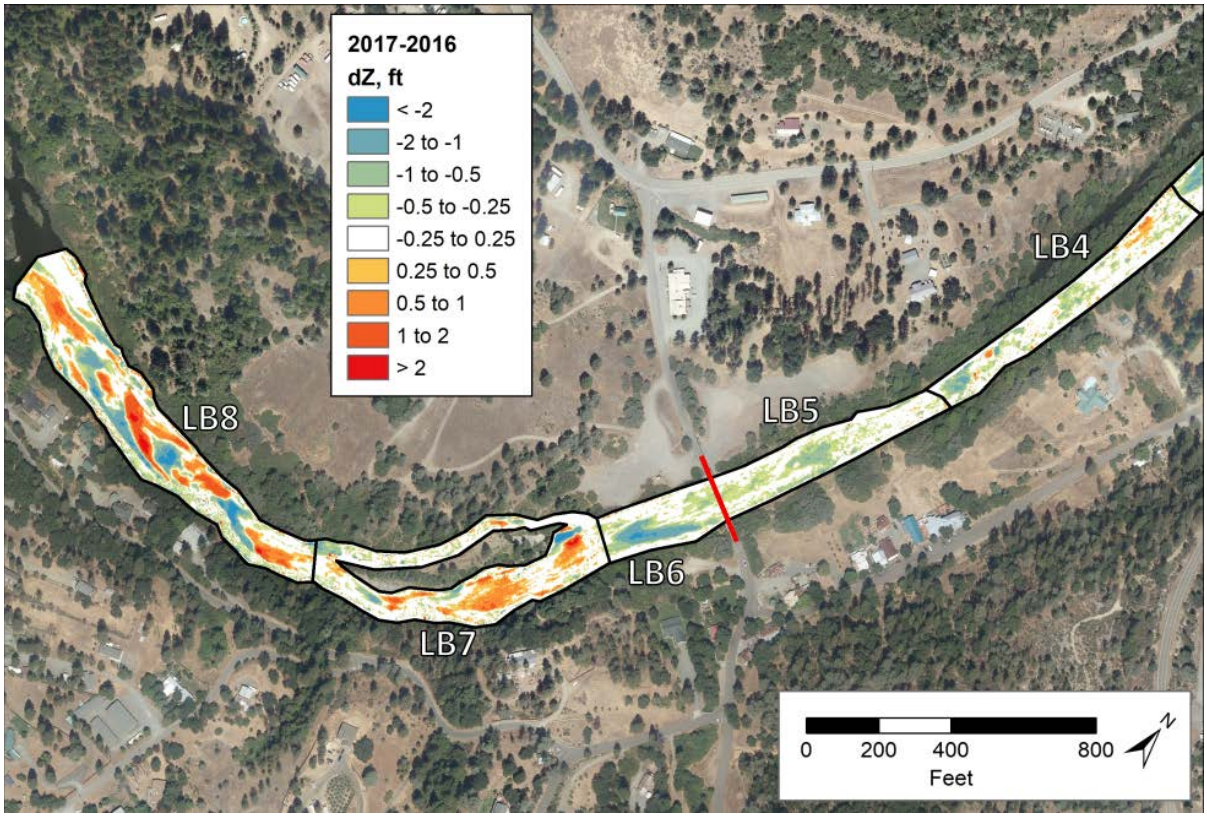

Figure 14: Bed elevation changes during the 2017 spring flow release in the downstream half of the Lewiston Bridges reach. *dZ* = change in bed elevation. The red line indicates the TRAL bedload sampling transect.

A portion of the material transported through LB zones 4-6 in 2017 appears to have deposited in LB7. The deposition is concentrated in two patches, one near the upstream boundary of the zone and the other near the zone's center. The area occupied by the more downstream of the two red patches has maintained a channel-spanning bar and riffle morphology since 1980 or before.

As in LB3, the distribution of 2017 erosion and deposition in zone LB8 shows the imprint of bedform migration, but here the pattern is better developed. Patches of red alternate with patches of blue throughout the zone, including an especially clear chevron shaped red patch that clearly outlines a linuoid bar in the zone's center.

Gravel Budgets in the Lowden/THG Reach

Gravel budgets for the Lowden/THG reach encompass the TRGVC bedload sampling transect in both years, so both budgets include estimated gravel fluxes at budget zone boundaries in addition to gravel storage changes. Due to the availability of topographic data, the 2016 gravel budget is restricted to the upstream third of the Lowden/THG reach, whereas the 2017 budget spans the entire reach.

The 2016 Flow Release

The 2015 topographic surveys in the Lowden Ranch area were restricted to analysis zones LR1, LR2, LR3, LR4, and LR5. Assessment of gravel dynamics during the 2016 flow release is therefore possible only in that portion of the Lowden/THG reach (Figure 15).

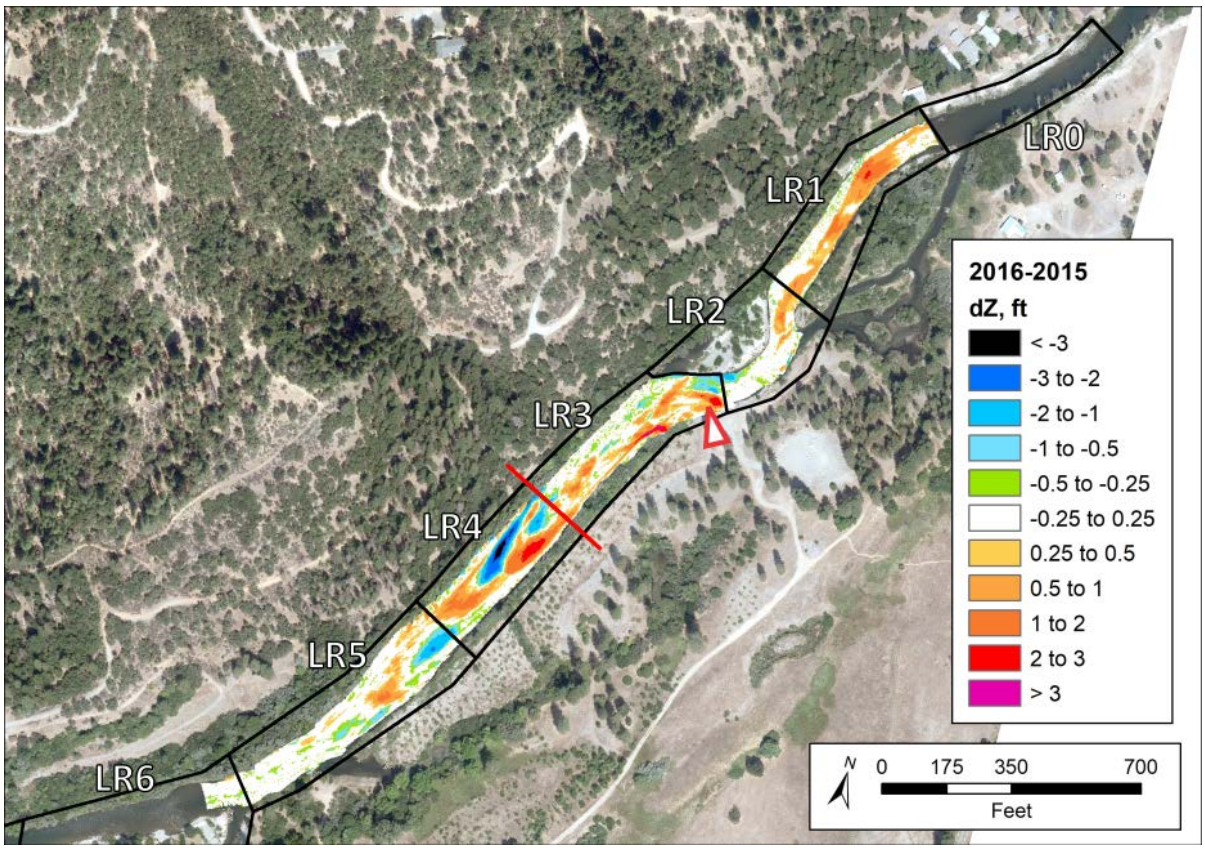

Figure 15: Bed elevation changes during the 2016 spring flow release at the upstream end of the Lowden/THG reach. *dZ* = change in bed elevation. The red line indicates the TRGVC bedload sampling transect

The upstream end of the Lowden/THG reach aggraded during the 2016 flow release, as shown qualitatively by the large region of red that spans zone LR1 and extends about a third of the way through zone LR2 in Figure 15. According to the 2016 gravel budget (Table 5), about 726 ± 117 yd^3 of gravel accumulated in zone LR1 and the upstream end of zone LR2 that year. Boundary fluxes propagated upstream from the measurement boundary at the downstream end of LR3 (the boxed cell in Table 5) indicate that 1685 ± 715 yd^3 entered LR1, so about 43% of the incoming flux was captured in the region of deposition spanning those two zones.

Zone LR3 also saw a net increase in gravel storage, but the magnitude of the increase was small relative to the volume of material supplied to the zone. Between the gravel augmentation at the upstream end of the zone and the flux entering from upstream, LR3 received a total input of about 2,400 ± 772 yd^3 of gravel during the 2016 flow release, whereas the net storage increase was just 20% of that figure. Storage changes in zone LR4 were even smaller relative to the fluxes in and out of that zone, with a net increase equivalent to less than 4% of the boundary fluxes. LR4 nonetheless displays large alternating patches of thick deposition and deep scour that track the propagation of a pair of dune-like bedforms that migrated approximately one channel width downstream during the 2016 flow release (Figure 15). Migration of those bedforms over the course of the 2016 flow release is perhaps more clearly illustrated in Figure 16, which displays bed elevations before and after the release rather than elevation changes.

Table 5: 2016 gravel budget for a portion of the Lowden/THG reach. Variables are: dZ = mean change in bed elevation, ΔV_b = change in gravel storage volume, G_a (yd^3) = augmentation volume, δV_b = uncertainty in gravel volume, F_i = gravel flux at downstream boundary of zone i, δF = cumulative uncertainty in gravel flux. All volumes given in substrate equivalent bulk density. Flux inside the box was estimated from field measurements.

Zone	dZ (ft)	ΔV_b (yd^3)	G_a (yd^3)	δV_b (yd^3)	F_i (yd^3)	δF (yd^3)
Flux from upstream					1685	± 715
LR1	0.417	692		± 83	993	± 641
LR2	0.033	34		± 52	959	± 628
Gravel augmentation input			1441	± 144		
LR3	0.189	468		± 190	1932	± 599
LR4	0.035	73		± 105	1859	± 608
LR5	−0.049	−144		± 147	2003	± 650

The primary morphologic changes in LR5 consist of a patch of scour 1 to 2 ft deep at the upstream boundary of the zone and some nearby diffuse patches of deposition that suggest the nascent development of a third bedform similar to those in LR4. The downstream half of LR5 is almost devoid of bed elevation changes. The total ΔV_b for the zone as a whole is slightly negative, with an estimated storage decrease that is approximately equal to its uncertainty margin. At 2,003 yd^3, the estimated volume of gravel exiting LR5 is equivalent to 84% of the total gravel supply immediately downstream from the gravel augmentation point.

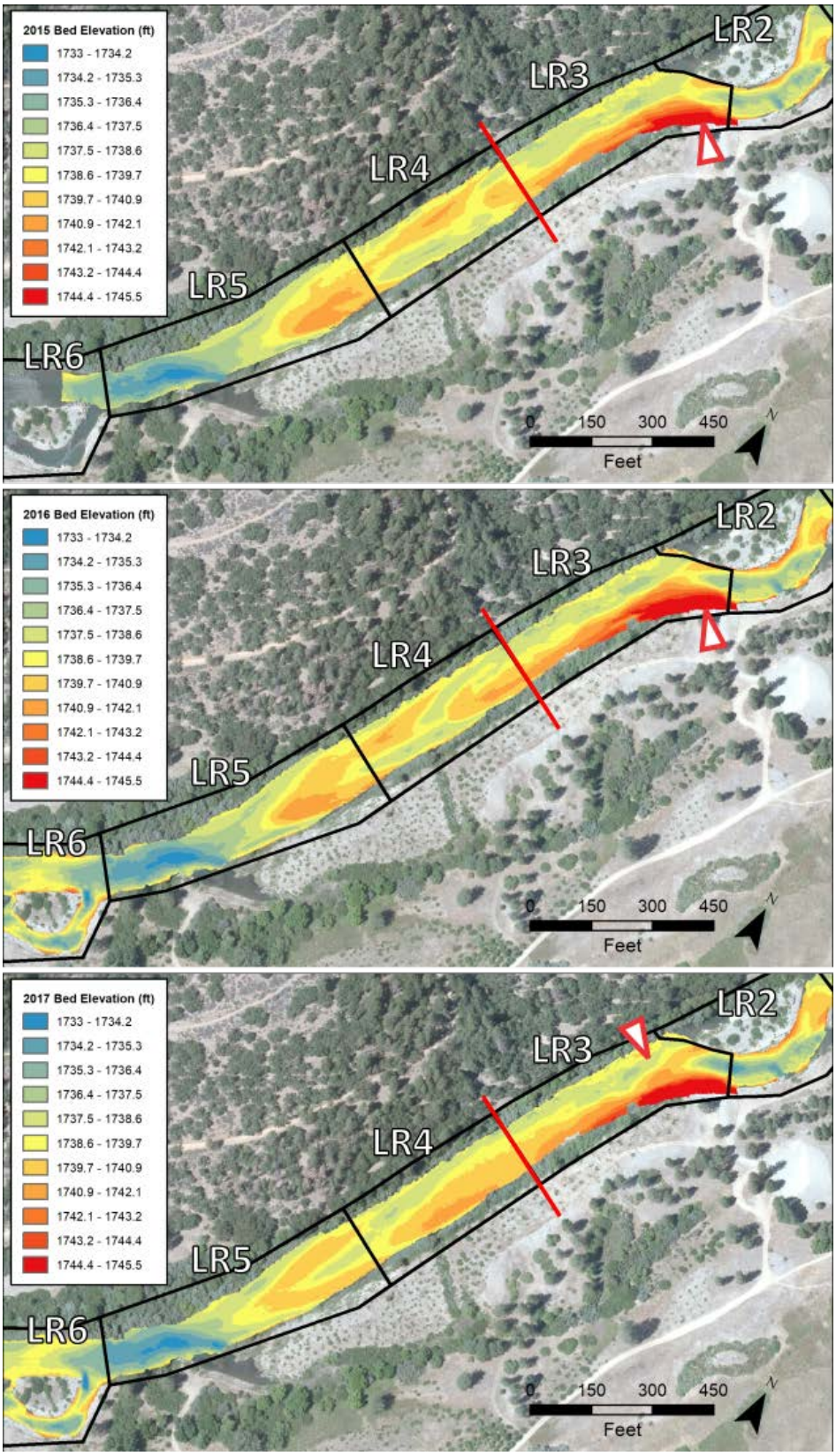

Figure 16: Bed elevation at the upstream end of the Lowden/THG reach after the 2015 (top), 2016 (middle), and 2017 (bottom) flow releases.

The 2017 Flow Release

Both the 2016 and 2017 terrain models cover a sufficient length of river to support development of a gravel budget that spans the full Lowden/THG reach (Figure 10). Due to its considerable length, the reach is split into three sections for displaying bed elevation changes. The first section, upper Lowden/THG, includes the five analysis zones used for the 2016 gravel budget, but the 2017 gravel budget is carried upstream through an additional analysis zone denoted LR0 (Figure 17).

An observant viewer may notice that the triangle indicating the gravel augmentation location in Figure 17 points at a slightly different location than in Figure 15. In 2017 the gravel was dropped into the middle of the channel with an excavator a few days prior to the rise of the flow release. The resulting in-channel stockpile, as well as a second stockpile introduced farther downstream, was surveyed to capture the final pre-release topography present at the site for a few days in April of 2017. The gravel budget presented herein, however, does not require these data. Instead, the topographic changes displayed in the figures and quantified in Table 6 are based on differences between the 2016 post-release morphology and the 2017 post-release morphology. The gravel volumes introduced as pre-release stockpiles are added into the gravel budget as if they had been injected during the rising limb of the release. A version of the Lowden/THG terrain model that incorporates the April 2017 pre-release survey data is used only to support morphodynamic modeling intended to assess whether the morphologic response of the Lowden area to the 2017 release was altered by the change in how gravel was introduced into the channel. That analysis, which is described in Appendix C, suggests that moving the gravel introduction point to the channel center in 2017 produced minor morphologic differences within a distance of about two channel widths from the augmentation, but had a negligible effect on erosion and deposition patterns farther downstream.

It is immediately apparent from the extent of color on Figure 17, as well as from the values of F_i in Table 6, that gravel fluxes in 2017 were much larger than in 2016. For example, the measured 2017 flux at the sediment monitoring transect (boxed value in the table) is 2.7 times larger than the corresponding figure for 2016. This magnitude of increase in the flux rate is in keeping with the difference in the peak flows for 2016 and 2017 of 9,500 ft^3/s and 12,000 ft^3/s, respectively. Given that the threshold for significant gravel transport in this reach is near 4,500 ft^3/s, these peaks correspond to excess discharges above threshold of 5,000 ft^3/s and 7,500 ft^3/s. These excess discharges assume values that have a ratio of 2.7 when raised to the power of 2.45, which is well within the range of exponents expected of 3-parameter bedload rating curves (Gaeuman et al. 2018).

The vast majority of the gravel flux that reached the upstream boundary of the Lowden/THG reach (> 96%) passed through LR0 and into LR1 (Table 6). As had been the case in 2016, LR1 and the upstream end of LR2 continued to accumulate gravel in 2017 but the proportion of the incoming load that was captured was considerably smaller in 2017 (18% in 2017 versus 43% in 2016).

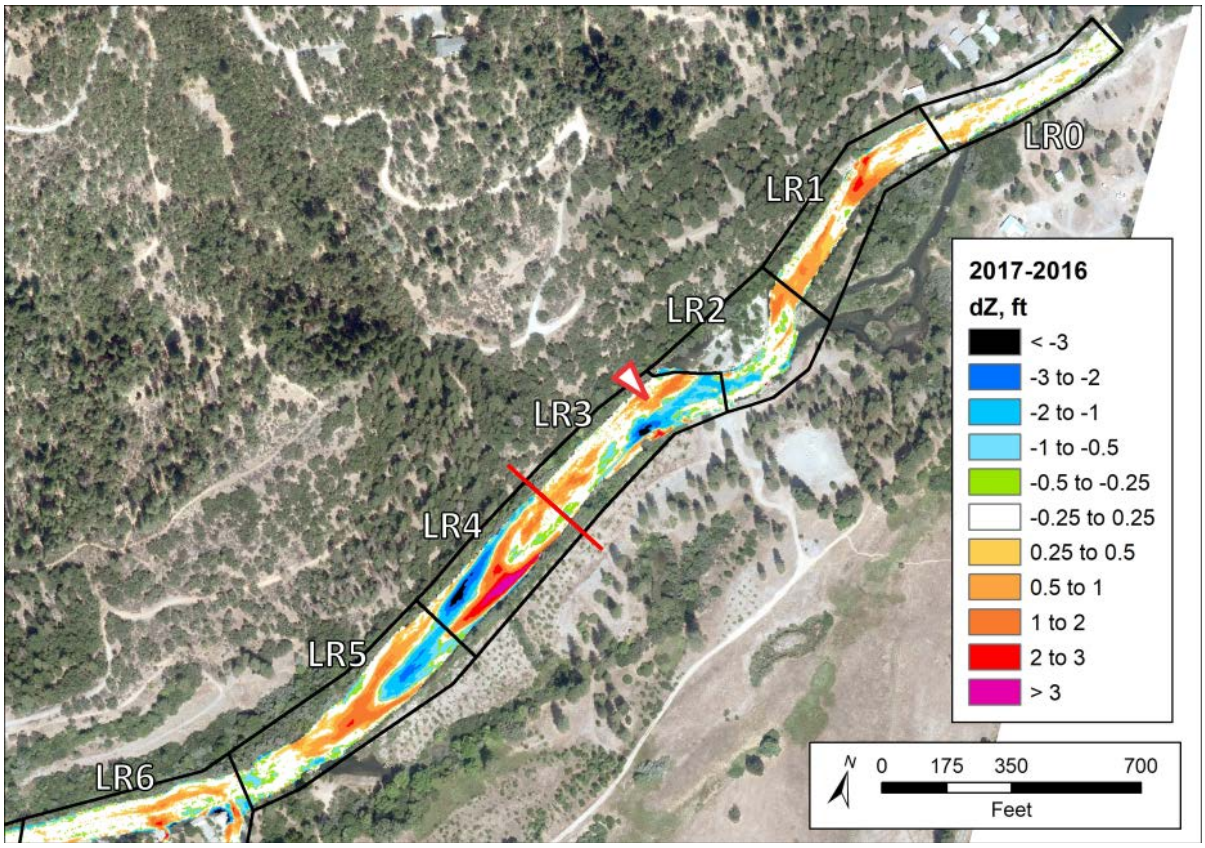

Figure 17: Bed elevation changes during the 2017 spring flow release at the upstream end of the Lowden/THG reach. *dZ* = change in bed elevation.

Larger deviations from the 2016 pattern appear farther downstream, beginning with a large patch of erosion ranging in depth from 1 to more than 3 ft that spans the boundary between LR2 and LR3 and extends downstream in the left half of the channel to about the mid-point of LR3. Together with a patch of deposition that appears on the right side of the channel near the upstream end of LR3, the 2017 configuration in this area essentially reverses the loci of erosion and deposition observed in 2016. It is tempting to attribute this reversal to the shift in the gravel augmentation location from the left bank toward the central part of the channel, but that interpretation is not supported by the morphodynamic modeling presented in Appendix C. In any case, the erosion and deposition in zone LR3 roughly balance, so that the estimated net storage change is smaller than its associated uncertainty margin and constitutes less than 2% of the flux at the downstream boundary of the zone.

The bedload dynamics in zones LR4 and LR5 changed considerably in 2017. First, the pair of bedforms that had been migrating through LR4 the previous year vanished. The bedform that had been present in the upstream left quadrant of LR4 appears to have attached to the left bank where it merged into a long lateral bar extending upstream to the gravel augmentation area (Figure 16). The material composing the second bedform in the downstream right quadrant of LR4 either joined the medial bar at the upstream end of LR5 or transported downstream past that bar. The medial bar itself, which had remained stationary with little change in morphology since 2011 (Gaeuman 2014a; Gaeuman et al. 2017), was flattened and

elongated by erosion through its center coupled with downstream deposition. These morphologic changes were associated with net deposition in both zones, although the total storage increase over both zones amounts to only about a fifth of the gravel flux through the area during the release.

Table 6: 2017 gravel budget for the Lowden/THG reach. Variables are: dZ = mean change in bed elevation, ΔV_b = change in gravel storage volume, G_a (yd^3) = augmentation volume, δV_b = uncertainty in gravel volume, F_i = gravel flux at downstream boundary of zone i, δF = cumulative uncertainty in gravel flux. All volumes given in substrate equivalent bulk density. Flux inside the box was estimated from field measurements.

Zone	dZ (ft)	ΔV_b (yd^3)	G_a (yd^3)	δV_b (yd^3)	F_i (yd^3)	δF (yd^3)
Flux from upstream					4868	± 1657
LR0	0.120	179		± 74	4690	± 1643
LR1	0.488	855		± 88	3835	± 1631
LR2	−0.049	−54		± 55	3889	± 1626
Gravel augmentation input			1260	± 126		
LR3	−0.025	−64		± 180	5213	± 1616
LR4	0.289	611		± 106	4602	± 1619
LR5	0.094	289		± 154	4314	± 1637
LR6	0.142	467		± 164	3846	± 1671
Gravel augmentation input			540	± 54		
LR7	0.058	213		± 191	4174	± 1711
LR8	0.073	177		± 121	3997	± 1755
LR9	0.052	92		± 88	3905	± 1791
LR10	−0.156	−201		± 64	4105	± 1820
LR11	−0.138	−240		± 87	4345	±1861
LR12	−0.349	−1043		± 149	5388	± 1940

Deposition of about 11% of the incoming gravel supply to zone LR6 reduced the gravel flux exiting that zone to approximately the same level estimated to have entered LR3 immediately upstream from the upstream gravel augmentation. Net deposition continued in zones LR7 through LR9, with the total gravel storage increase in those zones consuming about 90% of the augmentation volume placed in the channel near the center of zone LR7. Although LR9 showed a small overall increase in storage, deposition was confined to a small area near the zone's upstream boundary (Figure 18). Erosion dominated elsewhere in LR9, and extended downstream through the remainder of the reach. Erosion was especially widespread and deep in LR12, which spans a sharp bend in the valley that hosts a complex series of bedrock pools known as the SP/Ponderosa pool (Figure 19). More than 1,000 yd^3 of bed material was removed from the the pools and adjacent bars during the 2017 flow release.

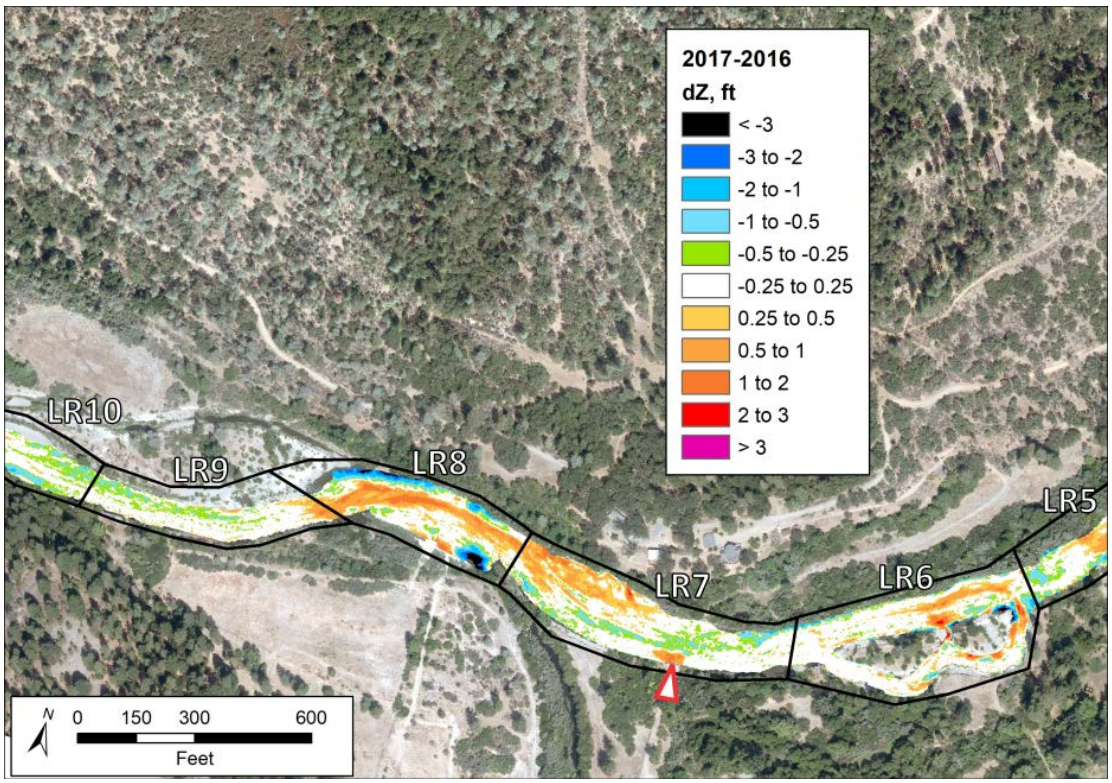

Figure 18: Bed elevation changes during the 2017 spring flow release in the middle of the Lowden/THG reach. dZ = change in bed elevation.

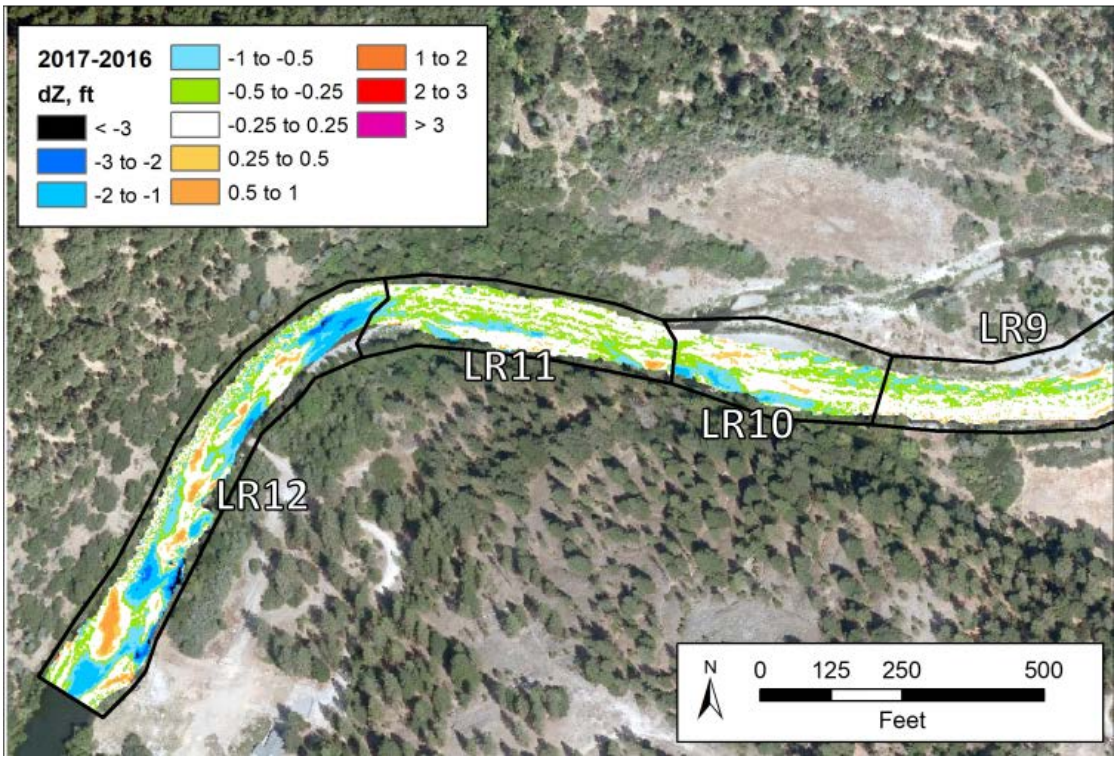

Figure 19: Bed elevation changes during the 2017 spring flow release at the downstream end of the Lowden/THG reach. dZ = change in bed elevation.

Gravel Activity in the Lewiston Bridges Reach

Gravel activity (G_i) computed for 2016 in the Lewiston Bridges reach decreased sharply from a maximum in analysis zone LB1 to about 44% of that maximum in LB2 (Figure 20a), where LB1 incorporates the combined activity in LB1a and LB1b. That decrease occurred despite the fact that LB2 experienced a somewhat larger increase in gravel storage that year than did LB1 (Table 3). The difference in activity levels, however, is more related to the the extent of erosion in the two zones. Widespread deposition is apparent in both zones on Figure 11, and LR1 also displays numerous small patches of erosion. LR2, on the other hand, includes almost no areas of erosion. The 2016 flow release was apparently capable of transporting gravel injected at the Diversion Pool beyond the New Lewiston Bridge, but was insufficient to maintain mobility beyond the head of the large island downstream from the bridge.

LB2 continued to be an area of net deposition in 2017, but that year's flow release appears to have been capable of maintaining gravel transport well beyond the New Lewiston Bridge. G_i in LR2 still decreased from a maximum value in LR1, but the magnitude of the decrease was smaller. Gravel storage in LB2 also continued to increase in 2017, but the storage increase was likely due to high rates of gravel delivery to the zone's upstream boundary rather than to a lack of transport within the zone. Evidence for that interpretation includes a near equality between the gravel flux estimated to have exited LR2 that year and the volume of the Diversion Pool gravel augmentation (Table 4).

The 2017 value of G_i in analysis zone LB3 is similar in magnitude to the value for LB2, although the dominant process shifted from deposition in LB2 to erosion in LB3. The relatively high level of G_i in LB3 reflects the migration of bedforms through the area, as described previously. G_i then plunges to very low values in LB4 and LB5, even though the local gravel flux rates in the area are similar to those computed for elsewhere in the reach. Activity in zone LB6 rebounds to a more moderate level, but erosion continues be the dominate process. Overall, the stretch of river spanning zones LB4 through LB6 appears to function as a transport reach that efficiently transmits bedload to zone LB7 immediately downstream from the Old Lewiston Bridge. Gravel activity in that zone is moderate, as there is very little erosion to complement the local deposition.

The second highest level of G_i anywhere in the Lewiston Bridges reach is attained in LB8. As in LB3, this high activity level is due to the previously-described bar migration through the zone, again demonstrating the effectiveness of G_i for identifying geomorphically active areas where bedload processes involve exchanges between the bedload and the stream substrate.

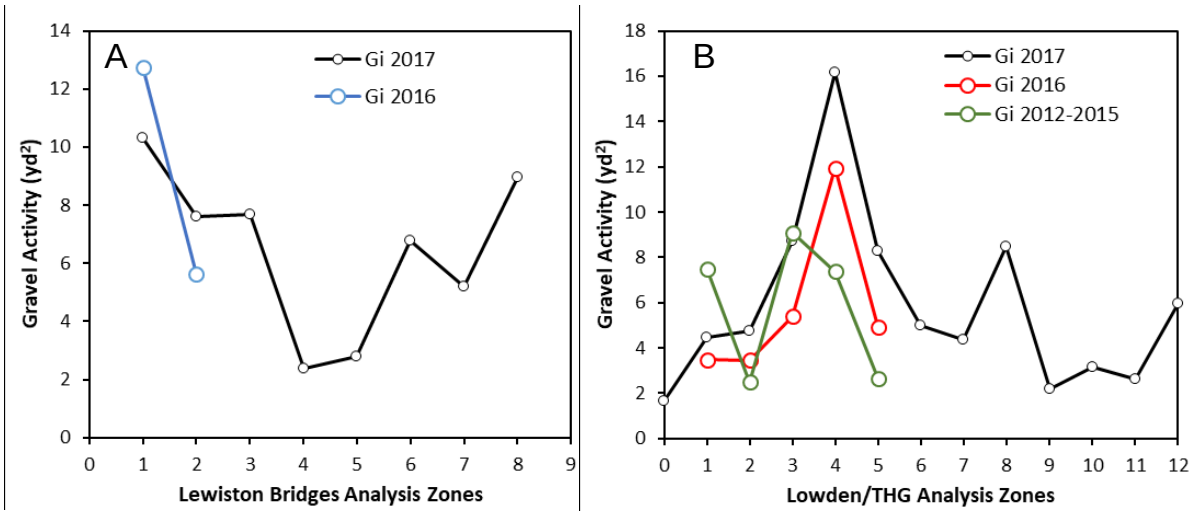

Figure 20: Gravel activity in a) the Lewiston Bridges reach and b) the Lowden/THG reach.

Gravel Activity in the Lowden/THG Reach

G_i profiles through the Lowden/THG reach for the 2016 and 2017 flow releases are almost identical in shape, although the 2017 profile is about 35% larger across the board (Figure 20b). The lowest values for both years occur in LR1 and LR2, upstream from the Lowden upstream gravel augmentation point. Activity predictably increases in zone LR3 downstream from the augmentation point in both years, then spikes to levels about twice as great in zone LR4. The very high activity levels in that zone correspond to the presence of migrating bedforms in 2016, and in 2017 to the destruction and transformation of those bedforms as described previously. Activity then drops back to moderate levels in LR5, where the primary topographic feature consisted of a medial bar that remained in an approximately fixed position.

It is instructive to compare the similar 2016 and 2017 G_i profiles through the five shared analysis zone with a profile developed for 2012-2015 using data reported by Gaeuman et al. (2017). That time interval, (referred to here as 2015 for brevity) includes the moderately large 2015 flow release that peaked at 8,830 ft^3/s and an associated gravel augmentation totaling 680 yd^3 at the upstream Lowden site. The peak value of G_i observed for 2015 occurs in LR3, upstream from the 2016 and 2017 peaks and immediately downstream from the augmentation location. The 2015 G_i profile then declines consistently downstream from LR3. This profile shape seems to indicate that the bulk of the gravel introduced at the upstream Lowden augmentation point was still upstream from LR4 in 2015, whereas by 2016 it had moved downstream and was making its way through LR4. The 2015 profile also differs from the later profiles in that LR1 also displayed relatively high values of G_i in 2015. A gravel budget for that time frame developed by Gaeuman et al. (2017) indicates that gravel storage in LR1 increased by about 1318 yd^3 – the largest storage change recorded for any analysis zone in the Lowden/THG reach during any time period. Gaeuman et al. (2017) described LR1 as containing a delta-like sediment wedge with small migrating dunes superimposed on its surface during the 2015 flow release.

PIT-tagged Tracers

This section summarizes interim results of an ongoing study with PIT-tagged tracer stones. Tracers introduced with the 2016 gravel injections at the Diversion Pool and at the upstream Lowden Ranch augmentation point have now been relocated twice (relocation for the third time is planned for late 2019). Current results include a comparison of travel distance and tracer recovery statistics for 2016 and 2017, plus observations regarding how the timing of introductions during the 2016 flow release affected tracer travel distances.

Tracer Recovery Efficiency

Due to a lack of experience tracking tracer stones in a stream as large as the Trinity River, the percentage of the tracer stones relocated in 2016 was rather low. At Lowden Ranch, where relatively simple morphology made the task somewhat easier, 72.9% of the tracers introduced during the 2016 flow release were detected the following summer (Table 7). Downstream from the Diversion Pool augmentation, however, the recovery percentage for 2016 was just 53.3%. In 2017, a more experienced crew using somewhat different equipment was able to relocate more than 70% of the tracers in the Diversion Pool area and nearly 80% of the tracers introduced at the upstream Lowden Ranch augmentation site.

The inability to locate a significant percentage of the tracers could arise in several ways. Tracers will go undetected if they are in locations that cannot be accessed with the mobile antenna used to stimulate the transmission of an RFID signal. The commercially available pole antennas used in 2016, for example, must get to within 2 to 3 ft of a PIT tag to generate a signal. Tags buried in thick alluvial deposits or located in relatively deep pools can be nearly impossible to access with that antenna. That source of non-detections was alleviated somewhat in 2017 by the use of a larger custom-built antenna with a detection range of up to 5 ft. Non-detections can also occur when two or more tags are located within the antenna detection distance of one another, such that simultaneous transmission of the tag signals interfere with each other. That source of non-detection may also have been alleviated to some extent by 2017 because the typical distance between deposited tracers increases with continued downstream transport.

Perhaps the most important potential source of non-detections is the possibility that some of the tracers have travelled beyond the downstream limits of the search. The available evidence, however, suggests that few tracers, if any, have left the search area. One line of evidence in support of that conclusion is that a large share of the tracers that were absent in 2016 reappeared in 2017. Of the 467 tracers that were apparently missing from the Diversion Pool area in 2016, 326 (70%) were successfully located the following year (Table 7). Likewise, 73% of the tracers missing from Lowden Ranch in 2016 were found in 2017.

The spatial distribution of tracers downstream from the gravel injection sites also strongly suggests that no tracers are located beyond the limits of the searches. Tracers tend to cluster together, most often in areas where the 2016 and 2017 gravel budgets indicate deposition. Near the Diversion Pool, for example, the downstream extent of the tracers in 2016 corresponds to a previously-described depositional region at the head of a large island in LB2 (Figure 21; Figure 11). In 2017, a cluster of about 70 tracers was found in the large prograding gravel lobe near the downstream end of LB2, as described in connection with the

2017 Lewiston Bridges gravel budget (Figure 21; Figure 12; Figure 13). The few tracers located downstream from that gravel lobe are also associated with a patch of deposition that suggests the presence of a small linguoid bar at the upstream end of the LB3 analysis zone. Relocation efforts extended through LB3 and included spot checks on depositional areas as far downstream as the Old Lewiston Bridge. Several tags were detected at a bar complex near the middle of LB3 (Figure 12), but those turned out to be leftover tags from a fish-tracking study performed several years earlier.

Table 7: Recovery statistics for the tracers introduced at the Diversion Pool and the upstream Lowden Ranch gravel augmentation sites. N_R, P_R, N_{F2017}, N_{L2017}, and $P_{R,\,R}$ denote the number of recovered tracers, the percentage of tracers recovered, the number of tracers found for the first time in 2017, the number of tracers found in 2016 but not in 2017, and the percentage of tracers relocated at least once.

	N_R	P_R	N_{F2017}	N_{L2017}	$P_{R,\,R}$
Diversion Pool					
2016	533	53.3			
2017	703	70.3	326	156	85.9
Lowden Ranch					
2016	729	72.9			
2017	790	79.0	197	136	92.6
Both Sites Combined					
2016	1262	63.1			
2017	1493	74.7	523	292	89.3

Tracers at Lowden Ranch are also associated with depositional areas identified in the gravel budget section. In 2016, the tracers were located in a nearly continuous band of deposition along the left channel margin downstream from the augmentation point (Figure 22; Figure 15). That cluster of tracers terminates abruptly on the slipface of the river-left bedform in the pair of migrating dune-like bedforms noted in the gravel budget section. Interestingly, dense clusters of tracers are also apparent in erosional areas to the right of that bedform. It appears that relatively coarse particles in the bedload transported onto the bedform crest that year tended to fall into the depressions vacated by the bedforms as they migrated downstream. By 2017, the tracer cluster together with the bedform on the left reached the upstream boundary of LR5. A narrower splay of tracers extends downstream through the scoured central portion of the medial bar in LR5 and into another deposition area. The last tracer located is coincident with the downstream limit of that deposition, even though the 2017 search extended through analysis zone LR7.

The locations of tracers detected in 2017 relative to net changes in bed elevations over the 2-year study period demonstrates a clear tendency for tracers to cluster in depositional areas. At Lowden Ranch, 70% of the tracers located in 2017 were in areas of net deposition. Bed elevations at those locations increased by an average of 1.3 ft, whereas the average decrease in bed elevation at the location of the remaining 30% of the tracers was about 30% smaller at 1.0 ft. At the Diversion Pool, 78% of the tracers were found in areas with net increases in bed elevations averaging 1.25 ft, whereas the elevation decreases at the locations of the remaining tracers averaged just 0.5 ft.

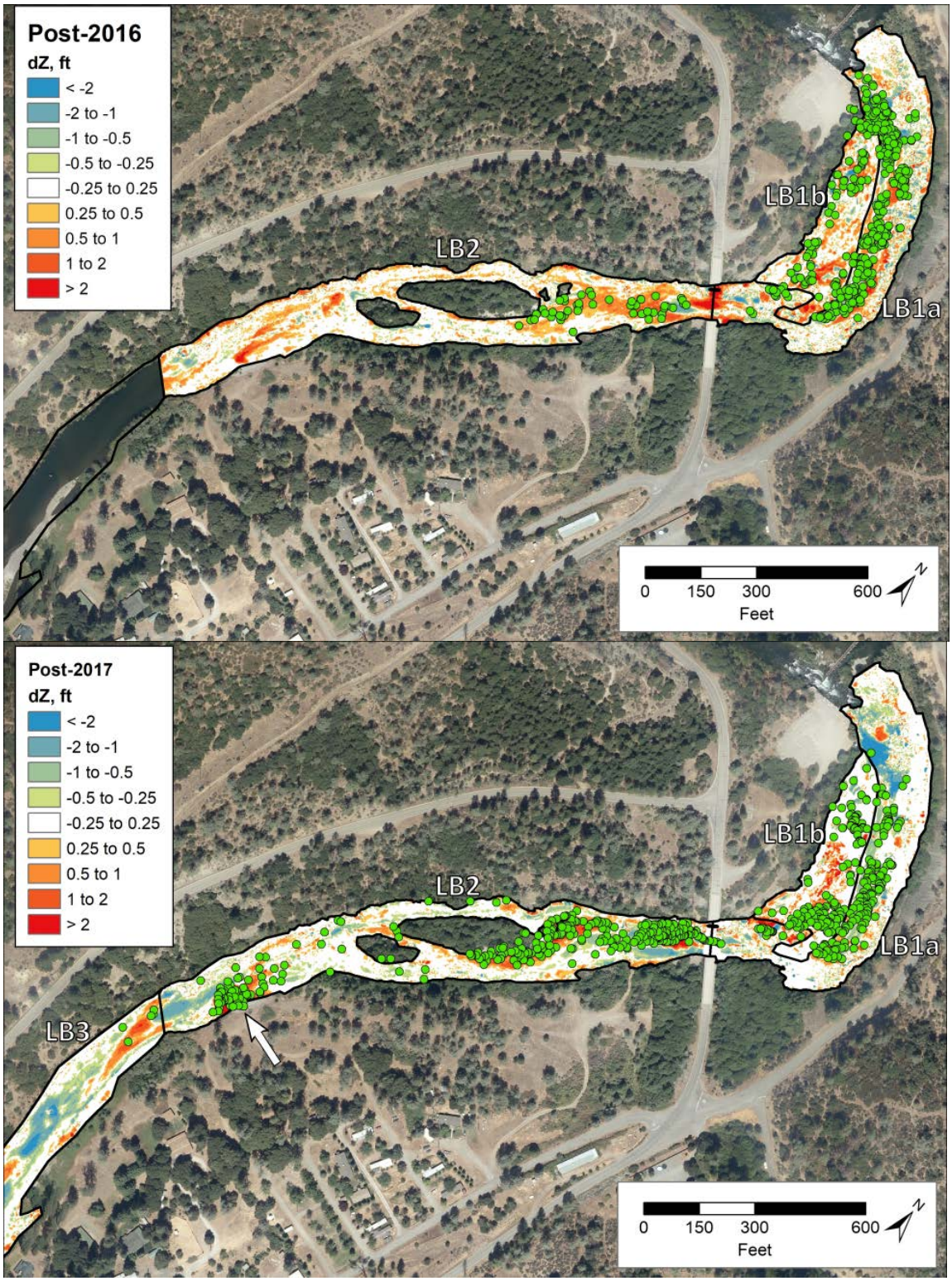

Figure 21: Green dots indicated tracer locations downstream from the Diversion Pool in 2016 (top) and 2017 (bottom). dZ = change in bed elevation. The white arrow indicates the position of the prograding gravel lobe described in the text.

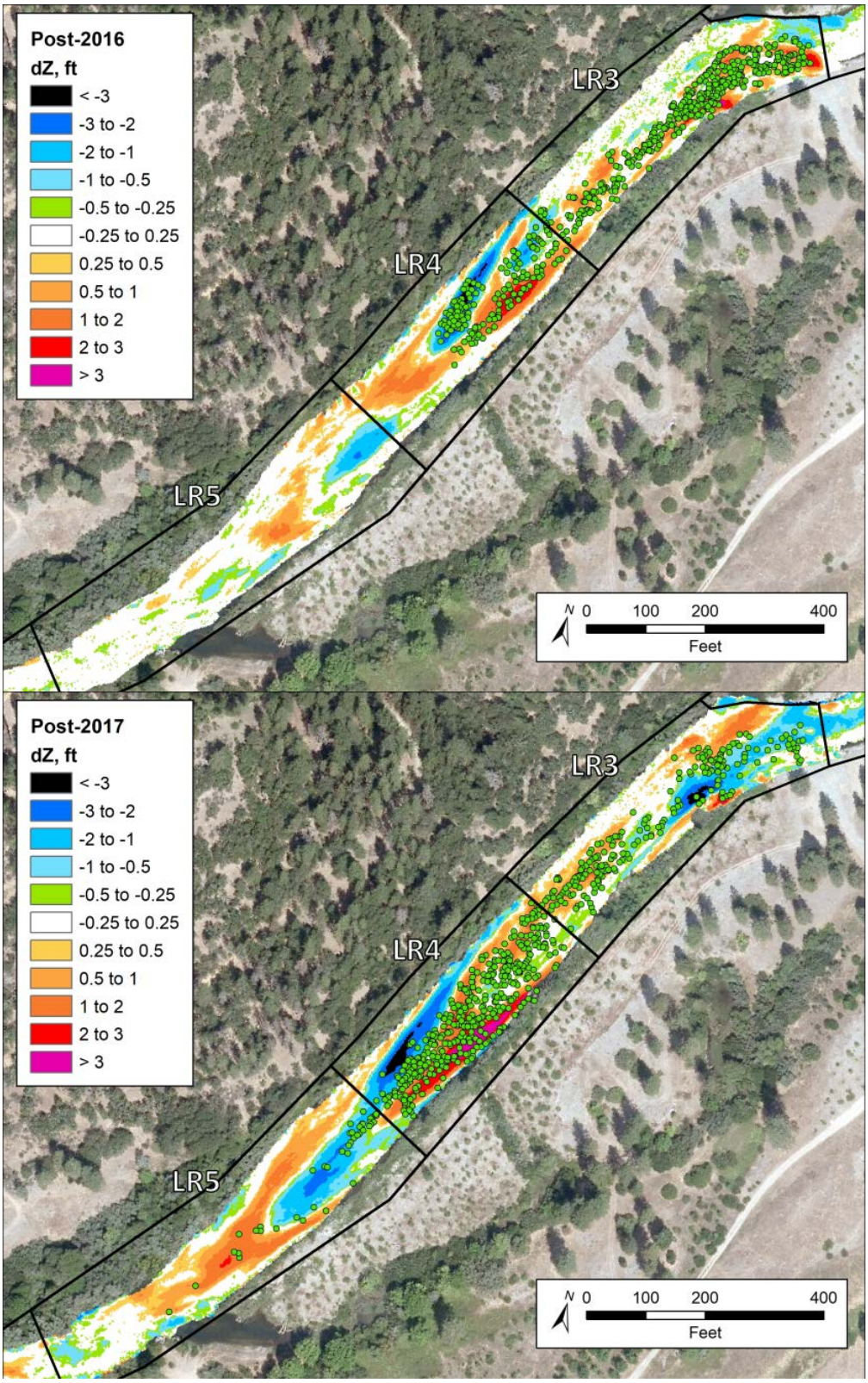

Figure 22: Tracer locations downstream from the upper Lowden Ranch augmentation point in 2016 (top) and 2017 (bottom). dZ = change in bed elevation.

Among the preliminary findings derived from the first two years of this multi-year study is that the tracer travel distances are surprisingly short, particularly the distances travelled in 2016. Of all tracers recovered at the Diversion Pool and Lowden sites in 2016, 91% and 78% were found in LB1 and LR3, the budget zones immediately downstream from the Diversion Pool and Lowden augmentation sites, respectively (Figure 23). This result is consistent with the gravel budget at the Diversion Pool, which indicates that the 2016 storage increase in LB1 was similar to or greater than the entire gravel augmentation volume that year. At Lowden Ranch, however, the 2016 gravel augmentations exceeded the storage increase in LR3 by a wide margin and bedload sampling indicates that the flux out of LR3 was similar to or greater than the augmentation volume containing the tracers. It appears that the dynamics associated with the augmentations can involve a large component of exchange between the introduced material and the pre-existing substrate. The types of exchange referred to herein is not limited to equilibrium exchanges between the bedload and substrate represented by models such as that of Toro-Escobar (1996). Rather, they include exchanges associated with variability in net erosion and deposition over a wide range of spatial scale.

The 2017 flow release was considerably more effective for moving the tracers downstream. At the Diversion Pool, slightly more than half of the tracers moved into LB2 and a few even reached the upstream end of LB3 in 2017. At Lowden Ranch, the majority of tracers (65%) were located in LR4, whereas nearly 6% had reached LR5.

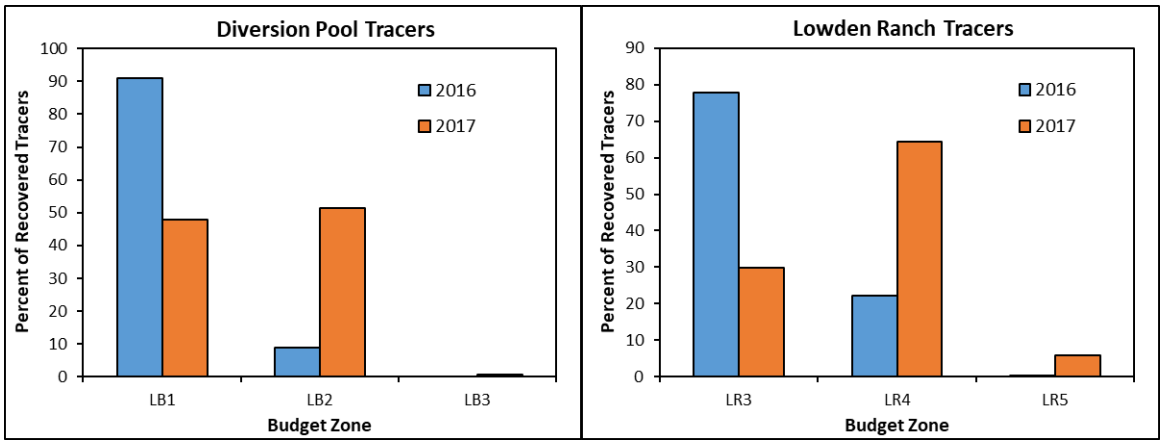

Figure 23: Percentages of recovered tracers located in gravel budget analysis zones in 2016 and 2017.

Other preliminary findings include observations on how the timing of the 2016 gravel augmentations affected tracer entrainment and transport. Recall that the 2016 flow release incorporated two flood peaks of equal magnitude, and that the 2016 gravel injections were implemented in four batches performed on four separate days. At the Diversion Pool, tracers introduced on the rising limb (May 8) or apex (May 9) of the first flood peak traveled more than 50% farther on average than tracers introduced on the rising limb (May 12) or apex (May 13) of the second flood peak (Table 8; Figure 24). There was virtually no difference, however, between the travel distances of the tracers introduced on the rising limb or peak of the same flood.

Table 8: Travel distance statistics for tracer stones during the 2016 flow release as a function of the injection date. N_R, μ_t, σ_t, and M_t denote the number of recovered tracers, the mean travel distance, the standard deviation of travel distance, and maximum travel distance.

	May 8, Rise	May 9, Peak	May 12, Rise	May 13, Peak
Diversion Pool				
N_R	126	125	132	148
μ_t	659	670	435	433
σ_t	421	435	227	223
M_t	1643	1619	967	1445
Lowden Ranch				
N_R	137	202	166	215
μ_t	600	282	466	250
σ_t	180	209	184	125
M_t	804	792	829	827

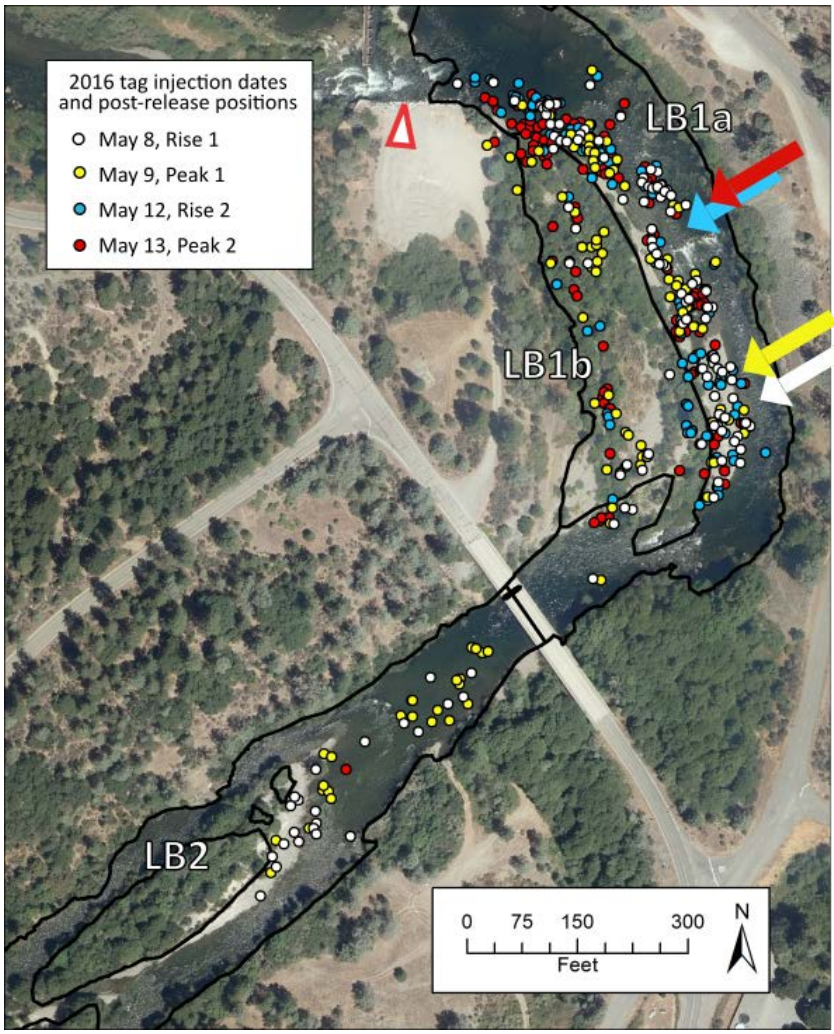

Figure 24: Tracer locations downstream from the Diversion Pool in 2016, color coded according to the time of their introduction into the stream. Colored arrows indicate the mean travel distance for each group.

The timing of gravel introduction had a very different effect at Lowden Ranch. At that site, the average travel distance of tracers introduced on either of the rising limbs (May 8 or 12) were about twice the travel distance of tracers introduced on the flood peaks (May 9 or 13) (Table 8; Figure 25). The distribution of the tracers clearly shows that gravel introduced at the peak of the flood has a tendency to deposit on the left bank immediately downstream from the augmentation point. As can be seen on Figure 16, the point bar on that bank is substantially higher than the channel bed. Material transported onto that surface during the flood peak is therefore no longer accessible to more moderate competent flows. Gravel introduced on the rising limb, on the other hand, stays within the bankfull channel as rising limb flows transport it into the straight reach beyond the point bar. Once beyond the bar, the gravel remains accessible for entrainment over a wide range of flows. Tracers introduced on the first rise traveled nearly 30% farther than those introduced on the second rise, a results that is easily explained by the fact that the first batch of tracers experienced two peaks whereas the second batch experienced only one peak. The travel distance associated with the tracers introduced on the two peaks, however, are nearly equal.

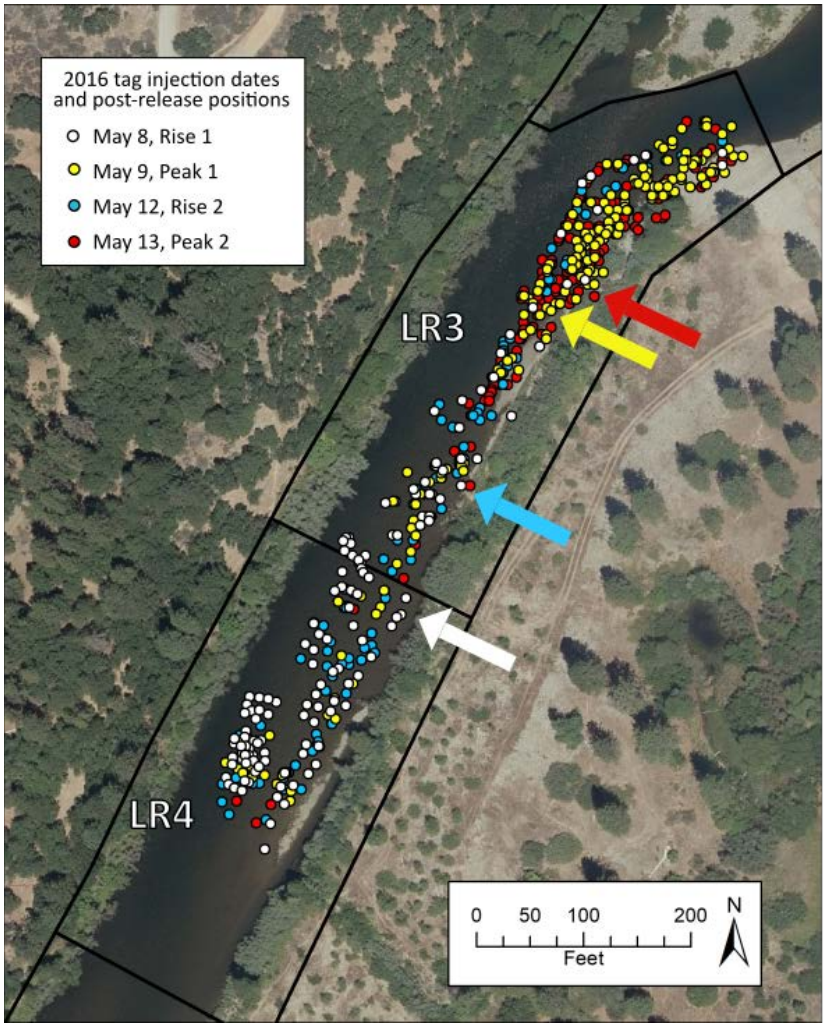

Figure 25: Tracer locations at Lowden Ranch in 2016, color coded according to the time of their introduction into the stream. Colored arrows indicate the mean travel distance for each group.

Integration of Gravel Budget and Tracer Results

The 2016 gravel budget for the Lewiston Bridges reach is in agreement with the PIT-tagged tracer stones relocated in 2016, in that both sets of data imply that all of the gravel added to the reach during the 2016 release deposited in analysis zones LB1 or LB2. The budget deviates from the tracer results, however, in that approximately two-thirds of the total increase in gravel storage occurred in LB2, whereas just 9% of the located tracers made it into LB2. Similarly, some aspects of the 2017 Lewiston Bridges gravel budget are consistent with tracer results while others are not. That budget shows a storage decrease in LB1 and an increase in LB2, which is consistent with an increase in the proportion of tracers found in LB2 to more than 50%. However, that budget also shows an estimated gravel flux into LB3 larger than the entire volume of the 2016 augmentation, whereas less than one-half of 1% of the tracers were recovered beyond the downstream boundary of LB2.

Inconsistencies between the estimated gravel fluxes and the tracer distributions appear in the Lowden Ranch/THG reach as well, despite the fact that the bedload sampling transect in the reach is located at the downstream boundary of analysis zone LR3, less than 600 ft downstream from the augmentation point. The 2016 gravel augmentation volume, which contained the tracers, accounted for about 62% of all gravel entering LR3 from all sources and about 75% of the gravel flux that exited the zone that year. Yet only 22% of the tracers relocated in 2016 were found beyond the zone's downstream boundary.

In 2017 gravel fluxes throughout the Lowden Ranch/THG reach were several times larger than in the previous year, and the relationship between the gravel budget fluxes and the tracer distribution varied spatially as the tracers spread downstream. The proportion of tracers found beyond the downstream boundary of LR3 after the 2017 flow release increased by a factor of more than 3 to 71%. Assuming that the percentage of tracers in a local area is proportional to the local abundance of the augmentation gravel they were introduced with, this suggests that slightly more than 700 yd^3 of the 2016 augmentation material exited LR3 in 2017. Net gravel storage in LR3, however, decreased by less than 10% of that volume. Thus, more than half of the 2016 augmentation gravel that remained in LR3 before the 2017 flow release was displaced by new gravel introduced during the release. The relatively high level of tracer mobility observed in LR3 diminished rapidly once tracers entered LR4. In LR4, relative tracer abundance increased from about 22% before the 2017 flow release to 65% after the release, which corresponds to an increase in the storage of 2016 gravel of about 627 yd^3. As the total gravel storage in LR4 increased by nearly the same amount (611 yd^3), it appears that the increase in gravel storage in LR4 during the 2017 release was almost entirely due to the transfer of gravel introduced as part of the 2016 gravel augmentation out of LR3. Moreover, the approximately 700 yd^3 of 2016 gravel that left LR3 during the 2017 release presumably joined the 310 yd^3 that was already in LR4 before the release, bringing the total quantity of 2016 gravel that was available for transport beyond the downstream boundary of LR3 to about 1016 yd^3. Of that total volume, the proportion of tracers retained in LR4 at the end of the release implies that only about 79 yd^3 (< 8%) of the 2016 gravel that made it into LR4 continued into LR5. Because that small volume of gravel amounts to less than 2% of the total gravel flux passing into LR5 that year, it can be concluded that the 2016 augmentation material represented by the tracers was disproportionately retained in LR4.

The discrepancies between the gravel budgets and the tracer distributions described above seem to require extensive and highly variable exchanges between the materials composing the streambed and the materials in active bedload transport. Subsurface bed material in this section of the Trinity River has a 90^{th}-percentile particle size of 122 mm but a median grain size near 20 mm (Viparelli et al. 2011). With median particle sizes of 73 mm, the typical tracer is equivalent to about the 80^{th}-percentile size of the native subsurface material (Figure 8). Similarly, the median size of the augmentation material (about 60 mm) is equivalent to about the 75^{th}-percentile size of the subsurface. Any process that sorts the bedload according to particle size, regardless of whether the sorting is in the horizontal or vertical dimensions, could therefore produce differences between the fluxes and transport distances of the tracers, the augmented gravel, and the total bedload.

The available evidence suggests that the exchange dynamics involve at least two particle size sorting processes that preferentially remove tracer stones and coarser fractions of the augmentation materials from the active bedload. The river downstream from the Diversion Pool is uncharacteristically steep through analysis zone LB1 and most of LB2 (Figure 26). Net gravel deposition near the augmentation point is nonetheless made possible by the considerable width of the floodway in the bend upstream from the New Lewiston Bridge (Figure 21). The tracer distribution in the bend suggests that augmented gravel accumulates along the right edge of the channel adjacent to the thalweg, perhaps because it is introduced into the channel faster than flow can disperse it downstream. Once emplaced, those deposits may steer flow toward erodible substrate elsewhere in the channel. Similarly, in 2016 the tracers at Lowden Ranch were concentrated along the left bank downstream from the augmentation point, whereas a band of erosion occupied the opposite side of the channel. Exchanges of this sort, which result from topographic steering of the flow when large quantities of gravel are introduced at a high rate, could account for the relative lack of tracer mobility observed in 2016 at both locations.

Gravel budget and tracer results were more compatible near the augmentation points in 2017, possibly due to the larger peak flows released that year or perhaps because new topographic structures arising from the 2017 gravel augmentations promoted scour of structures deposited the previous year. At both sites, however, tracer mobility was again anomalously low at more downstream locations. In both locations, this outcome appears to be the result of decreasing slope, which leads to the development of mobile bedforms. In the Lewiston Bridges reach, the downstream progress of tracers ends near the leading edge of the large prograding gravel lobe previously identified on the left bank near the downstream boundary of LB2 (Figure 21). That gravel lobe is located at a transition from the steep region near the Diversion Pool (slope = 0.006) to a stretch of channel spanning the downstream end of LB2 and all of LB3 where the channel slope averages 0.0014 (Figure 26). That decrease in slope is accompanied by a transition in the dominant style of bedload transport.

In the steeper reach upstream from the transition, mobile bedforms are generally absent. Instead, the dominant bed topography consists of large-scale static features, such as the large island in the middle of LB2, the channel constriction at the New Lewiston Bridge, and the expansive point-bar-like feature that comprises analysis zone LB1b. In the absence of

perturbations like gravel augmentations, bedload presumably moves over the bed surface in accordance with the standard bed layer model typically ascribed to coarse sediment transport in gravel-bed streams. That model describes interactions between the bedload and the substrate in terms of a thin active layer that interacts with bedload and a subsurface layer that remains stationary. Interactions between the subsurface and the active layer or the bedload layer occur only under conditions of net aggradation or degradation (Armanini and De Silvio 1988; Parker 1991; Hoey and Ferguson 1994; Toro-Escobar et al. 1996). The streambed is conceived as an essentially planar surface consisting of a mobile armor layer that mediates the transport of the smaller particles underneath (Parker and Klingeman 1982; Parker 2002). Under conditions of partial transport, the smaller particles in the active layer are entrained only when the coarser clasts that compose the armor are occasionally disturbed (Wilcock and McArdell 1993). The depth to which particles beneath the armor can exchange with the bedload is generally taken to be limited to a few times the diameter of the larger clasts (e.g., the 90th percentile) on the bed surface (Wilcock et al. 1996; DeVries 2002).

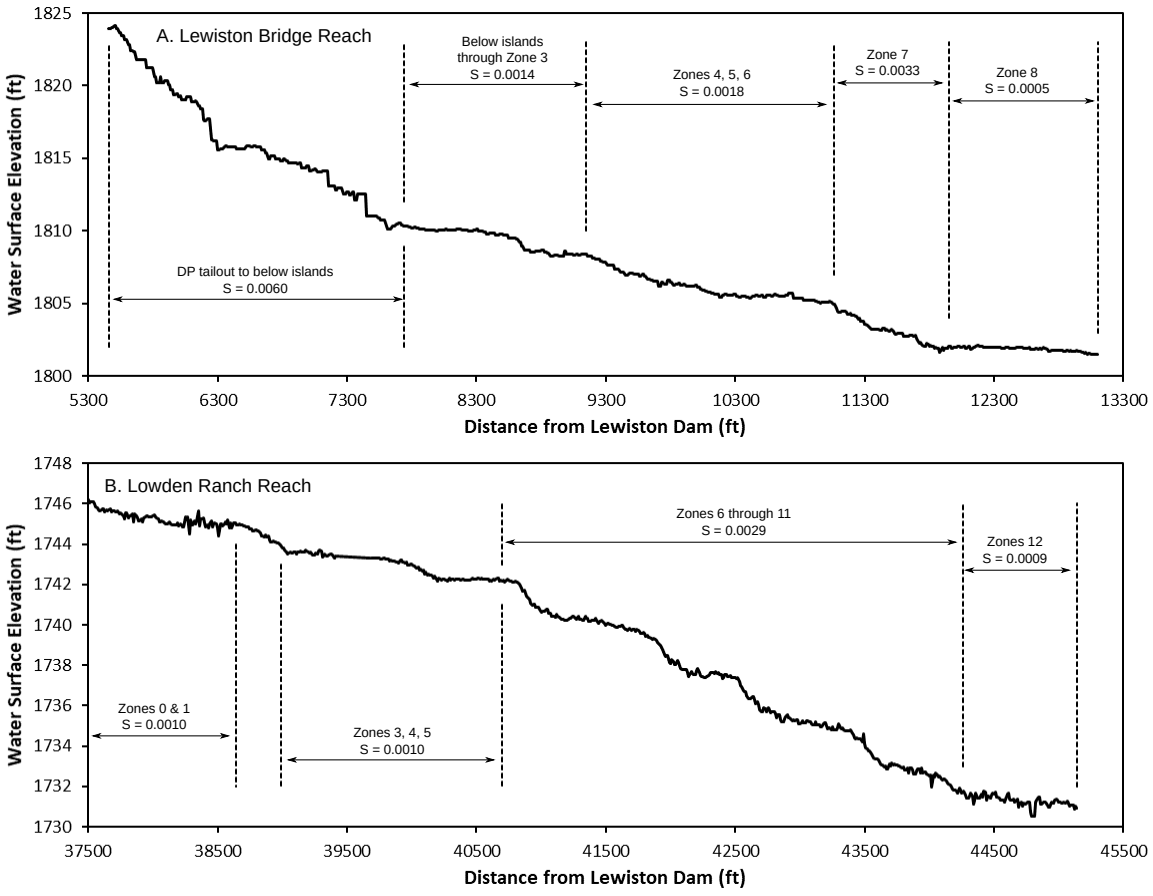

Figure 26: Water surface profiles at 2,000 ft^3/s through the Lewiston Bridges and Lowden Ranch/THG reaches. Islands referred to in top panel are can be seen in the center of Figure 21.

This plane-bed transport model ignores vertical sorting processes associated with the migration of bedforms. Migrating bedforms have been shown to promote vertical sorting that leads to a downward coarsening with depth below the surface (Blom et al. 2003; Blom and

Parker 2004). Bedforms migrate downstream as bedload particles are transported up their stoss faces to the crest, and then tumble down the steep lee face into the downstream trough. Coarser grains tend to roll farther down the lee face, potentially forming a nearly immobile layer at the base of the migrating bedforms. Turbulence generated by the bedforms serves to help winnow the finer fraction from the troughs (McLean et al. 1994).

The form of the prograding gravel lobe in LB2 is reminiscent of a delta, with a long, nearly flat stoss slope truncated by a lee face that stands at the angle of repose 4 to 5 ft above the baseflow water surface (Figure 13). Coarse particles entrained on its surface eventually avalanche down its leading edge, where they are buried as the deposit advances downstream. At least 70 tracers were found within this feature in 2017, whereas only four tracers escaped and reached the upstream end of LB3. The gravel budget, however, indicates that in 2017 between 867 and 2175 yd^3 of gravel moved past this feature into LB3. That gravel flux presumably contained a relatively large proportion of gravel sizes finer than the tracers. This delta-like depositional feature appears to function as a bedload filter that sequesters a large proportion of the coarse half of the bedload, while allowing most of the finer half to pass downstream. Particle fractions finer than the tracers were presumably more easily swept clear of burial at the leading edge or may have followed a different path through the area, perhaps avoiding the delta-like gravel deposit completely. Indeed, smaller more mobile gravel sizes transported at moderate discharges must necessarily bypass this feature, as its flat upper surface is barely inundated at 6,000 ft^3/s when most gravel fractions are being transported at significant rates.

In coarse-bedded streams, the development of mobile bedforms can be viewed as an adjustment that helps to convey bedload through regions of relatively low transport capacity. The sorting process described above moves the bed armor layer from the bed surface, where it exists in plane-bed transport, to the base of the bedforms. That coarse basal armor then appears at the surface only in the bedform troughs, while the relatively fine-grained bedforms translate across it (Wilcock and Southard 1989). That view is consistent with the observation that the topographic signature of bedform migration appears in areas where the channel slope is low.

In the Lewiston Bridges reach, evidence of bedform migration during the 2017 flow release begins at the gravel delta near the downstream end of LB2 and persists through much of analysis zone LB3 (Figure 12). It is absent in zones LB4 through LB7, but reappears with an especially clear footprint in LB8 (Figure 14). In LB4-LB6, the lack of bedforms corresponds to an increase in slope from 0.0014 to 0.0018 (Figure 26), as well as a narrowed channel that necessarily increases unit stream power. Channel slope approximately doubles to 0.0033 in LR7, where erosion and deposition patterns reflect the arrangement of static channel-scale features. Finally, the slope through LB8, where the imprint of bedform migration is most obvious, is exceptionally low at 0.0005.

Bedform migration in the Lowden Ranch/THG reach was most evident during the 2016 flow release throughout analysis zone LR4 (Figure 15). Similar bedform migration in LR4 occurred during the 2015 flow release (Gaeuman et al. 2017), and topographic changes during 2017 indicate that mobile bedform dynamics were beginning in LR5 (Figure 17).

Farther upstream in LR0 and LR1, a delta-like deposit was actively accumulating over the same time span. Gaeuman et al. (2017) described the early development of that sediment wedge during the 2015 flow release, and its volume has since continued to increase and shift downstream. The average slope through each of these areas is 0.001, which is half the average slope for the Lowden Ranch/THG reach as a whole. The slope spanning LR6 through LR 11, which contain no evidence of mobile bedforms (Figure 18; Figure 19), is nearly three times larger at 0.0029. Hints of bedform migration reappear in the erosion and deposition pattern in LR12 farther downstream where the slope flattens to 0.0009.

As described above, topographic steering, vertical sorting in bedforms, and a variety of other sorting mechanisms conspire to complicate attempts to relate tracer displacements to the total gravel fluxes through the study reaches. But the question as to whether tracer displacements can be assumed to represent the transport characteristics of the augmentation material alone remains to be addressed. For augmentation gravel introduced at the Diversion Pool in 2017, it seems likely that the tracers are representative of at least the coarser half of the material. That material, which is processed with a maximum screen diameter of 4 inches, has a median grain size of 55 mm and an interdecile size range (10^{th}- to 90^{th} percentile) of 28 to 83 mm. The interdecile size range for the tracers is 56 to 93 mm. Thus, the maximum tracer size is similar to the maximum augmentation material size, whereas the minimum tracer size is approximately equal to the median size of the augmentation material. Bedload theory supposes that the larger particles in a sediment mixture shelter smaller particles from the flow, whereas the large particles themselves are more fully exposed to the flow. These hiding and exposure effects are believed to counter the fact that greater forces are required to entrain large particles, so that large and small particles are entrained by approximately the same fluid force (Parker 2002; Wilcock and Crowe 2003). The hiding effect, however, is imperfect, such that the mobility of smaller particles is slightly greater than the mobility of larger particles. Moreover, this concept of so-called “equal mobility” arises in the context of equilibrium plane-bed bedload transport, and is perhaps less applicable to situations that involve complex lateral and vertical sorting processes or non-equilibrium conditions.

Given the discussions above involving vertical sorting associated with bedform dynamics, then, it cannot be assumed that the tracers accurately represent the transport behavior of the full range of grains sizes in the augmentation gravel. While a statement that the local tracer abundance corresponds to the local abundance of the coarse half of the particle size distribution of the augmentation gravel seems justified, it is entirely possible that the finer gravel sizes in the augmentation material are elsewhere.

Similar considerations apply at Lowden Ranch, except that the stockpile used to supply augmentation material at Lowden is coarser than the material used at the Diversion Pool in 2017. The Lowden stockpile was created during a 2010 channel rehabilitation project at that location. Processing specifications at the time called for a maximum screen diameter of 5 inches. The resulting size distribution had a median particle size of 64 mm and an interdecile range of 32 to 120 mm. Tracer displacements may therefore represent the transport characteristics of the Lowden augmentations somewhat better than they represent the Diversion Pool augmentation. However, due to the larger size of the Lowden stockpile

material, the transport characteristics of the augmentation material may differ from that of the native substrate more than is the case at the Diversion Pool.

Besides being larger due to the larger processing specification in use in 2010, the Lowden stockpile material contains a small percentage of clasts that are unambiguously too large to fit through a 5-inch screen. How these clasts got into the stockpile is not known with certainty, but the most likely explanation is that the contractor that processed the material used a 5-inch grizzly to remove the oversized clasts instead of a screen. A grizzly consist of parallel iron bars set at the specified spacing rather than square holes. Large cobbles and even small boulders can therefore pass a 5-inch grizzly, provided the stone measures less than 5-inches in one direction. The proportion of the Lowden stockpile material represented by these oversize clasts is small, so a typical pebble count analysis is unlikely to detect their presence. Still, the proportion is large enough that by 2016 a noticeable lag deposit of large cobbles and small boulders had accumulated at the upstream Lowden augmentation point. By 2017 the lag had grown to the point that TRRP staff considered it detrimental to the reach and to future gravel augmentation operations (Figure 27), and it was mechanically removed in the spring of 2018.

Figure 27: Lag deposit consisting of cobbles and occasional small boulder at the upstream Lowden Ranch gravel augmentation point after the 2017 flow release.

As of late 2019, approximately 3,000 yd^3 of processed gravel remain at the Lowden stockpile. Any future augmentations with that material will likely develop a similar lag deposit at the point of introduction, unless that material is reprocessed to remove the oversize clasts before placement.

Results of Pool Depth Monitoring

Background

In this section, changes in the depths of 105 pools are examined to assess the possibility that gravel augmentations or other management activities are systematically altering adult salmon holding habitats. As TRRP accelerated its gravel augmentation activities around 2008, certain public stakeholders began to express concerns that gravel additions to the river could result in the filling of some of the deep pools used as holding habitat by adult salmonids. Concern over potential pool filling intensified in late 2010 when a perception became widespread among local fishermen that holes and runs were filling with sediment throughout the river. TRRP addressed this concern by collecting bathymetry in 137 pools or other relatively deep parts of the river over a three-year period spanning 2009-2011 (Gaeuman and Krause 2013). That study showed that the majority of pools in the 40-mile stretch of river between Lewiston Dam and the North Fork Trinity River showed very little change. A small number of pools that had filled substantially were identified, but in nearly all cases the fill was the result of floodplain lowering on the insides of bends at channel rehabilitation sites. Gravel augmentation was found to be responsible for pool filling in just one of the 137 locations considered.

Although many stakeholders accepted the results of Gaeuman and Krause (2013), a small minority continue to believe that pool filling is widespread throughout the river. TRRP therefore suggested that potential changes in pool depths be re-assessed using the river-wide 2016 terrain model and multi-beam sonar data collected in the 2017. Those data are here compared with the river-wide 2011/2012 terrain model that defines the final bed elevations used in the 2013 analysis. As the 2011/2012 bathymetry was collected after the 2011 flow release and prior to the 2012 flow release, it is considered herein to represent 2011 bed elevations. Comparisons between 2011 and 2016 are possible for the full 40 miles of river upstream from the confluence with the North Fork Trinity River, as both terrain models cover that entire distance. In all, depth changes during 2011-2016 are evaluated at 105 pool locations. The 2017 sonar data, however, only covers the first 10 miles downstream from Lewiston Dam, so 2011-2017 and 2016-2017 comparisons are only possible for the 31 pools located within that portion of the river.

Quantifying Changes in Pool Morphology

Net changes in pool morphology between successive surveys can be assessed by changes in the frequency distribution of elevations in selected parts of the landscape. In the case of rivers, it is convenient to express elevations in terms of depths measured from a reference water surface. The advantage of that approach is that a water surface profile represents a sloping datum that effectively removes the longitudinal slope of the channel, making it possible to compare depths statistics drawn from different locations. Topographic changes in pools are summarized herein by year-to-year changes in the 50^{th}-, 75^{th}- 90^{th}- percentile depths (h_{50}, h_{75}, and h_{90}), where depths are measured from winter baseflow water surface elevations observed during a December 2011 LiDAR flight. At the time of the flight, flows ranged from 300 ft^3/s at Lewiston Dam to approximately 450 ft^3/s immediately upstream from the North Fork Trinity River. Use of these depth percentiles to describe pool morphology provides a

means to qualitatively evaluate changes in the overall sizes/volumes of the pools, as well as a means to quantify changes in their actual depths.

Pool Selection

Pools selected for analysis herein were objectively defined using output from a 2016 40-mile hydraulic model developed by Reclamation's Technical Services Center in Denver, CO. That model consists of a numeric mesh that reflects the 2016 channel configuration and 2016 topography (Bradley 2018). The model was run for discharge of 4,000 ft^3/s, and the output water surface elevations were converted to an ArcMap point shapefile. The water surface points were then joined to point files of bed elevations with 2-ft resolution that were extracted from the 2011, 2016, and 2017 terrain models and depths at each elevation point were computed. The next step was to extract only those areas from the depth point files that are at least 8 ft deep and also contain points with depths greater than 10 ft. Those areas were then converted to three sets of polygons, each corresponding to one of the three terrain models. The final step was to merge the sets of polygons to create a new polygon set defining pools only where pools in the original three sets overlap. The final set of 105 polygons are displayed on maps in Appendix D, where the appendix page number corresponds to the map number in Figure 27.

Figure 27: Index showing the longitudinal positions and orientations of maps of pool polygon locations in Appendix D.

The final polygons were assigned names according to local convention, nearby landmarks, or river mile distance from the confluence of the Trinity River with the Klamath River (Table 9). They also are numbered 1 through 105 from upstream to downstream, and assigned nominal water surface elevations based on the modeled 4,000 ft^3/s water surface. About a quarter of the polygons are in locations not considered by Gaeuman and Krause (2013), whereas the remainder are similar to polygons analyzed in that report. The names assigned to particular pool locations often differ from those used in the previous work, so Table 9 includes cross-referencing to polygons defined by Gaeuman and Krause (2013).

Table 9: List of the 105 pool polygons defined for this study with cross-reference to names and polygon ID numbers used by Gaeuman and Krause (2013), abbreviated as G&K(2013).

Polygon 1, Diversion Pool (RM 111.15): Same as in G&K(2013)

Polygon 2, Deadwood Creek Pool (RM 111.030: Same as in G&K(2013)

Polygon 3, New Bridge (RM 110.95): Combined polygons 3 and 4 referred to as Upper and Lower New Bridge in G&K(2013)

Polygon 4, Higgs (RM 110.7): Combined polygons 5 and 6 referred to as Upper and Lower B-2 in G&K(2013)

Polygon 5, Old Bridge (RM 110.2): Same as polygon 7 in G&K(2013)

Polygon 6, Hoadley Bar (RM 109.98): Same as polygon 8 in G&K(2013)

Polygon 7, Hoadley Pool (RM 109.9): Same as polygon 9 in G&K(2013)

Polygon 8, Upper Cemetery Pool (RM 109.47): Same as polygon 11 in G&K(2013)

Polygon 9, Cemetery Hole (RM 109.43): Same as polygon 12 in G&K(2013)

Polygon 10, Sawmill Burner (RM 109): Same as polygon 16 in G&K(2013) but the polygon has been expanded to cover more of the hole.

Polygon 11, Lower Burner (RM 108.9): Combined polygons 17 and 18 referred to as Lower Burner 1 and Lower Burner 2 in G&K(2013)

Polygon 12, Rush Creek Pool (RM 108.1): Same as polygon 21 in G&K(2013)

Polygon 13, Dark Gulch (RM 106.6): Referred to as polygon 25, Gold Bar in G&K(2013)

Polygon 14, Lower Dark Gulch (RM 106.5): Polygon 26, Lower Gold Bar in G&K(2013)

Polygon 15, RM106.25; surveyed 2009, 2011: Same as polygon 27 in G&K(2013)

Polygon 16, Dirty Bird (RM 105.72): Same as polygon 28 in G&K(2013) but the polygon has been expanded.

Polygon 17, Bucktail Island Bkwtr (RM 105.65): Same as polygon 29 in G&K(2013)

Polygon 18, Upper Bucktail Pool (RM 105.45): Same as polygon 30 in G&K(2013)

Polygon 19, Bucktail Hole (RM 105.4): Same as polygon 31 in G&K(2013)

Polygon 20, RM105.15: This is a new polygon not included by G&K(2013)

Polygon 21, Lowden Approach (RM 105.05): Referred to as polygon 33, Upper Lowden in G&K(2013)

Polygon 22, Lowden Bend (RM 104.95): Referred to as polygon 34, Lowden Forced Meander in G&K(2013)

Polygon 23, Lowden Floodplain Convergence (RM 104.65): Same as polygon 35 in G&K(2013)

Polygon 24, RM 104.5: This is a new polygon not included by G&K(2013)

Polygon 25, Wellock Pool (RM 104.3): Same as polygon 36 in G&K(2013)

Polygon 26, SP-Ponderosa (RM 103.85): Same as polygon 40 in G&K(2013)

Polygon 27, Tom Lang (RM 103.2): Same as polygon 42 in G&K(2013)

Polygon 28, RM102.95: Same as polygon 43 in G&K(2013)

Polygon 29, Stott Hole (RM 102.5): Same as polygon 44 in G&K(2013)

Polygon 30, RM102.1: Same as polygon 47 in G&K(2013)

Polygon 31, Society Pool (RM 101.8): Same as polygon 48 in G&K(2013)

Polygon 32, Montana (RM 101.35): Same as polygon 49 in G&K(2013)

Polygon 33, Snell (RM 101.15): Same as polygon 50 in G&K(2013)

Polygon 34, Crosby (RM 101.05): Same as polygon 51 in G&K(2013)

Polygon 35, RM100.85: Same as polygon 52 in G&K(2013)

Polygons 36, Leos (RM 100.6): Combined polygons 53 and 54 referred to as Leos 1 and Leos 2 in G&K(2013)

Polygon 37, Limekiln Trough (RM 100.1): Same as polygon 56 in G&K(2013)

Polygon 38, Lower Limekiln (RM 99.7): Same as polygon 57 in G&K(2013)

Polygon 39, Upper Steel Bridge (RM 99.45): Combined polygons 58 and 59 referred to as RM99.5 and Upper Steel Bridge in G&K(2013)

Polygon 40, RM99.15: Same as polygon 60 in G&K(2013)

Polygon 41, Steel Bridge (RM 98.95): Same as polygon 61 in G&K(2013)

Polygon 42, Steel Bridge Day Use (RM 98.55): Same as polygon 63 in G&K(2013)

Polygon 43, Lower Steel Bridge Day Use (RM98.4): Same location as polygon 64 referred to only by river mile in G&K(2013) but the polygon has been expanded.

Polygon 44, RM97.95: This is a new polygon not included by G&K(2013)

Polygon 45, McIntyre Pool (RM97.35): This is a new polygon not included by G&K(2013)

Polygon 46, Thistle Lane Pool (RM 96.95): This is a new polygon not included by G&K(2013)

Polygon 47, Indian Creek Backwater (RM 95.65): This is a new polygon slightly downstream of polygon 70, Upper Indian Creek Backwater defined by G&K(2013)

Polygon 48, Highway 299 Bridge (RM 94.1): Same as polygon 71 in G&K(2013)

Polygon 49, New DC Pool (RM 93.3): This is a new polygon not included by G&K(2013)

Polygon 50, The Bend (RM 92.95): Combined polygons 73 and 74 referred to as Upper Bend and Lower Bend in G&K(2013)

Polygon 51, Painted Rock (RM 92.7): Same as polygon 75 in G&K(2013)

Polygon 52, DC Campground (RM 92.4): This is a new polygon not included by G&K(2013)

Polygon 53, Upper Alcatraz (RM 92.33): This is the upstream part of as a single larger hole referred to by G&K(2013) as polygon 76, Alcatraz.

Polygon 54, Lower Alcatraz (RM 92.28): This is the downstream part of as a single larger hole referred to by G&K(2013) as polygon 76, Alcatraz.

Polygon 55, Upper Steiner (RM 92): Same location as polygon 79 referred as Lower Steiner by G&K(2013)

Polygon 56, X-factor (RM 91.6): Same as polygon 81 in G&K(2013)

Polygon 57, Skeletor (RM 91.5): Same as polygon 82 in G&K(2013)

Polygon 58, RM94.4: Same as polygon 83 in G&K(2013)

Polygon 59, Picnic Table (RM 91.5): Same as polygon 84 in G&K(2013)

Polygon 60, Chop Tree (RM 90.9): Same as polygon 85 in G&K(2013)

Polygon 61, Dump Hole (RM 90.75): Same as polygon 86 in G&K(2013)

Polygon 62, RM90.2: This is a new polygon not included by G&K(2013)

Polygon 63, Center Pin (RM 89.75): Same as polygon 87 in G&K(2013)

Polygon 64, Goat Hole (RM 89.45): Same as polygon 88 in G&K(2013)

Polygon 65, Goat Corner (RM89.35): This is a new polygon not included by G&K(2013)

Polygon 66, RM89.3: Same as polygon 89 in G&K(2013)

Polygon 67, Dutton (RM 89.15): Same as polygon 90 in G&K(2013)

Polygon 68, RM88.9: This is a new polygon not included by G&K(2013)

Polygon 69, RM88.9: Combined polygons 91 and 92 referred to as RM88.7 and RM88.65 in G&K(2013)

Polygon 70, RM88.4: This is a new polygon not included by G&K(2013)

Polygon 71, RM88.24: Same as polygon 93 in G&K(2013)

Polygon 72, RM88.1: Combined polygons 94 and 95 referred to as RM88.12 and RM88.07 in G&K(2013)

Polygon 73, Browns (RM 87.9): Combined polygons 96, 97, and 98 referred to as Browns 1, 2, and 3 in G&K(2013)

Polygon 74, RM87.5: This is a new polygon not included by G&K(2013)

Polygon 75, Jump Hole (RM87.45): This is a new polygon not included by G&K(2013)

Polygon 76, RM87.55: This is a new polygon not included by G&K(2013)

Polygon 77, Upper Camp (RM87.15): This is a new polygon not included by G&K(2013)

Polygon 78, Lower Camp (RM87): This is a new polygon not included by G&K(2013)

Polygon 79, RM86.9: This is a new polygon not included by G&K(2013)

Polygon 80, RM86.77: This is a new polygon not included by G&K(2013)

Polygon 81, Squatter Hole (RM86.55): This is a new polygon not included by G&K(2013)

Polygon 82, Johnson Point (RM86.45): This is a new polygon not included by G&K(2013)

Polygon 83, Steelhead Alley (RM 85.8): Same location as polygon 102 referred as Dutch by G&K(2013)

Polygons 84, Last Hole on the Left: Same as polygon 103 in G&K(2013)

Polygon 85, Chapman (RM83.2): This is a new polygon not included by G&K(2013)

Polygon 86, Icebox (RM 82.75): Same as polygon 108 in G&K(2013)

Polygon 87, RM82.6: This is a new polygon not included by G&K(2013)

Polygon 88, Eds (RM 82.3): Same as polygon 109 in G&K(2013)

Polygon 89, Sheridan Hole (RM 81.65): Same as polygon 111 in G&K(2013)

Polygon 90 Upper Sky Ranch (RM 80.7): Same location as polygon 114 referred to as Sky Ranch in G&K(2013)

Polygon 91, Lower Sky Ranch (80.45): Same as polygon 115 in G&K(2013)

Polygon 92, UJC 1 (RM 80.2): Same as polygon 116 in G&K(2013)

Polygon 93, UJC 2 (80.15): Same as polygon 117 in G&K(2013)

Polygon 94, Junction City Hole (RM 79.5): Same as polygon 119 in G&K(2013)

Polygon 95, RM78.95: This is a new polygon not included by G&K(2013)

Polygon 96, JC Campground 1 (RM 78.05): Same as polygon 121 in G&K(2013)

Polygon 97, JC Campground 2 (77.97): Same as polygon 122 in G&K(2013)

Polygon 98, McCartneys (RM 77.1): Same as polygon 126 in G&K(2013)

Polygon 99, Upper Bigfoot (RM 75.8): Same as polygon 129 in G&K(2013)

Polygon 100, Valdor (RM 75.05): Same as polygon 130 in G&K(2013)

Polygon 101, Coopers Bar (RM 74.85): Same as polygon 131 in G&K(2013)

Polygon 102, Rip-rap Hole (RM 74.65): Same as polygon 132 in G&K(2013)

Polygon 103, Lime Point (RM 74.5): Same as polygon 133 in G&K(2013)

Polygon 104, RM 73.3: Referred to as polygon 136, Screw Trap in G&K(2013)

Polygon 105, Pear Tree (RM 73.05): Same as polygon 137 in G&K(2013)

Pool depths within the polygons are determined by using the polygons to extract the bed elevations within each pool area from the terrain models. The elevations for each pool and available year combination are output to separate spreadsheets where the nominal water surface elevations assigned to each pool are subtracted from the elevations, yielding a distribution of depths. The median, 75th-percentile, and 90th-percentile depths (h_{50}, h_{75}, h_{90}) for each pool are extracted following Gaeuman and Krause (2013). The depth data are also plotted as cumulative frequency curves to facilitate inter-annual comparisons between depth distributions drawn from the same pool in different years. A complete list of the percentile statistics for all pool-year combinations is presented in Appendix E, and plots of cumulative depth frequency curves for all pools are presented in Appendix F. Changes in pool depth statistics over a time interval are obtained by subtracting the depth percentiles for a later year from the percentiles computed for an earlier year. The resulting quantities are positive for pools that filled and negative for pools that got deeper. The results of that operation are summarized below, and tabulated in full in Appendix G.

Depth Changes by Time Interval

The average changes in h_{50}, h_{75}, and h_{90} between 2011 and 2016 for all 105 pools are slightly negative, but average decreases are much smaller than the standard deviations (Figure 28). One-sample t-tests confirm that none of those decreases are statistically different from zero at the 95% confidence level.

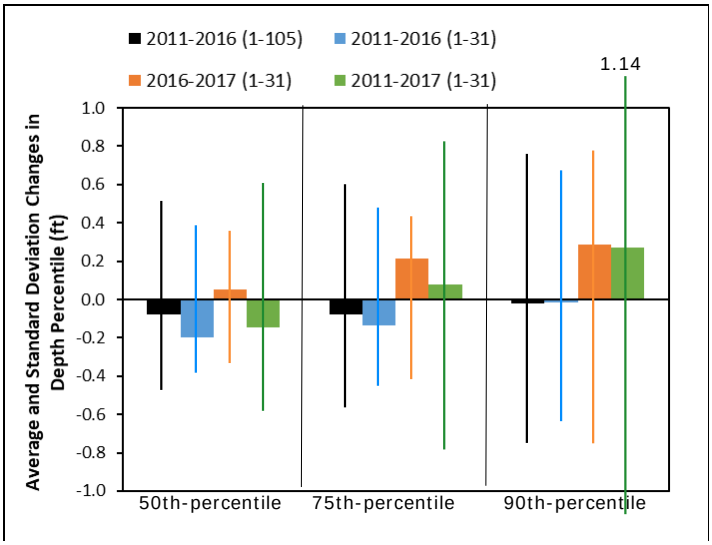

Figure 28: Average changes in h_{50}, h_{75}, and h_{90} for all three time intervals. 2011-2016 averages are presented for all 105 pools and for the subset of 31 pools surveyed in 2017. Columns indicate average changes and colored vertical lines indicate the associated standard deviation.

Although the magnitudes of the depth changes are small, plots of the 2011-2016 data show that negative changes outnumber positive changes by approximately a 3 to 2 ratio (Figure 29). Negative changes in h_{50} and h_{75} are particularly concentrated from river mile (RM) 106.6 to RM100.6. That concentration shows up in Figure 28 as the largest decreases in those two depths percentile recorded for any time interval involving the 31 pools surveyed in the upper 10 miles of river in 2017. The average decrease in h_{50} for those 31 pool in 2011-2016 (-0.2 ft)

is statistically different from zero at the 0.995% confidence level, and the probability that the decrease in the 75-percentile depth is different from zero approaches 0.9. However, changes in 90-percentile depths remain small and statistically insignificant with respect to any probability level. Changes during 2011-2016 in this stretch of river therefore consisted of slight decreases in pool volumes, while maximum depths remained essentially constant.

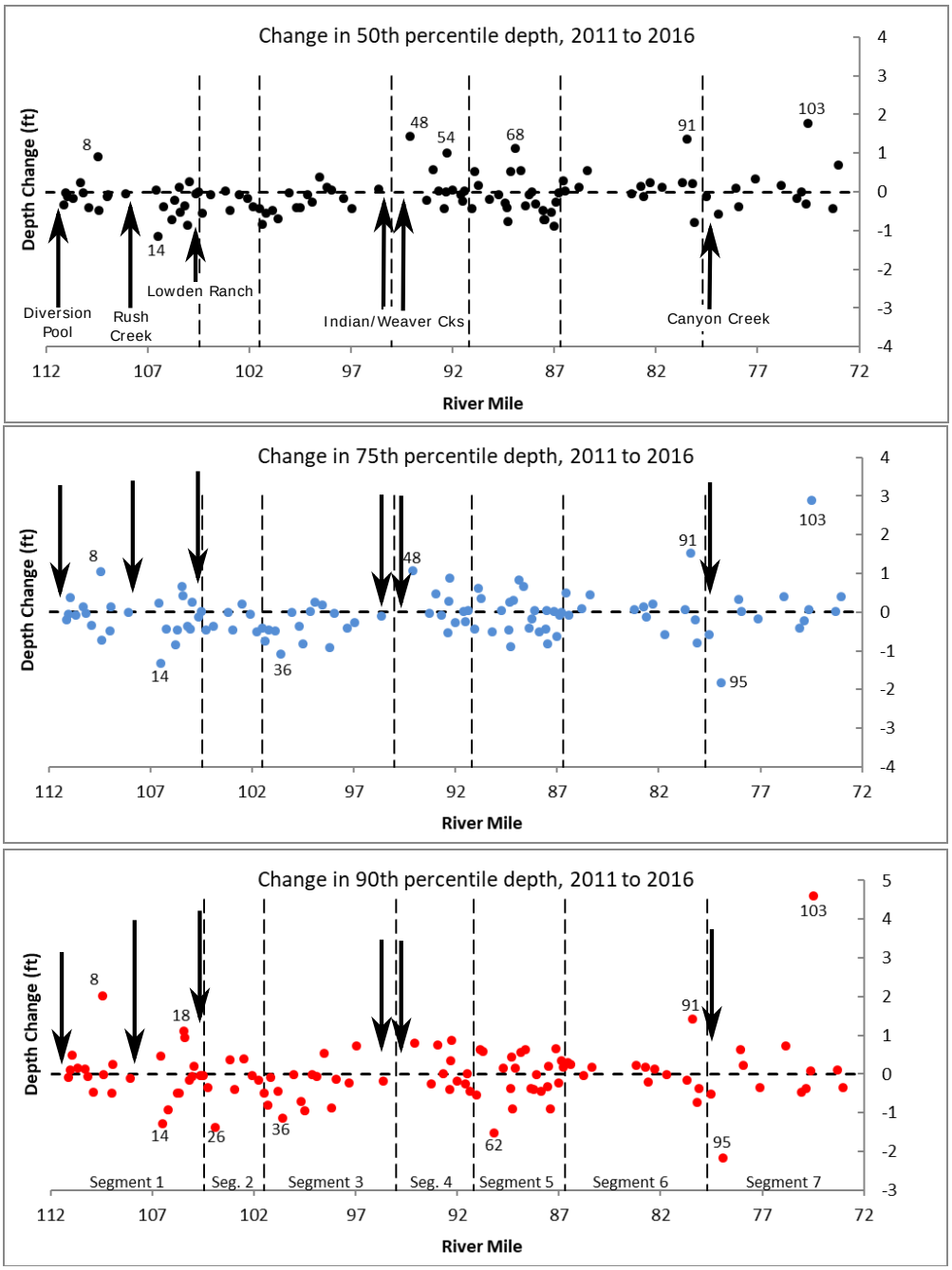

Figure 29: Changes in h_{50}, h_{75}, and h_{90} from 2011 through 2016 in all 105 pools. Data points indicating depth changes greater than 1 ft are labeled with the pool ID number. Arrows identify locations of gravel augmentations and significant tributary sources of gravel (labels in top panel). Labeled stream segments are those discussed by Gaeuman and Krause (2013).

The river miles that encompass the region of mostly negative changes in h_{50} begin at pool 13 (Dark Gulch) and extend downstream to about pool 36 (Leos). Dark Gulch is located immediately downstream from Rush Creek, the first important source of coarse sediment downstream from Lewiston Dam. It is plausible that recent gravel inputs from Rush Creek have contributed to the slight decreases in pool depths observed downstream from its confluence. The region in which pool depths are most likely to have been influenced by Rush Creek extends downstream to the point indicated by the arrow labeled as Lowden Ranch. Downstream from that point, slight decreases in h_{50} during that time interval could potentially also be linked to gravel augmentations at Lowden Ranch.

Pool depths in the upper river rebounded in 2017. Of the 31 pools surveyed that year, h_{50}, h_{75}, and h_{90} increased over their 2016 values in 21, 26, and 22 pools, respectively (Figure 30). The average changes from 2016 to 2017 were positive for in all three depth percentiles (Figure 28), and the magnitudes of the changes in the 75- and 90- percentiles were both large and significantly different from zero at the 0.95 probability level. Consequently, the average net changes in those percentiles over the full study period (2011-2017) for those pools were also positive. The net change in h_{50} remained slightly negative (-0.15 ft), but none of the net changes were statistically different from zero. The strong tendency for pool depths to increase in 2017 can likely be attributed to the large floods that occurred that extremely wet year. An instantaneous peak of 12,000 ft^3/s was released from Lewiston Dam that spring.

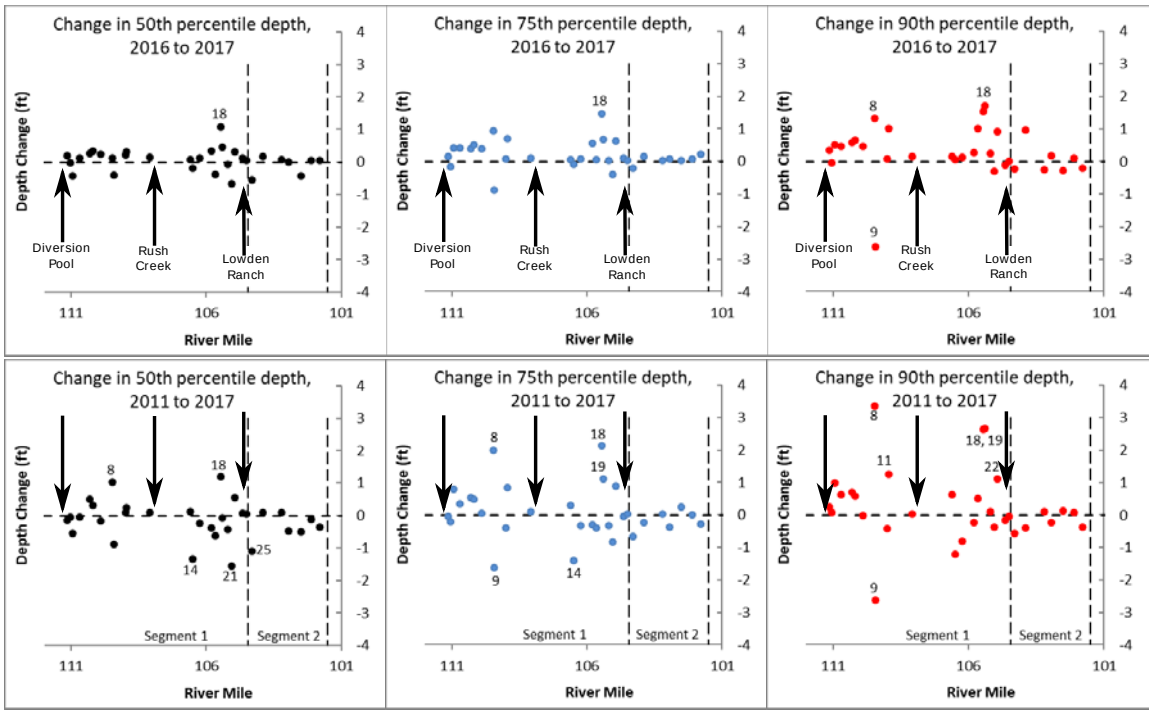

Figure 30: Changes in h_{50}, h_{75}, and h_{90} from 2016 to 2017 and from 2011 through 2017 in the 31 pools surveyed in 2017. Data points indicating depth changes greater than 1 ft are labeled with the pool ID number. Arrows identify the locations of gravel augmentation sites and significant tributary sources of gravel (labels in top panel. Labeled stream segments are those discussed by Gaeuman and Krause (2013).

Outlier pools with changes in depth percentiles greater than 1 ft are flagged in Figure 29 and Figure 30 with their ID numbers. Six of the 11 outliers identified for the 2011-2016 period displayed positive changes. Of the five pools that display a decrease in at least one depth percentile exceeding 1 ft in that time interval, Pool 14, Lower Dark Gulch, is the farthest upstream. With decreases in all three depth percentiles exceeding 1 ft, that pool filled more than any other during that time period. As that pool is nearly 5 miles downstream from the Diversion Pool and separated from it by numerous other pools that showed no tendency to fill, it would be difficult to argue that the changes at Lower Dark Gulch were related to gravel augmentation activities. It is, however, among the first pools downstream from Rush Creek, so deposition there could be related to gravel deliveries from that tributary source. Lower Dark Gulch changed little after 2016, so also appears as an outlier for two of the 2011-2017 depth percentiles.

Pool 26 (SP-Ponderosa) is the next pool downstream with a negative outlier statistic in 2011-2016. Values of h_{50} and h_{75} at SP-Ponderosa showed little change, but the h_{90} decreased by nearly 1.4 ft. In 2016-2017, however, h_{90} increased by about 1 ft, such that all depth statistics for the pool were within 0.4 ft of the 2011 values. The 2017 depth increases in SP-Ponderosa, as well as the general preponderance of increasing depths in most of the pools surveyed in 2017, could be interpreted as circumstantial evidence that causes other than gravel augmentations contributed to the 2011-2016 depth decreases observed downstream from Lowden Ranch. The hypothesis that augmentations were responsible for the slight depth decreases observed in 2011-2016 would seem to require an explanation for why those changes reversed in 2017 despite continued gravel augmentations at Lowden. The next pool with depth decreases exceeding 1 ft in 2011-2016, Pool 36 (Leos), marks the end of the 6-mile stretch of pools that mostly show negative depth changes for that period. All three depth percentiles for Leos declined in 2011-2016, and two of them, h_{75} and h_{90}, decreased by slightly more than 1 ft. No information is available about subsequent changes at Leos, as it is downstream from the section of river surveyed in 2017.

The remaining two pools displaying negative outlier statistics for 2011-2016 are located 15 miles or more downstream from any gravel augmentation activities. Pool 62 (RM90.2) also showed a relatively large decrease in h_{90} of about -1.5 ft, as well as smaller decreases in the other two depth percentiles. That pool is located about 800 ft downstream from the Lower Steiner Flat rehabilitation project that was implemented in 2012. It is therefore possible that Pool 62 received a pulse of bed material eroded from the project site as it adjusted to the high flows after construction. That adjustment would have most likely occurred during the wet winter of 2016. It is also likely that high peak flows during 2017, which reached 13,400 ft^3/s at this location (USGS gage at Douglas City), have since restored the pool to its former depth. Unfortunately, the 2017 data that would be necessary to test that hypothesis is not available in this part of the river. The final pool with fill statistics for 2011-2016 exceeded 1 ft is Pool 95 (RM78.95). That pool is located about a quarter of a mile downstream from Canyon Creek, a major tributary that arguably supplies more bed material to the Trinity River than any other tributary upstream from the North Fork Trinity River. The mouth of Canyon Creek supports a large delta that often spans half the width of the Trinity River

channel (see page D-20, Appendix D). Periodic fill and scour at this location is therefore unsurprising.

Only three pools display depth percentile changes greater than 1 ft for 2016-2017 (Figure 30). Two of those pools, Pool 8 (Upper Cemetery) and Pool 18 (Upper Bucktail) underwent positive changes. Those changes were sufficiently large that those pools also recorded increases of more than 1 ft over the full 2011-2017 study period for all three depth metrics. Only Pool 9 (Cemetery Hole) showed a decrease in a depth metric exceeding 1 ft during 2016-2017, when the h_{90} for the pool decreased by -2.61 ft. That magnitude of decrease is exceeded in this study only by the total decrease in the same percentile for the same pool over the full study period (-2.63 ft). This relatively large change is almost certainly due to hydraulic changes resulting from the Sawmill Rehabilitation Project, implemented in 2009. That project involved the expansion of a side channel that took flow out of the mainstem channel and conveyed it across the floodplain (see page D-2, Appendix D). Cemetery Hole has in fact been filling ever since that project was completed. Gaeuman and Krause (2013) reported decreases in h_{50}, h_{75}, and h_{90} from 2010 to 2011 of -0.48, -0.28, and -0.65 ft, respectively. They also found that limited survey data collected in 2009 prior to implementation of the Sawmill project suggests that depths in Cemetery Hole decreased by an average of -0.55 ft between 2009 and 2010, and attributed these decreases to an increase in the proportion of flood flows bypassing Cemetery Hole after completion of the Sawmill project.

While this account of pool depth changes is focused on instances in which pools filled, it is worth noting that the largest changes detected with this investigation were instances in which pools got deeper. In fact, there are five instances of pool depth percentiles larger than the maximum negative change noted in the previous paragraph. Pools 18 and 19, Upper Bucktail and Bucktail Hole, each slightly exceeded the maximum observed depth decrease with increases in their h_{90} values for 2011-2017 of 2.65 and 2.66 ft, respectively. The net increase in h_{90} for the same period in Pool 8, Upper Cemetery, was considerably larger at 3.36 ft. But the largest depth increase was observed in Pool 103, Lime Point, where the increase in h_{90} between 2011 and 2016 attained 4.61 ft and the increase in h_{75} for the same period registered a comparatively pedestrian 2.88 ft.

Conclusions

Topographic monitoring indicates that gravel augmentations at the upstream Lowden Ranch and Diversion Pool augmentation points in 2016 resulted large gravel storage increases in the first analysis zones downstream. This was especially true in the Lewiston Bridges reach downstream from the Diversion Pool, where the apparent gravel storage increase in analysis zone LB1 was approximately equal to the gravel augmentation volume. In LR3, the first analysis zone downstream from the upstream Lowden Ranch augmentation point, the storage increase in 2016 was equivalent to 32% of the augmentation volume.

The 2017 release, which reached a peak discharge 20% larger than the 2016 peak, was more effective for distributing the 2017 gravel augmentations downstream, as shown by decreases in gravel storage in both LB1 and LR3 that year. A particularly striking mobility increase in LB1 in 2017 may have been partially due to the use of augmentation material processed with a 4-inch screen, rather than a 5-inch screen as was the case with the other augmentations discussed in this report. Gravel storage continued to increase, however, in the next analysis zones downstream in both study reaches. In addition, gravel storage increased in LR7, the analysis zone that received the 2017 gravel augmentation at the downstream Lowden Ranch augmentation point. The storage increase in LR7 was equivalent to 39% of the downstream Lowden Ranch augmentation volume. The impact of the downstream augmentation on the Lowden Ranch gravel budget is nonetheless difficult to assess because storage increased in six consecutive zones from LR4 through LR9. Storage increases in the three zones downstream from the downstream Lowden Ranch augmentation, LR7 through LR9, amounted to a total volume equal to 90% of that augmentation.

Gravel fluxes through the Lowden Ranch/THG reach were much greater in 2017 than in 2016, in keeping with the larger peak discharge released in 2017. The total 2017 gravel flux measured at the TRGVC bedload sampling transect was 2.7 times larger than the 2016 gravel flux. A simple rating curve analysis with an assumed discharge threshold for significant gravel transport of 4,500 ft^3/s and exponent values ranging from 2 to 4 (Gaeuman et al. 2018) indicates that this increase is roughly in proportion to the magnitude of the flood event. Similar magnitudes of increase were found for the flux entering the reach at LR1, which increased by a factor of 2.8 over the 2016 flux, and the flux exiting LR5, which increased by a factor of 2.15. Overall, 2017 gravel fluxes estimated at analysis zone boundaries throughout the Lowden Ranch/THG reach were generally about double the 2017 gravel fluxes estimated at analysis zone boundaries in the Lewiston Bridges reach. Gravel fluxes for 2016 are available for the Lewiston Bridge reach only at the TRAL bedload sampling transect. The 2017 flux at that location was just 50% greater than the 2016 flux, a difference that according to a constant rating curve analysis is about half as great as would be expected from the larger flood peak in 2017.

Where available, estimated gravel fluxes do not necessarily correspond to the magnitude of net topographic change, as quantified by changes in gravel storage (ΔV_b), or to gross absolute change, as quantified by gravel activity (G_i). Local sections of the river can transmit large gravel fluxes (F_i) with or without large ΔV_b or large G_i. River sections in which F_i is large but ΔV_b and G_i are small can be thought of as transport regions that transmit bedload

downstream with minimal interaction within the reach. Large values of F_i coupled with large G_i define response regions with high rates of exchange between the bedload and the streambed. Large G_i can also appear where computed values of F_i are relatively small if the exchanges quantified by G_i are confined to a region small enough that it does not intersect a boundary where F_i is computed. Large positive values of ΔV_b define sediment sinks that sequester bedload for variable lengths of time, whereas large negative values of ΔV_b define sediment source areas. In both the Lewiston Bridges and Lowden Ranch/THG reaches of the Trinity River, analysis zones immediately downstream from gravel augmentation point appear to alternate between functioning as sediment sinks and sediment sources. Downstream from those zones, both reaches display a response region consisting of one or two zones in which G_i is high but absolute values of ΔV_b are low to moderate. G_i is especially high relative to ΔV_b in areas that contain migrating bedforms. Both reaches also feature transport regions that begin four analysis zones downstream from the gravel augmentation points and span multiple zones.

PIT-tagged tracer stones introduced during the 2016 flow release imply shorter transport distances than do the gravel fluxes derived from morphology-based gravel budgets. Short tracer transport distances downstream from the Diversion Pool in 2016 are in agreement with the large increase in gravel storage computed for analysis zones LB1 and LB2, but most of the increase occurred in LB2, whereas most of the tracers remained in LB1. In 2017, the Lewiston Bridges gravel budget indicated a gravel flux into LB3 larger than the entire volume of the 2016 gravel augmentation, but less than one-half of one percent of the tracers reached LB3. At Lowden Ranch, the volume of the 2016 gravel augmentation accounted for 75% of the gravel flux out of analysis zone LR3 where the augmentation was introduced into the river, but only 22% of the tracers it contained passed out of that zone. A large proportion of the tracers in LR3 moved into LR4 during the 2017 release, but a disproportionate number of then remained in LR4 relative to the large gravel fluxes that continued into LR5 that year.

The relatively short travel distances of the tracers implies extensive mass exchanges between the augmented gravel that contained them and the pre-existing substrate. Rapid introduction of augmentation gravel into the channel can potentially lead to topographic steering that causes scour elsewhere or lead to deposition of augmentation material in elevated areas. Vertical sorting processes, especially those associated with bedform migration, can bury coarser fractions of the augmentation material below the active substrate layer. The degree to which tracer displacements represent the transport characteristics of the augmentation material, as opposed to just its coarser fractions, remains unresolved.

An evaluation of 105 pools in the Trinity River between Lewiston Dam and the North Fork Trinity River showed essentially no change in pool depths or volumes from 2011 through 2016. A slight decrease in pool volumes during that period was detected among 31 pools within 10 miles of Lewiston Dam, but those same pools increased in both depth and volume the following year (2016 to 2017), resulting in small but statistically insignificant increase in the 75^{th}- and 90^{th}-percentile depths for the full study period (2011 through 2017). Several pools showed changes in at least one depth percentile that exceeded 1 ft, but more than half of those changes involved depth increases, as did the largest change magnitudes. Only three pools showed sustained decreases in multiple depth percentiles exceeding 1 ft. Two of those

pools are located immediately downstream from large tributary sources of coarse sediment (Rush Creek and Canyon Creek), whereas the cause of fill in the third pool is unclear. Overall, there is little evidence to suggest that pools are systematically filling or that gravel augmentation plays an important role in pool evolution.

Recommendations

The results of the gravel augmentation monitoring described in this report indicate that the augmented gravel propagates downstream slowly. It is therefore recommend that the TRRP immediately begin work to identify additional augmentation sites and obtain the environmental permitting necessary to implement augmentations at those sites. Varying the locations of gravel augmentations from year to year would promote local geomorphic change and increase gravel dispersion, which would likely produce greater habitat benefits over longer stretches of the river. It would also reduce the risk of local habitat simplification associated with the oversupply of gravel to a limited area, as has been suggested in related studies.

The current evidence suggests that the mobility of augmented gravel is low relative to the mobility of the existing substrate, as inferred from total gravel fluxes into and through the study reaches. The use of augmentation material processed with a maximum screen size of 4 inches, rather than material processed with a 5-inch screen, is recommended. Studies to evaluate the degree to which augmentation materials are sorted into mobile fractions that join the downstream gravel flux and immobile fractions that go into long-term storage are needed to better understand interactions between the augmented gravel and the bedload in transport. One such study would consist of comparing bulk substrate samples obtained from mobile versus fixed bedforms and surface pebble counts obtained in those areas, as well as in bedform troughs.

Gravel stockpiled at Lowden Ranch contains a small but important fraction of oversized cobbles that resulted in the formation of a coarse lag deposit at the upstream Lowden Ranch augmentation site. Reprocessing that material to remove coarse lag before future placement in the river is proposed.

Bedload transport sampling near gravel augmentation monitoring sites supports the development of morphology-based gravel budgets that include estimated gravel fluxes throughout the study reaches. It should be considered a key component of all future efforts to monitor the fate of augmented gravel and its effects on downstream morphology.

References

Ashmore, P.E. and M.A. Church. 1998. Sediment transport and river morphology: A paradigm for study, in *Gravel-bed Rivers in the Environment*, edited by P.C. Klingeman, R.L. Beschta, P.D. Komar and J.B. Bradley, Water Resources Publications, LLC. Highlands Ranch, CO, pp 115-148.

Armanini, A. and G. Di Silvio. 1988. A one-dimensional model for the transport of a sediment mixture in non-equilibrium conditions. *Journal of Hydraulic Research,* 26:275-292.

Arnaud, F., H. Piegay, L. Vaudor, L. Bultingaire, and G. Fantino. 2015. Technical specifications of low-frequency radio identification bedload tracking from field experiments: Differences in antennas, tags, and operators. *Geomorphology,* 238, 37-46

Bartley, R. and Rutherfurd, I. 2005. Measuring the reach-scale geomorphic diversity of streams: application to a stream disturbed by a sediment slug. *River Research and Applications*, 21:39-59.

Blom, A. and G. Parker. 2004. Vertical sorting and the morphodynamics of bed form-dominated rivers: A modeling framework. *Journal of Geophysical Research*, 109, F02007, doi:10.1029/2003JF000069.

Blom, A., J.S. Ribberink, and H.J. de Vriend. 2003. Vertical sorting in bed forms: Flume experiments with a natural and trimodal sediment mixture. *Water Resources Research,* 39(2), 1025, doi:10.1029/2001WR1088.

Bradley, D.N. and G.E. Tucker. 2012. Measuring gravel transport and dispersion in a mountain river using passive radio tracers. *Earth Surface Processes and Landforms,* (2012) doi:10.1002/esp.3223.

Bradley, D.N. 2017. Direct observation of heavy-tailed storage times of bed load tracer particles causing anomalous superdiffusion. *Geophysical Research Letters*, 44, 12,227-12,235,doi:10.1002/2017GL075045.

Bradley, D.N. 2018. *Trinity River 40 mile hydraulic model: update with 2016 Topography*. USBR Technical Services Center, Technical Report SRH-2018-11, Denver, CO, http://www.trrp.net/library/document/?id=2359.

Church, M. 1995. Geomorphic response to river flow regulation: Case studies and time-scales. *Regulated Rivers: Research and Management,* 11:3-22.

DeVries, P. 2002. Bedload layer thickness and disturbance depth in gravel bed streams. *Journal of Hydraulic Engineering,* 128(11):983-991.

Gaeuman, D. 2011. *Water year 2010 implementation monitoring report*. Trinity River Restoration Program Technical Report TR-TRRP-2011-1, Weaverville, CA, http://www.trrp.net/library/document/?id=1811.

Gaeuman, D. 2013. *Monitoring the effectiveness of gravel augmentations for Salmonid habitat improvement downstream from dams.* US Bureau of Reclamation Science and Technology Project Completion Report, Project 0295, USBR Technical Services Center, Denver, CO, https://www.usbr.gov/research/projects/detail.cfm?id=295

Gaeuman, D., 2014a. High-flow gravel injection for constructing designed in-channel features. *River Research and Applications,* doi:10.1002/rra.2662.

Gaeuman, D. 2014b. *Analyses to support gravel augmentation recommendations for the Trinity River, California*. Trinity River Restoration Program Technical Report TR-TRRP-2014-1, Weaverville, CA, http://www.trrp.net/library/document/?id=2197.

Gaeuman, D. and Boyce, J. 2018. Effects of gravel supply on gravel bar morphology and physical habitat in a reach of the Trinity River, California, USA, *Proceedings of the 12th International Symposium on Ecohydraulics,* Aug. 19-24, 2018, Tokyo, Japan.

Gaeuman, D. and A. Krause, 2013. *Assessment of pool depth changes in the Trinity River between Lewiston Dam and the North Fork Trinity River*. Trinity River Restoration Program Technical Report TR-TRRP-2013-1, Weaverville, CA, http://www.trrp.net/library/document/?id=2110.

Gaeuman, D., A. Martin, and N.A. Som, 2019. Effect of increasing bed material storage on bed relief and rearing habitat in a reach of the Trinity River, California. *SEDHYD 2019, Proceedings of the Federal Interagency Sedimentation and Hydrologic Modeling Conference*, June 24-28, Reno NV.

Gaeuman, D., B. Schmandt, and R.L. Stewart. 2016b. *Seismic monitoring of bedload transport in a large gravel-bed river*, US Bureau of Reclamation, Denver, CO. Science and Technology Program Project No. 5561 Completion Report, ST-2016-5561-1, https://www.usbr.gov/research/projects/detail.cfm?id=5561.

Gaeuman, D., J.C. Schmidt, and P.R. Wilcock. 2003. Evaluation of in-channel gravel storage with morphology-based gravel budgets developed from planimetric data. *Journal of Geophysical Research* 108(F1), 6001, doi:10.1029/2002JF000002.

Gaeuman, D. and R.L. Stewart. 2019. WY2015 Trinity River gravel augmentation implementation monitoring, Trinity River Restoration Program Technical Report, TR-TRRP-2019-2, Weaverville, CA, http://www.trrp.net/library/document?id=2357..

Gaeuman, D., R.L. Stewart, and T. Buxton. 2016a. First steps toward a river corridor management strategy, Trinity River Restoration Program Technical Report TR-TRRP-2016-1, Weaverville, CA, http://www.trrp.net/library/document/?id=2294.

Gaeuman, D., R.L. Stewart, and S. Pittman. 2018. Toward the prediction of bed load rating curve parameter values: The influence of scale, particle size, and entrainment threshold, *Water Resources Research,* 54, 3313-3334, doi:10.1002/2017WR021627.

Gaeuman, D., R.L. Stewart, and C. Pryor. 2017. Geomorphic response to gravel augmentation and high-flow dam release in the Trinity River, California. *Earth Surface Processes and Landforms,* 42:2523-2540, doi:10.1002/esp.4191.

GMA (GMA Hydrology). 2016. *2015 Diversion Pool survey report*, Report to the Trinity River Restoration Program, Weaverville, CA.

GMA (GMA Hydrology). 2017a. *Lowden Meadows repeat bathymetry survey report*. Report to the Trinity River Restoration Program, Weaverville, CA.

GMA (GMA Hydrology). 2017b. *2016 Trinity River focal reach survey report*. Report to the Trinity River Restoration Program, Weaverville, CA, http://www.trrp.net/library/document?id=2389.

GMA (GMA Hydrology). 2018. *2017 Trinity River sediment transport monitoring report*. Report to the Trinity River Restoration Program, Weaverville, CA, http://www.trrp.net/library/document?id=2361.

Grams, P.E., D.J. Topping, J.C. Schmidt, J.E. Hazel, Jr., and M. Kaplinski. 2013. Linking morphodynamic response with sediment mass balance on the Colorado River in Marble Canyon: Issues of scale, geomorphic setting, and sampling design. *Journal of Geophysical Research,* 118(2):361-381, doi:10.1002/jgrf.20050.

Ham, D.G. and M. Church. 2000. Bed-material transport estimated from channel morphodynamics: Chilliwack River, British Columbia. *Earth Surface Processes and Landforms*, 25:1123-1142.

Hamilton, L.C., 1990. *Modern data analysis: a first course in applied statistics*. Brooks/Cole Publishing Company, Belmont, CA, 684 pp.

Hoey, T.B. and R.I. Ferguson. 1994. Numerical simulation of downstream fining by selective transport in gravel bed rivers: Model development and illustration. *Water Resources Research,* 30:2251-2260.

Humphries, R., J.G. Venditti, and L.S. Sklar. 2012. Experimental evidence for the effect of hydrographs on sediment pulse dynamics in gravel-bedded rivers. *Water Resources Research,* 48(1), doi:10.1029/2011WR010419.

Kondolf, G.M. and P.R. Wilcock, 1996. The flushing flow problem: Defining and evaluating objectives. *Water Resources Research,* 32:2589-2599.

Krause, A.F. 2012. History of mechanical sediment augmentation and extraction on the Trinity River, California, 1912-2011. Trinity River Restoration Program Technical Report. TR-TRRP-2012-2, Weaverville, CA.

Lane, S.N., Westaway, R.M. and Hicks, D.M. 2003. Estimation of erosion and deposition volumes in a large, gravel-bed, braided river using synoptic remote sensing. *Earth Surface Processes and Landforms* 28:249-271.

Liébault, F., H. Bellot, M. Chapuis, S. Klotz, and M. Deschâtres (2012), Bedload tracing in a high-sediment-load mountain stream, *Earth Surface Processes and Landforms*, 37, 385-399.

Lisle, T.E. 1982. Effects of aggradation and degradation on riffle-pool morphology in natural gravel channels, Northwestern California. *Water Resources Research,* 18:1643–1651.

Lisle, T.E., Iseya, F. and Ikeda, H. 1993, "Response of a channel with alternate bars to a decrease in supply of mixed-size bed load: a flume experiment," *Water Resources Research*, 29(11):3623-3629.

Lisle, T. E., J. E. Pizzuto, H. Ikeda, F. Iseya, and Y. Kodama. 1997. Evolution of a sediment wave in an experimental channel. *Water Resources Research,* 33:1971-1981.

Madej, M.A. 1999. Temporal and spatial variability in thalweg profiles of a gravel-bed river. *Earth Surface Processes and Landforms,* 24(12):1153-1169.

Madej, M.A. and V. Ozaki. 2006. Channel response to sediment wave propagation and movement, Redwood Creek, California, USA. *Earth Surface Processes and Landforms,* 21:911-927.

Madej, M.A. and V. Ozaki. 2009. Persistence of effects of high sediment loading in a salmon-bearing river, northern California, in L.A. James, S.L. Rathburn, and G.R. Whittecar, eds., *Management and restoration of fluvial systems with broad historical changes and human impacts*: Geological Society of America Special Paper 451, pp. 43-55.

Marineau, M.D., S.A. Wright, and D. Gaeuman. 2016. Calibration of sediment-generated noise measured using hydrophones to bedload sediment in the Trinity River, California. *River Flows 2016: Proceedings of the 8th International Conference on Fluvial Hydraulics*, St. Louis, MO.

McLean, S. R., J. M. Nelson, and S. R. Wolfe. 1994. Turbulence structure over two-dimensional bed forms: Implications for sediment transport. *Journal of Geophysical Research,* 99:12729– 12747.

Milhous, R.T. 1998. Modelling of instream flow needs: The link between sediment and aquatic habitat. *Regulated Rivers: Research and Management,* 14:79-94.

Ock, G., D. Gaeuman, J. McSloy, and G.M. Kondolf. 2015. Ecological functions of restored gravel bars, the Trinity River, California. *Ecological Engineering*, 83:49-60.

Olinde, L. and J.P.L. Johnson (2015), Using RFID and accelerometer-embedded tracers to measure probabilities of bed load transport, step lengths, and rest times in a mountain stream. *Water Resources Research*, 51, 7572-7589, doi:10.1002/2014WR016120.

Pace, K.M., D. Tullos, C. Walter, S. Lancaster, and C. Segura. 2016. Sediment pulse behavior following dam removal in gravel-bed rivers. *River Research and Applications*, doi:10.1002/rra.3064.

Parker, G. 1991. Selective sorting and abrasion of river gravel. I. Theory. *Journal of Hydraulic Engineering*, 117:113-149.

Parker, G. 2002. Equal mobility of gravel in streams: The remains of the day. *Water Resources Research*, 38(11), 1264, doi:10.1029/2001WR000669.

Parker, G., P.C. Klingeman, 1982. On why gravel bed streams are paved. *Water Resources Research*, 18(5): 1409-1423.

Petts, G.E. and I. Maddock. 1996. Flow allocation for in-river needs. In *River Restoration*, G.E. Petts and P. Calow, eds. Blackwell Science, London.

Phillips, C.B., R.L. Martin, and D.J. Jerolmack (2013), Impulse framework for unsteady flows reveals superdiffusive bed load transport, *Geophysical Research Letters*, 40, 1328-1333.

Phillips, C.B. and D.J. Jerolmack (2014), Dynamics and mechanics of bed-load tracer particles, *Earth Surface Dynamics*, 2, 513-530.

Rantz, S.E. and others. 1982. Measurement and computation of streamflow, US Geological Survey Water-Supply Paper 2175, 631 pp.

Richter, B.D., J.V. Baumgartner, R. Wigington and D.P. Braun. 1997. How much water does a river need? *Freshwater Biology*, 37:231-249.

Sklar, L.S., J. Fadde, J.G. Venditti, P. Nelson, M.A. Wydzga, Y. Cui, and W.E. Dietrich. 2009. Translation and dispersion of sediment pulses in flume experiments simulating gravel augmentation below dams. *Water Resources Research*, 45, W08439, doi:10.1029/2008WR007346.

Stanford, J.A., J.V. Ward, W.J. Liss, C.A. Frissell, R.N. Williams, J.A. Lichatowich and C.C. Coutant. 1996. A general protocol for restoration of regulated rivers. *Regulated Rivers: Research and Management*, 12:391-413.

Toro-Escobar, C.M., G. Parker, and C. Paola. 1996. Transfer function for the deposition of poorly sorted gravel in response to streambed aggradation. *Journal of Hydraulic Research,* 34:35-53.

USDOI (United States Department of the Interior), 2000. *Record of Decision: Trinity River mainstem fishery restoration final environmental impact statement/environmental impact report*. Washington D.C.

USFWS and HVT (United States Fish and Wildlife Service and Hoopa Valley Tribe), 1999. *Trinity River Flow Evaluation Study*, Report to the Secretary of the Interior, US Department of the Interior, Washington, D.C.

Viparelli, E., D. Gaeuman, P.R. Wilcock, and G. Parker. 2011. A model to predict the evolution of a gravel bed river under an imposed cyclic hydrograph and its application to the Trinity River. *Water Resources. Research*, 47, W02533, doi:10.1029/2010WR009164.

Wilcock, P.R., A. Barta, C.C. Shea, G.M. Kondolf, W.V.G. Matthews, and J. Pitlick. 1996. Observations of flow and sediment entrainment on a large gravel-bed river. *Water Resources Research,* 32(9):2897-2909.

Wilcock, P.R. and J.C. Crowe. 2003. Surface-based transport model for mixed-size sediment. *Journal of Hydraulic Engineering,* 129:120-128.

Wilcock, P.R. and B.W. McArdell. 1993. Surface-based fractional transport rates: mobilization thresholds and partial transport of a sand-gravel sediment. *Water Resources Research,* 29(4):1297-1312.

Wilcock, P.R., and J.B. Southard. 1989. Bed load transport of mixed size sediment: Fractional transport rates, bed forms, and the development of a coarse bed surface layer. *Water Resources Research,* 25:1629-1641.

Williams, G.P. and M.G Wolman. 1984. *Downstream Effects of Dams on Alluvial Rivers*. United States Geological Survey, Professional Paper 1286.

Yarnell S.M., Mount J.F. and Larsen E.W. 2006. The influence of relative sediment supply on riverine habitat heterogeneity. *Geomorphology*, 80:310-324.

Zunka, J.P.P., Tullos, D.D. and Lancaster, S.T. 2015. Effects of sediment pulses on bed relief in bar-pool channels. *Earth Surface Processes and Landforms*, doi:10.1002/esp.3697.

Appendix A: Assessment of Elevation Bias in 2017 Sonar Data

The spatial extents of the 2017 sonar surveys make it possible to evaluate bed elevation changes relative to the 2016 topography over several miles (many km) of channel. Among the analyses performed using these data was a preliminary sediment budget extending from the Diversion Pool gravel injection location to a point immediately upstream from the mouth of Rush Creek. As described in the main body of the report, the river channel is partitioned into a series of analysis zone in which changes in bed material storage (i.e., deposition volumes minus erosion volumes) are quantified. Gravel fluxes measured at the TRAL sediment monitoring location provides an internal boundary condition that, when combined with the storage changes, supports estimation of gravel fluxes across the zone boundaries.

The stretch from the TRAL sediment monitoring transect to Rush Creek spans 2.3 miles (3.7 km). The initial gravel budget developed for this stretch indicates a consistent increase in gravel fluxes with distance downstream from TRAL during the 2017 flow release, reaching a maximum of 13690 ± 5335 tons (12440 ± 4850 Mg) just upstream from Rush Creek. For comparison, the estimated flux at TRAL of 4330 ± 1340 tons (3935 ± 1220 Mg) is less than a third as large. The implied consistent dominance of erosion over such a long reach of river, as well as the 3-fold increase in flux relative to TRAL, was judged to be unlikely. Moreover, the magnitude of the flux at Rush Creek is considered to be nearly impossible given that a large delta at the tributary mouth creates a backwater pool that extends at least 1700 ft (520 m) upstream from the confluence area. The extents and persistence of the Rush Creek pool is such that previous studies conclude that no gravel can pass the pool and recommend excavation of the delta itself to allow coarse bed material to route through the area (USFWS and HVT 1999).

Similarly, an initial 2017 gravel budget developed for the Lowden Ranch reach and carried 3 (4.8 km) miles downstream from the TRGVC sediment monitoring location also indicates a persistent increase in gravel flux with downstream distance. Taken together, these preliminary budget results strongly suggest the presence of a negative bias in the 2017 multibeam sonar survey relative to the 2016 survey, and inspired the following analyses intended to verify the bias and quantify its magnitude.

The potential bias was first evaluated by assessing the apparent change in bed elevations over the full domain covered by the 2017 multibeam data. To reduce the computational load, the elevation change grid developed for 2017-2016 was divided into 6 segments, and the mean bed elevation change (ΔZ) and corresponding gravel volume change (ΔV) within each segment were computed for each (Table A-1). All segments except Salt Flat showed negative values of ΔZ of about 0.1 ± 0.05 ft (0.03 ± 0.015 m). The positive change in the Salt Flat segment of 3742 yd^3 (2860 m^3) is the result of sediment input from Rush Creek, which enters the Trinity River near the upstream end of that segment. Although the 2017 multibeam survey was limited to the thalweg area near the Rush Creek delta, independent terrestrial surveys

performed data was confined to the increase in gravel storage volume detected within the stream channel from the repeat multibeam surveys is similar to the 3096 yd^3 (2366 m^3) of gravel that Gaeuman and Stewart (2017) estimated was removed from the Rush Creek delta that year.

Table A-1: River segments defined for analysis of potential bias magnitude. Grid cells are 4 ft^2 (0.37 m^2) in area. The Lowden/THG, Lewiston Bridges, and Sawmill/Rush Ck Pool segments correspond to reaches defined for detailed sediment budget analyses discussed in the main body of the report.

	Grid Cells	Mean ΔZ (ft)	Mean ΔV (yd^3)
Lewiston Bridges	270580	-0.048	-1933
Cemetery	69079	-0.049	-496
Sawmill/Rush Ck Pool	200199	-0.146	-4319
Salt Flat	150120	0.168	3742
Lowden/THG	225356	-0.057	-1895
Poker Bar	335037	-0.135	-6685
All Segments	1250371	-0.063	-11587
Injection Inputs		0.019	3550
Total, less Inputs		-0.082	

Summing the total volume changes and dividing by the total area yields a mean change in bed elevation for the entire domain surveyed with multibeam sonar in 2017 of −0.063 ft (−0.019 m). Accounting for the volume of gravel injected into the river during the flow release increases this first-order estimate for the negative elevation bias associated with the 2017 multibeam data to −0.082 ft (−0.025 m). Inherent in this bias estimate is the assumption that the difference between the gravel fluxes that entered and exited the analysis domain at its upstream and downstream boundaries was small relative to the volume changes within the domain. For context, the flux of 4330 tons (3935 Mg) estimated for the TRAL sediment sampling is equivalent to about 2690 yd^3 (2056 m^3) of substrate volume, suggesting that the difference between the fluxes entering and exiting the domain is small relative to the total storage change.

A second analysis for estimating the bias magnitude is based on the hypothesis that bed elevation changes occur in active portions of the stream bed, whereas other parts of the bed are essentially inactive and undergo little or no change in bed elevations. This hypothesis is supported by observations that areas with larger versus smaller bed elevation changes tend to appear in discrete patches (Figure A-1), as well as by studies showing that bed material transport is often restricted to distinct lanes within the total channel width (Gaeuman and Pittman 2010; Williams et al. 2015). In areas where elevation change does occur, absolute scour and fill depths will vary spatially from a relatively small value to a local maximum. Because inactive areas, on the other hand, are defined by elevation changes that are consistently near zero, it seems likely that the total area with elevation change near zero will exceed the total areas with elevation changes of any other magnitude. Furthermore, changes near zero occur in patches, whereas changes of non-zero magnitude are often distributed along contours ringing erosional or

depositional features on the elevation-change surface. This implies that the average distance between points of zero change should be smaller than the average distance between points of any other non-zero magnitude.

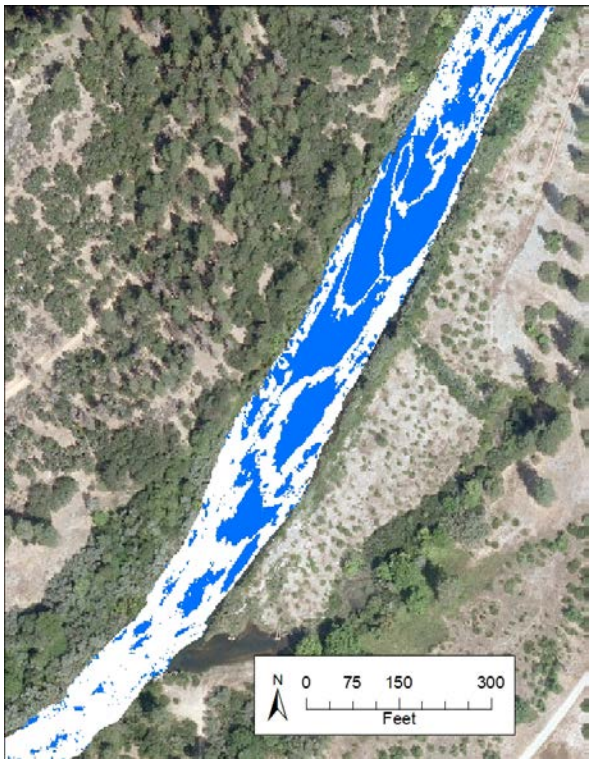

Figure A-1: Portion of the Lowden Ranch reach showing patches of absolute bed elevation change between 2015 and 2016 greater than 0.3 ft (0.09 m) in blue and patches of change less than 0.3 ft (0.09 m) in white.

These expectations were used to evaluate the probable magnitude of bias between the 2016 and 2017 sonar surfaces by applying different bias corrections to the 1.4-mile (2.25 km) section of channel referred to as the Lowden/THG reach in the main body of the report. Bias corrections ranging from −0.2 to 0.3 ft (−0.06 to 0.09 m) were added to the 2017-2016 change surface in increments of 0.05 ft (0.015 m), and the number of grid cells with absolute change magnitudes less than 0.1 ft (0.03 m) for each correction were tabulated. In addition, the average distance between the center of each grid cells and the center of its nearest neighbor was computed (NND). Graphs of both variables as functions of the bias correction have a parabolic form with an apex near the center of the correction range (Figure A-2). The optimal corrections to maximum the cell count and minimize NND were estimated with fitted quadratic functions that yielded optimal correction values of 0.058 ft (0.0176 m) for cell count and 0.059 ft (0.0179 m) for NND. These results indicate that the 2017 sonar surface may be biased low relative to the 2016 surface by about 0.06 ft (0.018 m).

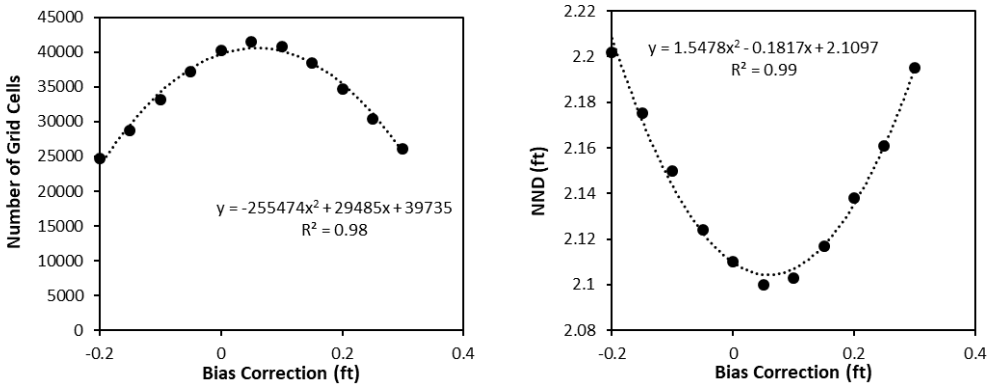

Figure A-2: Graphs of the number of grid cells in the 2017-2016 bed elevation change surface with absolute value less than 0.1 ft (0.03 m) (left) and the average distance to nearest neighbor (NND) (right) as functions of the bias correction applied.

A final assessment of potential bias involved consideration of the bias corrections that would cause the gravel budgets described in the main body of this report to produce unrealistic flux estimates. Experimentation with the gravel budget for the Lowden/THG reach indicated that an assumed negative bias greater than −0.1 ft (0.03 m) would cause the gravel flux upstream from the gravel injection point to exceed the gravel flux a short distance downstream from the into the reach. As this seems highly unlikely, bias exceeding that magnitude were rejected. As decreasing the assumed negative bias to values closer to zero results in an increasing tendency for fluxes to show a consistent increase in the downstream direction, a value of −0.07 ft (0.02 m) was selected as the smallest negative bias that produced believable results. Use of that value results in an output flux out the reach that is 13% larger than input flux at the upstream boundary of the reach.

Similar experimentation with the Diversion Pool gravel budget showed that assumed negative biases greater than −0.15 ft (0.045 m) will produce negative gravel fluxes in the approach to the Rush Creek pool. Decreasing the negative bias rapidly increases the flux through the Rush Creek pool. By the time the bias reaches −0.07 ft (0.02 m) the estimated flux through the pool is 4920 ± 2800 yd^3 (3760 ± 2140 m^3), which was considered unrealistically large. An assumed bias of −0.1 ft (0.03 m), however, reduces the output flux to 3382 ± 2800 yd^3 (2586 ± 2140 m^3). That result seems possible, particularly if one considers the potential for error in the flux measured at the sediment sampling transect. If that measured flux is reduced by 30% in keeping with the uncertainty margins adopted herein for that type of measurement, the output flux through the Rush Creek pool becomes 2576 ± 2672 yd^3 (1969 ± 2043 m^3). That is, the output flux become smaller than the uncertainty in its estimate and potentially very close to zero.

Taken together, the above results indicate that the relative bias between the 2017 and 2016 sonar surfaces is between −0.07 and −0.15 ft (0.02 and 0.045 m). That range is

accommodated with a best estimate of −0.1 ft (0.03 m) supplemented with an uncertainty margin of ± 0.05 ft (0.015 m).

References

Gaeuman, D. and Pittman, S. 2010. Relative contribution of sand and gravel bedload transport to acoustic Doppler bed-velocity magnitudes in the Trinity River, California. In: *Bedload-surrogate monitoring technologies*, J.R. Gray, J.B. Laronne, and J.D.G. Marr, editors, US Geological Survey Scientific Investigations Report 2010-5091, https://pubs.usgs.gov/sir/2010/5091/papers/Gaeuman_Pittman.pdf.

Gaeuman, D. and R.L. Stewart. 2017. *Sediment transport in the Trinity River, CA: Data synthesis 2004-2015*. Trinity River Restoration Program Technical Report. TR-TRRP-2017-1, Weaverville, CA, http://www.trrp.net/library/document/?id=2357.

USFWS and HVT (United States Fish and Wildlife Service and Hoopa Valley Tribe), 1999. *Trinity River Flow Evaluation Study*, Report to the Secretary of the Interior, US Department of the Interior, Washington, D.C.

Williams, R. D., C. D. Rennie, J. Brasington, D. M. Hicks, and D. Vericat. 2015. Linking the spatial distribution of bed load transport to morphological change during high-flow events in a shallow braided river. *J. Geophys. Res. Earth Surf.*, 120, 604–622, doi:10.1002/2014JF003346.

Appendix B: Bedload Sampling Uncertainty

Tests of the variability in sampled coarse bedload transport rates were performed at each of the four sediment sampling locations along the Trinity River during the 2016 and 2017 spring flow releases, for a total of 8 test datasets (GMA 2017; GMA 2018). Each test consisted of 6 to 13 repeated bedload sampler deployments at the same vertical over a 30-minutes period when water discharge (Q) was essentially constant (Table B-1). It should be noted that the term "sampler deployment" means that the sampler was placed on the bed for 30 seconds, and then emptied before the next deployment. This differs from a bedload sample, which in this report refers to a set of deployments at multiple verticals spanning the stream channel and is intended to characterize the transport rate across the full channel width.

Table B-1: Coarse bedload transport rates computed from repeated sampler deployments at the same vertical. Q_b = transport rate of bedload > 8 mm in diameters in tons/day.

2016 Flow Release				2017 Flow Release			
TRAL	TRGVC	TRLG	TRDC	TRAL	TRGVC	TRLG	TRDC
8560 ft^3/s	9655 ft^3/s	9700 ft^3/s	10075 ft^3/s	10700 ft^3/s	6230 ft^3/s	6750 ft^3/s	7550 ft^3/s
Q_b	Q_b	Q_b	Q_b	Q_b	Q_b	Q_b	Q_b
45.00	35.87	73.61	67.24	49.68	49.89	61.42	34.99
56.47	94.22	67.30	80.85	432.95	0.00	21.41	151.87
42.14	83.98	22.00	47.48	258.21	29.39	10.39	32.77
40.09	243.48	71.57	100.87	249.49	0.34	10.47	28.14
20.54	153.48	47.91	42.02	165.81	0.04	10.53	60.17
18.30	234.21	143.94	50.26	271.89	1.26	5.66	43.41
98.66	118.57	49.96	36.15		0.00	7.53	50.29
8.46	180.48	63.69	30.46		0.00	0.62	56.99
48.49	122.43	98.46	26.03			3.95	0.37
23.51	165.94	58.11	32.76			3.64	138.90
			31.68				
			14.66				
			67.99				

The variability in these test datasets does not directly represent the potential uncertainty in bedload fluxes over a flood hydrograph because the number of bedload samples collected over the flood event and the range of discharges sampled are both important factors. The importance of discharge stems from the dependence on bedload variability on transport rate when transport conditions are near the threshold of entrainment. At those low transport rates, the chance capture of a single large gravel clast (or failure to capture a large gravel clast) can result in large differences in sample sizes obtained under identical conditions (Wilcock 1988; Gaeuman et al 2009). The number of samples used to compute a load estimate (n) is also clearly an important variable, since flux estimates computed from a large number of samples are likely to be more accurate than estimates based on just a few samples. To incorporate these factors, the variability in samples sizes within each of the 8 test datasets was characterized by their coefficients of variation, defined as:

$$\sigma_v^* = \sigma_v/\mu_v \quad (1)$$

where σ_v is the standard deviation of sample sizes within an individual test dataset and μ_v is the mean sample size for the dataset. The notation used for the coefficient of variation itself (σ_v^*) reflects that it is equivalent to a dimensionless standard deviation.

Transport intensity when the test datasets were collected is expressed with a dimensionless sediment transport rating curve [Gaeuman et al. 2018]:

$$g_v^* = ((Q_v - Q_c)/ Q_c)^b \quad (2)$$

where Q_v is the discharge when the test samples were obtained, and Q_c and b are rating curve parameters fit to all the bedload samples obtain during that event. Those parameters were fit to the data according to method described by Gaeuman et al. (2018) and Gaeuman et al. (2015). The 8 values of σ_v^* were then plotted as a function of g_v^* and fit with a power function for estimating the expected dimensionless standard deviation for sets of sampler deployments (σ_{ev}^*) as a function of dimensionless transport intensity (Figure B-1):

$$\sigma_{ev}^* = 1.37 g_v^{*-0.259} \quad (3)$$

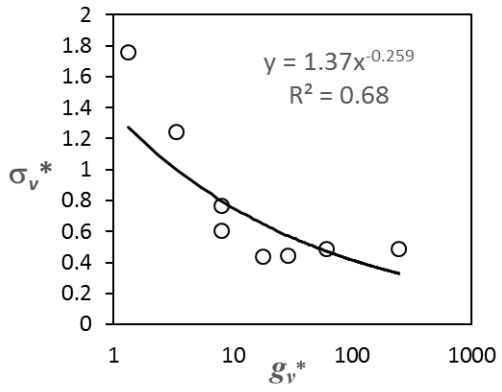

Figure B-1: σ_v^* plotted as a function of g_v^* with power function fit.

Replacing g_v^* in equation (3) with the average dimensionless transport intensities for all n samples collected at each site during each of the two releases (g_μ^*) yields the average variability in sample sizes for each of the 8 sample datasets (σ_{es}^*). The dimensionless standard error of the mean for each of those datasets (E_s^*) is computed as:

$$E_s^* = \sigma_{es}^*/n^{0.5} \quad (4)$$

where n is the number of bedload samples used to estimate the sediment flux. Although each of the 8 sample datasets has unique values of n and and g_μ^*, their respective values of E_s^* are remarkably consistent (Table B-2). Four of the datasets have $E_s^* = 0.11$ and the remaining four have values of 0.05, 0.07, 0.9, and 0.1.

Table B-2: Variables discussed in the text for the sample datasets collected at the four sediment monitoring locations in 2016 and 2017.

	2016 Flow Release				2017 Flow Release			
	TRAL	TRGVC	TRLG	TRDC	TRAL	TRGVC	TRLG	TRDC
Q_c ft³/s	2815	2930	2015	1200	1730	2965	2650	2545
b	2.92	3.46	2.51	2.75	2.5	3.29	2.75	3.09
g_μ*	6.49	9.70	20.12	161.55	49.47	11.57	9.84	25.18
σ_{es}*	0.84	0.76	0.63	0.37	0.50	0.73	0.76	0.59
n	64	53	72	53	21	40	68	39
E_s*	0.11	0.11	0.07	0.05	0.11	0.11	0.09	0.1

Because the *n* bedload samples used to compute loads consist of multiple sampler deployments, the loads are actually computed with a larger "sample" in the statistical sense than is used to compute E_s*. Individual bedload samples in the Trinity River typically consist of about 10 sampler deployments at verticals spaced across the channel width. However, most of the coarse bedload is captured at a few to several verticals where most of the water is conveyed. Sampler deployments in locations with lower conveyance may yield no coarse bedload at all. Rather than attempting to incorporate this added complexity, the distinction between *n* and the number of sampler deployments used in the variability tests is ignored. As defined here, *n* results in a more conservative estimate of E_s*.

References

Gaeuman, D., E. D. Andrews, A. Krause, and W. Smith (2009), Predicting fractional bedload transport rates: Application of the Wilcock-Crowe equations to a regulated gravel-bed river, Water Resour. Res., 45, W06409, doi:10.1029/2008WR007320.

GMA (GMA Hydrology). 2017. *2016 Trinity River sediment transport monitoring report*. Report to the Trinity River Restoration Program, Weaverville, CA, http://www.trrp.net/library/document?id=2361.

GMA (GMA Hydrology). 2018. *2017 Trinity River sediment transport monitoring report*. Report to the Trinity River Restoration Program, Weaverville, CA, http://www.trrp.net/library/document?id=2317.

Wilcock, P. R. (1988), Methods for estimating the critical shear stress of individual fractions in mixed-size sediments, Water Resour. Res., 24, 1127– 1135, doi:10.1029/WR024i007p01127.

Appendix C: Morphodynamic Modeling

The 2017 gravel augmentation at the upstream Lowden Ranch augmentation point was implemented at a much lower discharge than augmentation during previous spring flow releases. The relatively low discharge also made it possible for the gravel to be introduce into the flow much close to the channel thalweg. Morphodynamic modeling was employed to assess the possibility that differences in how the 2017 gravel augmentations were implemented are responsible for some apparent differences in the geomorphic response observed in the reach downstream compared to previous years. Morphodynamic modeling, which simulates sediment erosion, transport and deposition, was performed using the "mobile" module of SRH-2D. The computational mesh developed for this purpose was created using SMS software from Aquaveo. The mesh spans the upstream half of the Lowden/THG gravel budget reach defined in the main body of the report (Figure 1). Mesh elements within the main channel are rectangular with dimensions of approximately 12 by 20 ft (240 ft^2 in area) (3.6 by 6 m (22 m^2 in area)), whereas floodplain areas that become inundated during the model run are triangular and range in area from about 190 to 400 ft^2 (18 to 37 m^2). Mannings *n* was set to 0.03 in the main channel area, 0.045 is floodplain areas with scattered vegetation, and 0.06 in areas with dense riparian vegetation.

Two versions of the pre-release topography were created by mapping slightly different ground elevation to the mesh. For one version, ground elevations were derived from a modified version of the 2017 terrain model that accounts for topographic changes produced from the gravel augmentations performed at the beginning of the 2017 flow release. The bed in the immediate vicinity of the upstream and downstream Lowden Ranch augmentations was resurveyed during the brief period of low flow between the augmentations and the rising limb of the flood. Those new survey data, obtained with a combination of wading with a survey rod and single beam sonar deployed from an inflatable kayak, were mapped to the model mesh in place of the data collected the previous summer. For the other version of the mesh, ground elevations were derived directly from the 2017 terrain model with no modification. Instead, special functionality within SRH-2D was used to simulate a high-flow gravel "injection" similar to the 2016 implementation in which a front-end loader dumped loads of gravel into the flow from the left bank during the peak of the release.

A flow hydrograph simulating the high-flow portion of the 2017 flow release was developed for the model runs. The hydrograph consists of a sequence of 28 steady discharges with durations ranging from 5 to 180 hours and a total duration of 680 hours. Each of the steady flow periods was selected to approximate a portion of the 15-minute instantaneous flow record recorded at the TRGVC gage. A comparison with the 15-minute gage record showed that the modeled hydrograph differs from the gaged instantaneous flows by just 3% on average.

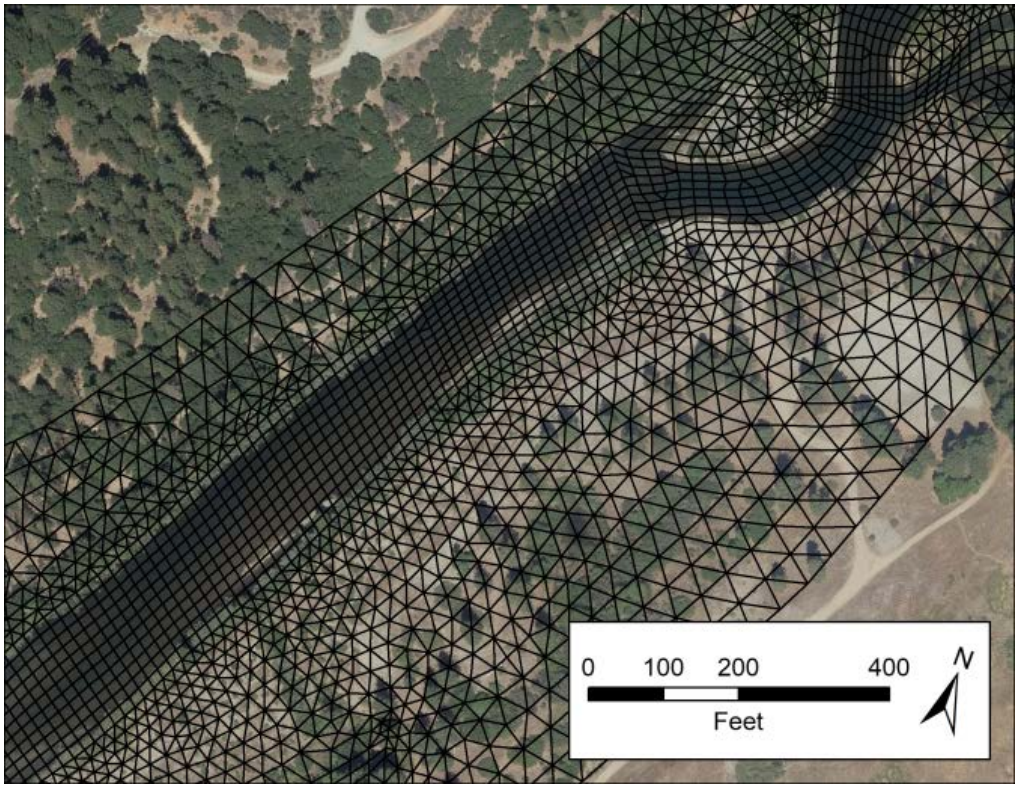

Figure 1: The computational mesh used to perform morphodynamic modeling in the upstream half of the Lowden/THG reach.

The results of any sediment transport model depend heavily on how the sediments involved are defined and the parameters chosen to simulate the transport process. Because the Trinity River is a gravel bed stream with little or no material less than 0.5 mm present in its bed (Wilcock et al. 1996), the sediment sizes available for transport span the following 8 size classes: 0.5-2 mm, 2-4 mm, 4-8 mm, 8-16 mm, 16-32 mm, 32-64 mm, 64-128 mm, and 128-256 mm. Various percentages are then assigned to those size classes to represent the particle size distributions of different components of the systems, such as the composition of the bed surface and subsurface layers. The size distribution of the channel subsurface was estimated as the average distribution of 8 bulk samples collected in 2014 at sites located both upstream and downstream from Lowden Ranch (Figure 2). Coarse-scale surface facies mapping in the field established that surface particle sizes differ in different parts of the Lowden Ranch reach. For practical reasons, the spatial variability in surface particles sizes is represented in the model by just two surface facies. The size distribution of a finer facies with a median particle size near 55 mm was estimated from surface pebble counts collected at the TRGVC sediment monitoring transect. This finer surface distribution was applied to most of the channel area in the upstream part of the model and extending about 1300 ft (400 m) downstream from the upstream gravel augmentation point, including the area where new gravel was injected just prior to the flood peak. The distribution of a coarser facies was developed by visually estimating the median and 90^{th}-percentile particles sizes in relatively coarse areas within the reach and stretching the cumulative distribution associated with finer surface layer to the right to match the larger grain sizes to those percentiles. This coarser

surface distribution was most applicable farther downstream where substrate conditions and previous topographic studies (e.g. Gaeuman et al. 2017) indicate that gravel injected upstream had not yet arrived.

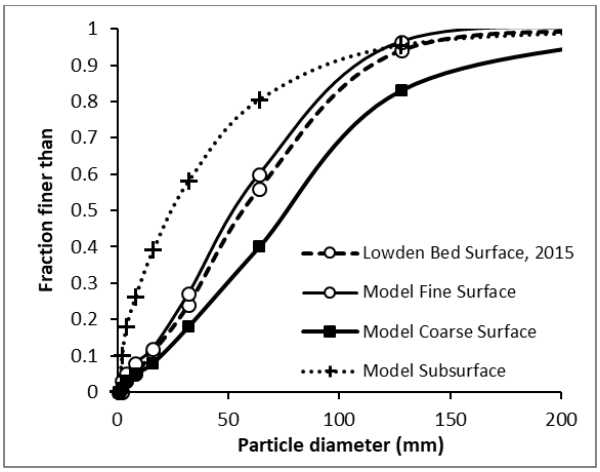

Figure 2: Two modeled surface particle size distributions and the subsurface distribution compared to 2015 pebble count data at Lowden Ranch, shown with the size class breaks used in the model setup.

SRH-2d supports several different sediment transport functions. In this case, the Wilcock-Crowe equations (Wilcock and Crowe 2003) as modified for the Trinity River (Gaeuman et al. 2009) were selected. This set of equations evaluates transport rate for individual size fractions of coarse sediment by estimating the reference shear stress for significant bedload transport for each fraction according to:

$$\frac{\tau_{ri}}{\tau_{rm}} = \left[\frac{D_i}{D_{sm}}\right]^{\frac{0.7}{1+exp\left(1.9-\frac{D_i}{D_{sm}}\right)}} \qquad (3)$$

where τ_{ri} and τ_{rm} are the reference shear stresses for size fraction i and for the mean grain size on the bed surface, respectively, whereas D_i and D_m are those respective grain sizes. The unknown term τ_{rm} is estimated with:

$$\tau_{rm} = [T_1 + (T_2 - T_1)exp(-20F_s)][\rho g R D_{sm}] \qquad (4)$$

where ρ is the density of water, g is gravitational acceleration, R is the submerged specific gravity of the sediment, F_s is the cumulative fraction of relatively fine surface material that directly influences the mobility of the mean particles size, and T_1 and T_2 are adjustable parameters. The value of F_s is controlled by a third user-specified parameter, D_SAND, which represents the particle size defining F_s. Default values of T_1, T_2, and are D_SAND are 0.021, 0.0365, and 2 mm, respectively.

Several options are available for setting the sediment flux at the upstream boundary of the model domain. For this modeling exercise, the upstream boundary flux was set to the

capacity transport rate calculated with the transport function given the substrate composition and channel geometry at the upstream boundary. For this purpose, the bed surface near the upstream boundary was set to the coarser surface particle size distribution and bed elevations were set to have constant values so that channel geometry in the area would remain constant over the course of the model run. Areas outside the main channel throughout the model domain were set to be non-erodible to prevent unrealistic floodplain and bank erosion.

The model was calibrated by comparing the modeled gravel fluxes summed over the flow release with measured fluxes at the TRGVC transect and estimated fluxes at five other analysis zone boundaries. Such comparisons are accomplished by inserting monitoring lines into the model mesh, where water and sediment discharge across a transect is logged throughout the model run. The TRGVC transect corresponds to the downstream boundary of Lowden Ranch analysis zone LR3. Modeled fluxes were also computed at monitoring lines corresponding to the downstream boundaries of analysis zones LR1, LR2, LR4, and LR5, and at the upstream boundary of zone 0 (LR0). Values of T_1, T_2, and D_SAND were then adjusted to 1) exactly match the modeled gravel flux at TRGVC to the measured value, and 2) minimize the differences between the modeled fluxes and the fluxes estimated from gravel storage change results and equations (1a) and (1b). After numerous iterations using the mesh with the modified 2017 topography, an acceptable calibration was obtained with T_1, T_2, and D_SAND values of 0.0228, 0.04, and 8 mm, respectively (Table 1). The same parameters values were applied to the model run incorporating the mesh with unmodified 2017 topography and a simulated gravel injection from the left bank.

	LR0, in	LR1, out	LR2, out	TRGVC	LR4, out	LR5, out
Measured Flux				5213		
Budget Estimate	4868	3835	3889		4602	4314
Calibrated Model	5682	1341	2306	5241	4759	4142
Percent Error	17	−65	−41	<1	4	−4

Table 1: Results of calibration to match the gravel flux measured at TRGVC in 2017 and approximate the fluxes at analysis zone boundaries estimated in the 2017 gravel budget. Fluxes given in yd^3 of bulk substrate.

Both model scenarios were run, and output consisting of depths of erosion or deposition values assigned to each model mesh element were imported into ArcMap as polygon shapefiles. Subtracting the bed-level changes assigned to the in-channel gravel placement scenario from the gravel injection scenario yields the predicted deviation from the injection scenario due to the different placement method. The results of that operation is displayed in Figure 3, which shows that differences exceeding 0.2 ft are limited to the immediate vicinity of the gravel augmentation, as well as around the two island about 1600 ft downstream. In the areas of the augmentations themselves, relative erosion exceeding 2 ft is predicted where the injection would have been placed and relative deposition up to 1 ft is predicted at and upstream from the location where the in-channel stockpile was placed. Differences indicated near the islands reflect the inherent inability of a depth-average two-dimensional model to accurately simulate hydraulics and morphodynamics in a complex channel. The slightly different hydraulic fields entering the island area produce slightly different patterns of

erosion and deposition that further alter the local hydraulic field, creating a feedback loop that accelerates divergence of the numerical solutions.

The essential result of these simulations, however, is that virtually no difference in erosion or deposition is predicted through the straight response reach where the bulk of the gravel placed in 2016 and 2017 deposited. According to these simulations, differences in the gravel placement method at the upper augmentation point did not materially alter geomorphic responses in analysis zones LR3, LR4, and LR5.

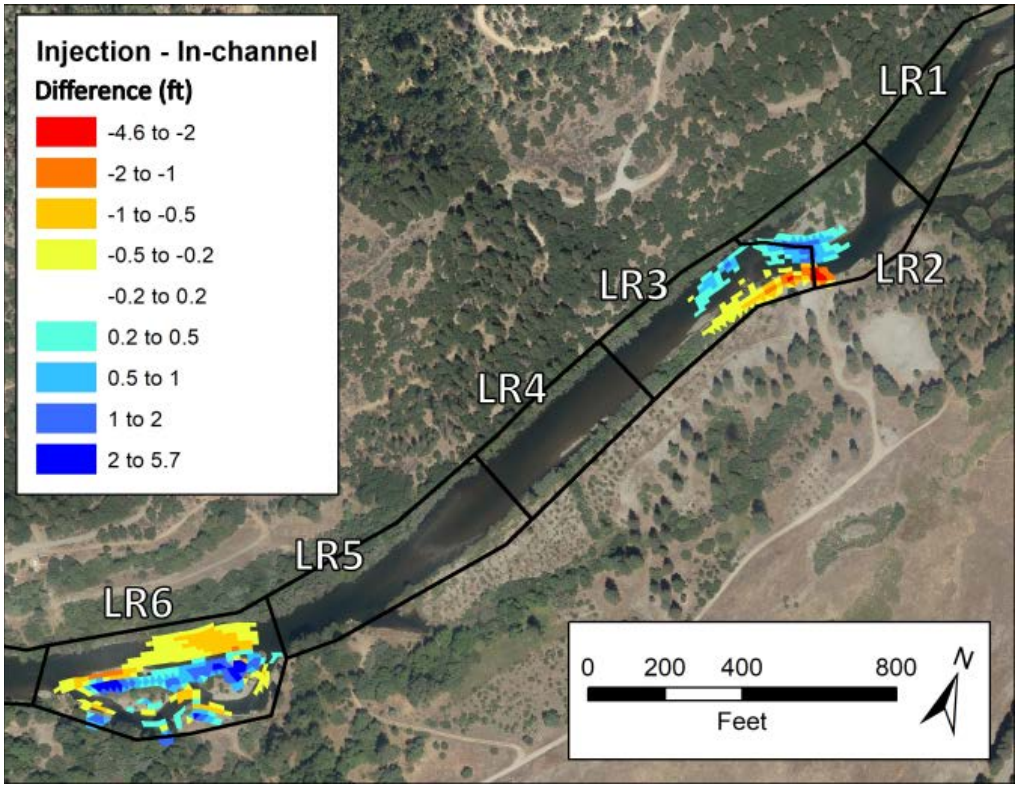

Figure 3: Model output showing the differences in the erosion and deposition values predicted for the model run with high-flow gravel injection and the model run with gravel placed in the channel prior to the flow release.

References

Gaeuman, D., E.D. Andrews, A. Krause and W. Smith. 2009. Predicting fractional bedload transport rates: application of the Wilcock-Crowe equations to a regulated gravel-bed river. *Water Resources Research*, 45, W06409, doi:10.1029/2008WR007320.

Wilcock, P.R. and J.C. Crowe. 2003. Surface-based transport model for mixed-size sediment. *Journal of Hydraulic Engineering*, 129:120-128.

Appendix D: Pool Polygon Location Maps

Locations of analysis polygon use to assess changes in pool depths are shown in yellow on aerial photographs with the polygon ID numbers in black font.

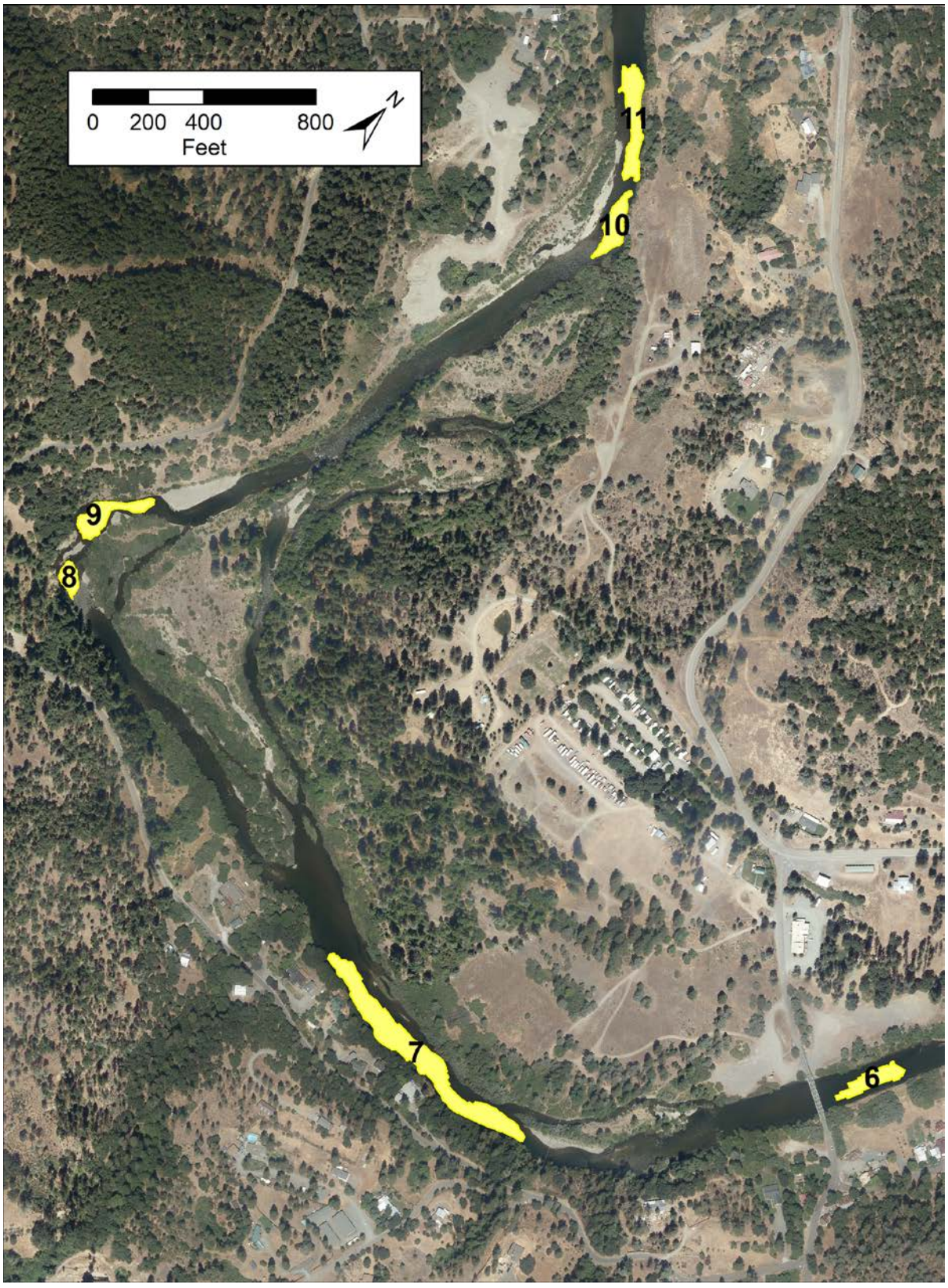
0 200 400 800
Feet
N
11
10
9
8
7
6

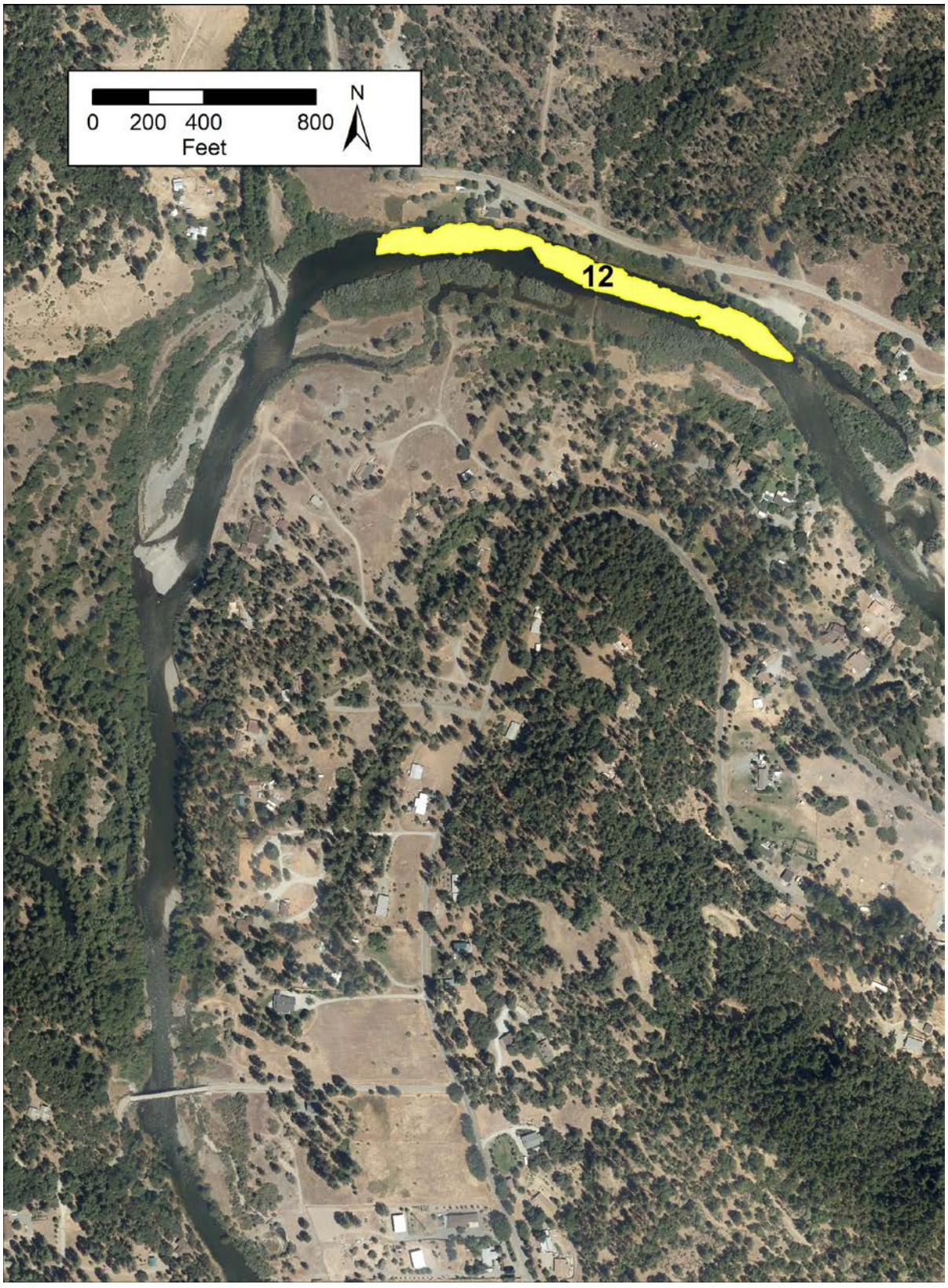
0 200 400 800
Feet
N
12

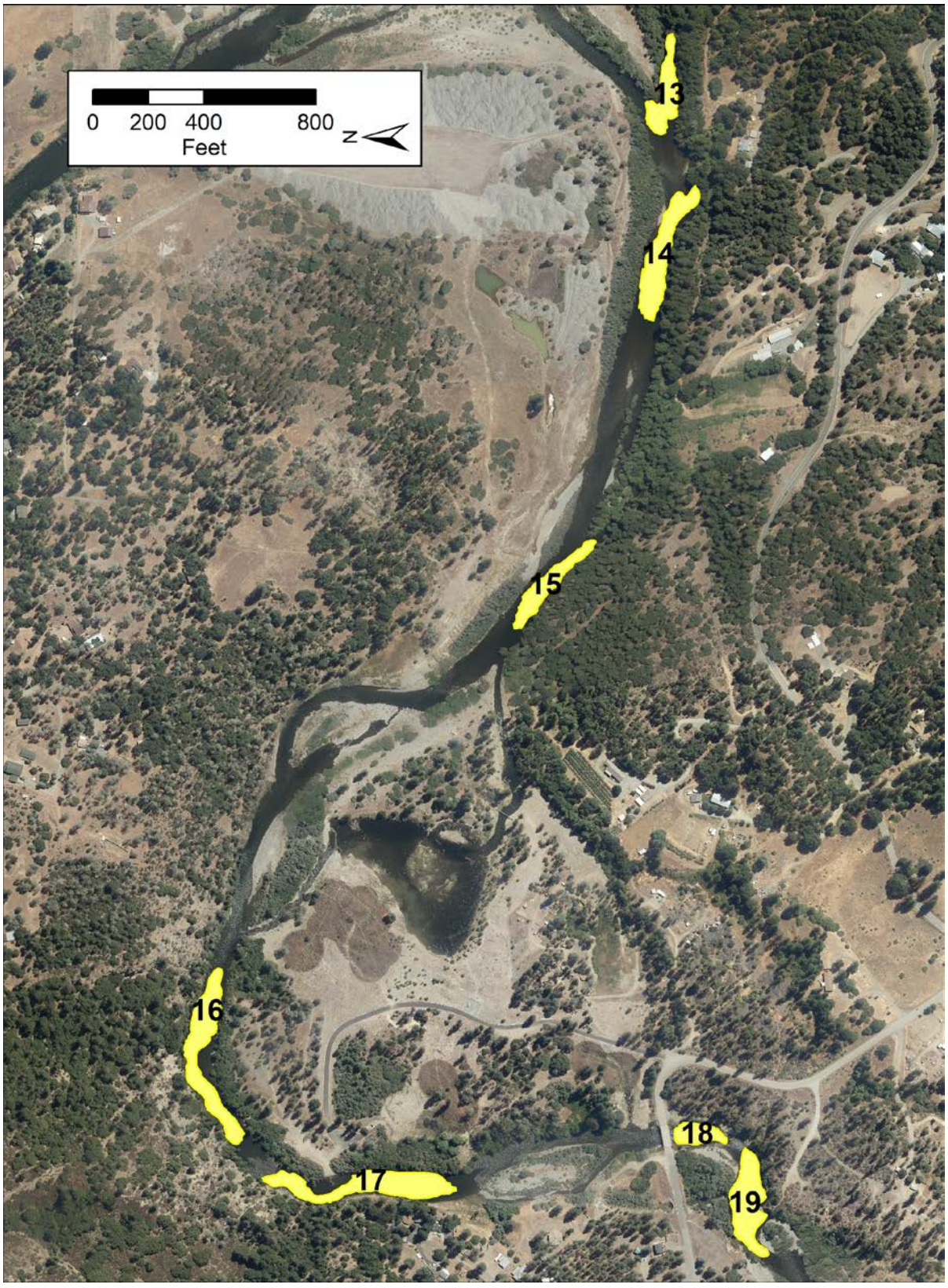
0 200 400 800
Feet
N
13
14
15
16
17
18
19

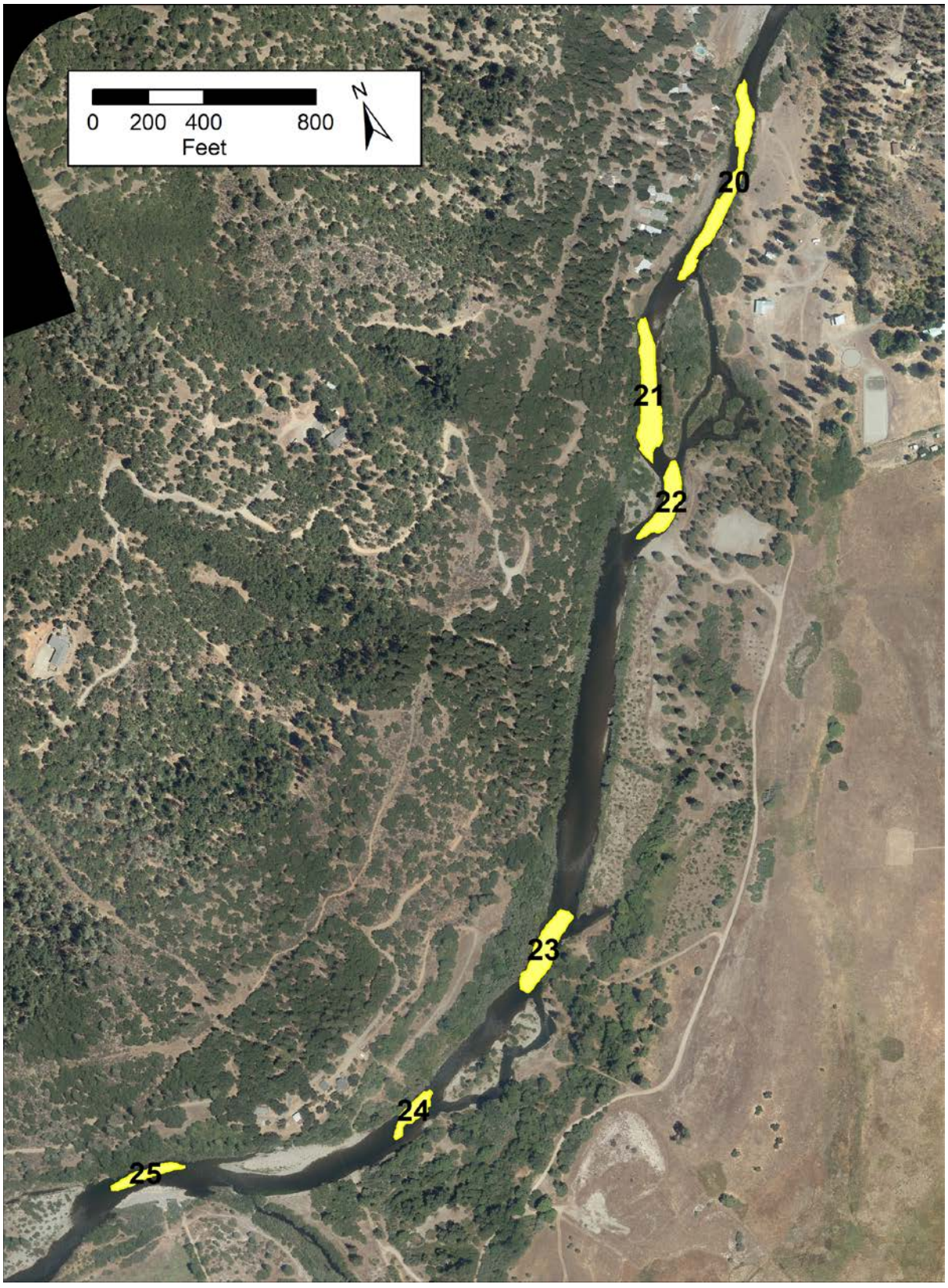
0 200 400 800
Feet
N
20
21
22
23
24
25

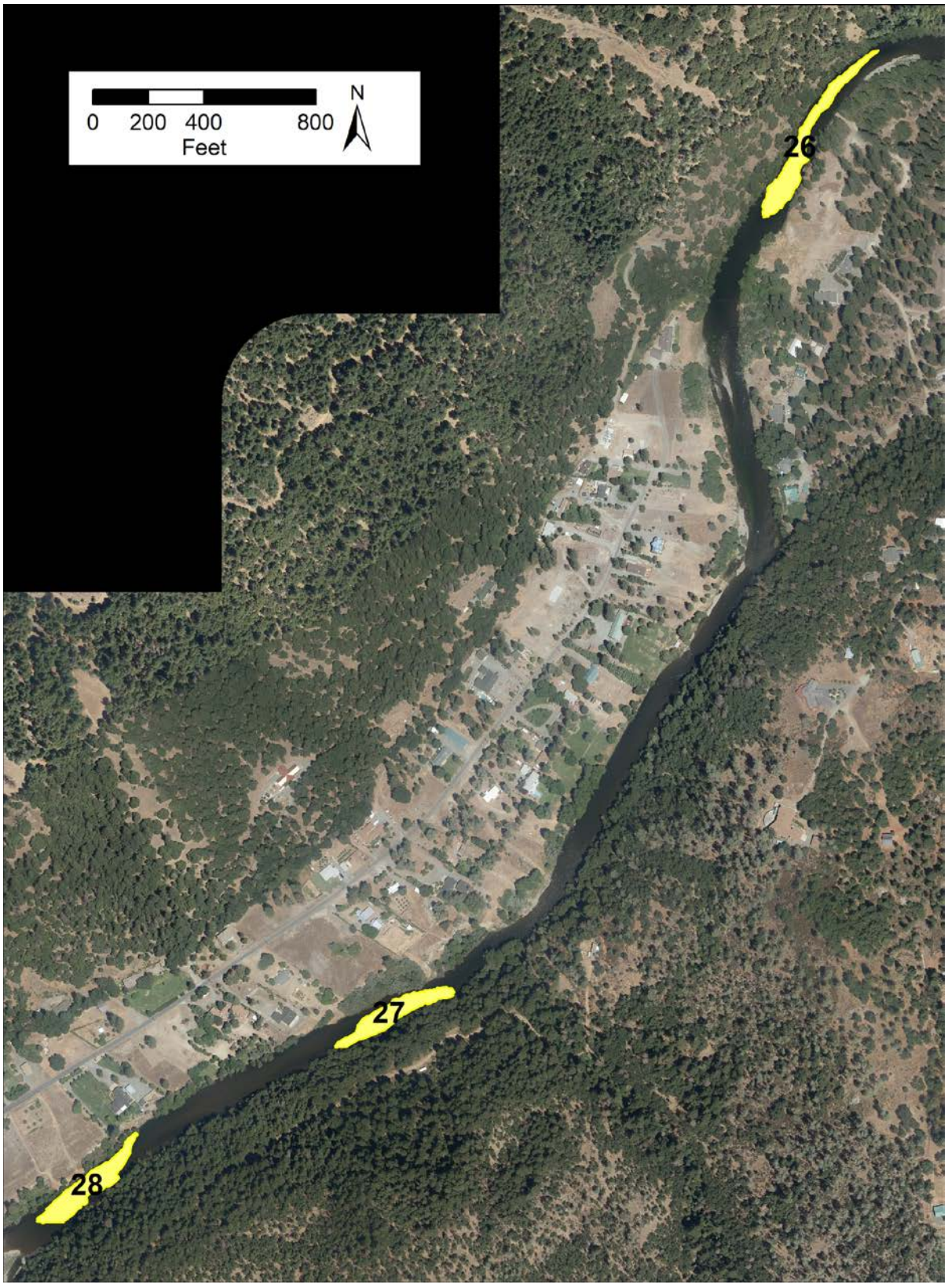
0 200 400 800
Feet
N
26
27
28


33
32
31
30
29
0 200 400 800
Feet
N

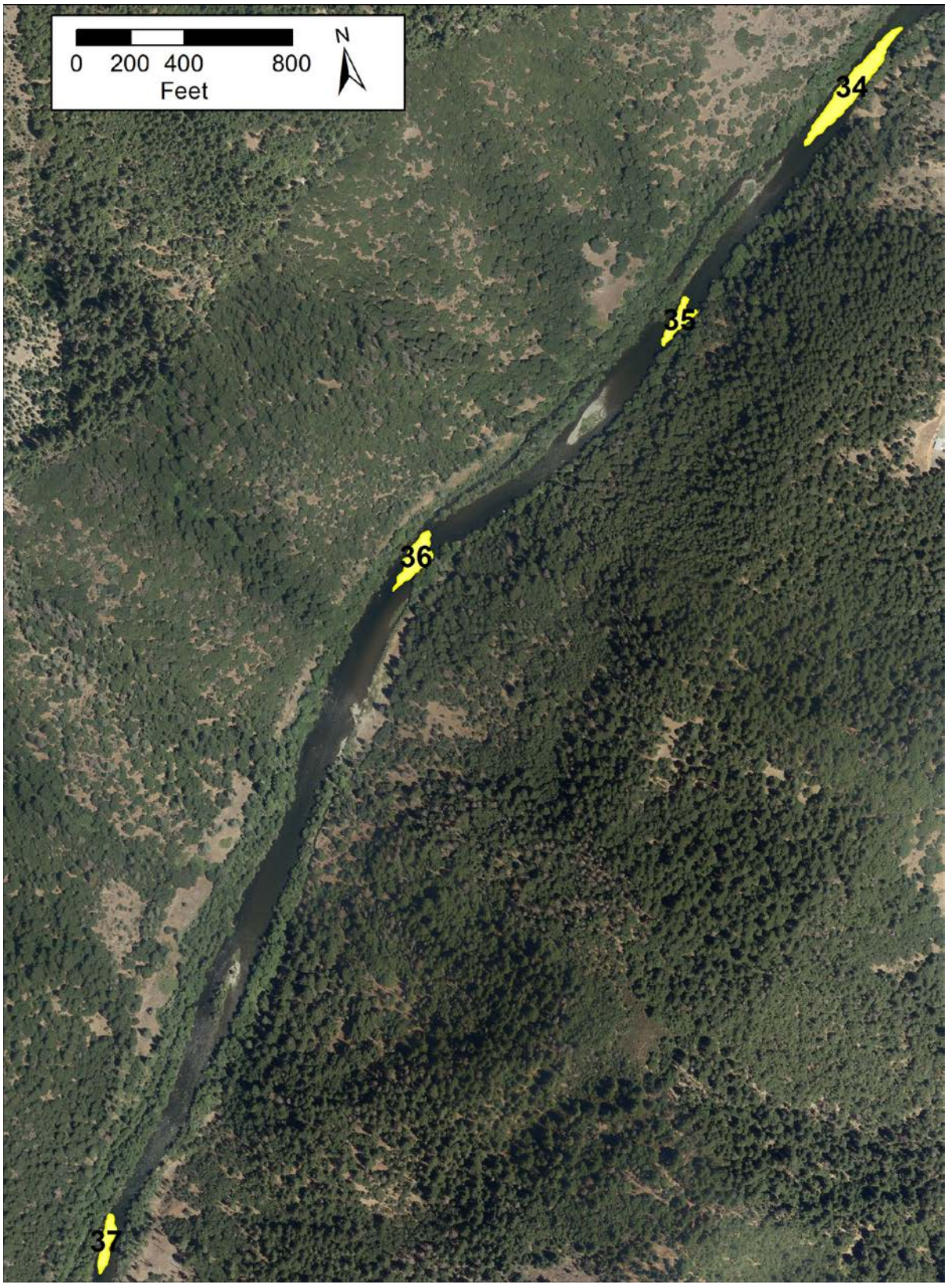
0 200 400 800
Feet
N
34
35
36
37

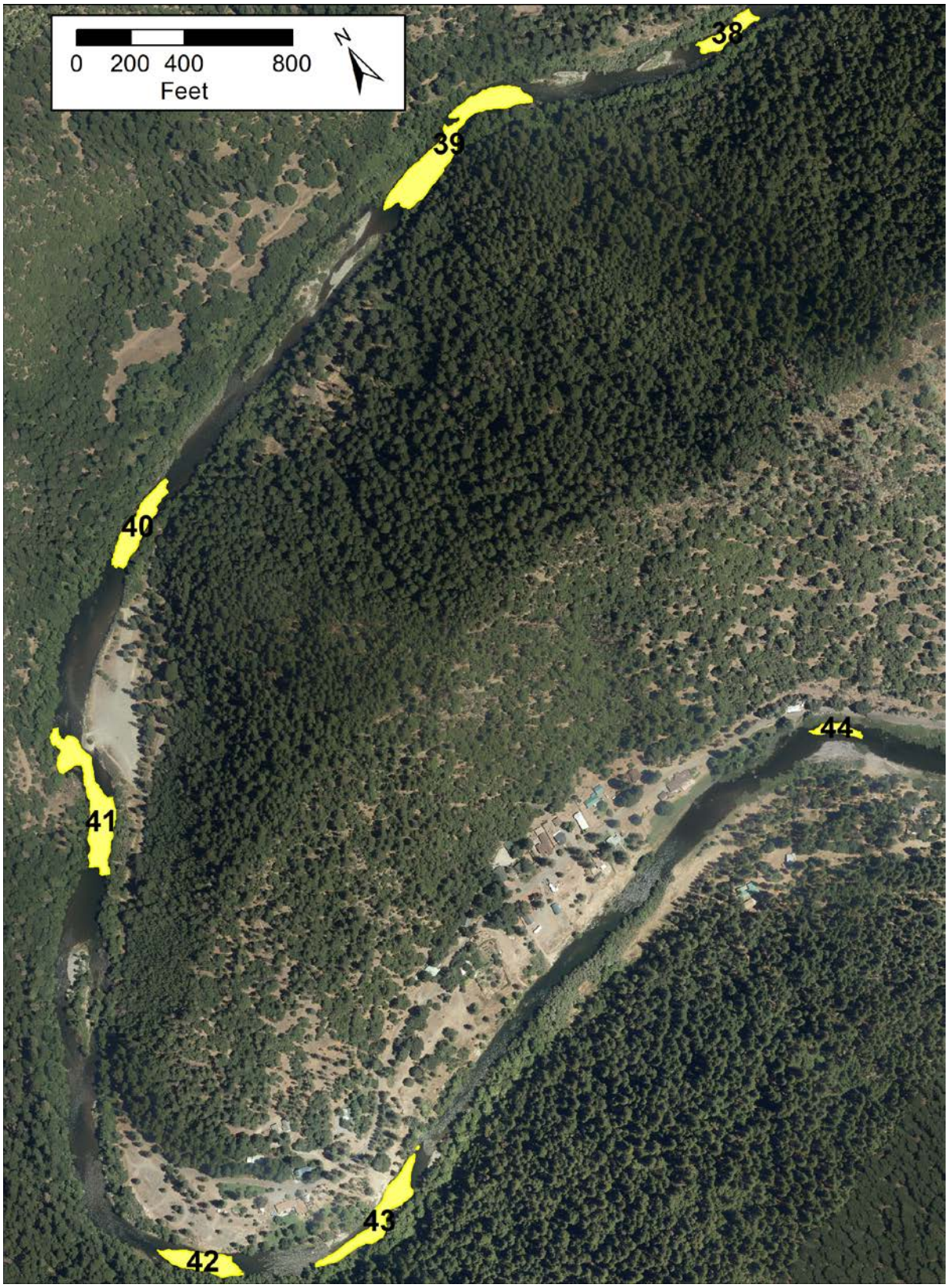
0 200 400 800
Feet
N
38
39
40
41
42
43
44


0 200 400 800
Feet
N
45
46
47

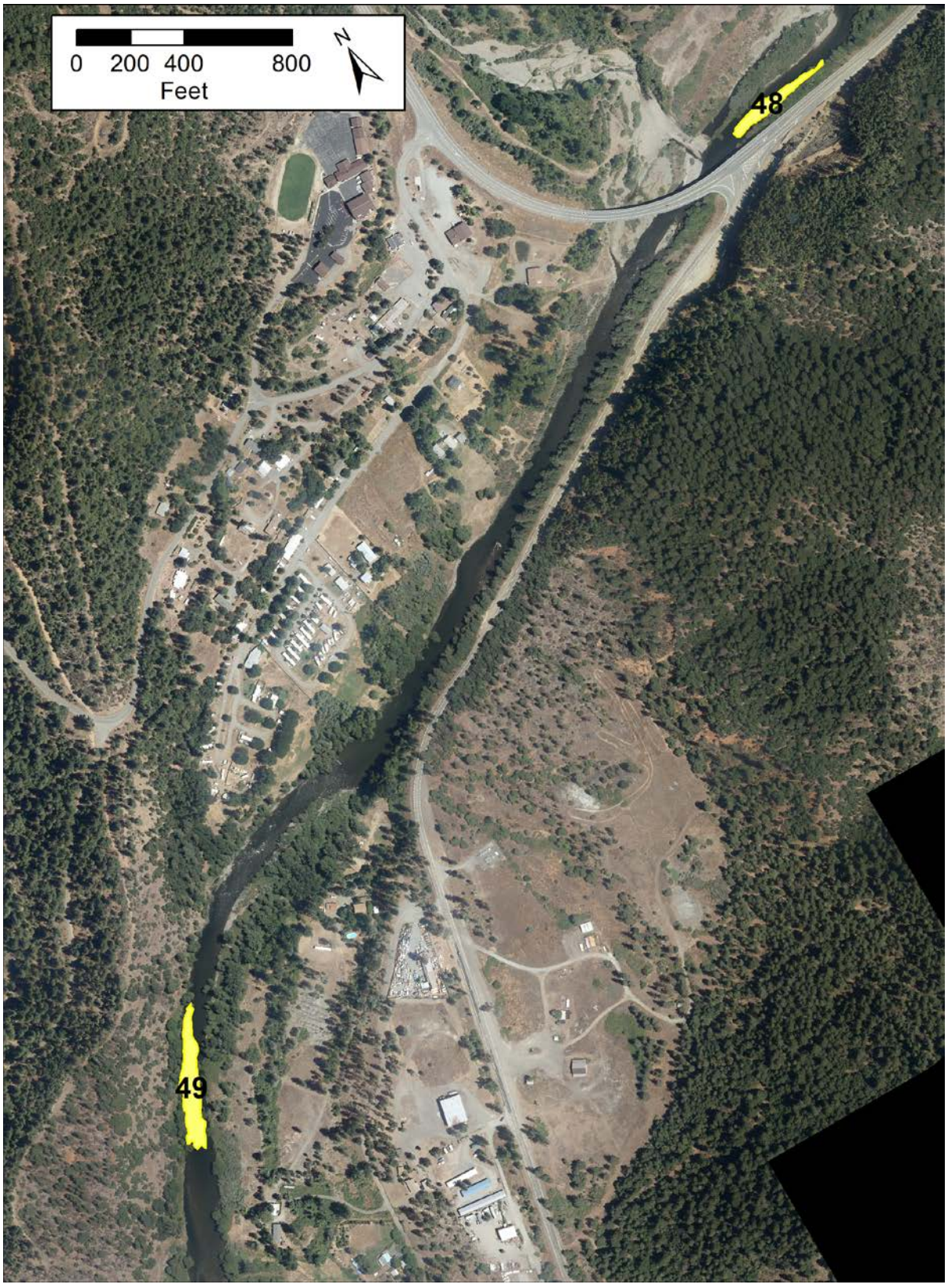
0 200 400 800
Feet
N
48
49

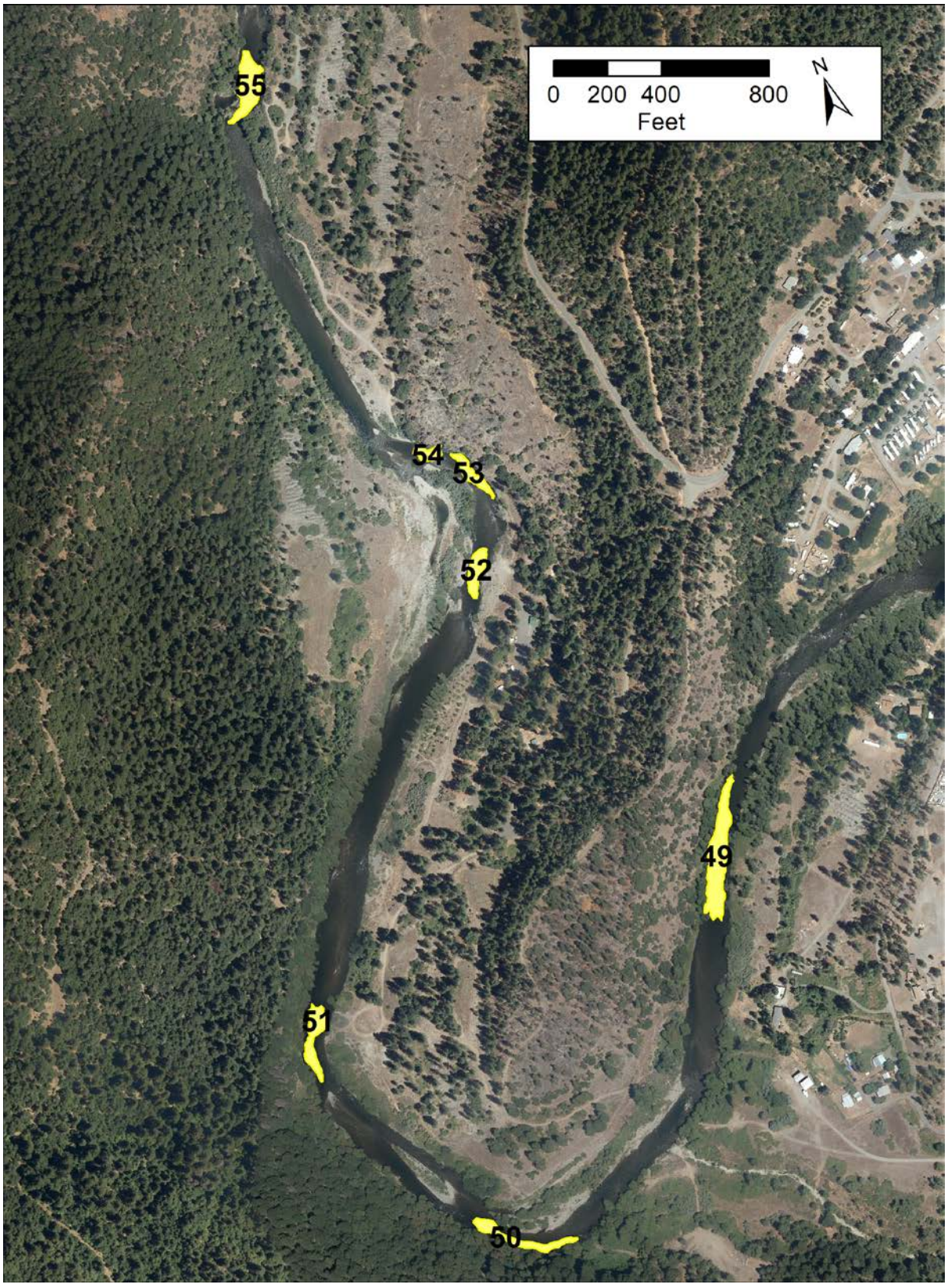
55
0 200 400 800
Feet
N
54
53
52
49
51
50

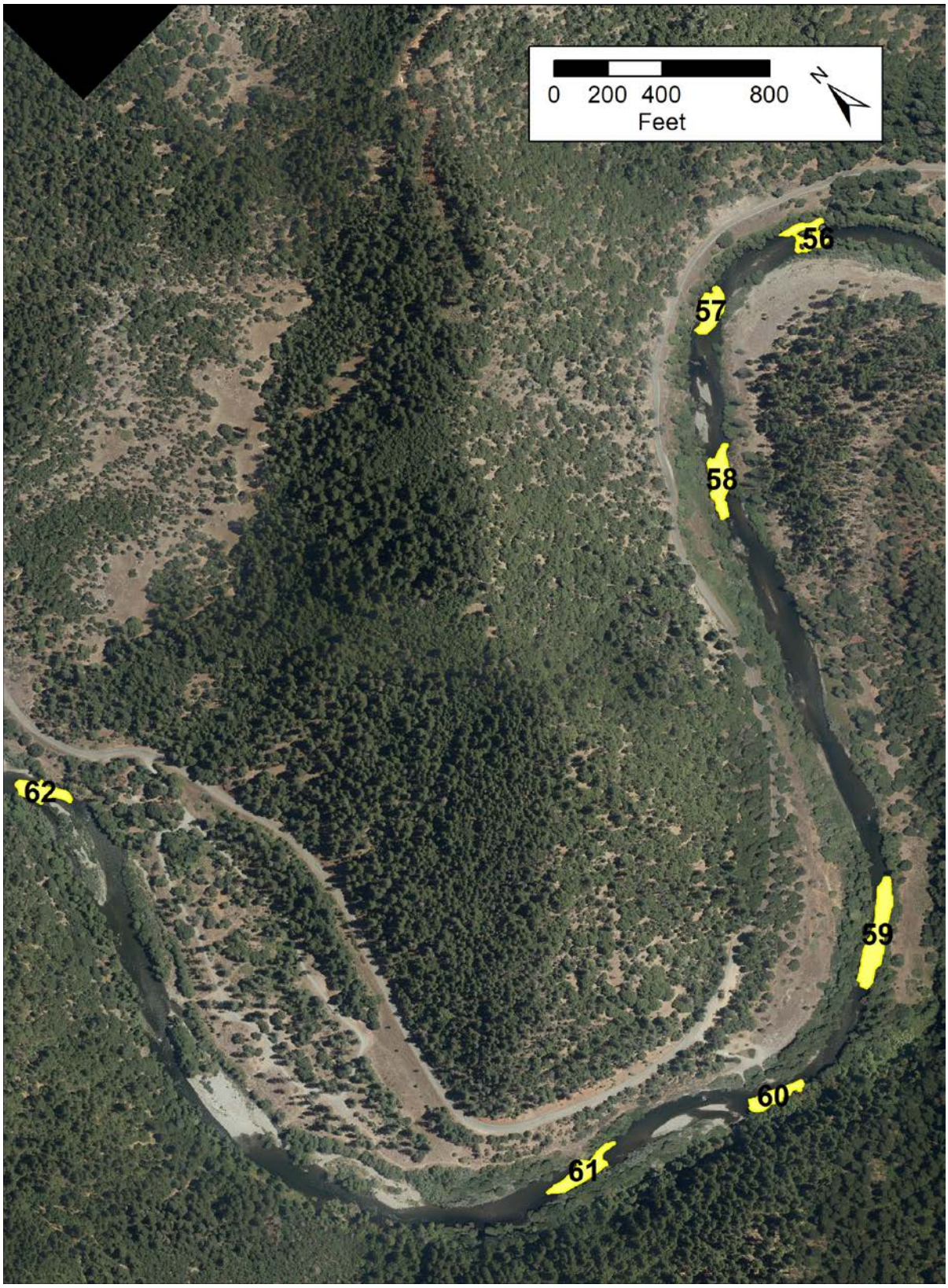
0 200 400 800
Feet
N
56
57
58
59
60
61
62

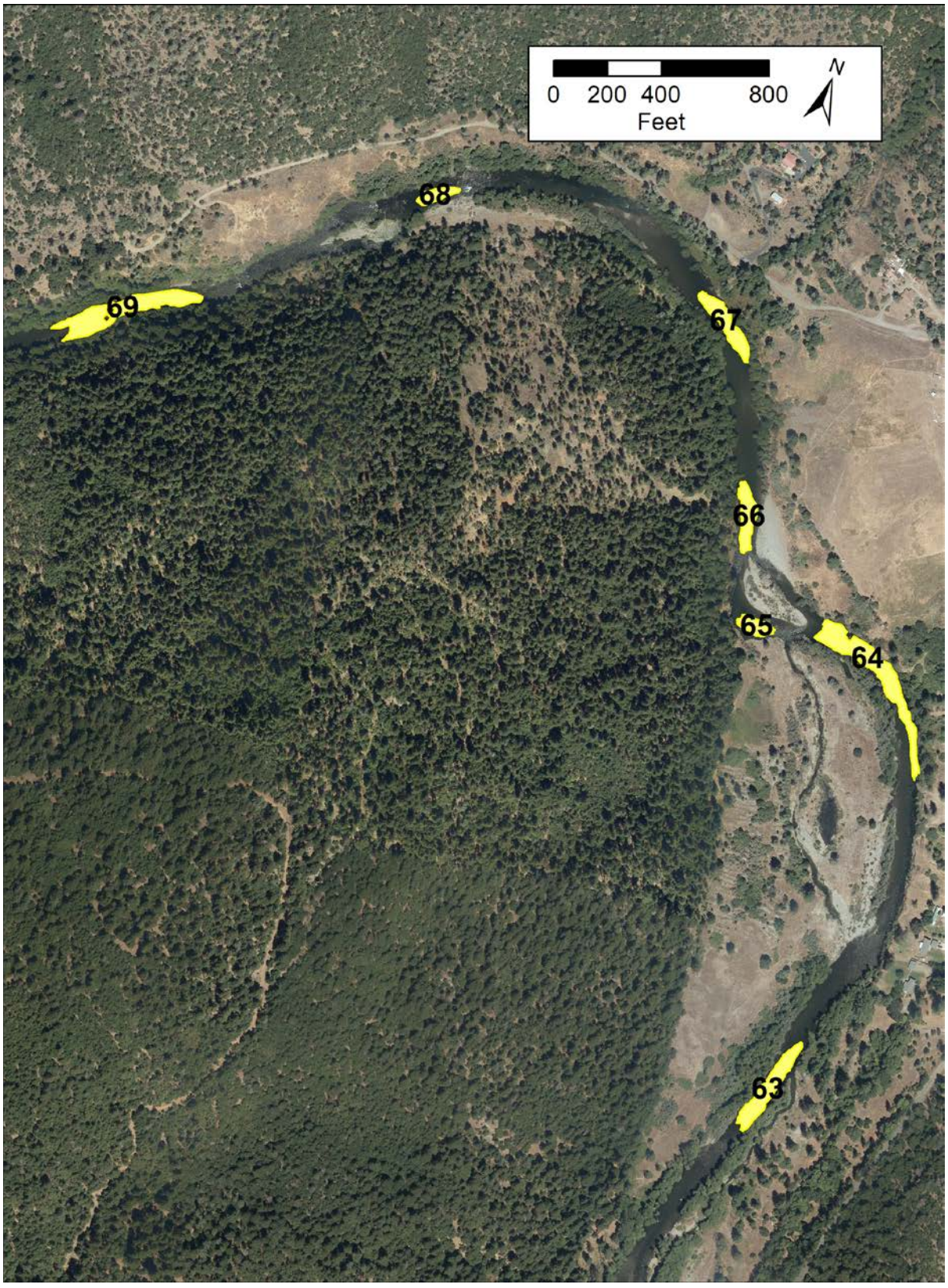
0 200 400 800
Feet
N
68
69
67
66
65
64
63

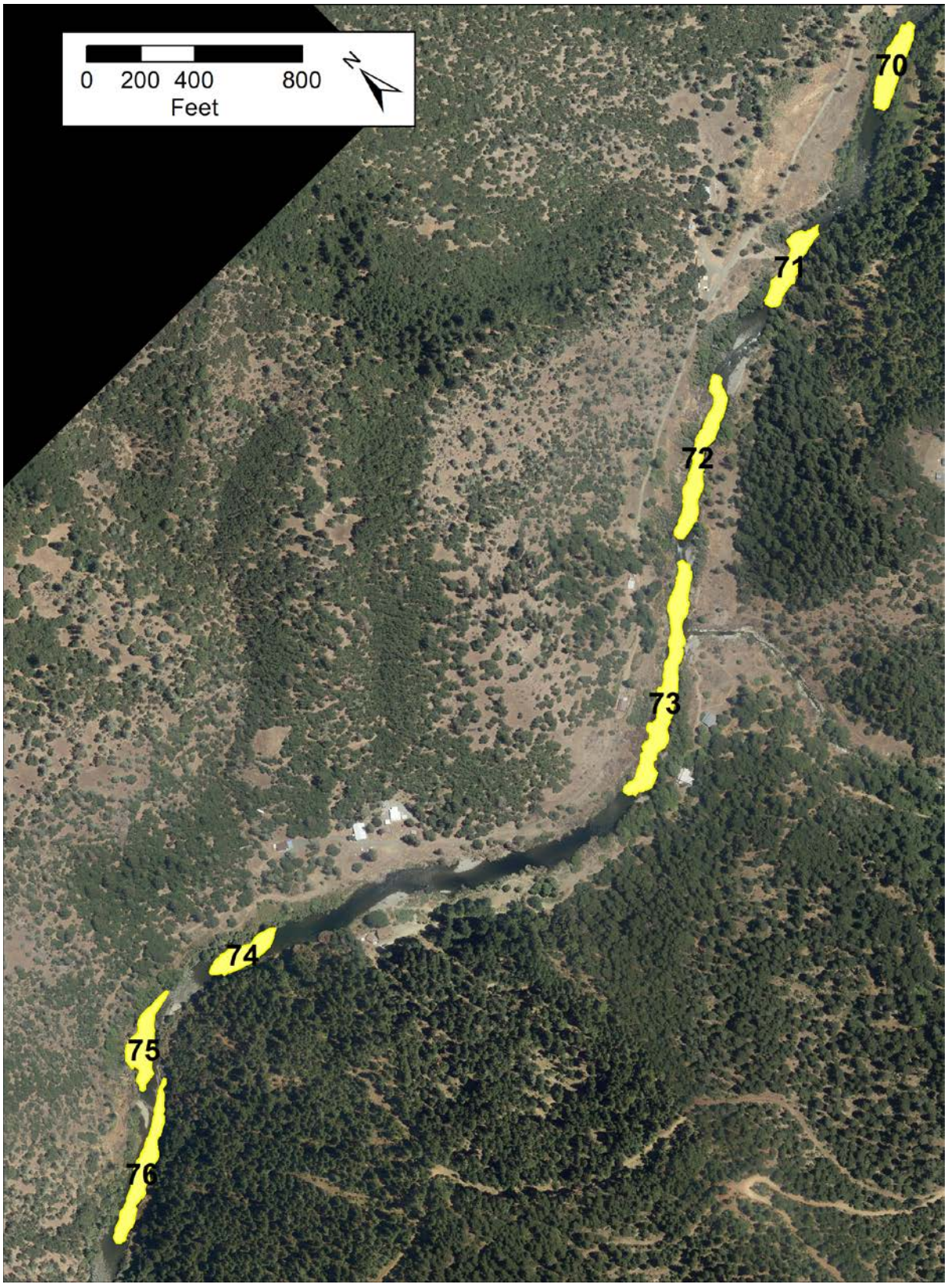
0 200 400 800
Feet
N
70
71
72
73
74
75
76

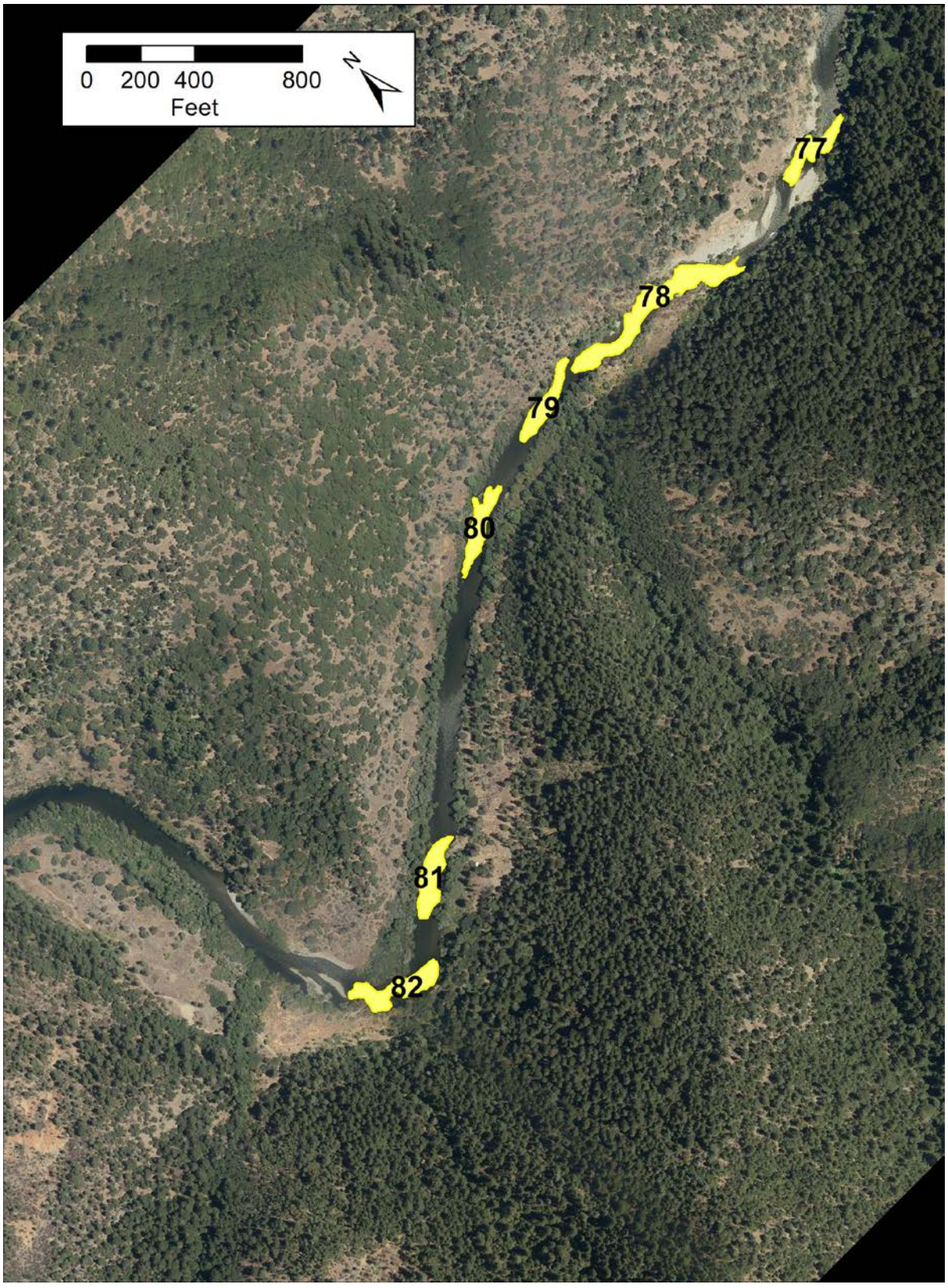
0 200 400 800
Feet
N
77
78
79
80
81
82


0 200 400 800
Feet
N
84
83


0 200 400 800
Feet
N
88
87
86
85


0 200 400 800
Feet
N
91
90
89


0 200 400 800
Feet
N
95
94
93
92


0 200 400 800
Feet
N
98
97
96

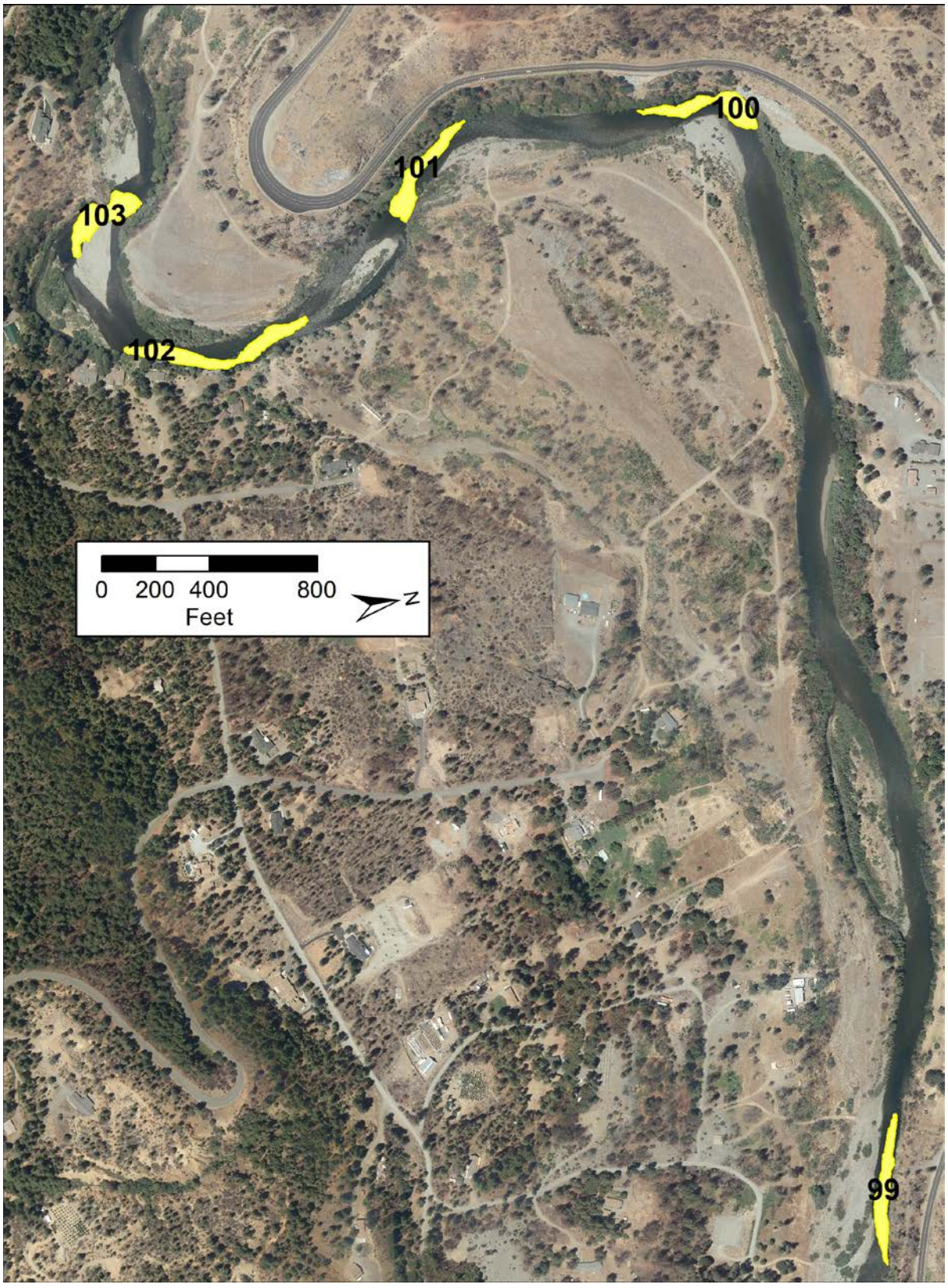
100
101
103
102
0 200 400 800
Feet
N
99

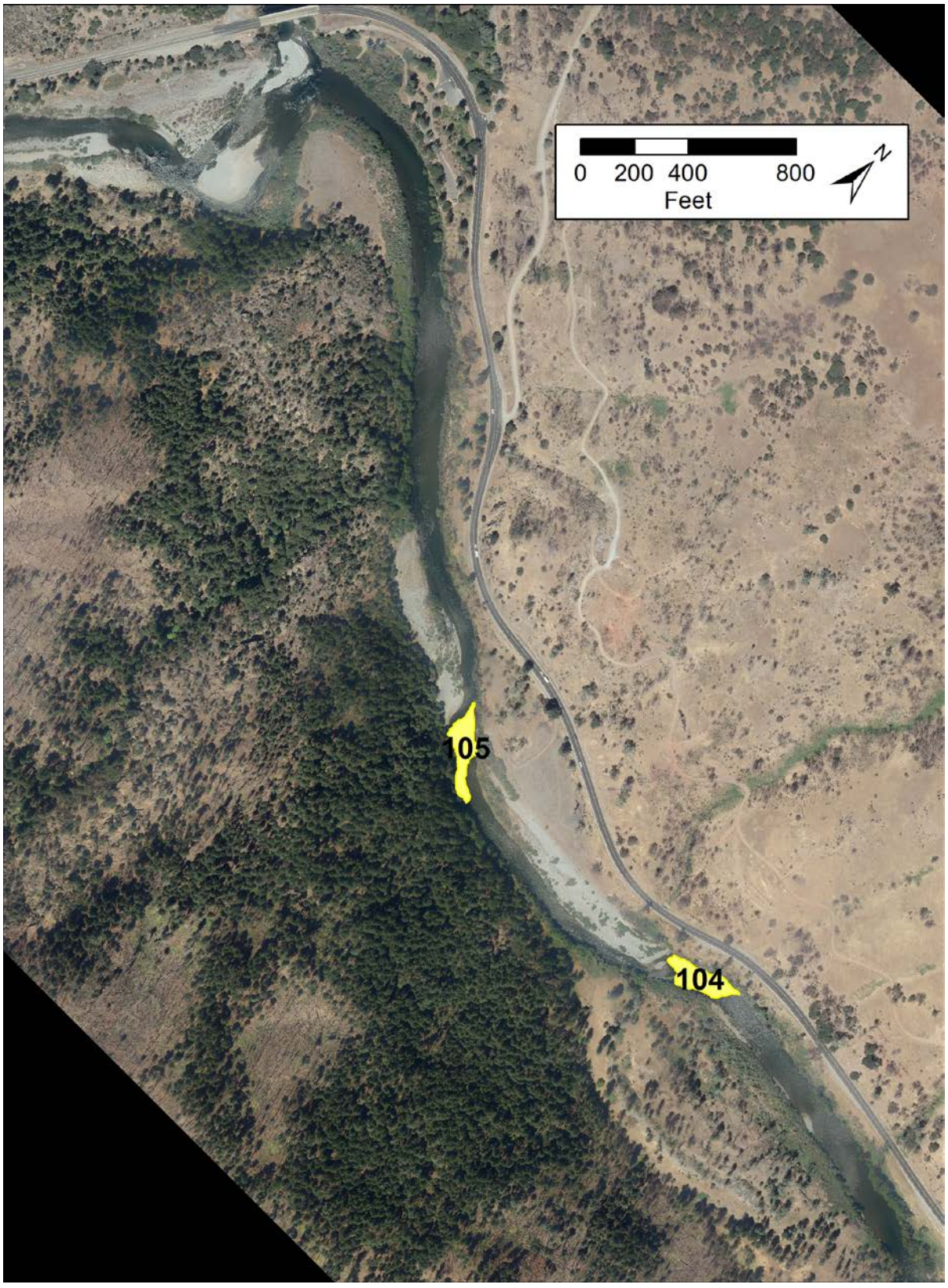
0 200 400 800
Feet
N
105
104

Appendix E: Pool Depth Statistics

Pool depth statistics derived from 2011-2017 surveys. Units are ft.

No.	Name	Year	RM	WSEL	Max_D	50P_D	75P_D	90P_D
1	Diversion Pool	2011	111.15	1822	13.74	8.55	10.74	12.06
1	Diversion Pool	2016	111.15	1822	14.19	8.22	10.55	11.97
1	Diversion Pool	2017	111.15	1822	15.29	8.41	10.69	12.32
2	Deadwood	2011	111.05	1816.8	11.42	5.36	6.36	7.50
2	Deadwood	2016	111.05	1816.8	11.55	5.33	6.31	7.61
2	Deadwood	2017	111.05	1816.8	10.83	5.31	6.16	7.58
3	New Bridge	2011	110.95	1813.8	11.57	6.61	8.16	9.27
3	New Bridge	2016	110.95	1813.8	13.06	6.49	8.54	9.75
3	New Bridge	2017	110.95	1813.8	14.56	6.07	8.96	10.26
4	Higgs	2011	110.7	1808.2	10.01	4.83	5.49	6.17
4	Higgs	2016	110.7	1808.2	9.79	4.67	5.41	6.33
4	Higgs	2017	110.7	1808.2	9.97	4.78	5.82	6.79
5	Cableway	2011	110.32	1803.7	4.87	3.67	4.07	4.31
5	Cableway	2016	110.32	1803.7	5.75	3.92	4.21	4.43
5	Cableway	2017	110.32	1803.7	6.35	4.18	4.60	5.02
6	Old Bridge	2011	110.2	1803.3	5.56	4.24	4.45	4.66
6	Old Bridge	2016	110.2	1803.3	5.06	4.21	4.43	4.59
6	Old Bridge	2017	110.2	1803.3	5.57	4.54	4.93	5.24
7	Hoadley	2011	109.9	1800	13.57	6.36	7.82	9.59
7	Hoadley	2016	109.9	1800	13.24	5.95	7.49	9.11
7	Hoadley	2017	109.9	1800	12.96	6.19	7.88	9.57
8	Upper Cemetery	2011	109.47	1794.4	11.88	6.41	8.32	9.41
8	Upper Cemetery	2016	109.47	1794.4	14.09	7.33	9.36	11.44
8	Upper Cemetery	2017	109.47	1794.4	15.27	7.45	10.31	12.77
9	Cemetery	2011	109.43	1793.1	14.56	5.09	7.23	9.52
9	Cemetery	2016	109.43	1793.1	13.44	4.60	6.50	9.51
9	Cemetery	2017	109.43	1793.1	10.41	4.20	5.61	6.89
10	Sawmill Burner	2011	109	1787.65	8.16	3.67	5.24	6.29
10	Sawmill Burner	2016	109	1787.65	7.09	3.55	4.76	5.79
10	Sawmill Burner	2017	109	1787.65	7.04	3.77	4.85	5.86
11	Lower Burner	2011	108.95	1787.6	10.38	4.89	6.15	8.05
11	Lower Burner	2016	108.95	1787.6	11.22	4.83	6.30	8.29
11	Lower Burner	2017	108.95	1787.6	11.65	5.13	6.99	9.30
12	Rush Pool	2011	108.1	1780.75	11.06	5.30	6.45	7.80
12	Rush Pool	2016	108.1	1780.75	10.47	5.26	6.45	7.68
12	Rush Pool	2017	108.1	1780.75	10.44	5.40	6.56	7.83
13	Dark Gulch	2011	106.6	1760.35	11.93	6.75	8.46	9.53
13	Dark Gulch	2016	106.6	1760.35	11.66	6.81	8.69	10.00
13	Dark Gulch	2017	106.6	1760.35	11.96	6.88	8.75	10.15
14	Lower Dark Gulch	2011	106.5	1759.9	9.41	6.28	7.43	8.21
14	Lower Dark Gulch	2016	106.5	1759.9	8.86	5.12	6.11	6.93
14	Lower Dark Gulch	2017	106.5	1759.9	7.94	4.93	6.02	6.99
15	RM106.25	2011	106.25	1756.15	8.31	4.16	4.63	5.39
15	RM106.25	2016	106.25	1756.15	6.18	3.78	4.20	4.46
15	RM106.25	2017	106.25	1756.15	5.60	3.91	4.29	4.59

16	Dirty Bird	2011	105.8	1751.5	11.09	5.19	6.62	7.74
16	Dirty Bird	2016	105.8	1751.5	10.13	4.47	5.77	7.25
16	Dirty Bird	2017	105.8	1751.5	9.95	4.80	6.32	7.52
17	Bucktail Island Bkwtr	2011	105.67	1749.8	11.00	5.40	6.49	7.32
17	Bucktail Island Bkwtr	2016	105.67	1749.8	12.15	5.18	6.04	6.83
17	Bucktail Island Bkwtr	2017	105.67	1749.8	12.10	4.79	6.10	7.84
18	Upper Bucktail	2011	105.45	1746.9	14.62	5.15	8.86	11.20
18	Upper Bucktail	2016	105.45	1746.9	14.74	5.26	9.53	12.32
18	Upper Bucktail	2017	105.45	1746.9	16.04	6.34	11.00	13.85
19	Bucktail	2011	105.4	1746.7	22.19	6.92	9.61	13.49
19	Bucktail	2016	105.4	1746.7	23.57	6.39	10.04	14.43
19	Bucktail	2017	105.4	1746.7	23.12	6.84	10.72	16.15
20	RM105.15	2011	105.2	1743.2	7.37	3.53	4.01	4.65
20	RM105.15	2016	105.2	1743.2	7.17	3.17	3.65	4.50
20	RM105.15	2017	105.2	1743.2	7.86	3.11	3.69	4.75
21	Lowden Approach	2011	105.05	1741.9	7.87	4.74	5.45	6.04
21	Lowden Approach	2016	105.05	1741.9	7.71	3.87	5.02	5.97
21	Lowden Approach	2017	105.05	1741.9	7.88	3.19	4.62	5.67
22	Lowden Bend	2011	104.95	1741.9	6.93	4.34	4.92	5.41
22	Lowden Bend	2016	104.95	1741.9	7.15	4.60	5.18	5.60
22	Lowden Bend	2017	104.95	1741.9	7.80	4.90	5.81	6.53
23	Lowden Convergence	2011	104.65	1740.3	7.40	5.15	5.74	6.27
23	Lowden Convergence	2016	104.65	1740.3	7.47	5.11	5.61	6.22
23	Lowden Convergence	2017	104.65	1740.3	6.87	5.22	5.71	6.12
24	RM104.5	2011	104.5	1737.8	5.52	3.83	4.09	4.30
24	RM104.5	2016	104.5	1737.8	4.72	3.84	4.10	4.27
24	RM104.5	2017	104.5	1737.8	4.67	3.88	4.13	4.27
25	Wellock	2011	104.3	1735.5	6.34	5.23	5.56	5.78
25	Wellock	2016	104.3	1735.5	6.24	4.68	5.10	5.44
25	Wellock	2017	104.3	1735.5	5.80	4.14	4.90	5.22
26	SP-Ponderosa	2011	103.9	1729.1	12.76	6.64	8.42	10.31
26	SP-Ponderosa	2016	103.9	1729.1	10.79	6.56	8.05	8.94
26	SP-Ponderosa	2017	103.9	1729.1	12.14	6.73	8.19	9.91
27	Tom Lang	2011	103.2	1719.6	9.44	4.88	5.99	6.85
27	Tom Lang	2016	103.2	1719.6	9.39	4.90	5.99	7.21
27	Tom Lang	2017	103.2	1719.6	9.58	4.98	6.02	6.96
28	RM102.95	2011	102.95	1719	6.50	4.56	5.03	5.42
28	RM102.95	2016	102.95	1719	5.91	4.08	4.58	5.01
28	RM102.95	2017	102.95	1719	6.14	4.08	4.65	5.18
29	Stott	2011	102.5	1713.5	19.75	8.27	12.66	16.87
29	Stott	2016	102.5	1713.5	20.46	8.20	12.87	17.26
29	Stott	2017	102.5	1713.5	20.54	7.76	12.91	16.99
30	RM102.1	2011	102.1	1709	6.56	4.11	4.70	5.25
30	RM102.1	2016	102.1	1709	6.10	3.95	4.64	5.22
30	RM102.1	2017	102.1	1709	6.09	4.00	4.71	5.33
31	Society Pool	2011	101.8	1706	12.71	8.39	10.30	11.01
31	Society Pool	2016	101.8	1706	12.71	8.00	9.80	10.84
31	Society Pool	2017	101.8	1706	13.24	8.04	10.02	10.64
32	Montana	2011	101.35	1697.3	10.58	5.72	7.28	8.83

32	Montana	2016	101.35	1697.3	9.39	4.88	6.53	8.02
33	Snell	2011	101.17	1694.8	10.82	5.06	6.76	8.73
33	Snell	2016	101.17	1694.8	10.75	4.51	6.30	8.64
34	Crosby	2011	101.5	1694.4	10.46	6.42	7.74	8.90
34	Crosby	2016	101.5	1694.4	10.25	6.00	7.32	8.40
35	Limekiln	2011	100.85	1692.45	5.97	4.94	5.16	5.39
35	Limekiln	2016	100.85	1692.45	5.26	4.45	4.67	4.95
36	Leos	2011	100.6	1689.3	10.61	6.86	7.86	8.63
36	Leos	2016	100.6	1689.3	10.02	6.17	6.78	7.48
37	Limekiln Trough	2011	100.05	1682.3	9.13	4.86	5.33	5.98
37	Limekiln Trough	2016	100.05	1682.3	8.60	4.83	5.32	5.96
38	Lower Limekiln	2011	99.7	1677	11.33	6.13	8.62	10.28
38	Lower Limekiln	2016	99.7	1677	10.76	5.72	8.26	9.57
39	Upper Steel Bridge	2011	99.5	1675	14.46	5.77	7.87	10.18
39	Upper Steel Bridge	2016	99.5	1675	13.91	5.36	7.05	9.24
40	RM99.15	2011	99.15	1671.2	9.12	6.04	7.16	7.81
40	RM99.15	2016	99.15	1671.2	8.96	5.97	7.18	7.80
41	Steel Bridge	2011	98.9	1669.8	19.66	7.81	9.02	11.86
41	Steel Bridge	2016	98.9	1669.8	19.62	7.55	9.28	11.79
42	Steel Bridge Day Use	2011	98.55	1663.7	15.93	6.34	10.14	13.09
42	Steel Bridge Day Use	2016	98.55	1663.7	16.51	6.72	10.32	13.62
43	Low St Brdg Day Use	2011	98.2	1660	16.96	3.57	6.62	10.82
43	Low St Brdg Day Use	2016	98.2	1660	17.41	3.68	5.71	9.94
44	RM97.95	2011	97.95	1655.3	6.54	4.13	4.74	5.27
44	RM97.95	2016	97.95	1655.3	6.41	4.19	4.71	5.14
45	McIntyre Pool	2011	97.35	1650.4	15.89	5.79	8.04	10.80
45	McIntyre Pool	2016	97.35	1650.4	14.33	5.63	7.62	10.56
46	Thistle Lane Pool	2011	96.95	1644.6	7.37	4.27	4.88	5.60
46	Thistle Lane Pool	2016	96.95	1644.6	9.47	3.83	4.62	6.32
47	Ind. Ck Backwater	2011	95.65	1636.3	12.24	7.24	8.78	9.94
47	Ind. Ck Backwater	2016	95.65	1636.3	12.45	7.31	8.68	9.76
48	299 Bridge	2011	94.1	1617.5	5.99	2.76	3.67	4.50
48	299 Bridge	2016	94.1	1617.5	6.18	4.20	4.73	5.30
49	New DC Pool	2011	93.3	1607.1	9.82	4.40	5.36	6.56
49	New DC Pool	2016	93.3	1607.1	9.27	4.19	5.34	6.31
50	Reading Crk Point	2011	92.95	1603.5	10.28	5.18	6.25	7.39
50	Reading Crk Point	2016	92.95	1603.5	10.55	5.75	6.73	8.15
51	Painted Rock	2011	92.7	1598.6	15.88	6.73	8.91	11.34
51	Painted Rock	2016	92.7	1598.6	15.17	6.75	8.83	11.35
52	DC Campground	2011	92.4	1593.8	11.29	6.96	8.46	9.66
52	DC Campground	2016	92.4	1593.8	11.25	6.53	7.92	9.26
53	Upper Alcatraz	2011	92.33	1591.6	9.97	4.59	5.94	7.10
53	Upper Alcatraz	2016	92.33	1591.6	10.45	4.60	6.21	7.45
54	Lower Alcatraz	2011	92.28	1591.55	12.87	6.04	8.10	10.09
54	Lower Alcatraz	2016	92.28	1591.55	14.43	7.04	8.99	10.97
55	Upper-steiner	2011	92	1587	17.51	6.55	9.37	11.84
55	Upper-steiner	2016	92	1587	16.53	6.61	9.09	11.66
56	X-factor	2011	91.6	1582.1	11.13	5.32	6.64	8.59
56	X-factor	2016	91.6	1582.1	10.70	5.24	6.66	8.33

57	Skeletor	2011	91.5	1579.9	16.55	7.20	9.95	12.54
57	Skeletor	2016	91.5	1579.9	16.38	6.97	9.71	12.56
58	Mid-Steiner	2011	91.4	1578	12.37	4.57	7.15	10.17
58	Mid-Steiner	2016	91.4	1578	11.87	4.59	7.19	9.73
59	Picnic Table	2011	91.05	1575	10.04	5.36	6.73	8.06
59	Picnic Table	2016	91.05	1575	9.44	4.93	6.29	7.51
60	Chop Tree	2011	90.9	1572	8.92	4.32	5.45	6.67
60	Chop Tree	2016	90.9	1572	8.88	4.84	6.06	7.29
61	Dump Hole	2011	90.75	1570.9	8.78	4.54	5.70	6.50
61	Dump Hole	2016	90.75	1570.9	7.95	4.71	6.06	7.09
62	RM90.2	2011	90.2	1562	10.33	3.94	5.87	8.44
62	RM90.2	2016	90.2	1562	8.97	3.74	5.37	6.91
63	Center Pin	2011	89.75	1558.4	5.26	3.79	4.07	4.30
63	Center Pin	2016	89.75	1558.4	4.88	3.73	4.11	4.46
64	Goat Hole	2011	89.4	1555.4	15.91	5.85	8.32	10.63
64	Goat Hole	2016	89.4	1555.4	15.43	5.56	7.85	10.26
65	Goat Corner	2011	89.35	1554.2	10.10	4.98	6.54	8.17
65	Goat Corner	2016	89.35	1554.2	9.99	4.58	6.80	8.62
66	RM89.3	2011	89.3	1552.8	8.85	5.50	6.75	7.55
66	RM89.3	2016	89.3	1552.8	7.60	4.74	5.86	6.66
67	Dutton	2011	89.15	1552.5	12.94	6.42	8.42	10.07
67	Dutton	2016	89.15	1552.5	12.85	6.95	8.72	10.22
68	RM88.9	2011	88.9	1547.2	8.80	5.59	6.54	7.23
68	RM88.9	2016	88.9	1547.2	8.52	6.72	7.37	7.78
69	RM88.65	2011	88.65	1540	14.18	4.27	5.83	8.39
69	RM88.65	2016	88.65	1540	14.05	4.82	6.49	9.01
70	RM88.4	2011	88.4	1537.7	11.11	6.24	7.12	7.99
70	RM88.4	2016	88.4	1537.7	9.96	5.87	6.71	7.61
71	RM88.24	2011	88.23	1534	21.90	9.17	14.90	18.85
71	RM88.24	2016	88.23	1534	21.33	9.09	14.73	18.45
72	RM88.1	2011	88.1	1529.5	13.54	5.13	6.91	9.14
72	RM88.1	2016	88.1	1529.5	13.71	5.14	6.96	9.13
73	Browns	2011	87.9	1527.1	12.96	4.14	5.86	8.91
73	Browns	2016	87.9	1527.1	12.45	3.83	5.36	8.47
74	RM87.5	2011	87.5	1525.1	12.31	5.49	6.75	8.20
74	RM87.5	2016	87.5	1525.1	12.25	4.77	6.79	8.41
75	Jump Hole	2011	87.45	1523.5	16.95	6.88	9.86	12.84
75	Jump Hole	2016	87.45	1523.5	16.33	6.17	9.05	11.94
76	RM87.55	2011	87.55	1523	11.62	5.49	6.71	7.89
76	RM87.55	2016	87.55	1523	10.37	5.01	6.28	7.56
77	Upper Camp	2011	87.15	1521.1	15.41	5.94	7.27	9.23
77	Upper Camp	2016	87.15	1521.1	17.03	5.41	7.30	9.88
78	Lower Camp	2011	87	1517.5	14.07	4.38	6.60	8.91
78	Lower Camp	2016	87	1517.5	13.69	3.50	5.97	8.69
79	RM86.9	2011	86.9	1517.3	6.81	4.02	4.75	5.31
79	RM86.9	2016	86.9	1517.3	7.01	3.76	4.67	5.65
80	RM86.77	2011	86.77	1517	10.77	4.40	6.55	7.55
80	RM86.77	2016	86.77	1517	10.90	4.38	6.55	7.72
81	Squatter Hole	2011	86.55	1514.5	10.20	3.97	5.23	6.86

81	Squatter Hole	2016	86.55	1514.5	9.76	4.26	5.73	7.16
82	Johnson Point	2011	86.45	1513.8	16.62	5.54	7.53	9.35
82	Johnson Point	2016	86.45	1513.8	16.97	5.57	7.45	9.59
83	Steelhead Alley	2011	85.8	1508.9	6.86	4.37	5.08	5.53
83	Steelhead Alley	2016	85.8	1508.9	7.13	4.49	5.16	5.50
84	Last Hole on Left	2011	85.4	1506	9.66	5.27	6.53	7.91
84	Last Hole on Left	2016	85.4	1506	9.19	5.83	6.99	8.09
85	Chapman	2011	83.2	1481.9	6.86	3.94	4.72	5.42
85	Chapman	2016	83.2	1481.9	7.09	3.90	4.78	5.65
86	Icebox	2011	82.75	1479.9	7.84	4.67	5.35	5.94
86	Icebox	2016	82.75	1479.9	7.94	4.81	5.50	6.11
87	RM82.6	2011	82.6	1478	5.97	4.18	4.61	5.00
87	RM82.6	2016	82.6	1478	5.17	4.07	4.49	4.79
88	Eds Hole	2011	82.3	1474.5	9.43	3.91	4.35	4.86
88	Eds Hole	2016	82.3	1474.5	9.72	4.14	4.57	5.00
89	Sheridan Hole	2011	81.7	1469.7	13.51	4.72	8.21	10.64
89	Sheridan Hole	2016	81.7	1469.7	13.38	4.85	7.63	10.62
90	Upper Sky Ranch	2011	80.7	1460.2	17.33	6.06	7.37	10.72
90	Upper Sky Ranch	2016	80.7	1460.2	16.71	6.30	7.43	10.57
91	Lower Sky Ranch	2011	80.45	1455.8	11.44	5.22	7.29	9.07
91	Lower Sky Ranch	2016	80.45	1455.8	14.89	6.58	8.81	10.50
92	UJC 1	2011	80.2	1452.6	13.33	5.75	7.87	9.63
92	UJC 1	2016	80.2	1452.6	12.19	5.97	7.68	8.90
93	UJC 2	2011	80.1	1452.6	15.03	7.38	9.07	11.39
93	UJC 2	2016	80.1	1452.6	14.29	6.59	8.27	11.01
94	JC Hole	2011	79.53	1445.2	23.12	8.30	12.90	16.64
94	JC Hole	2016	79.53	1445.2	21.66	8.19	12.31	16.12
95	RM78.95	2011	78.95	1436.4	15.05	5.87	7.89	10.71
95	RM78.95	2016	78.95	1436.4	12.87	5.30	6.07	8.55
96	JC Campground 1	2011	78.05	1422.9	12.24	6.12	7.78	9.22
96	JC Campground 1	2016	78.05	1422.9	13.22	6.21	8.11	9.85
97	JC Campground 2	2011	77.95	1421.1	10.72	5.99	7.81	8.95
97	JC Campground 2	2016	77.95	1421.1	10.91	5.61	7.84	9.18
98	McCartneys	2011	77.1	1411.1	14.22	6.10	8.23	10.24
98	McCartneys	2016	77.1	1411.1	14.27	6.43	8.05	9.90
99	Upper Bigfoot	2011	75.83	1394.6	8.62	4.23	5.37	6.66
99	Upper Bigfoot	2016	75.83	1394.6	9.81	4.39	5.76	7.39
100	Valdor	2011	75.05	1387.8	12.59	6.42	8.16	9.62
100	Valdor	2016	75.05	1387.8	11.00	6.25	7.74	9.15
101	Coopers Bar	2011	74.85	1385.2	14.10	7.54	9.41	11.21
101	Coopers Bar	2016	74.85	1385.2	13.40	7.54	9.20	10.83
102	Riprap	2011	74.6	1383.2	13.33	6.39	8.13	10.53
102	Riprap	2016	74.6	1383.2	13.55	6.09	8.20	10.61
103	Lime Point	2011	74.5	1379.6	14.76	4.19	6.65	8.97
103	Lime Point	2016	74.5	1379.6	20.82	5.97	9.53	13.58
104	RM73.3	2011	73.3	1365	17.39	6.43	10.99	15.03
104	RM73.3	2016	73.3	1365	18.39	5.99	11.01	15.14
105	Pear Tree	2011	73.03	1362.6	16.38	5.27	7.16	10.78
105	Pear Tree	2016	73.03	1362.6	16.31	5.97	7.56	10.44

Appendix F: Cumulative Pool Depth-frequency Curves

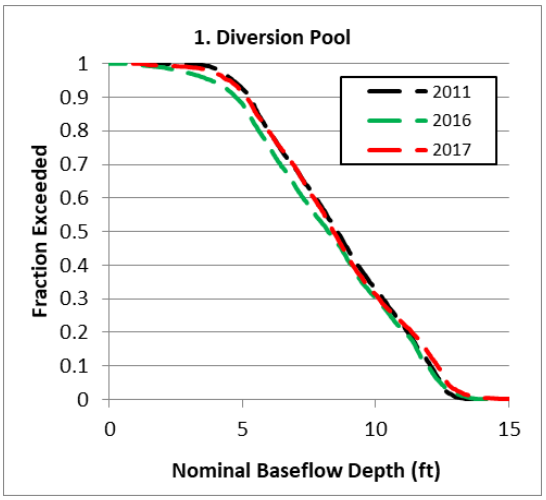

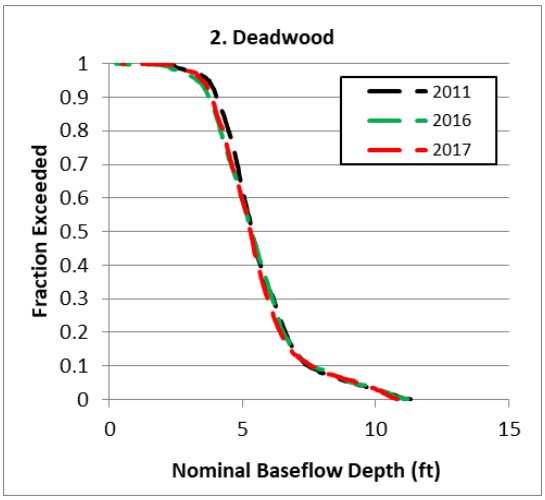

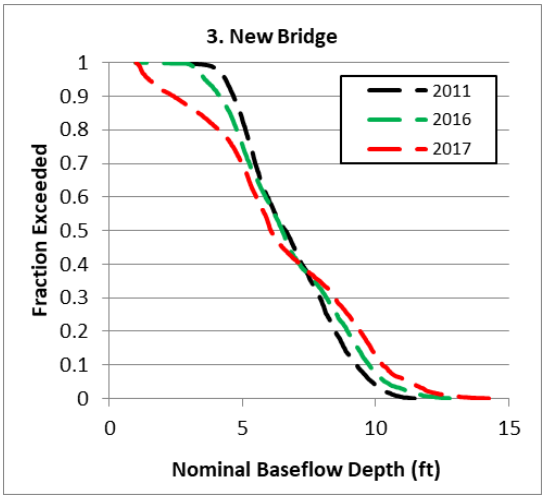

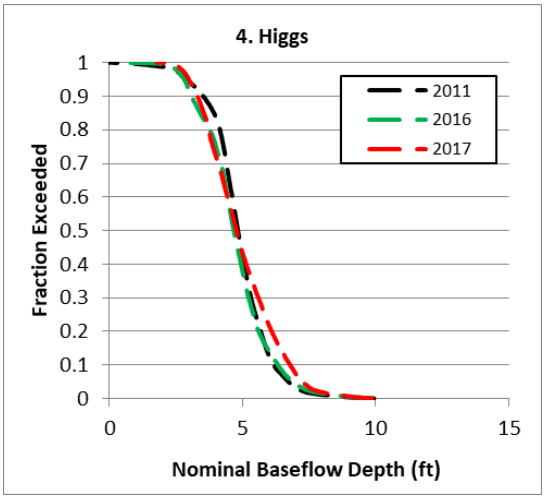

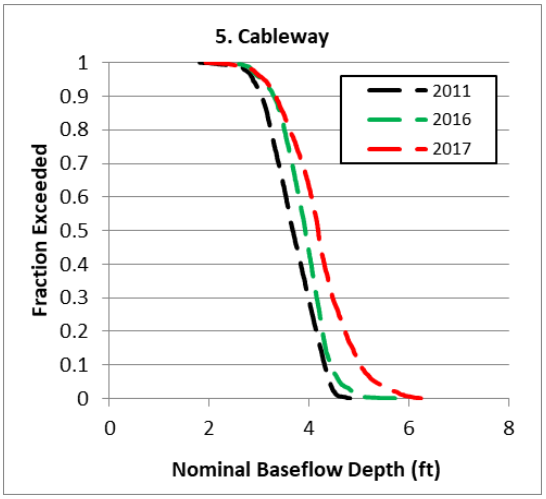

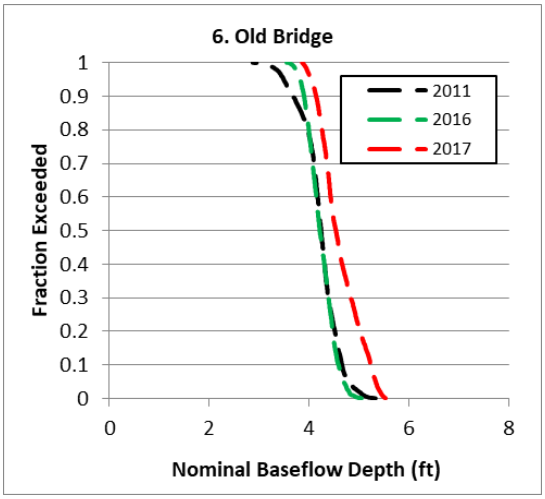

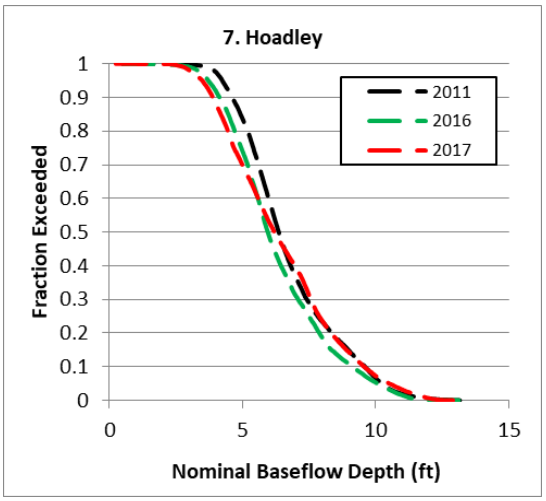
7. Hoadley
Fraction Exceeded
Nominal Baseflow Depth (ft)
2011
2016
2017

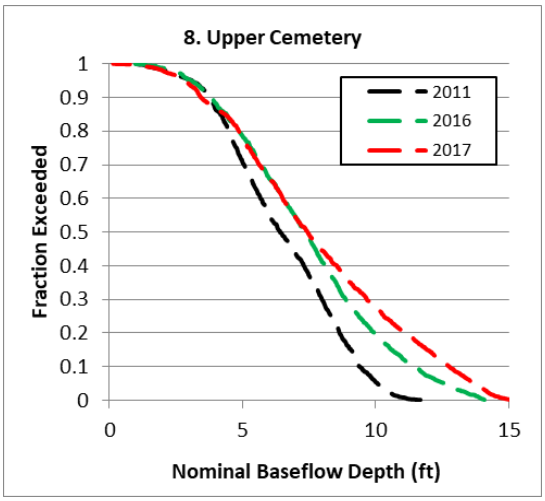
8. Upper Cemetery
Fraction Exceeded
Nominal Baseflow Depth (ft)
2011
2016
2017

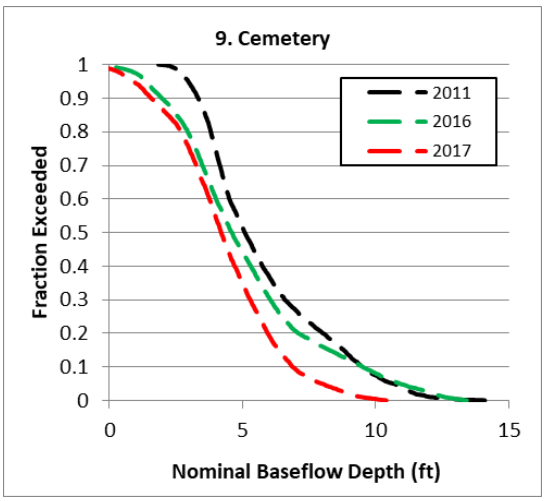
9. Cemetery
Fraction Exceeded
Nominal Baseflow Depth (ft)
2011
2016
2017

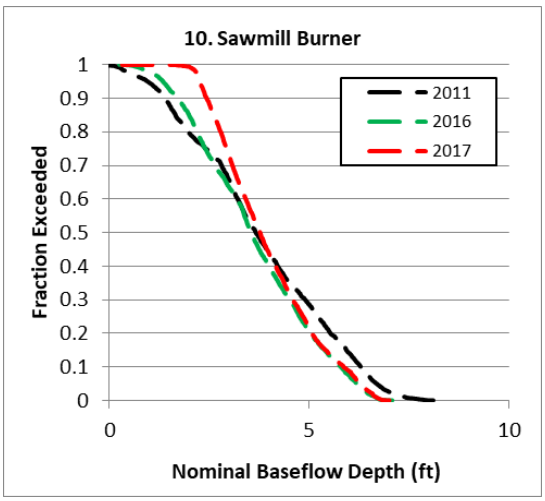
10. Sawmill Burner
Fraction Exceeded
Nominal Baseflow Depth (ft)
2011
2016
2017

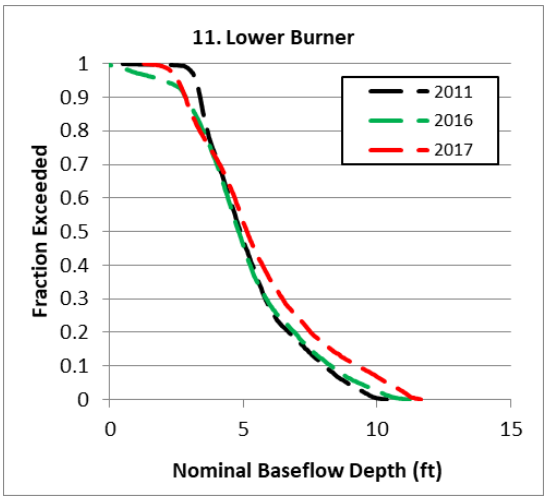
11. Lower Burner
Fraction Exceeded
Nominal Baseflow Depth (ft)
2011
2016
2017

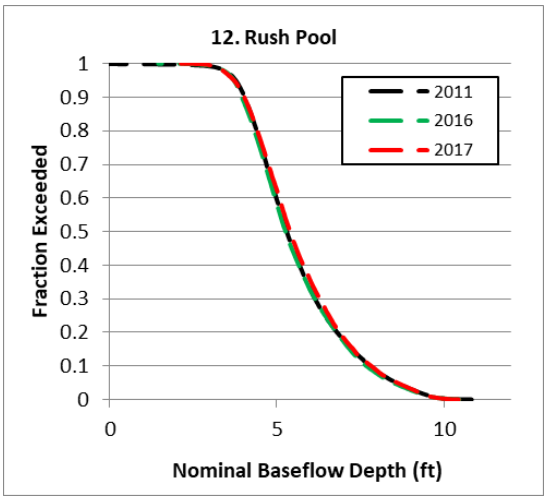
12. Rush Pool
Fraction Exceeded
Nominal Baseflow Depth (ft)
2011
2016
2017

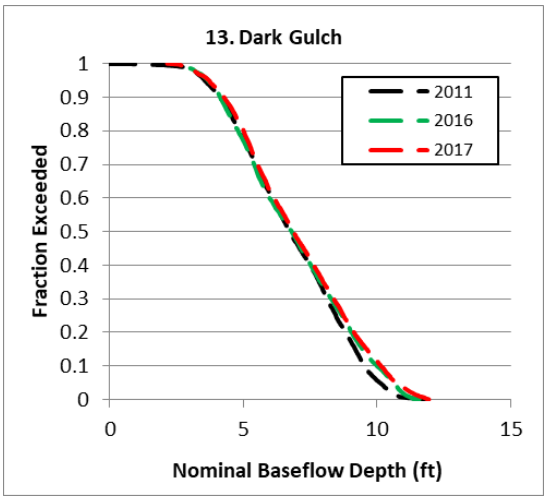
13. Dark Gulch
Fraction Exceeded
Nominal Baseflow Depth (ft)
2011
2016
2017

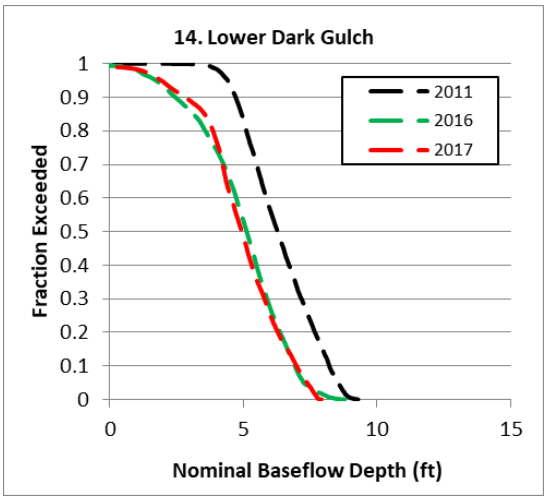
14. Lower Dark Gulch
Fraction Exceeded
Nominal Baseflow Depth (ft)
2011
2016
2017

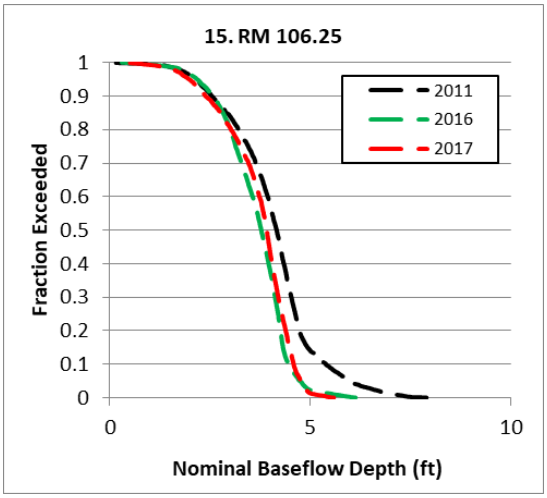
15. RM 106.25
Fraction Exceeded
Nominal Baseflow Depth (ft)
2011
2016
2017

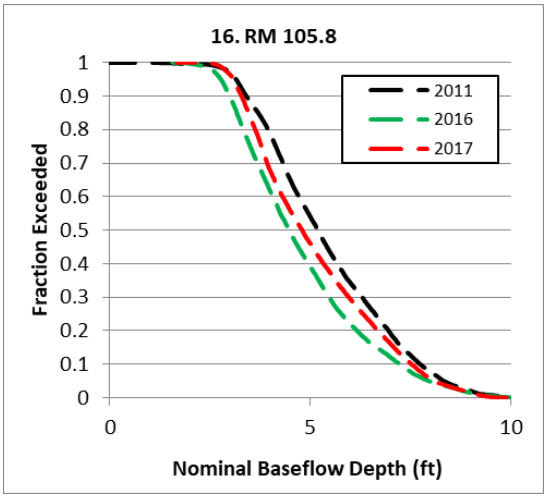
16. RM 105.8
Fraction Exceeded
Nominal Baseflow Depth (ft)
2011
2016
2017

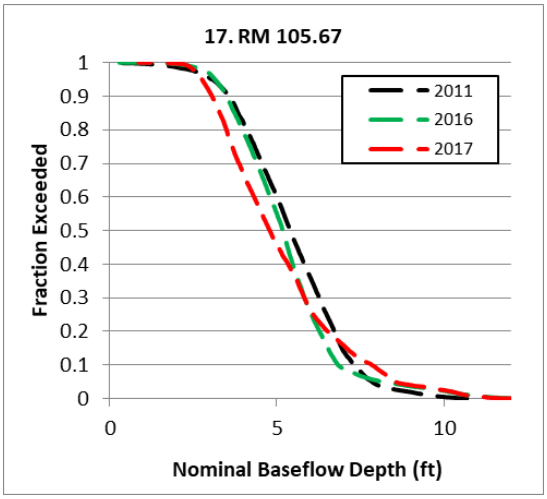
17. RM 105.67
Fraction Exceeded
Nominal Baseflow Depth (ft)
2011
2016
2017

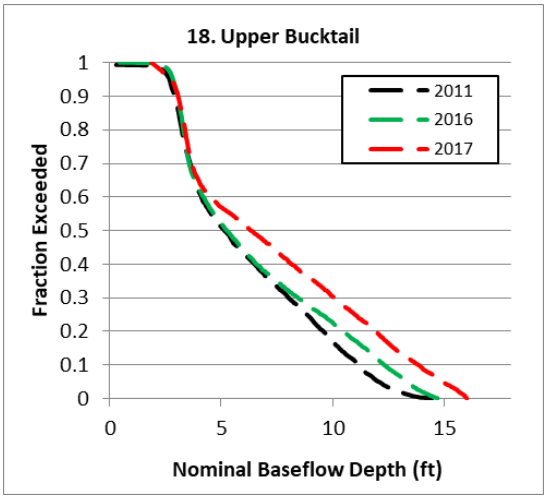
18. Upper Bucktail
Fraction Exceeded
Nominal Baseflow Depth (ft)
2011
2016
2017

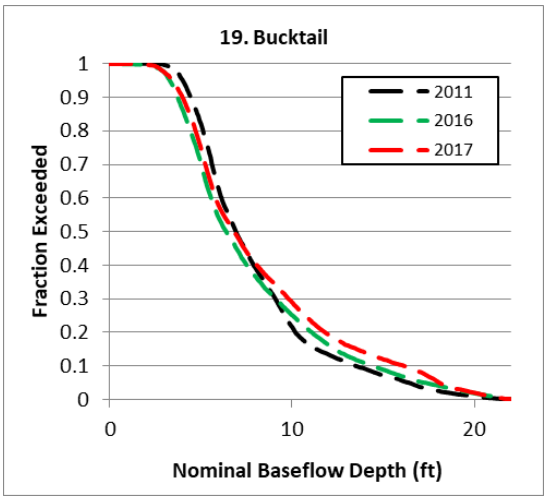
19. Bucktail
Fraction Exceeded
Nominal Baseflow Depth (ft)
2011
2016
2017

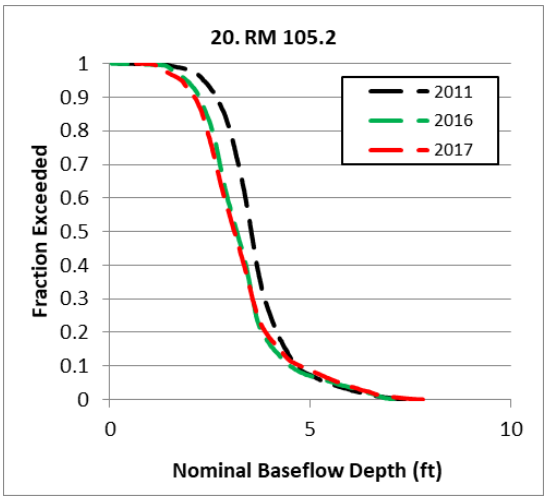
20. RM 105.2
Fraction Exceeded
Nominal Baseflow Depth (ft)
2011
2016
2017

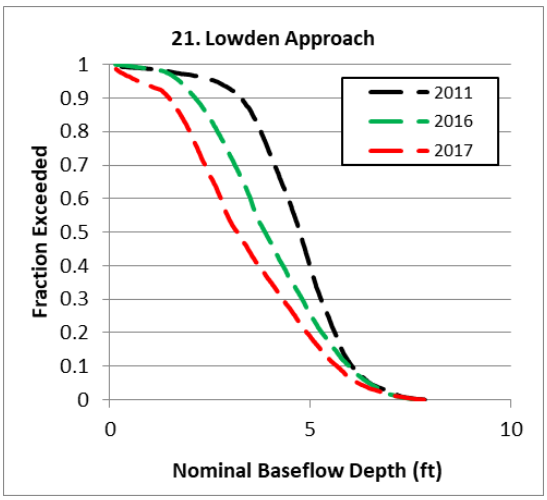
21. Lowden Approach
Fraction Exceeded
Nominal Baseflow Depth (ft)
2011
2016
2017

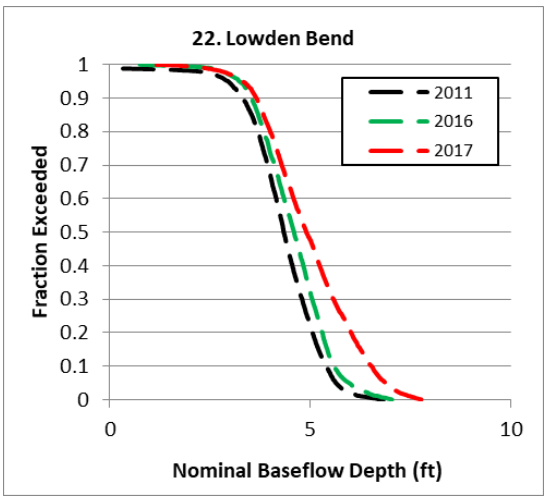
22. Lowden Bend
Fraction Exceeded
Nominal Baseflow Depth (ft)
2011
2016
2017

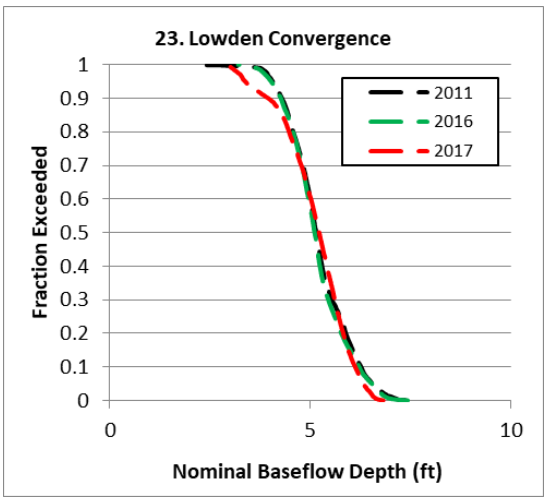
23. Lowden Convergence
Fraction Exceeded
Nominal Baseflow Depth (ft)
2011
2016
2017

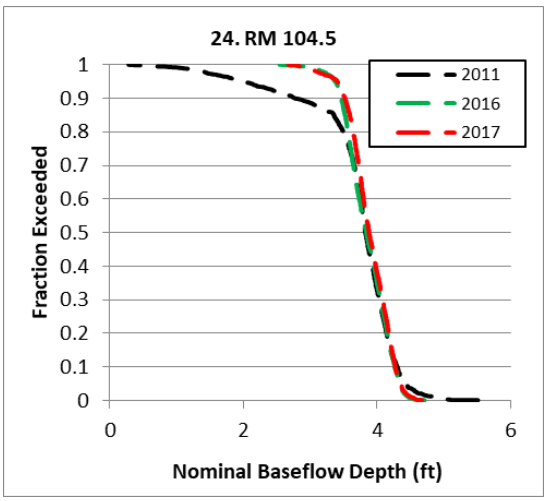
24. RM 104.5
Fraction Exceeded
Nominal Baseflow Depth (ft)
2011
2016
2017

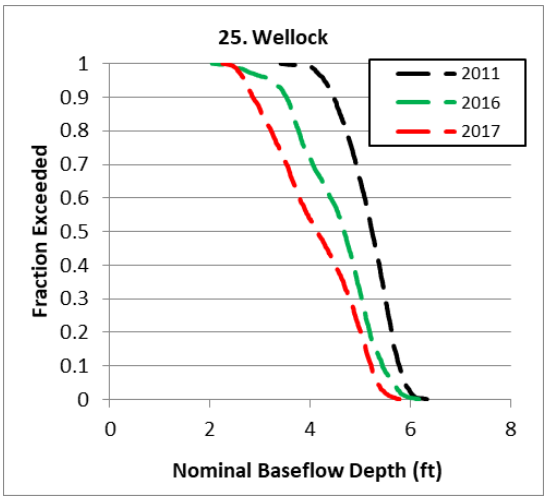
25. Wellock
Fraction Exceeded
Nominal Baseflow Depth (ft)
2011
2016
2017

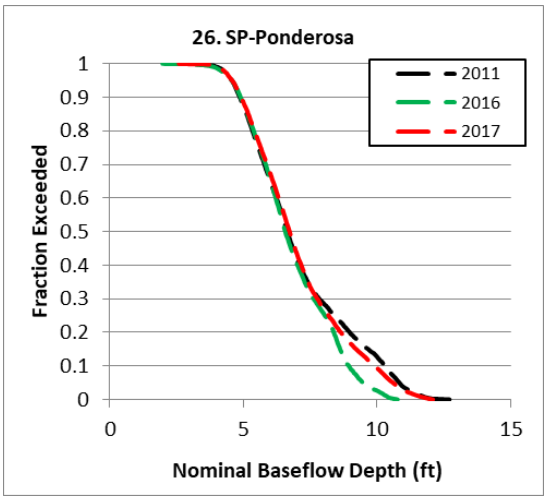
26. SP-Ponderosa
Fraction Exceeded
Nominal Baseflow Depth (ft)
2011
2016
2017

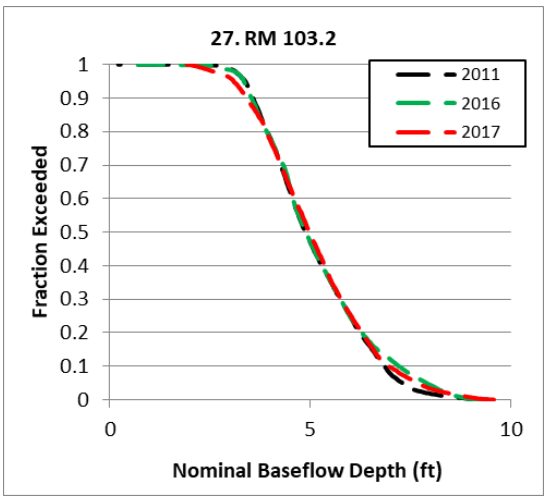
27. RM 103.2
Fraction Exceeded
Nominal Baseflow Depth (ft)
2011
2016
2017

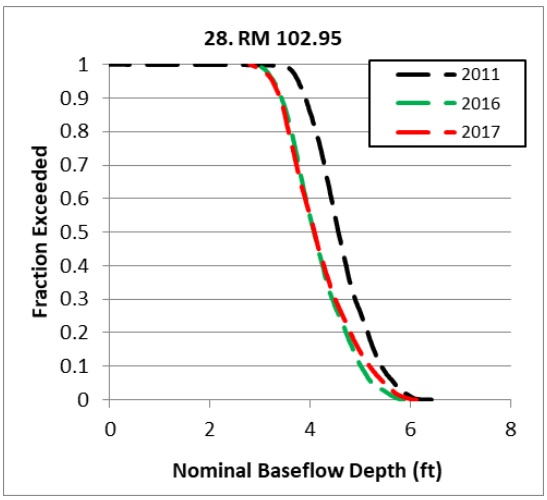
28. RM 102.95
Fraction Exceeded
Nominal Baseflow Depth (ft)
2011
2016
2017

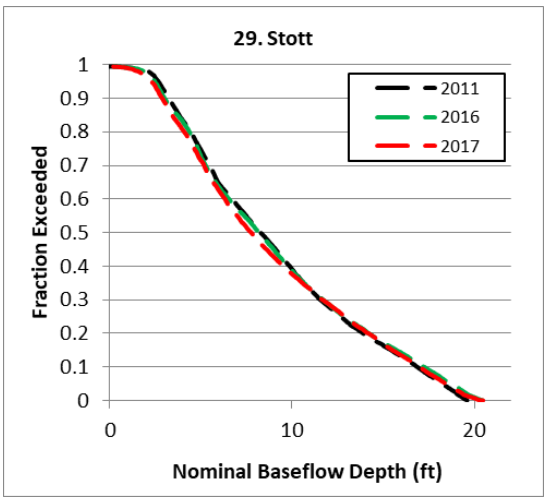
29. Stott
Fraction Exceeded
Nominal Baseflow Depth (ft)
2011
2016
2017

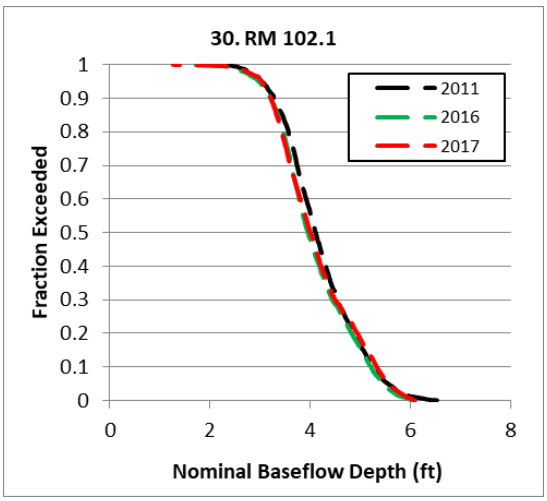
30. RM 102.1
Fraction Exceeded
Nominal Baseflow Depth (ft)
2011
2016
2017

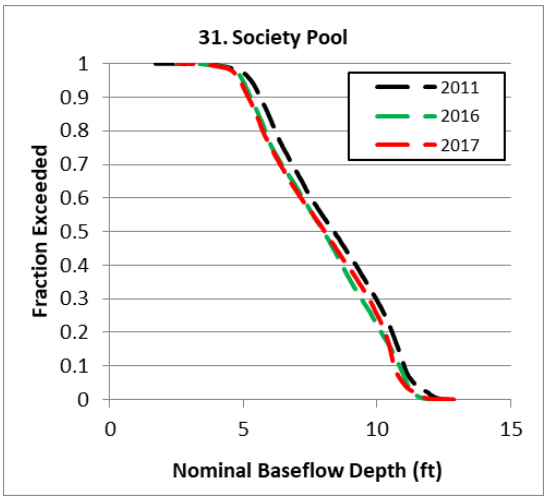
31. Society Pool
Fraction Exceeded
Nominal Baseflow Depth (ft)
2011
2016
2017

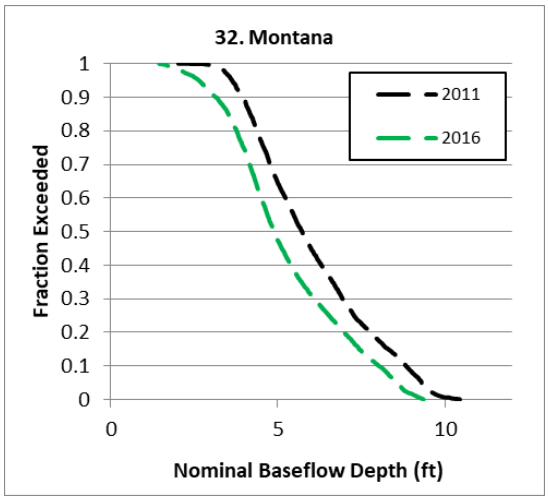
32. Montana
Fraction Exceeded
Nominal Baseflow Depth (ft)
2011
2016

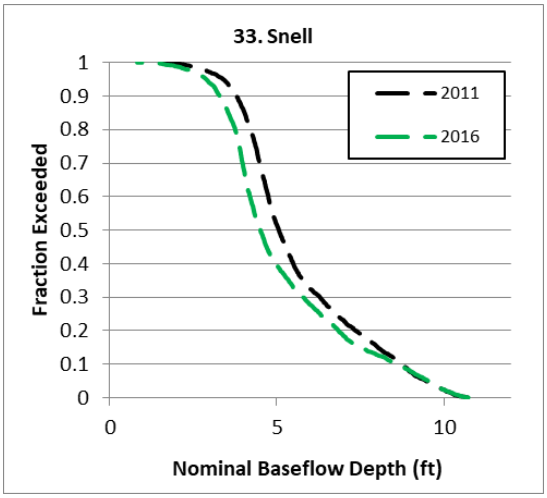
33. Snell
Fraction Exceeded
Nominal Baseflow Depth (ft)
2011
2016

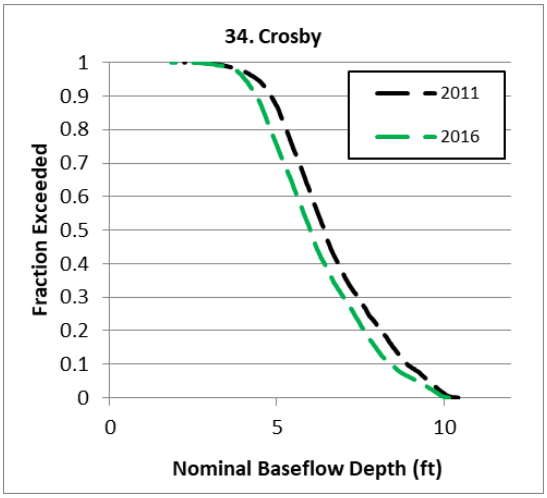
34. Crosby
Fraction Exceeded
Nominal Baseflow Depth (ft)
2011
2016

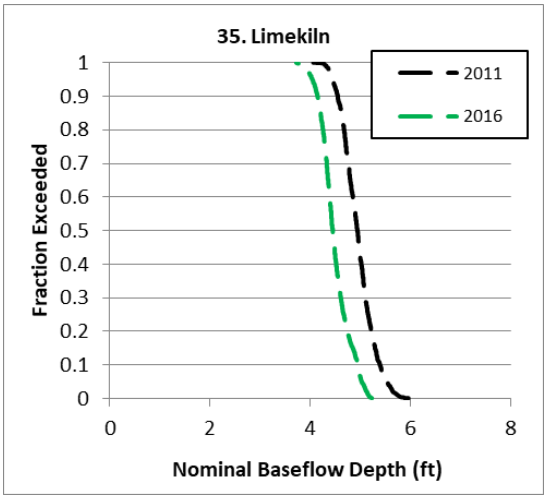
35. Limekiln
Fraction Exceeded
Nominal Baseflow Depth (ft)
2011
2016

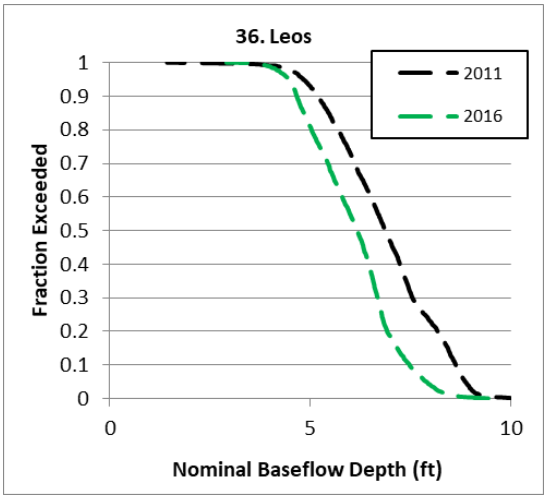
36. Leos
Fraction Exceeded
Nominal Baseflow Depth (ft)
2011
2016

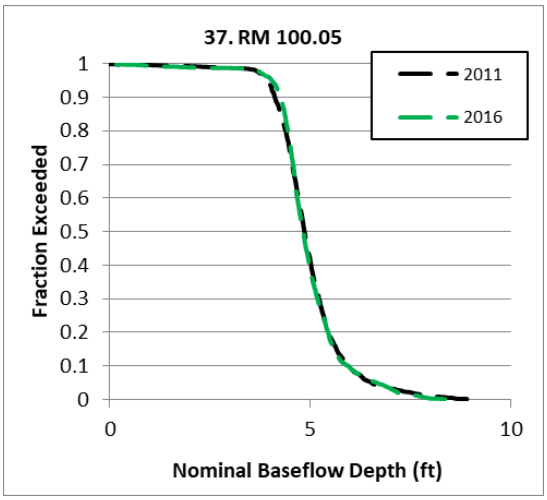
37. RM 100.05
2011
2016
Fraction Exceeded
Nominal Baseflow Depth (ft)

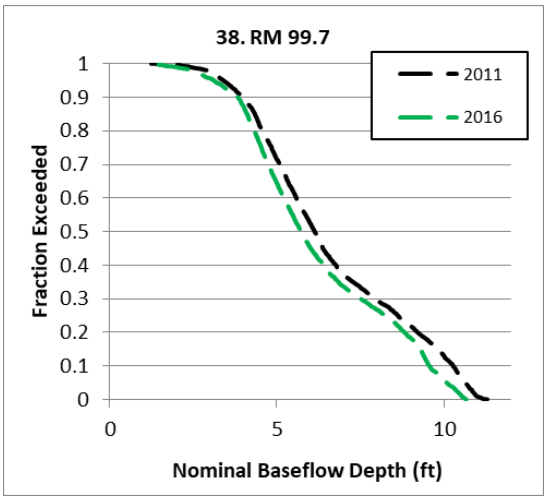
38. RM 99.7
2011
2016
Fraction Exceeded
Nominal Baseflow Depth (ft)

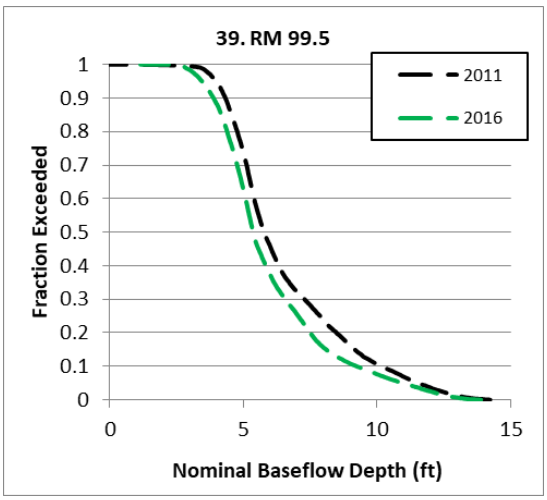
39. RM 99.5
2011
2016
Fraction Exceeded
Nominal Baseflow Depth (ft)

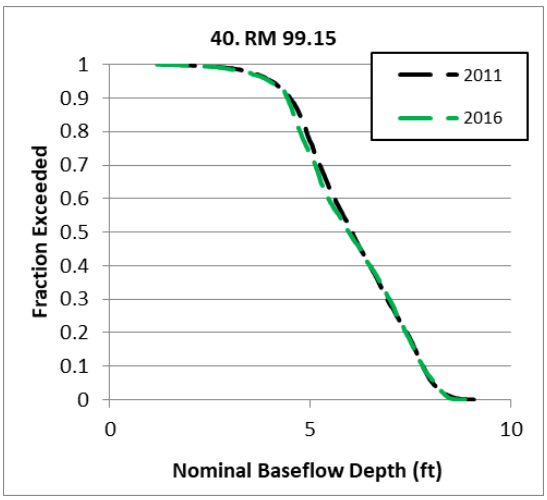
40. RM 99.15
2011
2016
Fraction Exceeded
Nominal Baseflow Depth (ft)

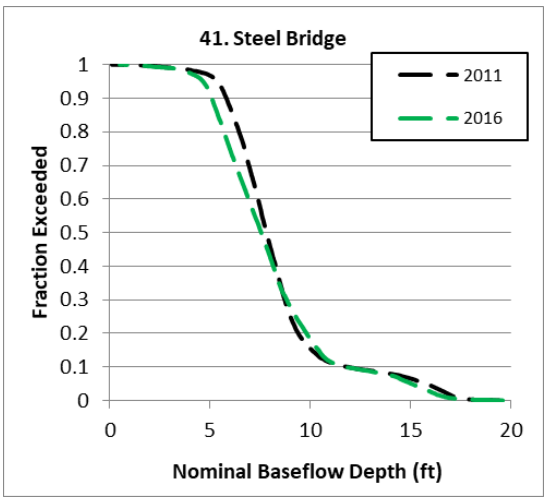
41. Steel Bridge
2011
2016
Fraction Exceeded
Nominal Baseflow Depth (ft)

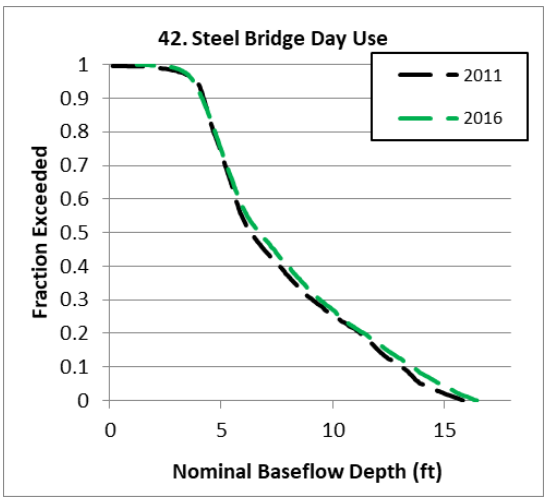
42. Steel Bridge Day Use
2011
2016
Fraction Exceeded
Nominal Baseflow Depth (ft)

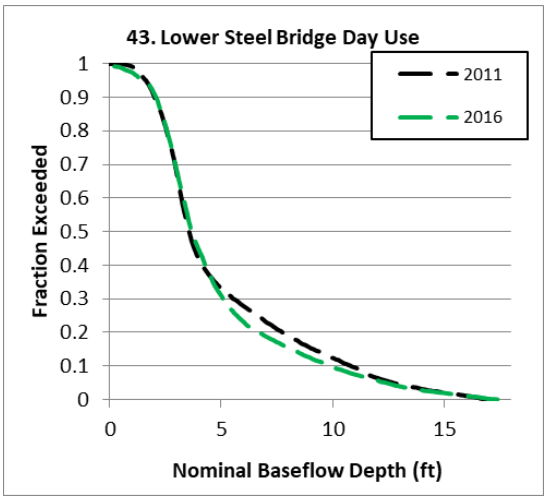
43. Lower Steel Bridge Day Use
2011
2016
Fraction Exceeded
Nominal Baseflow Depth (ft)

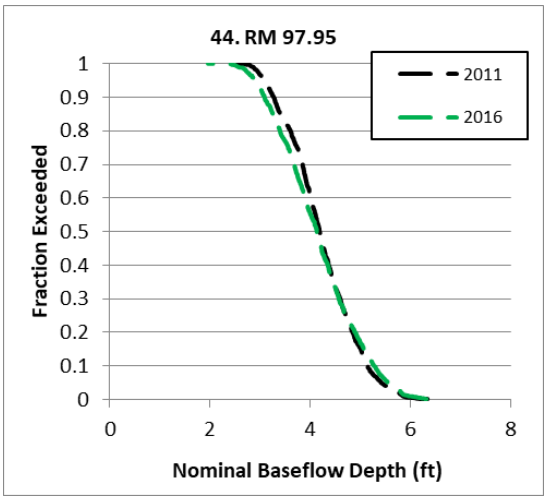
44. RM 97.95
2011
2016
Fraction Exceeded
Nominal Baseflow Depth (ft)

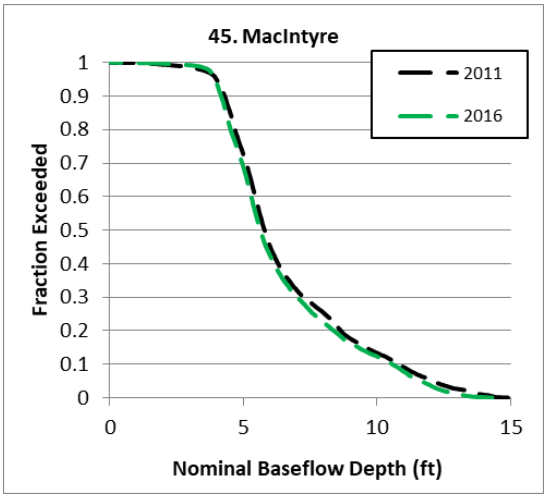
45. MacIntyre
2011
2016
Fraction Exceeded
Nominal Baseflow Depth (ft)

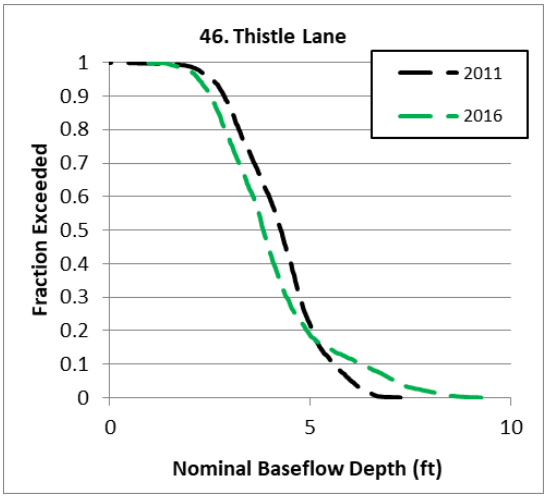
46. Thistle Lane
2011
2016
Fraction Exceeded
Nominal Baseflow Depth (ft)

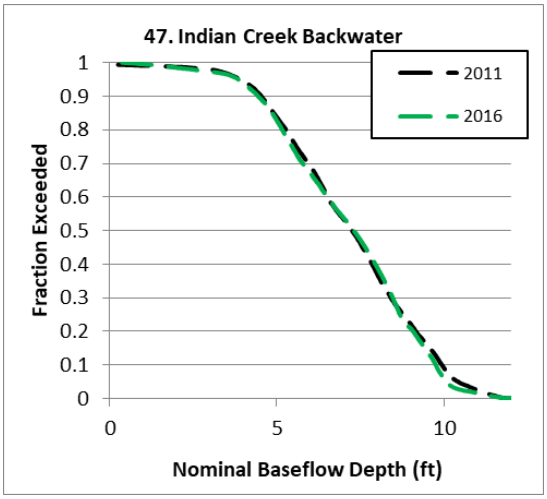
47. Indian Creek Backwater
2011
2016
Fraction Exceeded
Nominal Baseflow Depth (ft)

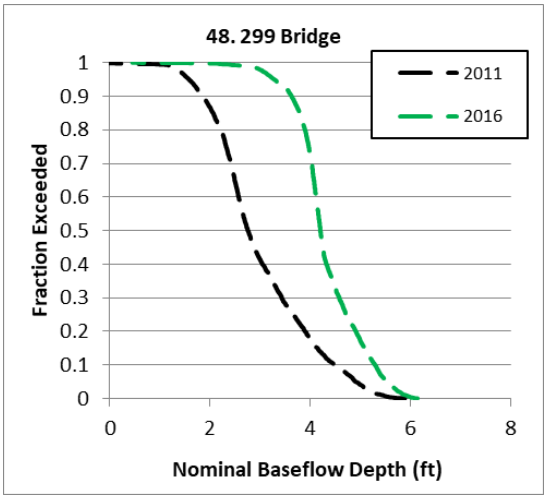
48. 299 Bridge
2011
2016
Fraction Exceeded
Nominal Baseflow Depth (ft)

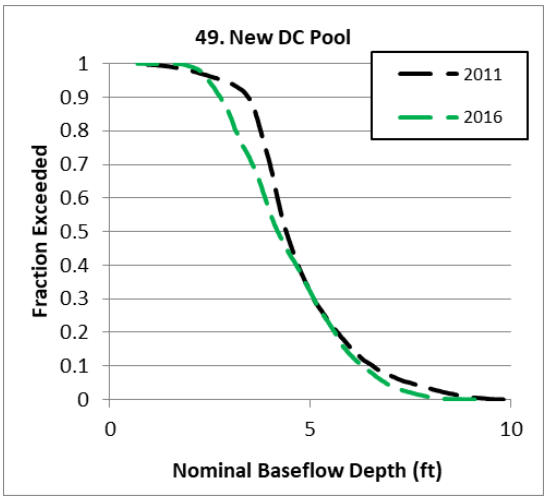
49. New DC Pool
2011
2016
Fraction Exceeded
Nominal Baseflow Depth (ft)

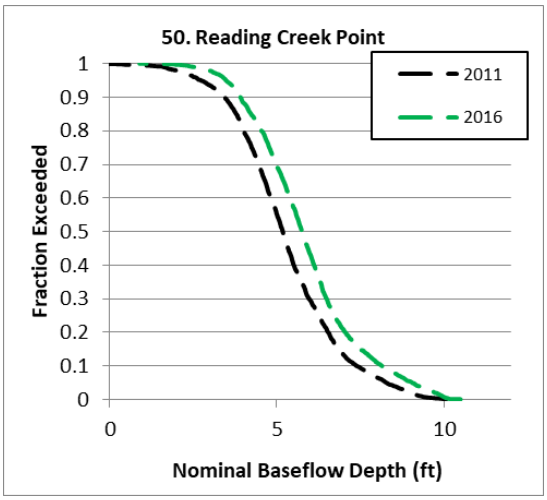
50. Reading Creek Point
2011
2016
Fraction Exceeded
Nominal Baseflow Depth (ft)

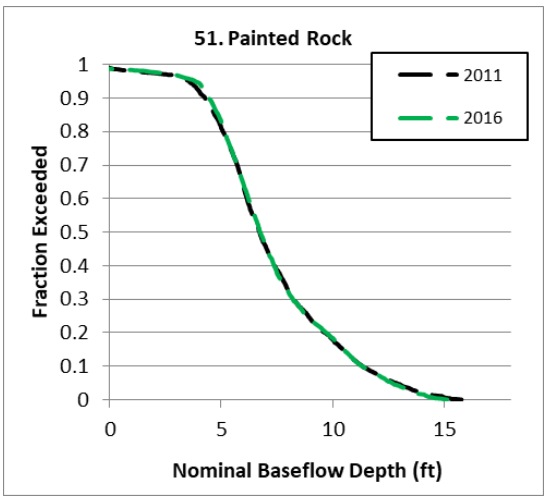
51. Painted Rock
2011
2016
Fraction Exceeded
Nominal Baseflow Depth (ft)

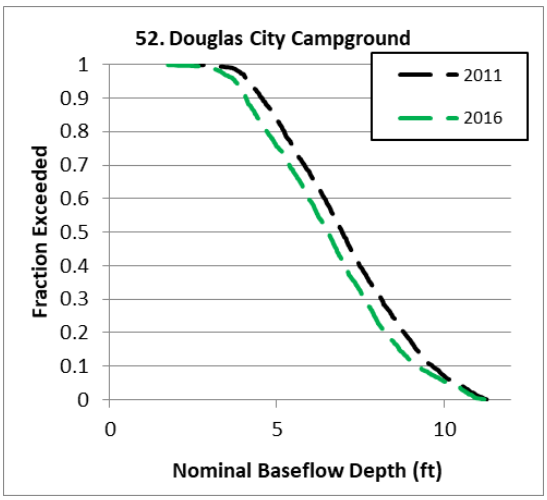
52. Douglas City Campground
2011
2016
Fraction Exceeded
Nominal Baseflow Depth (ft)

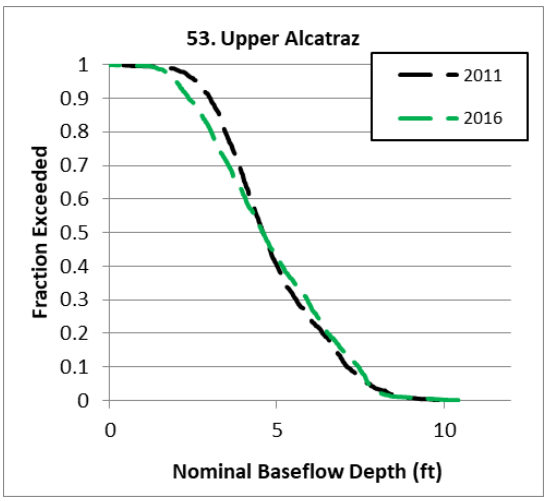
53. Upper Alcatraz
2011
2016
Fraction Exceeded
Nominal Baseflow Depth (ft)

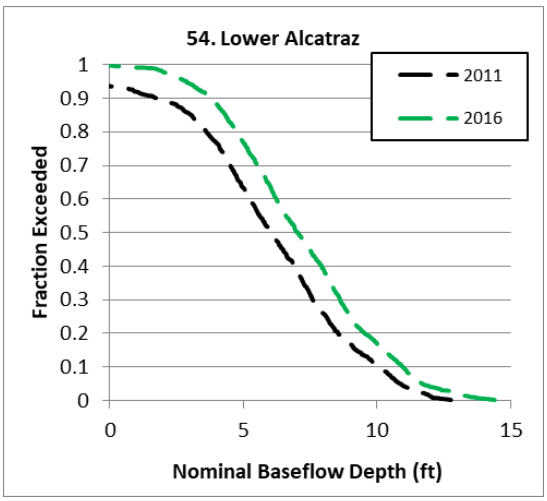
54. Lower Alcatraz
2011
2016
Fraction Exceeded
Nominal Baseflow Depth (ft)

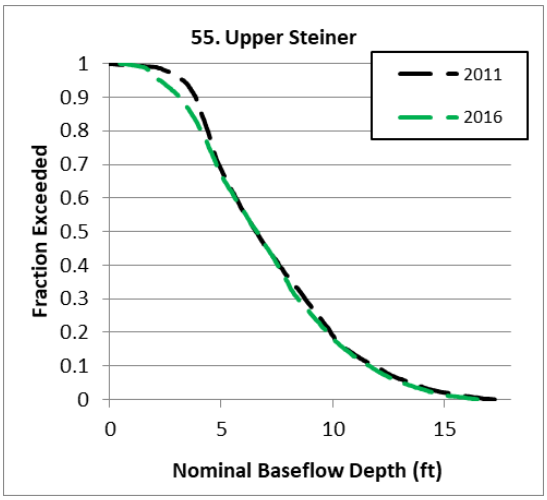
55. Upper Steiner
2011
2016
Fraction Exceeded
Nominal Baseflow Depth (ft)

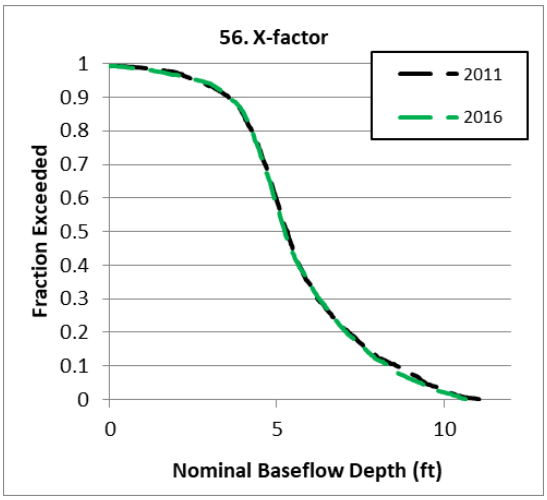
56. X-factor
2011
2016
Fraction Exceeded
Nominal Baseflow Depth (ft)

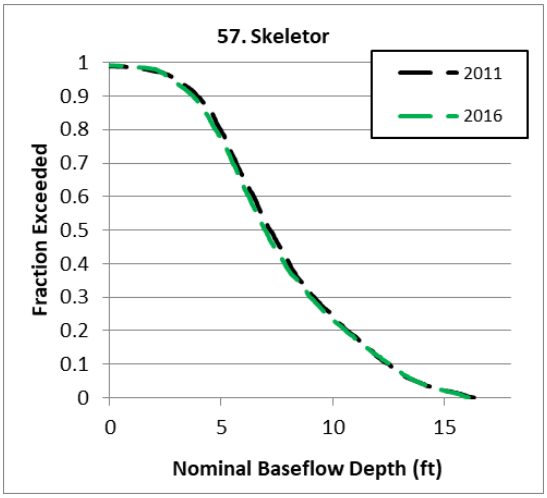
57. Skeletor
2011
2016
Fraction Exceeded
Nominal Baseflow Depth (ft)

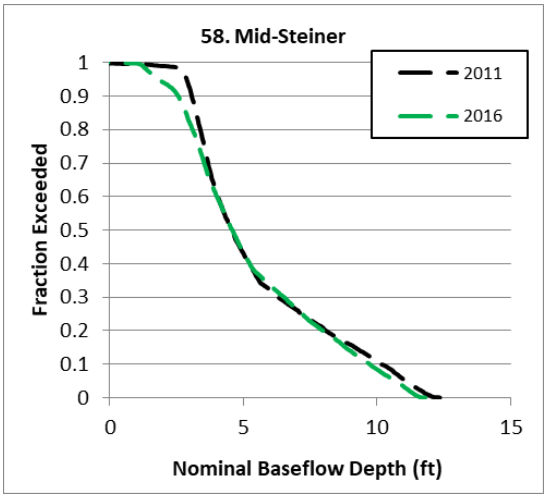
58. Mid-Steiner
2011
2016
Fraction Exceeded
Nominal Baseflow Depth (ft)

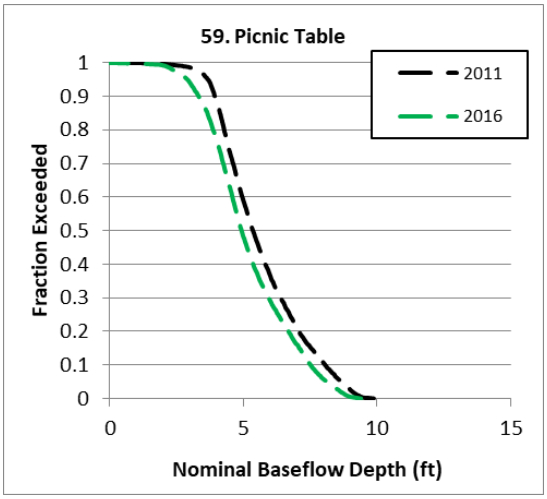
59. Picnic Table
2011
2016
Fraction Exceeded
Nominal Baseflow Depth (ft)

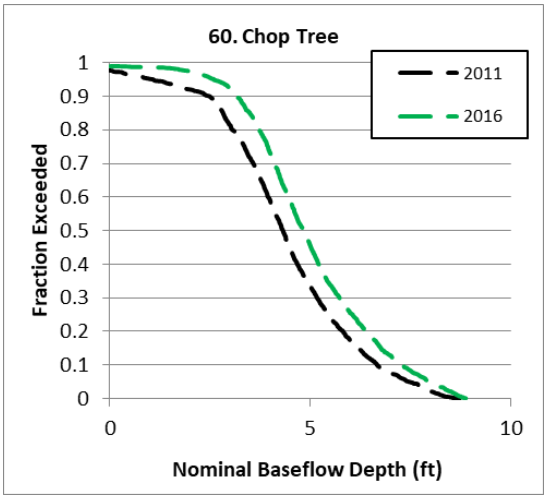
60. Chop Tree
2011
2016
Fraction Exceeded
Nominal Baseflow Depth (ft)

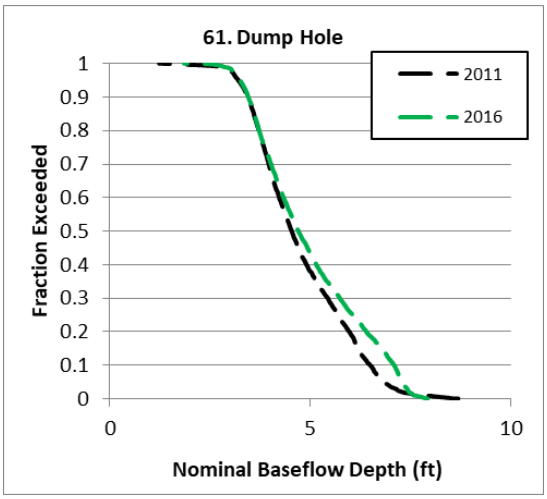
61. Dump Hole
2011
2016
Fraction Exceeded
Nominal Baseflow Depth (ft)

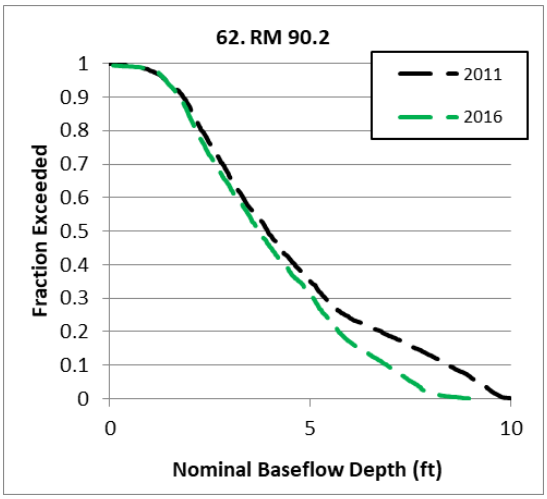
62. RM 90.2
2011
2016
Fraction Exceeded
Nominal Baseflow Depth (ft)

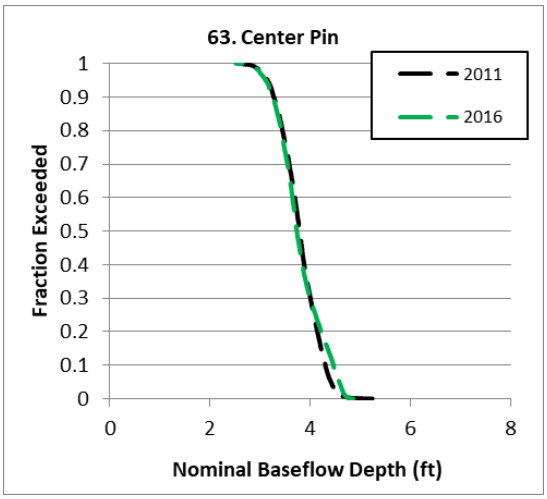
63. Center Pin
2011
2016
Fraction Exceeded
Nominal Baseflow Depth (ft)

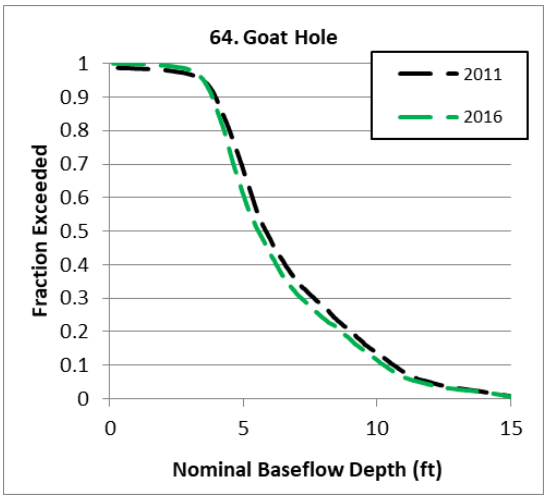
64. Goat Hole
2011
2016
Fraction Exceeded
Nominal Baseflow Depth (ft)

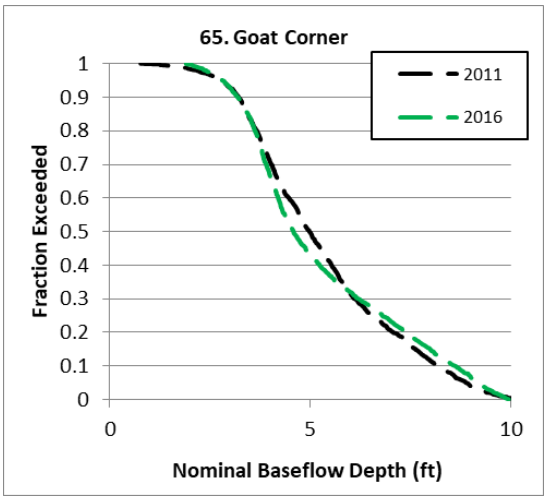
65. Goat Corner
2011
2016
Fraction Exceeded
Nominal Baseflow Depth (ft)

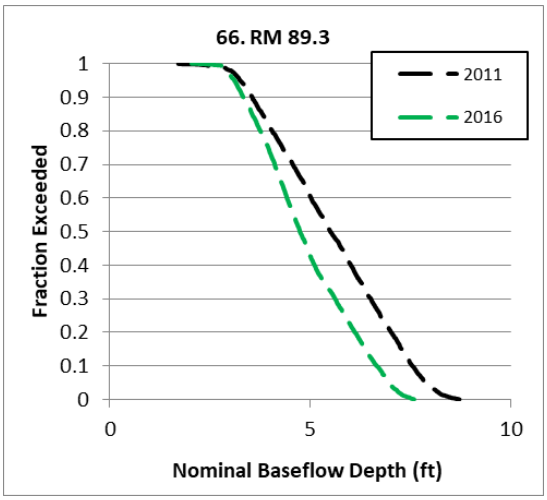
66. RM 89.3
2011
2016
Fraction Exceeded
Nominal Baseflow Depth (ft)

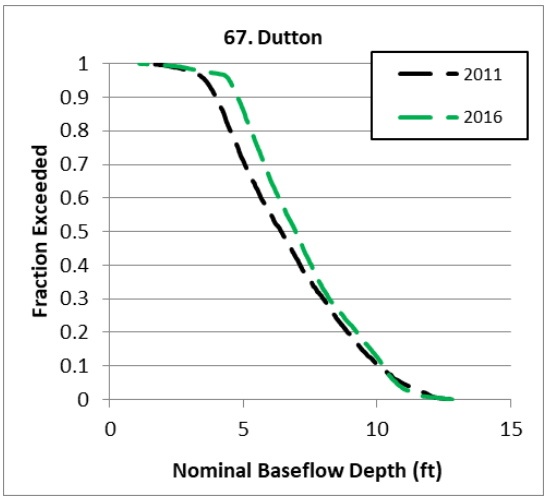
67. Dutton
2011
2016
Fraction Exceeded
Nominal Baseflow Depth (ft)

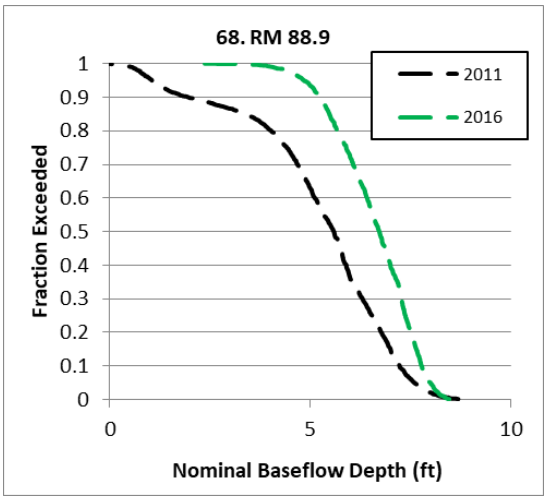
68. RM 88.9
2011
2016
Fraction Exceeded
Nominal Baseflow Depth (ft)

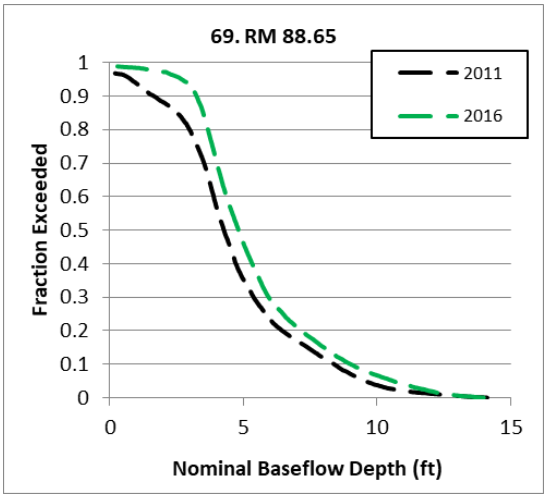
69. RM 88.65
2011
2016
Fraction Exceeded
Nominal Baseflow Depth (ft)

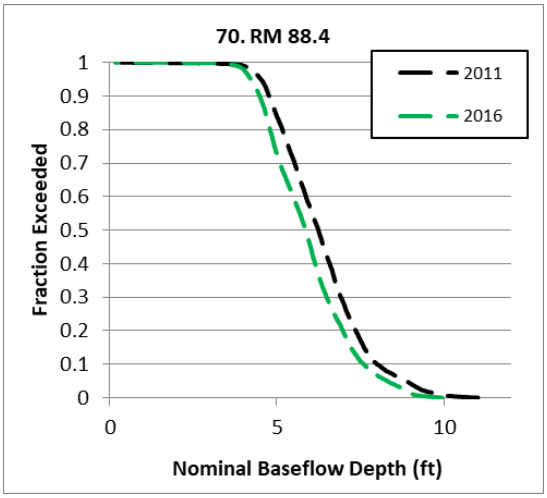
70. RM 88.4
2011
2016
Fraction Exceeded
Nominal Baseflow Depth (ft)

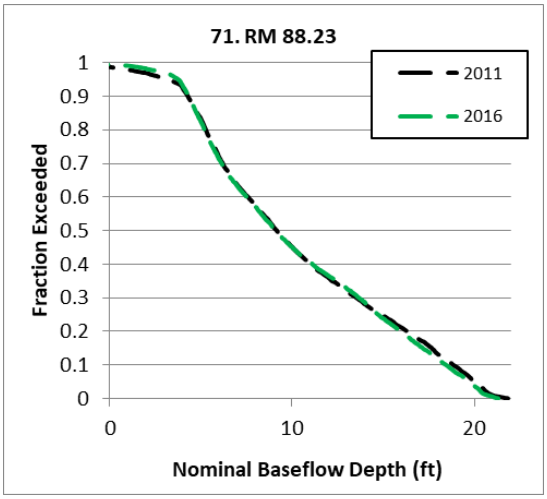
71. RM 88.23
2011
2016
Fraction Exceeded
Nominal Baseflow Depth (ft)

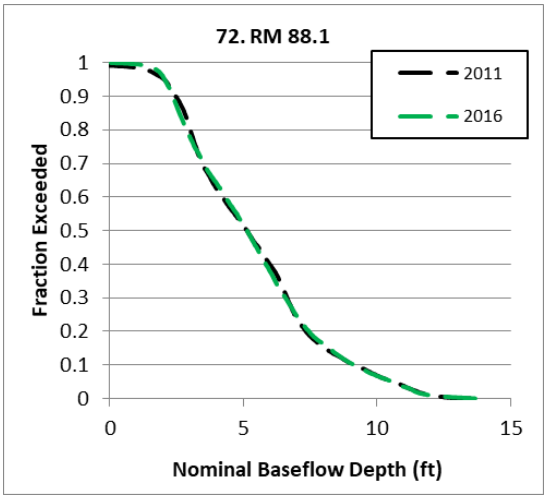
72. RM 88.1
2011
2016
Fraction Exceeded
Nominal Baseflow Depth (ft)

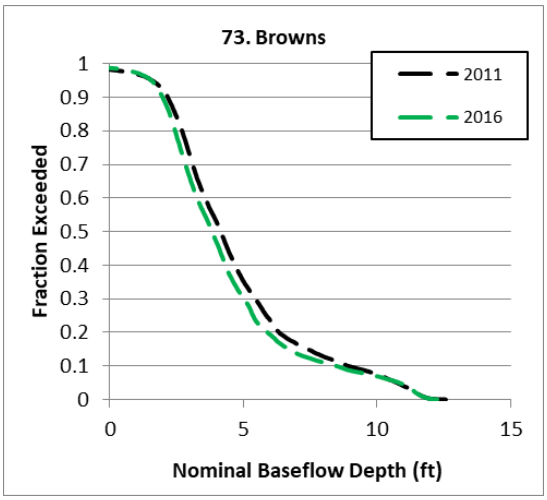
73. Browns
2011
2016
Fraction Exceeded
Nominal Baseflow Depth (ft)

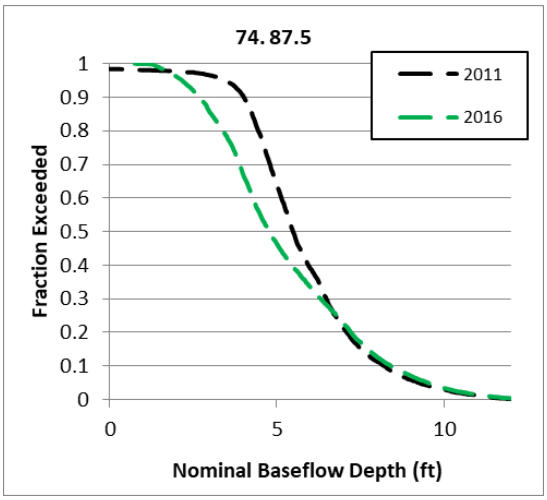
74. 87.5
2011
2016
Fraction Exceeded
Nominal Baseflow Depth (ft)

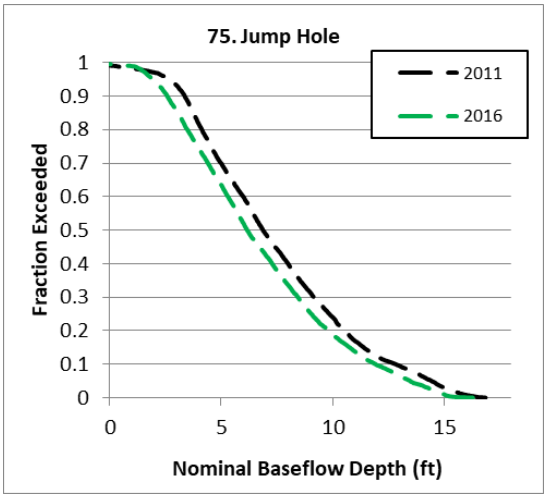
75. Jump Hole
2011
2016
Fraction Exceeded
Nominal Baseflow Depth (ft)

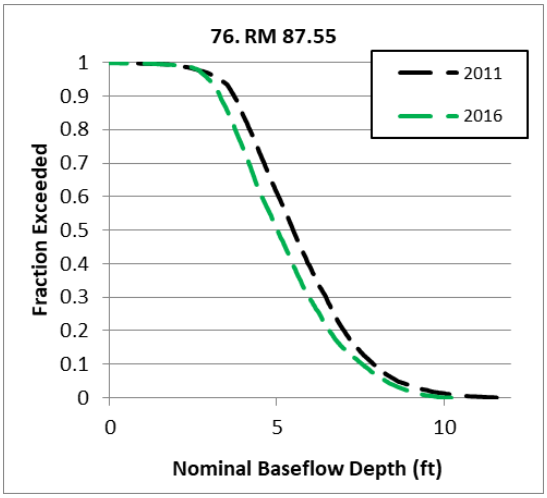
76. RM 87.55
2011
2016
Fraction Exceeded
Nominal Baseflow Depth (ft)

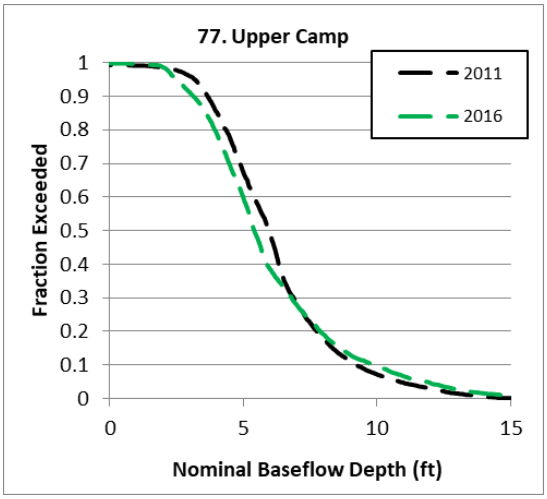
77. Upper Camp
2011
2016
Fraction Exceeded
Nominal Baseflow Depth (ft)

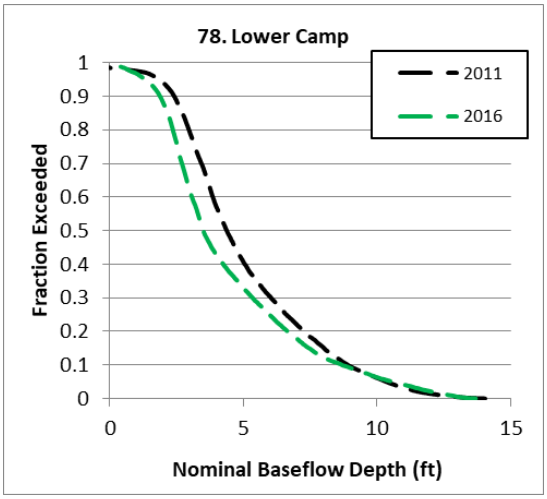
78. Lower Camp
2011
2016
Fraction Exceeded
Nominal Baseflow Depth (ft)

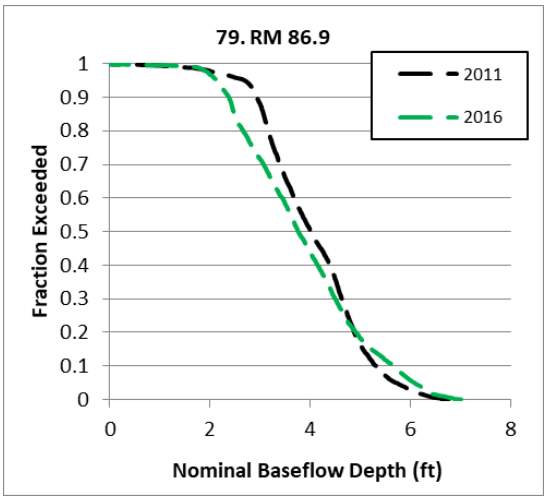
79. RM 86.9
2011
2016
Fraction Exceeded
Nominal Baseflow Depth (ft)

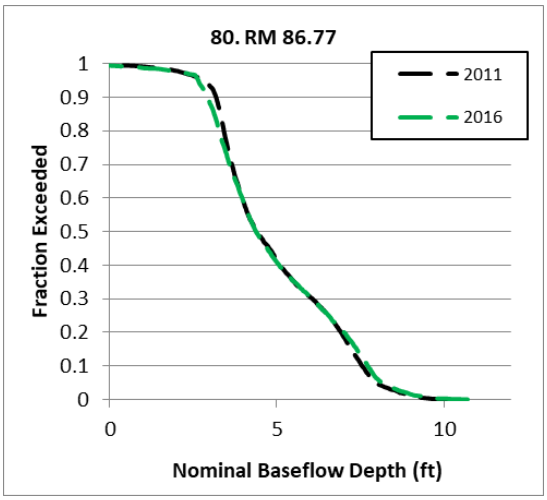
80. RM 86.77
2011
2016
Fraction Exceeded
Nominal Baseflow Depth (ft)

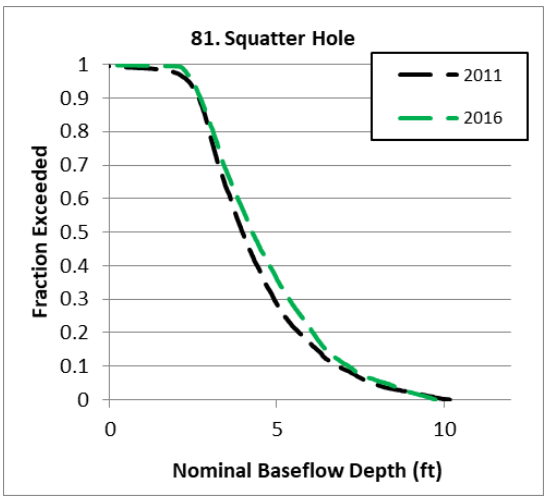
81. Squatter Hole
2011
2016
Fraction Exceeded
Nominal Baseflow Depth (ft)

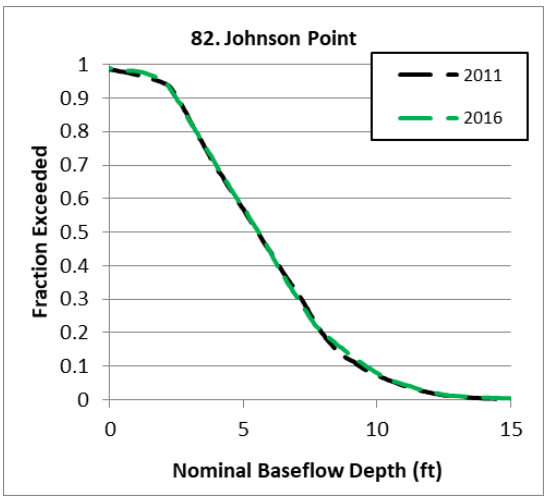
82. Johnson Point
2011
2016
Fraction Exceeded
Nominal Baseflow Depth (ft)

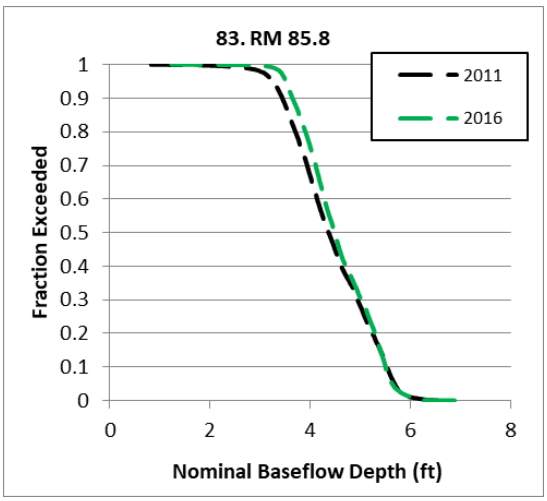
83. RM 85.8
2011
2016
Fraction Exceeded
Nominal Baseflow Depth (ft)

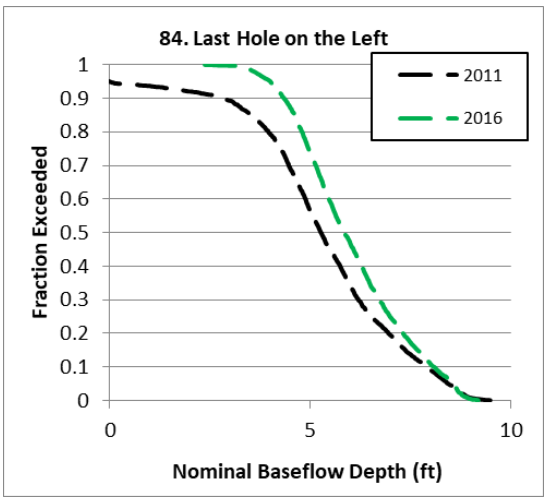
84. Last Hole on the Left
2011
2016
Fraction Exceeded
Nominal Baseflow Depth (ft)

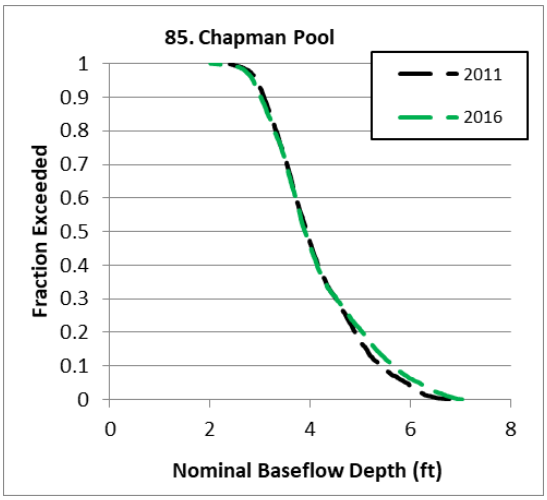
85. Chapman Pool
2011
2016
Fraction Exceeded
Nominal Baseflow Depth (ft)

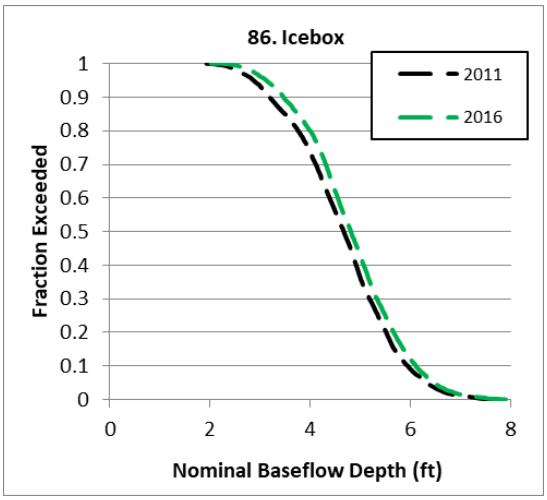
86. Icebox
2011
2016
Fraction Exceeded
Nominal Baseflow Depth (ft)

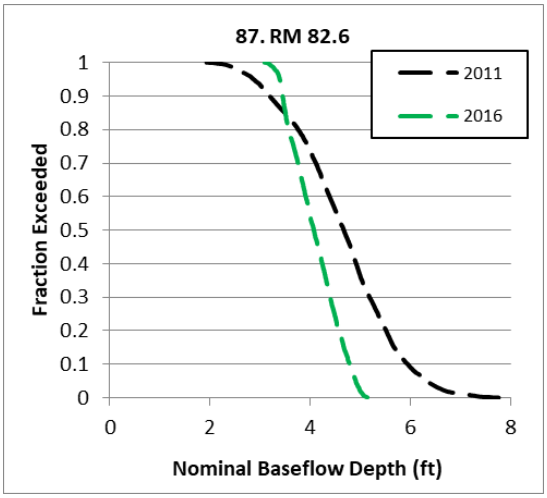
87. RM 82.6
2011
2016
Fraction Exceeded
Nominal Baseflow Depth (ft)

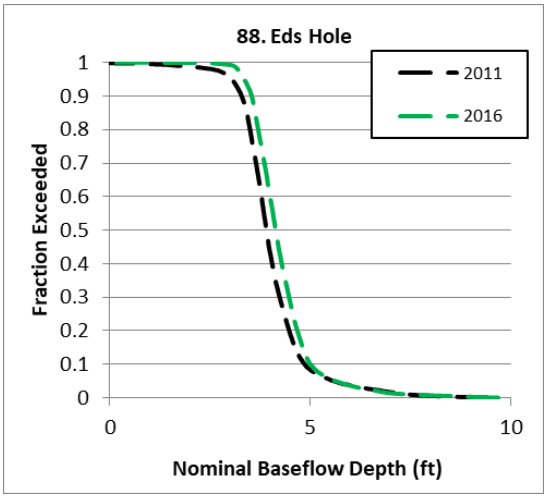
88. Eds Hole
2011
2016
Fraction Exceeded
Nominal Baseflow Depth (ft)

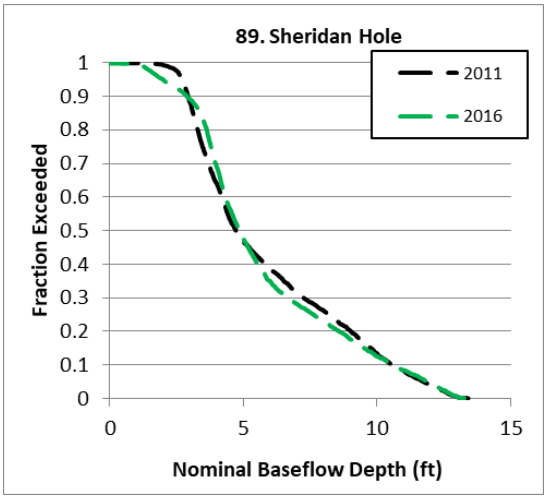
89. Sheridan Hole
2011
2016
Fraction Exceeded
Nominal Baseflow Depth (ft)

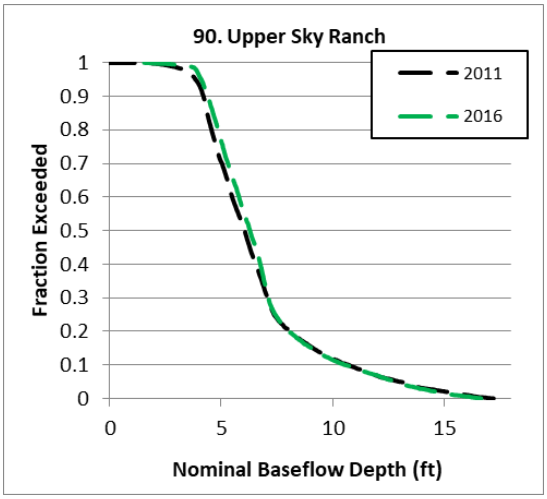
90. Upper Sky Ranch
2011
2016
Fraction Exceeded
Nominal Baseflow Depth (ft)

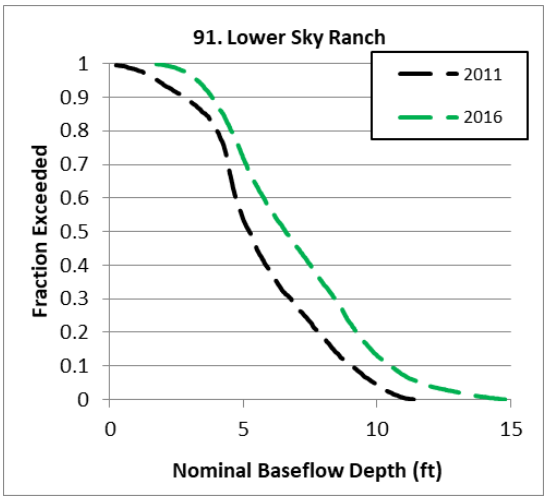
91. Lower Sky Ranch
2011
2016
Fraction Exceeded
Nominal Baseflow Depth (ft)

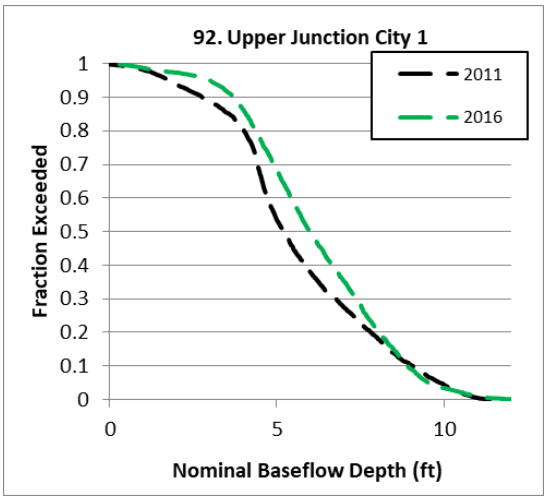
92. Upper Junction City 1
2011
2016
Fraction Exceeded
Nominal Baseflow Depth (ft)

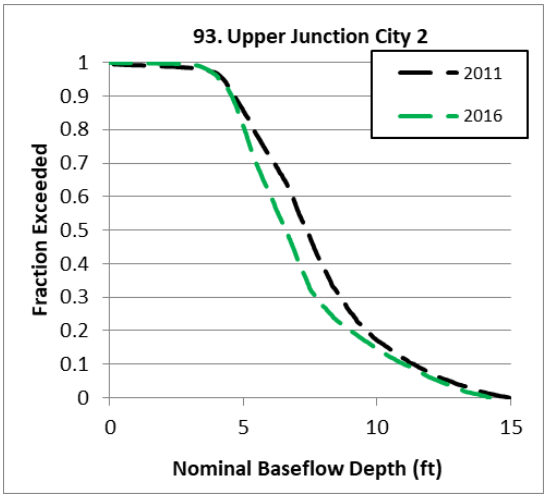
93. Upper Junction City 2
2011
2016
Fraction Exceeded
Nominal Baseflow Depth (ft)

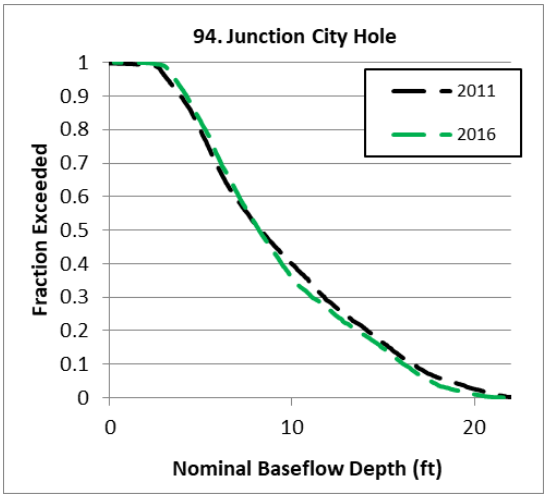
94. Junction City Hole
2011
2016
Fraction Exceeded
Nominal Baseflow Depth (ft)

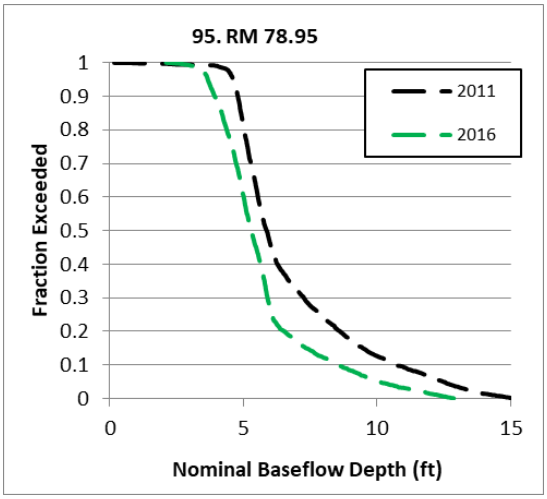
95. RM 78.95
2011
2016
Fraction Exceeded
Nominal Baseflow Depth (ft)

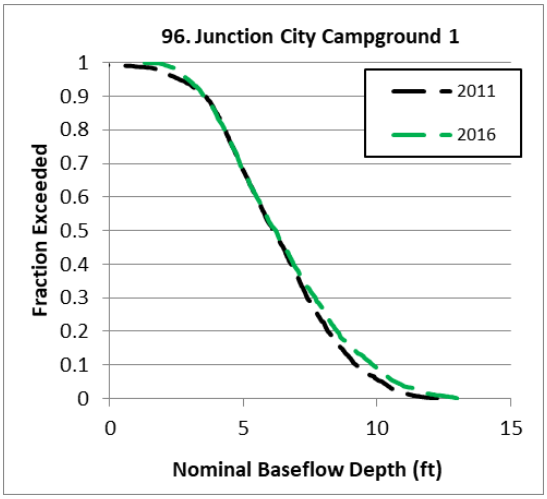
96. Junction City Campground 1
2011
2016
Fraction Exceeded
Nominal Baseflow Depth (ft)

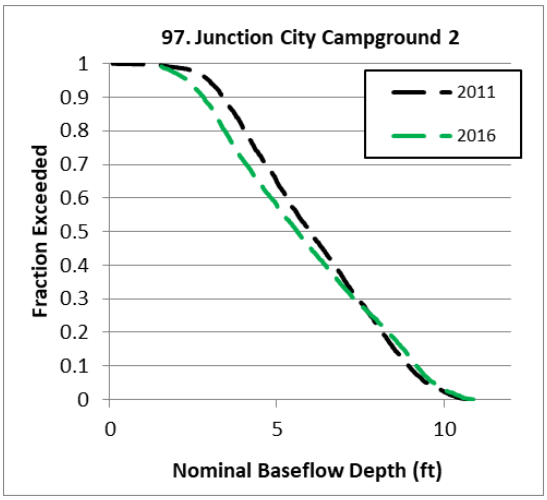
97. Junction City Campground 2
Fraction Exceeded
Nominal Baseflow Depth (ft)
2011
2016

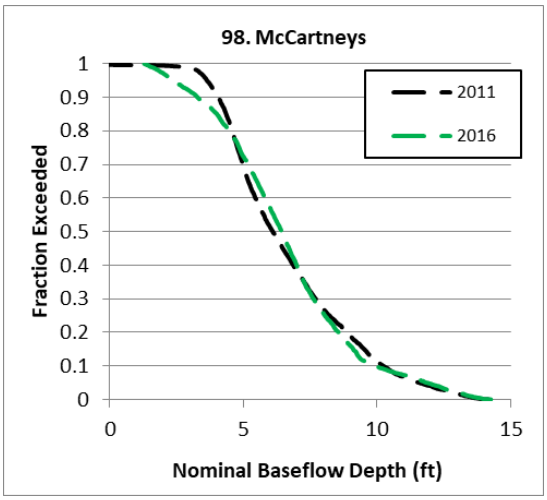
98. McCartneys
Fraction Exceeded
Nominal Baseflow Depth (ft)
2011
2016

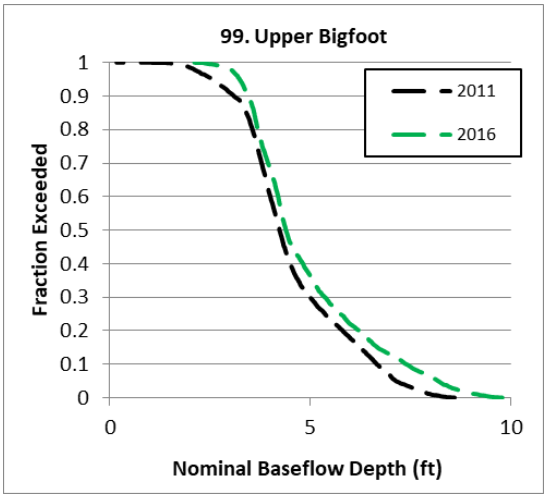
99. Upper Bigfoot
Fraction Exceeded
Nominal Baseflow Depth (ft)
2011
2016

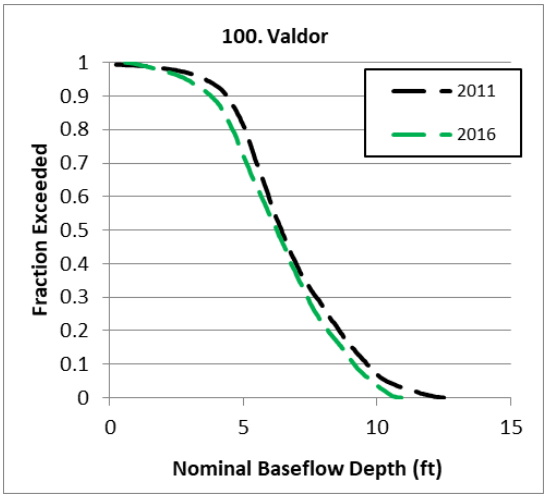
100. Valdor
Fraction Exceeded
Nominal Baseflow Depth (ft)
2011
2016

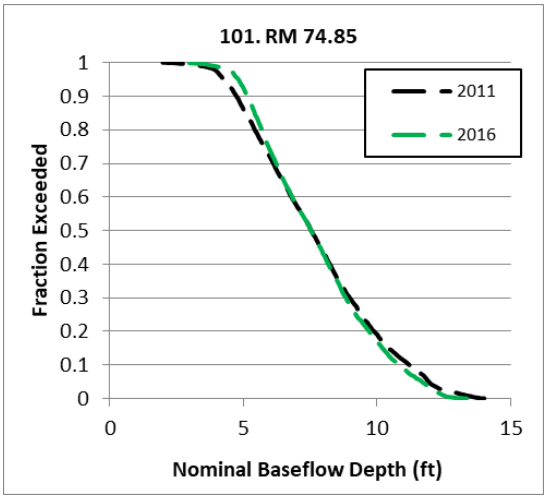
101. RM 74.85
Fraction Exceeded
Nominal Baseflow Depth (ft)
2011
2016

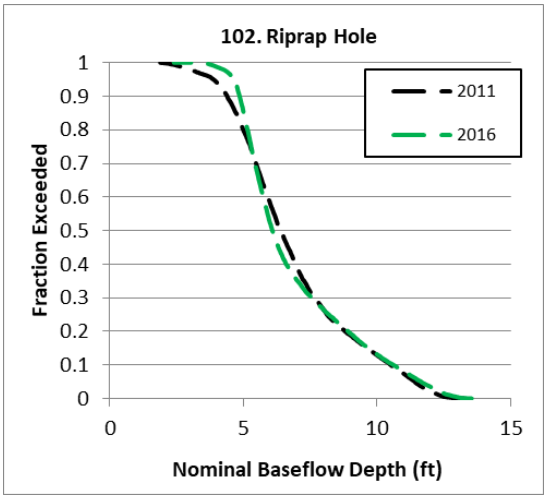
102. Riprap Hole
Fraction Exceeded
Nominal Baseflow Depth (ft)
2011
2016

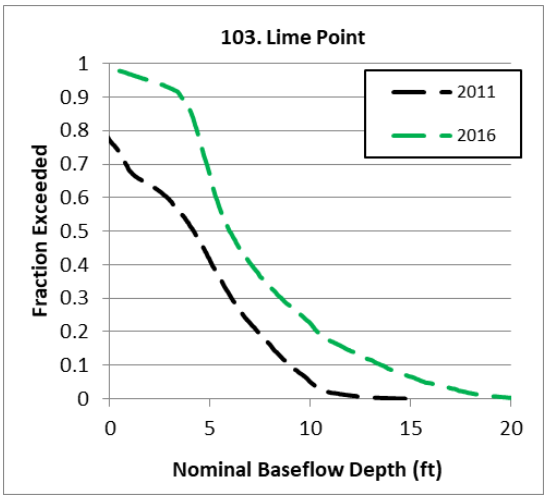
103. Lime Point
Fraction Exceeded
Nominal Baseflow Depth (ft)
2011
2016
0
0.1
0.2
0.3
0.4
0.5
0.6
0.7
0.8
0.9
1
0
5
10
15
20

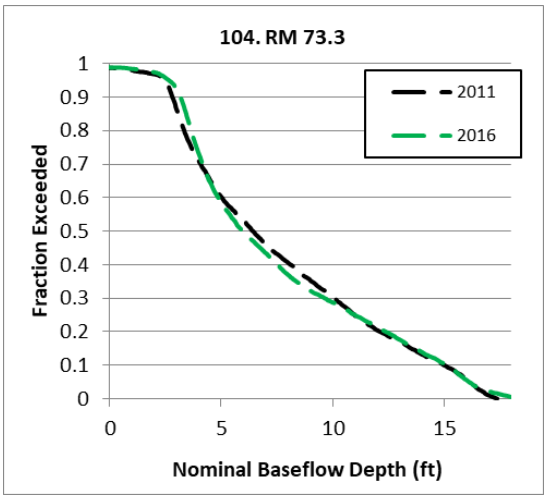
104. RM 73.3
Fraction Exceeded
Nominal Baseflow Depth (ft)
2011
2016
0
0.1
0.2
0.3
0.4
0.5
0.6
0.7
0.8
0.9
1
0
5
10
15

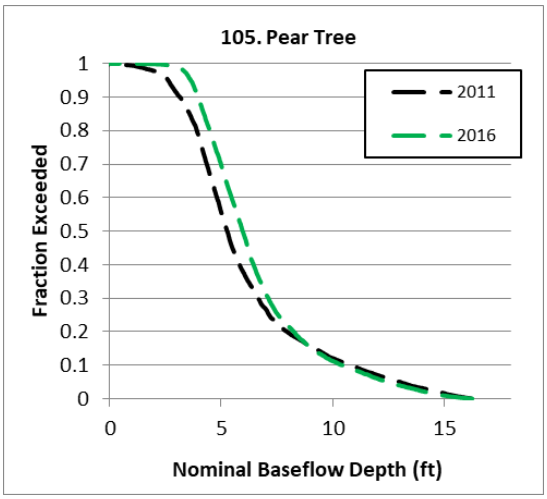
105. Pear Tree
Fraction Exceeded
Nominal Baseflow Depth (ft)
2011
2016
0
0.1
0.2
0.3
0.4
0.5
0.6
0.7
0.8
0.9
1
0
5
10
15

Appendix G: Pool Depth Change Statistics

Changes in median, 75th-percentile, and 90th-percentile depths in ft at polygon locations.

			2011-2016			2016-2017			2011-2017		
No.	Name	RM	Δmedian	Δ75th	Δ90th	Δmedian	Δ75th	Δ90th	Δmedian	Δ75th	Δ90th
1	Diversion Pool	111.15	-0.33	-0.19	-0.09	0.19	0.14	0.35	-0.14	-0.05	0.26
2	Deadwood	111.05	-0.03	-0.05	0.11	-0.02	-0.15	-0.03	-0.05	-0.20	0.08
3	New Bridge	110.95	-0.12	0.38	0.48	-0.42	0.42	0.51	-0.54	0.80	0.99
4	Higgs	110.7	-0.16	-0.08	0.16	0.11	0.41	0.46	-0.05	0.33	0.62
5	Cableway	110.32	0.25	0.14	0.12	0.26	0.39	0.59	0.51	0.53	0.71
6	Old Bridge	110.2	-0.03	-0.02	-0.07	0.33	0.50	0.65	0.30	0.48	0.58
7	Hoadley	109.9	-0.41	-0.33	-0.48	0.24	0.39	0.46	-0.17	0.06	-0.02
8	Upper Cemetery	109.47	0.92	1.04	2.03	0.12	0.95	1.33	1.04	1.99	3.36
9	Cemetery	109.43	-0.49	-0.73	-0.01	-0.40	-0.89	-2.62	-0.89	-1.62	-2.63
10	Sawmill Burner	109	-0.12	-0.48	-0.50	0.22	0.09	0.07	0.10	-0.39	-0.43
11	Lower Burner	108.95	-0.06	0.15	0.24	0.30	0.69	1.01	0.24	0.84	1.25
12	Rush Pool	108.1	-0.04	0.00	-0.12	0.14	0.11	0.15	0.10	0.11	0.03
13	Dark Gulch	106.6	0.06	0.23	0.47	0.07	0.06	0.15	0.13	0.29	0.62
14	Lower Dark Gulch	106.5	-1.16	-1.32	-1.28	-0.19	-0.09	0.06	-1.35	-1.41	-1.22
15	RM106.25	106.25	-0.38	-0.43	-0.93	0.13	0.09	0.13	-0.25	-0.34	-0.80
16	Dirty Bird	105.8	-0.72	-0.85	-0.49	0.33	0.55	0.27	-0.39	-0.30	-0.22
17	Bucktail Island Bkwtr	105.67	-0.22	-0.45	-0.49	-0.39	0.06	1.01	-0.61	-0.39	0.52
18	Upper Bucktail	105.45	0.11	0.67	1.12	1.08	1.47	1.53	1.19	2.14	2.65
19	Bucktail	105.4	-0.53	0.43	0.94	0.45	0.68	1.72	-0.08	1.11	2.66
20	RM105.15	105.2	-0.36	-0.36	-0.15	-0.06	0.04	0.25	-0.42	-0.32	0.10
21	Lowden Approach	105.05	-0.87	-0.43	-0.07	-0.68	-0.40	-0.30	-1.55	-0.83	-0.37
22	Lowden Bend	104.95	0.26	0.26	0.19	0.30	0.63	0.93	0.56	0.89	1.12
23	Lowden Convergence	104.65	-0.04	-0.13	-0.05	0.11	0.10	-0.10	0.07	-0.03	-0.15
24	RM104.5	104.5	0.01	0.01	-0.03	0.04	0.03	0.00	0.05	0.04	-0.03
25	Wellock	104.3	-0.55	-0.46	-0.34	-0.54	-0.20	-0.22	-1.09	-0.66	-0.56
26	SP-Ponderosa	103.9	-0.08	-0.37	-1.37	0.17	0.14	0.97	0.09	-0.23	-0.40

27	Tom Lang	103.2	0.02	0.00	0.36	0.08	0.03	-0.25	0.10	0.03	0.11
28	RM102.95	102.95	-0.48	-0.45	-0.41	0.00	0.07	0.17	-0.48	-0.38	-0.24
29	Stott	102.5	-0.07	0.21	0.39	-0.44	0.04	-0.27	-0.51	0.25	0.12
30	RM102.1	102.1	-0.16	-0.06	-0.03	0.05	0.07	0.11	-0.11	0.01	0.08
31	Society Pool	101.8	-0.39	-0.50	-0.17	0.04	0.22	-0.20	-0.35	-0.28	-0.37
32	Montana	101.35	-0.84	-0.75	-0.81						
33	Snell	101.17	-0.55	-0.46	-0.09						
34	Crosby	101.5	-0.42	-0.42	-0.50						
35	Limekiln	100.85	-0.49	-0.49	-0.44						
36	Leos	100.6	-0.69	-1.08	-1.15						
37	Limekiln Trough	100.05	-0.03	-0.01	-0.02						
38	Lower Limekiln	99.7	-0.41	-0.36	-0.71						
39	Upper Steel Bridge	99.5	-0.41	-0.82	-0.94						
40	RM99.15	99.15	-0.07	0.02	-0.01						
41	Steel Bridge	98.9	-0.26	0.26	-0.07						
42	Steel Bridge Day Use	98.55	0.38	0.18	0.53						
43	Low St Brdg Day Use	98.2	0.11	-0.91	-0.88						
44	RM97.95	97.95	0.06	-0.03	-0.13						
45	McIntyre Pool	97.35	-0.16	-0.42	-0.24						
46	Thistle Lane Pool	96.95	-0.44	-0.26	0.72						
47	Ind. Ck Backwater	95.65	0.07	-0.10	-0.18						
48	299 Bridge	94.1	1.44	1.06	0.80						
49	New DC Pool	93.3	-0.21	-0.02	-0.25						
50	The Bend	92.95	0.57	0.48	0.76						
51	Painted Rock	92.7	0.02	-0.08	0.01						
52	DC Campground	92.4	-0.43	-0.54	-0.40						
53	Upper Alcatraz	92.33	0.01	0.27	0.35						
54	Lower Alcatraz	92.28	1.00	0.89	0.88						
55	Upper-steiner	92	0.06	-0.28	-0.18						
56	X-factor	91.6	-0.08	0.02	-0.26						
57	Skeletor	91.5	-0.23	-0.24	0.02						

58	Mid-Steiner	91.4	0.02	0.04	-0.44
59	Picnic Table	91.05	-0.43	-0.44	-0.55
60	Chop Tree	90.9	0.52	0.61	0.62
61	Dump Hole	90.75	0.17	0.36	0.59
62	RM90.2	90.2	-0.20	-0.50	-1.53
63	Center Pin	89.75	-0.06	0.04	0.16
64	Goat Hole	89.4	-0.29	-0.47	-0.37
65	Goat Corner	89.35	-0.40	0.26	0.45
66	RM89.3	89.3	-0.76	-0.89	-0.89
67	Dutton	89.15	0.53	0.30	0.15
68	RM88.9	88.9	1.13	0.83	0.55
69	RM88.65	88.65	0.55	0.66	0.62
70	RM88.4	88.4	-0.37	-0.41	-0.38
71	RM88.24	88.24	-0.08	-0.17	-0.40
72	RM88.1	88.1	0.01	0.05	-0.01
73	Browns	87.9	-0.31	-0.50	-0.44
74	RM87.5	87.5	-0.72	0.04	0.21
75	Jump Hole	87.45	-0.71	-0.81	-0.90
76	RM87.55	87.55	-0.48	-0.43	-0.33
77	Upper Camp	87.15	-0.53	0.03	0.65
78	Lower Camp	87	-0.88	-0.63	-0.22
79	RM86.9	86.9	-0.26	-0.08	0.34
80	RM86.77	86.77	-0.02	0.00	0.17
81	Squatter Hole	86.55	0.29	0.50	0.30
82	Johnson Point	86.45	0.03	-0.08	0.24
83	Steelhead Alley	85.8	0.12	0.08	-0.03
84	Last Hole on Left	85.4	0.56	0.46	0.18
85	Chapman	83.2	-0.04	0.06	0.23
86	Icebox	82.75	0.14	0.15	0.17
87	RM82.6	82.6	-0.11	-0.12	-0.21
88	Eds Hole	82.3	0.23	0.22	0.14

89	Sheridan Hole	81.7	0.13	-0.58	-0.02
90	Upper Sky Ranch	80.7	0.24	0.06	-0.15
91	Lower Sky Ranch	80.45	1.36	1.52	1.43
92	UJC 1	80.2	0.22	-0.19	-0.73
93	UJC 2	80.1	-0.79	-0.80	-0.38
94	JC Hole	79.53	-0.11	-0.59	-0.52
95	RM78.95	78.95	-0.57	-1.82	-2.16
96	JC Campground 1	78.05	0.09	0.33	0.63
97	JC Campground 2	77.95	-0.38	0.03	0.23
98	McCartneys	77.1	0.33	-0.18	-0.34
99	Upper Bigfoot	75.83	0.16	0.39	0.73
100	Valdor	75.05	-0.17	-0.42	-0.47
101	Coopers Bar	74.85	0.00	-0.21	-0.38
102	Riprap	74.6	-0.30	0.07	0.08
103	Lime Point	74.5	1.78	2.88	4.61
104	RM73.3	73.3	-0.44	0.02	0.11
105	Pear Tree	73.03	0.70	0.40	-0.34